UNIVERSITY OF LONDON THESIS

Degree *PhD*   Year *2006*   Name of Author *HO, Szeman*

Injectable Biodegradable Poly(ester-co-ether) Methacrylate Monomers for Bone Tissue Engineering and Drug Delivery Applications

Thesis submitted by

Sze Man Ho

For the degree of
DOCTOR OF PHILOSOPHY

Division of Biomaterials and Tissue Engineering
Eastman Dental Institute
University College London
256 Gray's Inn Road
London
WC1X 8LD

-2006-

UMI Number: U592960

UMI

Dissertation Publishing

ProQuest®

Dedicated to

my Parents, my Sister and my Brother

Declaration

I hereby certify that the work embodied in this thesis is the result of my own investigations, except where otherwise stated.

In the synthesis of the monomers section, the NMR spectra were collected with the assistance of Dr Geoff Kelly at the NMR Centre of National Institute for Medical Research. In the degradation study, the mechanical analyses of the polymers were carried out with assistance from Roopa Prabhakar, a PhD student at that time at the Eastman Dental Institute, UCL. In the composite study, the bulk phosphate glass was made, and the ion chromatograms were collected, by Dr Ifty Ahmed, a post-doctoral researcher then at the Eastman Dental Institute, UCL. The calcium phosphate particles were prepared and supplied by Dr. Mike Hofmann and Prof. Uwe Gbureck, from the Universities of Birmingham and Wurzburg. The Raman mapping spectra were obtained by Dr Simon Fitzgerald of Horiba Jobin Yvon Ltd.

Acknowledgements

Firstly I would like to sincerely thank my main supervisor, Dr. Anne Young, for her invaluable advice, support and guidance throughout the project. I would like to express my gratitude for the time that she dedicated to this project and the fact that she was always available to help whenever I needed her. I would like to thank my second supervisor, Professor Nikos Donos, for his assistance.

Secondly I would like to thank all at the Eastman Dental Institute for their help and time, with special thanks to Dr. Showan Nazhat for his help on mechanical analysis. Thanks also go to my colleague, Roopa Prabhakar for her assistance in conducting the mechanical analyses of the polymers and Dr Ifty Ahmed, for making the bulk phosphate glass and collecting the ion chromatography data.

I would like to acknowledge Dr Geoff Kelly at the NMR Centre of National Institute for Medical Research, for his assistance with collection of the NMR spectra; Dr. Mike Hofmann and Professor Uwe Gbureck, from the Universities of Birmingham and Wurzburg for supplying the calcium phosphate particles, and Dr Simon Fitzgerald of Horiba Jobin Yvon Ltd for collecting the Raman mapping spectra.

The Engineering and Physical Sciences Research Council (EPSRC) and the UCL Clinical Research and Development Committee (CRDC) are also acknowledged for their financial support for this project.

I would like to take this opportunity to thank Ifty Ahmed, Roopa Prabhakar, Danny Leung, Anita Patel and Graham Palmer for their support and encouragement during this PhD, especially Ifty and Roopa, whose friendship is no doubt one of my biggest gains in these four years.

Finally I would like to thank my family for supporting me to complete this PhD.

Abstract

The aim of this project was to produce strong, fast photocuring polymer adhesives and composites for biomedical applications that degrade and can release drugs at a controllable rate after set. Five ABA triblock poly(lactide-co-propylene glycol-co-lactide)s with 7, 17 or 34 propylene glycol and 2, 4 or 8 lactic acid units in each B and A block respectively, end capped with methacrylate groups, were prepared. Using FTIR, Raman and NMR, the relative lactide, polypropylene glycol and methacrylate levels in the monomer were proved controllable and as expected from reactant ratios. Polymerisation rates upon blue light exposure for 60, 120 or 240 s using 0.5, 1 or 2 wt% initiators were determined. The shortest monomer with 0.5 wt% initiator achieved 96 % conversion by 120 s after start of 60 s illumination, forming a semi-rigid polymer that in water degraded almost linearly with time with 19 wt% material loss over 14 weeks. Raising initiator concentration reduced polymerisation rate on the lower surface of samples. Increasing the number of lactic acid units in each A block from 2 to 8 enhanced water sorption and increased average total mass loss in 14 weeks to 60 wt% but degradation rate decreased with time. Monomers produced with longer polypropylene glycol B blocks required longer periods of light exposure for full cure and the final more flexible polymers exhibited slower non-linear degradation. Drug release was controlled by varying monomer composition and drug loading level. With hydrophobic ketoprofen, release was more enhanced from rapid-eroding, high water-absorbing polymers. Release of the more water-soluble chlorhexidine diacetate and prednisolone were affected more by polymer swelling and drug diffusion rates through the polymer. Two highly soluble phosphate glasses (67 wt%) were added to one monomer producing composites without losing the

rapid set capacity of the polymer. Within a few days in water the glass was leached out providing a means to generate a porous structure. Replacement of phosphate glass with β−tricalcium phosphate and monocalcium phosphate monohydrate filler increased the composite modulus by an order of magnitude upon water sorption, buffered the acidic polymer degradation products and raised the polymer erosion rate significantly. Through further investigations, these polymers and composites should potentially provide a new range of injectable biodegradable slow drug-releasing adhesive materials for various applications in bone tissue engineering and drug delivery.

Table of Contents

3   SYNTHESIS AND POLYMERISATION KINETICS OF MONOMERS

List of Tables

List of Figures

20

List of Abbreviations

ATR FT-IR	Attenuated total reflectance Fourier transform infra-red spectroscopy
BMP	Bone morphogenetic protein
BP	Benzoyl peroxide
Ca^{2+}	Calcium cation
$CaCO_3$	Calcium carbonate
CaO	Calcium oxide
CaP	Calcium phosphate
CDA	Chlorhexidine diacetate
CPC	Calcium phosphate cements
CPH	1,6-bis (p-carboxyphenoxy) hexane
CPP	1,3-bis(p-carboxyphenoxy) propane
CQ	Camphoroquinone
DCPA	Dicalcium phosphate anhydrous (i.e. monetite)
DCPD	Dicalcium phosphate dihydrate (i.e. brushite)
DMA	Dynamic mechanical analysis
DMPA	2,2-dimethoxy-2-phenyl acetophenone
DMPT	N,N-dimethyl-p-toluidine
DPFDMA	Di(propylene fumarate)-dimethacrylate
D-PLA	Poly-D-lactic acid / poly-D-lactide
D,L-PLA	Poly-D,L-lactic acid / poly-D,L-lactide
D,L-PLGA	Poly(D,L-lactic-co-glycolic acid)
D,L-PLGA/PEG	Poly(D,L-lactic-co-glycolic acid) / poly(ethylene glycol)
EDAX	Energy dispersive X-ray analysis
4EDMAB	Ethyl-4-N,N-dimethyl aminobenzoate
Fe_2O_3	Iron oxide
FT-IR	Fourier transform infra-red spectroscopy
GL	Glycolide
HA	Hydroxyapatite
HEMA	Hydroxyethyl methacrylate

IC	Ion chromatography
Ka	Acid dissociation constant
$L_{critical}$	Critical dimension
LA	Lactide
L-PLA	Poly-L-lactic acid / poly-L-lactide
m	Length of lactide or glycolide linkage in lactic or glycolide acid units on either side of PPG
Mn	Number-average molecular weight
M_w	Molecular weight (g/mol)
MA	Methacrylate
MAC	Methacryloyl chloride
MCPH	Dimethacrylated 1,6-bis (p-carboxyphenoxy) hexane
MCPP	Dimethacrylated 1,3-bis(p-carboxyphenoxy) propane
MCPM	Monocalcium phosphate monohydrate
MMA	Methylmethacrylate
MSA	Dimethacrylated sebacic acid
MRI	Magnetic resonance imaging
n	Propylene glycol units
Na^+	Sodium cation
Na_2O	Sodium oxide
NMR	Nuclear magnetic resonance spectroscopy
NVP	N-vinylpyrrolidone
P	Phosphorus
PnLm / PnGm	Intermediate poly(propylene glycol-co-ester) products
PnLmDMA / PnGmDMA	Final poly(propylene glycol-co-ester) dimethacrylate monomers
PCL	Poly(ε-caprolactone)
PCLTMA	Trimethacrylated poly(ε-caprolactone)
PCPH	Poly[1,6-bis (p-carboxyphenoxy) hexane]
PDO	Poly(dioxanone)
P(EAD-SA)	Poly(erucic acid dimer-sebacic acid)
PEG	Poly(ethylene glycol)
PEG-DMA	Dimethacrylated poly(ethylene glycol)
PGA	Poly(glycolide) or poly(glycolic acid)

PLA	Poly(lactide) or poly(lactic acid)
PLGA	Poly(lactide-co-glycolide) or poly(lactic acid-co-glycolic acid)
PMMA	Poly(methyl methacrylate)
PMSA	Dimethacrylated poly(sebacic acid)
PO_4^{3-}	Orthophosphate
P_2O_5	Di-phosphorous pentoxide
$P_2O_7^{4-}$	Pyrophosphate
$P_3O_9^{3-}$	Cyclic trimetaphosphate
$P_3O_{10}^{5-}$	Tripolyphosphate
PPF	Poly(propylene fumarate)
PPF-DA	Diacrylated poly(propylene fumarate)
PPG	Poly(propylene glycol)
PPGLADMA	Poly(propylene glycol-co-lactide) dimethacrylate
PSA	Poly(sebacic acid)
PVP	Poly(vinyl pyrrolidone)
RSD	Relative standard deviation
SA	Sebacic acid
SC-CO$_2$	Supercritical carbon dioxide
SEM	Scanning electron microscopy
Sn(Oct)$_2$	Stannous octoate (Sn (II) 2-ethylhexanoate)
T_c	Crystallisation temperature
T_g	Glass transition temperature
T_m	Melting temperature
β-TCP	β-tricalcium phosphate
TEA	Triethylamine
TGF-β1	Transforming growth factor β1
UV	Ultraviolet
UV/vis	Ultraviolet/ visible spectroscopy
XRD	X-ray diffraction
XRPD	X-ray powder diffraction
μ	Dipole moment
δ	Ratio of loss to storage modulus of a material (i.e. Tan delta)

Keys for Equations

Chapter 2 Analytical Techniques

Energy	Energy of an electromagnetic light beam
f	Frequency of an electromagnetic light beam (Hz)
υ	Wavenumber of an electromagnetic light beam (cm^{-1})
λ	Wavelength of an electromagnetic light beam (nm)
h	Planck's constant
c	Velocity of light
I_o	Intensity of light incident on an absorbing system
I_t	Transmitted intensity of light incident on an absorbing system
c	Concentration of a homogenous light absorbing system ($moldm^{-3}$ or % m/v)
l	Path-length that an incident light has to pass (cm)
A	Absorbance of a homogenous light absorbing system
k	Absorptivity of a homogenous light absorbing system
σ	Stress applied to a material in DMA (Pa)
ε	Amount of displacement by which a material is deformed (i.e. strain) in DMA (%)
σ_o	Maximum stress applied to a material in DMA (Pa)
ε_o	Strain at the maximum stress in DMA (%)
ω	Frequency of oscillation
δ	Phase lag/ tan delta
E^*	Complex modulus of a material (Pa)
E'	In-phase storage (real or elastic) modulus of a material (Pa)
E''	Out-of-phase loss (imaginary or viscous) modulus of a material (Pa)
F	Level of variable i being investigated in a factorial analysis experiment (can be +1, 0 or -1)
Q_c	Measured outcome of cth sample in factorial analysis

Chapter 3 Synthesis and Polymerisation Kinetics of Monomers

Y_I	Reaction yield of intermediate products ($PnLm$ or $PnGm$) (%)
Y_E	Reaction yield of end products ($PnLm$DMA or $PnGm$DMA) (%)
Y_O	Reaction yield of overall monomer synthesis (%)
G_{obt}	Obtained mass of product (g)
G_{exp}	Expected mass of product (g)
a_{LA} or a_{GL}	Fraction of units that are ester in intermediate product ($PnLm$ or $PnGm$)
a_{MA}	Fraction of units that are methacrylates in end product ($PnLm$DMA or $PnGm$DMA)
n	Propylene glycol units
m	Length of lactide or glycolide linkage in lactic or glycolide acid units on either side of PPG
A_v	Absorbance of a FT-IR peak at wavenumber v cm^{-1}
I	Peak height of a Raman peak
P	Peak area of a NMR signal
m_{calc}	Calculated lactoyl/glycoyl chain lengths of monomer
LA_{tot} or GL_{tot}	Molar ratios of total lactide or glycolide to PG for monomer
LA_e or GL_e	Number of end lactic acid or glycolic acid groups per PG unit
MA	Number of methacrylate groups per PG unit
M_{mw}	Calculated molecular weight of synthesised monomer (g/mol)
PPG_{mw}	Molecular weight of PPG (g/mol)
PG_{mw}	Molecular weight of PG (i.e. 58 g/mol)
LA_{mw}	Molecular weight of lactic acid (i.e. 72 g/mol)
GL_{mw}	Molecular weight of glycolic acid (i.e. 58 g/mol)
MA_{mw}	Molecular weight of methacrylate (i.e. 85 g/mol)
m_{pred}	Expected length of lactide or glycolide linkage in lactic or glycolide acid units on either side of PPG
x_{exp}	Percentage of OH groups that would be expected (from simple probabilities) to be reacted after the first reaction stage
H_0	Pre-polymerisation Raman peak height at 1640 cm^{-1}
H_f	Post-polymerisation Raman peak height at 1640 cm^{-1}

Q_f	Final polymerisation percentage of monomer (%)
Q_t	Polymerisation percentage of monomer as a function of time
ΔA_t	Absorbance difference at 1736 and 1716 cm^{-1} at time t
ΔA_0	Absorbance difference at 1736 and 1716 cm^{-1} at time 0 before start of light exposure
ΔA_f	Absorbance difference at 1736 and 1716 cm^{-1} at end of time-based IR run

Chapter 4 Polymer Degradation

RSD	Relative standard deviation
s	Sample standard deviation
$\bar{x}$	Sample mean
ΔW	Wet mass change of specimen (%)
W_t	Mass of 'wet' specimen at time t (g)
W_0	Mass of 'wet' specimen at time 0 (g)
ρ_t	Density of specimen at time t (g/cm^3)
V_t	Volume of specimen at time t (cm^3)
ρ	Density of specimen (g/cm^3)
ρ_{water}	Density of water (g/cm^3) at the operating temperature (°C)
M	Mass of 'wet' specimen measured in water (g)
V	Volume of specimen (cm^3)
ρ_0	Density of specimen at time 0 (g/cm^3)
$\Delta\rho$	Density change of specimen (%)
ΔV	Volume change of specimen (%)
C_a	Cumulative moles of acid released in 10 ml storage solution per specimen
$[H^+]$	Molar hydrogen ion concentration (mol dm^{-3})
ΔW_P	Polymer mass loss (%)
W_{Pmol}	Mass of degradation products per mole of acid released (g/mol)
$\Delta E'$	Storage modulus change of specimen (%)
E'_t	Storage modulus of specimen at time t (kPa)
E'_0	Storage modulus of specimen at time 0 (kPa)

Chapter 5 Drug Release

ΔW_D	Total percentage mass loss of specimen
ΔW_P	Percentage mass loss due to polymer erosion
W_D	Total specimen mass loss (g)
W_0	Initial specimen mass (i.e. at 0 hr) (g)
C_D	Cumulative mass of drug released (g)
W_{Pmol}	Mass of polymer erosion per mole of acid released (g/mol)
K	Ratio of absorbance at an absorption minimum and maximum
λ_1	Wavelength at absorption minimum of drug
λ_2	Wavelength at absorption maximum of drug
A_i	Absorbance due to impurity
A_d	Absorbance due to pure drug
A_s	Absorbance of drug-containing sample
D	Mass of drug released from specimen (g)
g	Gradient of the calibration curve of the drug
u	Dilution factor for solution of drug-containing sample
V_s	Storage solution volume (i.e. 10 ml).
MA_{den}	Methacrylate density (mol/g)

Chapter 6 Polymer composites

x_i	Mass fraction of individual component in wet composite (polymer, i=1; filler, i=2; water, i=3)
W_i	Mass of individual component in composite (g)
$\sum W_i$	Sum of mass of individual component in composite (g)
ρ	Density of specimen (g/cm^3)
ρ_i	Density of individual component in composite (g/cm^3)
$\sum V_i$	Sum of volume of individual component in composite (cm^3)
z	Total mass loss fraction of specimen
z_1	Polymer mass loss fraction

z_2	Filler mass loss fraction
y_1	Fraction of dried composite that is polymer
y_2	Fraction of dried composite that is filler
$y_{i,0}$	Initial fraction of polymer or filler in composite at time 0
C_a	Cumulative moles of acid released in 10 ml storage solution per specimen
I_{mM}	Ion release of phosphorus atom (mM)
I_{ppm}	Ion release of phosphate species (ppm)
n	Number of phosphorus atom in phosphate species (e.g. 3 in $P_3O_9^{3-}$)
P_{mw}	Molecular weight of phosphate species (g/mol)
C_I	Cumulative ion release (mM)
Vol	Polymerisation shrinkage of specimen (%)
V_c	Volume change per mole of any methacrylate (i.e. 22.5 cm^3/mol)
f	Polymerisation fraction of specimen
m	Polymer mass content (wt%)
M_{MA}	Molecular weight of monomer per mole of methacrylate (g/ mol)
Heat	Amount of heat generated by polymerisation of specimen (kcal/cm^3)
H	Heat per mole of methacrylate monomer reacted (i.e. 14 kcal/mol)

1 Literature Review

1.1   Introduction

The presence of biodegradable materials in the field of bone tissue engineering has grown significantly over the past two decades with applications in dental, maxillofacial and orthopaedic surgeries (1). This is because the potential market and demand for better filler materials are increasing in relation to the increased cases of bone fractures / diseases worldwide due to an ageing population, a growing problem of obesity and lack of exercise in the general population, as well as an increasing number of road traffic injuries. It has been postulated that road traffic injuries will rise from ninth rank in 1999 to third by 2020 as the leading cause of ill health worldwide (2). In the United Kingdom alone an osteoporosis-related fracture occurs every three minutes at a daily cost of £5 million to the NHS (3).

Tissue engineering is a rapidly developing biomaterial field which is concerned with the augmentation, regeneration or replacement of tissue or organ of the body. The approach is based on the use of an artificial extra-cellular matrix that allows living cells/ tissues to be assembled either in the body or in bioreactors that overtime develop into the required functional tissue or organ (4-6). Tissue engineering, as it applies to bone, particularly focuses on the treatment of bone defects as a result of trauma or tumour resection, the healing of fracture non-unions, the enhancement of normal fracture healing, and possibly in the future, the regeneration of complex functional components of the skeleton such as weight - bearing joints (7).

Materials for bone tissue engineering can be classified as either man-made or of natural origin. Natural materials include bone grafts (i.e. autograft or allograft) and natural polymers (i.e. collagen). Synthetic materials include metals, ceramics and

synthetic polymers. Each class has its associated problems and with advancement in bone tissue engineering it has become necessary to develop new materials that meet more demanding expectations. These range from the ability of materials to provide mechanical support during tissue regeneration and gradually degrade to biocompatible products to the more complex ability of the material to incorporate cells, growth factors etc. and provide osteoconductive and osteoinductive environments. In addition, the development of *in situ* polymerisable materials that can function as cell delivery systems in the form of an injectable and biodegradable liquid / paste are becoming increasingly more attractive. Many of the currently available polymers do not fulfil all of these requirements and significant changes to their chemical structures may be required if they are to be better formulated for bone tissue engineering applications. In recent years a lot of interest has focused on developing injectable and biodegradable polymer compositions in which mechanical and degradation properties can be tailored to suit various end applications and to avoid the need for surgical insertion and removal.

The injectable and biodegradable polymers under development in this project are produced from fluid monomers. They can be moulded into any shape or be injected directly into a space in the body via minimally invasive surgical procedures. They should then solidify rapidly at 37°C either by light exposure or using chemical initiators. Once solidified, they should provide initial support and substitute for the non-functioning damaged tissue. Through manipulation of their structures and fabrication, they could allow space for cells/ growth factors/ drugs to be incorporated and potentially be used in various bone tissue engineering and drug delivery applications. With subsequent degradation at a suitable rate into components that are safely removed by the body, the need for expensive and potentially damaging device removal surgery is eliminated.

1.2   Monomer and polymer definitions

Polymers are macromolecules composed of many repeating units called monomers that generally have carbon atom backbones, although oxygen, nitrogen, silicon and sulphur can also be present (8). If only a few monomer units are joined together during polymerisation, the resultant low-molecular-weight polymer is an oligomer. The degree of polymerisation refers to the total number of monomeric units including end groups, and hence determines both chain length and molecular weight. A homopolymer is formed when identical monomers react, whereas a copolymer is produced when two or more different monomers react (Figure 1.1). This copolymer can be random, block or graft, whereby different monomeric units are distributed randomly, in blocks, or with one polymer branching from the backbone of the other, respectively (9). Block copolymers can include those of a diblock (i.e. AB), triblock (i.e. ABA), or multiblock (i.e. -[AB]-).

-A-A-A-A-A-A-A-   Homopolymer

-A-B-B-A-B-A-A-   Random co-polymer

-A-A-B-B-A-A-B-B-   Block co-polymer

-A-A-A-A-A-A-A-A   Graft co-polymer
  | |
  B-B-B-   B-B-B-
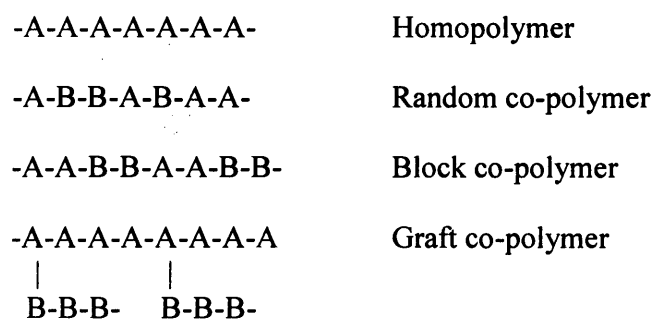
Figure 1.1. Representations of homopolymer and copolymers. A and B are hypothetical monomers.

1.2.1 Nomenclature

In a molecular formula or polymer name the monomeric structural unit is usually provided in brackets e.g. poly(ethylene glycol). In a graphical formula the end functional groups are often placed outside the brackets (see for example Figure 1.2)

(a)   (b)
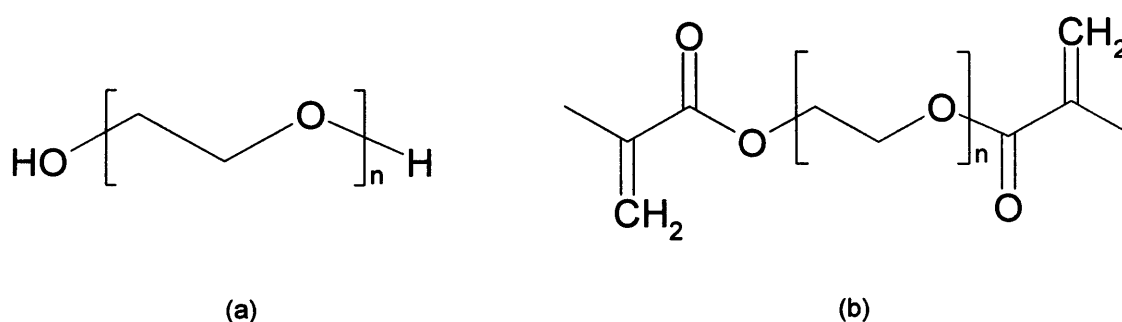
Figure 1.2. (a) Poly(ethylene glycol) with diol end groups and (b) Poly(ethylene glycol) dimethacrylate with vinyl end groups.

1.2.2 Physical properties

Some of the physical properties of polymers that can affect their working properties, such as degradation and mechanical strength, are as follows:

1.2.2.1 Molecular weight and polydispersity

A polymer sample is made up of individual molecules that have a distribution of degrees of polymerisation that can be affected by the synthetic methods used. If all polymers in a given sample are made up of the same number of monomers, the sample is monodisperse. This is rare in synthetic polymers, and the sample is a mixture of different molecular-weight molecules (i.e. polydisperse) (10). As molecular weight can affect the

properties of the polymer, a polymer synthesis should produce molecules of controllable sizes/ lengths with a narrow distribution.

1.2.2.2 Crystallinity

Polymers may be either semi-crystalline or amorphous (11). Amorphous polymers have disordered and random chains. These polymers cannot undergo crystallisation and melting, but undergo a glass transition (see section 1.2.2.3). Semi-crystalline polymers have regular repeating units that allow the chains to fold in a compact, orderly packed fashion, forming regions called crystallites. They have a crystallisation temperature (T_c) and melting temperature (T_m). No polymer can completely organise into a fully crystalline material such that amorphous areas still exist in semi-crystalline polymers. Crystallinity can be induced by the use of homogenous chain lengths, cooling of molten polymer, evaporation of polymer solutions, or heating of a polymer under vacuum or in an inert atmosphere (to prevent oxidation) at a specified temperature (called annealing) (12). The degree of crystallinity can also be changed by the use of co-monomers in the synthesis. Monomers which are of different structures do not typically co-crystallise and crystallinity can be reduced by increasing the composition of the amorphous monomer. Semi-crystalline polymers are generally stiffer, more resistant to solvents, and of higher density than their amorphous counterparts.

1.2.2.3 Thermal properties

The glass transition temperature (T_g), exhibited by the amorphous regions of a polymer, is the point at which the material changes from a glassy state into a rubbery state (12). At temperatures below T_g, a polymer acts more like a glass (i.e. brittle, stiff and rigid), whilst at temperatures above T_g, a polymer acts more like a rubber (i.e. flexible).

As the temperature increases, the kinetic energy of the molecules increases with increasing vibrational and rotational freedom resulting in more segmental motion of the polymer chains. The value of T_g therefore depends on the level of rotational freedom and segmental motion of the polymer. For the increased motion to take place, the space between the atoms (the free volume) must increase. Generally the higher the molecular weight of a polymer, the fewer the chain ends and the lower the free volume, and the higher the T_g. Similarly, the bulkier the substituents on the polymer backbone (e.g. branching), the less will be its flexibility (i.e. rotational freedom) and the higher the T_g. Increasing the polarity of the monomeric units also leads to higher T_g because of increased dipole-dipole interaction.

The melting temperature (T_m) of a crystalline polymer is the point when the thermal energy becomes so great that the chains become totally mobile and the polymer flows. Unlike amorphous polymers which liquefy gradually over a broad temperature range above the T_g, semi-crystalline polymers melt over a relatively narrow temperature range. T_m is affected by similar factors to T_g. A rigid, branched polymer with many cyclic units would have a high T_m, whereas a flexible, chain polymer would have a low T_m (9).

1.3   History of medical polymers

For hundreds of years crutches and wooden legs have been examples of simple yet useful attempts to improve bone fractures. With the advancement of technical skills and knowledge, materials such as wood, clay, stones and plaster components have been applied on the outer surface of injured limbs. Since 1892, when Plaster of Paris ($CaSO_4$)

was first used as a bone cement, ceramics were often chosen for fracture fixation (13). Then from the early 1940s, use of synthetic polymers, such as nylon sutures for medical applications, began to emerge. The use of polymeric bone cements for fracture fixation was pioneered in 1951, when Charney first anchored an endoprosthesis with a self-curing polymethacrylate cement (14). In the 1960s the suitability of polymers which were biodegradable was recognised for reparative medical applications (15). Polyesters made of glycolic or lactic acid were among these first synthetic biodegradable polymers, and were explored as resorbable sutures/ fibres (16). The wide acceptance of the lactide/ glycolide polymers as suture materials led to a variety of other possible clinical applications including ligament reconstruction, parenteral drug controlled release, vascular grafts, nerve, dental and fracture repairs (16) and promoted the biomedical use of other biodegradable polymers (17). Polyanhydrides, for example, were first synthesised in the early 1900s (18). Originally used for textile applications in 1930s (18), they were later proposed as biodegradable carriers for controlled drug delivery systems in the early 1980s (19). Another biodegradable polymer, poly(propylene) fumarate, was first synthesised in 1988 (20) and has since been investigated for use as bone cements and scaffolds (21-24). Research has continued to (i) optimise the properties and performance of the classic original materials such as polyesters *in vivo*; and (ii) develop new synthetic polymers.

1.4   End Applications

The potential end applications in bone tissue engineering and drug delivery for the injectable biodegradable polymers being developed are vast and may include the following:

✓ As bone cements to provide structural support for fractured bones (25;26)

✓ As orthopaedic fixation devices (pins, screws, plates) (15;27)

✓ As rigid porous two- or three-dimensional scaffolds (28-30)

✓ As flexible materials / implants to act as substitutes for damaged tissues around bones such as cartilage repair (13;31)

✓ As controlled drug/ bioactive agent delivery carriers (32-34)

1.4.1 Bone cements and fracture fixation

Surgical resections, traumatic injuries, cancer treatment and congenital abnormalities are often associated with abnormal bone shape or segmental bone loss. Restoration of normal structure and function in these cases requires replacement of the damaged or missing bone. This may involve surgical transplant of natural tissue from an uninjured location elsewhere in the body. This approach, however, is limited by availability, inadequate blood supply and secondary deformities at the donor sites. Allograft (where bone is transplanted between two individuals) provides an alternative procedure but is associated with possible transfer of diseases and immunological reactions from the host, poor osteogenic capacity and high costs (35). Biodegradable polymers can therefore be used as substitutes.

Every bone in the body is composed of a honey-comb medullary cavity containing cancellous (trabecular, spongy) bone, which is surrounded by a solid bone cortex composed of cortical (compact) bone (36). Under most conditions bone is capable of regenerating itself in minor fractures (37). When a fracture occurs, inflammatory cells flood the damaged site and segregate it from surrounding tissues and vasculature. These inflammatory factors partially digest the broken bone ends and provide growth factors for

reparative cells (known as mesenchymal cells). These reparative cells accumulate at the site and differentiate into chondrocytes or osteoblasts to form a new cartilage and bone mass (soft callus). The cartilage is then resorbed and replaced by new bone mass that is subsequently remodelled to restore the original osseous anatomy and function (35;38). The time for this bone union varies, but normally can be achieved in about 4-8 weeks (15).

In 5 to 10 % of fractures, however, this sequence of facture repair cannot be completed due to instability of the fracture gap, interposition of soft tissues, infection, inadequate blood supply, nutritional and metabolic abnormalities and neural element disruption (7). This results in a prolonged non-union condition. Furthermore, when a fracture occurs in the lower extremity, immediate mechanical support of the bone is needed for continued limb loading. In these cases biodegradable polymers can be used as bone cements for fracture repair, for example, by filling in a bone defect.

Commercially available bone cements today are usually a mixture of poly(methyl methacrylate) (PMMA) and a copolymer of methylmethacrylate (MMA). MMA monomer is used in the curing process of the bone cement, with benzoyl peroxide (BP) as initiator and N,N-dimethyl-p-toluidine (DMPT) as accelerator to enable thermal polymerisation. This forms rigid polymers that can be of the required dimension and functionally replace the damaged bone or secure metallic orthopaedic implants (39).

1.4.2 Orthopaedic fixation devices

Biodegradable materials have been used in the shape of screws, pins, plugs and plates (9;27;40) for orthopaedic, oral and maxillofacial surgery. With a material that is injectable and photo-crosslinkable, flexible fracture fixation plates could be developed from partially reacted monomers. The flexible plates could then be contoured *in vivo* and

subsequently further exposed to light to complete the crosslinking polymerisation and to produce a rigid plate (41). Currently the majority of the polymeric fixation devices on the market are neither injectable nor photo-crosslinkable; they are made of L-poly(lactide) (L-PLA), poly(glycolide) (PGA) and copolymers of PLA and PGA (11).

1.4.3 Cartilage repair

Cartilage repair represents a special challenge in bone tissue engineering as cartilage itself has very low or no regeneration potential (13). The mechanism of repair is complex and it has been suggested to involve initially the eruption of marrow into the empty defect. This causes the marrow to fill completely the defect with osteoprogenitor cells that aggregate and multiply and then differentiate into cartilage, and eventually this cartilage is replaced by bone at the base with a covering of fibrous tissue. The extent and rate of the defect repair is, however, dependent on the amount of marrow that provides the progenitor cells (38).

Currently the treatment of cartilage repair involves cell implantation into the cartilage defect or stimulation of cell migration to the lesion site (38). One of the challenges in achieving successful treatment is getting the cells to adhere to the site and to produce a durable matrix with living cells that matures into a tissue that duplicates the original tissue (37). Naturally derived polymers such as fibrin glues and alginate gels have been explored for injectable cartilage applications (13). Synthetic biodegradable polymers can therefore also be used as matrices filled with cells to serve simultaneously as delivery vehicles and for fixation. The latter can be achieved through crosslinking the matrix to the lesion wall. An injectable and crosslinkable polymer, poly(ethylene oxide)

dimethacrylate, has been studied for this purpose (13) although this polymer is not biodegradable.

1.4.4 Two- or three-dimensional tissue engineering scaffolds

Synthetic biodegradable polymers can be used to create porous scaffolds to allow room for bone cellular attachment, migration, proliferation and the resultant guided tissue in-growth and vessel formation (1). A cellular component can also be seeded into the material before implantation (42). The physical appearance of scaffold implants depends on the application and implantation site. Scaffolds can be membranes, meshes, plates, screws, plugs, or rods. For example, scaffold plates that cover cranial defects serve as a guide and prevent non-desired tissues, like fibrous tissue, from growing in and filling the defect, thereby enhancing healing compared to non-covered defects (28). The physical factors that determine the success of a scaffold include its pore size for tissue growth, pore interconnectivity for access to nutrients and transport of waste products, and pore shape and roughness for better cell spreading (30). Scaffold materials that have been investigated for bone and cartilage tissue engineering include hydroxyapatite (30), poly(α-hydroxy esters) (28;43) and collagen (44).

1.4.5 Controlled drug/ bioactive agent delivery

Biodegradable polymers can be developed specifically as drug / bioactive agent delivery systems alone or in conjunction with all of the applications previously mentioned. As the rate of infection following total joint replacement surgery may be as high as 11 % (45), it is therefore of interest to minimise this by incorporating various antibiotics into cements for slow release at the surgical site. The synthetic polymer can also be made to

contain bioactive molecules to increase repair rate (46), or to control release of peptides, proteins and DNA (47;48).

Since the last two decades, various polymeric devices like parenteral depot systems, microspheres, nanoparticles, implants and films (16;47-49) have been fabricated using synthetic biodegradable polymers for the delivery of a variety of drug classes. For example, antibiotics have been incorporated into a resorbable cement for the treatment of chronic bone infections such as bacterial osteomyelitis (45), and osteoinductive proteins and peptides, such as recombinant growth factors and bone morphogenetic proteins, have been added into synthetic polymers to speed up recovery (42;50). The drug/ bioactive agent release can include both sustained delivery over days/ weeks/ months/ years (51) and targeted delivery (e.g. to a tumour, diseased blood vessel etc.) on a one-time or sustained basis (52). In sustained delivery controlled therapeutic concentrations of the drugs/ bioactive agents can be released in the local vicinity of the material thereby reducing possible systemic side effects and avoiding unnecessary drug metabolism that would reduce its effectiveness. Some studies have used polymers to protect the drugs/ bioactive agents from premature inactivation (45). A successful use of synthetic polymers for drug delivery is the implantable contraceptive Norplant™, which comprises a silicone rubber (polydimethysiloxane) tube filled with a steroid dispersion; drug release is controlled by the permeability of the steroid through the tube wall (53).

1.5   Requirements

The polymeric materials should be designed with respect to the clinical requirements in order to engineer a clinically relevant device. The material properties of

the ideal polymer for the above end applications form a template for the development of the poly(ester-co-ether) methacrylate monomers in this project. These properties should include the following:

1.5.1 Suitable mechanical characteristics

An ideal material should provide immediate mechanical support for a fracture but also not impose stress shielding as the fracture heals (13). In other words the material should possess mechanical properties similar to those of the tissue it is replacing in order to provide structural stability to a damaged site without absorbing all of the mechanical stresses. For example, a bone cement should have similar compressive modulus to that of human trabecular bone i.e. ~100-1000 MPa (54).

1.5.2 Biodegradability

There have been many definitions for biodegradable polymers. Okada (55) has defined biodegradable polymers as 'polymers that are degraded and catabolised, eventually to carbon dioxide and water, by microorganisms (bacteria, fungi, etc) under natural environment'. Vert (29) has defined biodegradable polymers as "polymeric materials or devices which break down due to macromolecular degradation" and which "can be attacked by biological elements so that the integrity of the system and in some cases but not necessarily, of the macromolecules themselves, is affected and produces fragments or other degradation products. Such fragments can move away from their site of action but not necessarily from the body". As it applies to the body this 'attack' of the polymeric systems could be either through hydrolysis or enzymatic or cellular degradation (51).

The material should degrade at a rate that is coupled to the rate of tissue formation so that slow transfer of the mechanical load to the healing bone/ damage site is facilitated (13). Long-term toxicity problems are also avoided by the gradual degradation of the materials, as the small amount of constituents released daily from the slowly degrading device can be easily handled by the tissue elimination routes. As the degraded materials may be removed by the body naturally, the need for a second surgery to remove the medical device is eliminated.

1.5.3 Injectability

To enable materials to be easily moulded to fill in different shapes and cracks they should initially possess a liquid or putty-like consistency but subsequently react to form a polymer of exactly the required dimensions when placed within the body. The materials can be injected either directly underneath the skin or via a small surgical opening thereby avoiding the need for invasive surgical incisions. They can then be solidified *in situ* in a timely fashion by light or chemical means or a combination of both. Heat generated by this curing reaction should be as minimal as possible to reduce damage to the surrounding tissue (13). The adhesion of the polymer to the biological surface of surrounding tissue is improved because of intimate contact of the polymer with the tissue during formation and the micromechanical interlocking that can result from surface micro-roughness (39).

1.5.4 Readily made drug releasing

Drugs can be incorporated into polymers in a number of ways. The drugs may be miscible with the monomers but if not they can be finely ground and dispersed within the monomer. The resultant monomer/ drug mixtures can then be injected and solidified *in*

situ as an injectable implant or be polymerised *ex vivo* prior to placement into the body. The latter may be powdered into nanoparticles and then introduced into the body as a suspension in a liquid. This 'drug-polymer nanoparticle' method can provide more control of the particle size and consequently of the drug release rates. The drugs incorporated must not react with the polymer or interfere with the fabrication process. One study for example (56), found that the incorporation of chlorhexidine diacetate (CDA) in a tetrahydrofurfuryl methacrylate/ poly(ethyl methacrylate) polymer system hindered polymerisation resulting in a higher level of residual monomer and low molecular weight components being leached from the polymer. This was possibly due to the multiple amine groups on the CDA molecule which can mop up free radicals via their protonation (on the chlorhexidine or acetate ion), resulting in formation of new ion pairs between the DMPT- and BP-based ions and the CDA. In a polymeric system, the drugs encapsulated are released either by diffusion through the polymer barrier, or by erosion of the polymer material, or by a combination of both diffusion and erosion mechanisms (57;58). If the device is used purely as a drug delivery carrier it would be ideal that the completeness of polymer erosion coincides with the end of drug release (51).

1.5.5 Promotion of cellular growth

Use of new polymers for bone repair provides many advantages over tradition allograft bone grafting but a disadvantage can be that they lack biological activity to promote bone formation. These materials can, however, be made to deliver growth factors such as bone morphogenetic proteins (BMPs) to augment bone healing or to have void spaces within their structures (i.e. as scaffolds) to allow cells such as osteoblasts to migrate into and proliferate. These void spaces may be created either through degradation

of the material with time at a designed rate or by a fabrication process during polymerisation. The latter can involve use of leachable porogens, such as sugar spheres (43) or sodium chloride (59); phase separation techniques (60); or expansion of the material into a foam through release of carbon dioxide during polymerisation (42;61). It has been determined in several studies (9;62;63) that the minimum pore size for effective bone ingrowth is approximately 100 μm. Pore connectivity was also found (30) to be important for forming channels to allow supply of oxygen and nutrients for deep tissue growth and transfer of waste products out of the matrix. Through use of a leachable porogen, Hedberg *et al* (59) constructed crosslinkable poly(propylene fumarate) (PPF) composite scaffolds incorporated with poly(D,L-lactic-co-glycolic acid) / poly(ethylene glycol) (D,L-PLGA/PEG) blend microparticles that were loaded with an osteogenic peptide. In this way, the drug/ bioactive molecules were protected by the polymeric carriers from any adverse effects of exposure to free radicals during curing of the composite, whilst the embedding of these microparticles in the polymer composites further modulated the release kinetics of the loaded compounds. Use of methods like this therefore should allow the easily damaged osteogenic peptides or proteins to be incorporated into an injectable and polymerisable system to create a potentially osteoinductive material.

1.5.6 Biocompatibility

Biocompatibility has been defined as 'local biological tolerance of the given material manifested by absence of acute and chronic inflammatory responses' (64). In other words the material must not provoke an irresolvable inflammatory response that might lead to host rejection and / or the formation of an impenetrable fibrous capsule

around the implant (24) or demonstrate extreme immunogenicity or cytotoxicity (13). Additionally implants in direct contact with both the bony and the soft tissues should not induce bone resorption, while the soft tissue should be firmly attached to the implant surface preventing fluid accumulation which might lead to infection (64). Biocompatibility should apply to the intact material as well as the degradation products (13). In some studies polymeric materials have been incorporated with hydroxyapatite or calcium phosphates, including for example phosphate-based glasses, in an attempt to increase their biocompatibility, allow more rapid tissue repair and enable further control over their degradation and mechanical properties(23;65-69).

Table 1.1. Properties of products currently on the market or under development for bone tissue engineering and drug delivery applications.

	Class of products	Example materials within class [i]	Elastic modulus E (GPa) [ii]	Biodegra-dable [iii]	Injectable	Drug releasing	Biocom-patible [iv]
Commercialised products	Metal	Stainless steel, cobalt-chromium alloy, titanium and its alloy	110 – 253	✗	✗	✗	✗
	Poly(methyl methacrylate)	-	1.1 - 2.2	✗	✓	✓	✓ (strikethrough)
	Poly(α-hydroxy esters)	D,L-PLA	1 – 3	12 -16 m	✗	✓	✓ (strikethrough)
		L-PLA	3 – 5	3 - 5 yr			
		PGA	6 – 7	6 - 12 m			
		P(D,L-LA-co-GA) 50:50	1 – 3	1 - 2 m			
	Poly(ε-caprolactone)	-	0.4	2 - 3 yr	✗	✓	✓
	Ceramics	Calcium phosphate	40 – 117	decades	✓	✓	✓
Products mainly under development	Poly(ether-esters)	PDO	1.5	6 – 12 m	✓	✓	✓
		PEG/ PLA	-	days - weeks			
	Poly(anhydrides)	PSA	0.1	1 dy	✓	✓	✓
		PMSA	~1.4	2 dy			
		PCPH	0.0013	1 yr			
	Poly(propylene fumarate)	PPF/NVP	~0.06	months	✓	✓	✓ (strikethrough)
		PPF/PEG-DMA	0.03 - 0.06				
		PPF/PPF-DA	0.019 - 0.34				

[i] PLA = poly(lactide); PGA = poly(glycolide); PDO = poly(dioxanone); PEG = poly(ethylene glycol); PSA = poly(sebacic acid); PMSA= dimethacrylated poly(sebacic acid); PCPH = poly[1,6-bis (p-carboxyphenoxy) hexane]; PPF = poly(propylene fumarate); NVP = N-vinylpyrrolidone; PEG-DMA = dimethacrylated poly(ethylene glycol); PPF-DA = diacrylated poly(propylene fumarate).

[ii] Youngs modulus of human cortical bone is 15-30 GPa; human trabecular bone is ~100-1000 MPa and [iii] yr = year; m = month; dy = day.

[iv] Strikethrough the 'tick' means initial or late biocompatibility problem may occur; for more details on biocompatibility of the materials, see later.

58

1.6   Products on the Market

Table 1.1 compares the properties of selected materials currently available on the market or under development. These materials are generally classified into metals, ceramics, natural and synthetic polymers. Each class of materials has its short-comings and none contains all the desired properties required for all bone tissue engineering and drug delivery applications.

1.6.1 Metals and alloys

In orthopaedic applications metals (and alloys) have been used almost exclusively for load-bearing implants such as hip and knee prostheses and as fracture fixation wires, pins, screws, and plates. Apart from being non-injectable and non-biodegradable, a major clinical problem associated with metallic implants is 'stress shielding' (27). Bone is a dynamic material and remodels itself in accord with the applied stresses to achieve and maintain density and structural integrity (70). The elastic moduli of metals can be at least five to ten times greater than that of natural bone (70), as a result almost the entire mechanical load is transferred from the bone to the metal implant during fracture healing process. This creates a 'disuse' situation where the bone is not subject to the normal force-induced remodelling at the site of facture, and the consequent mechanical integrity of the bone structure is compromised. Resorption of the bone and subsequent possible re-fracture can therefore occur when the implant is removed (71). Furthermore, in long-term application the metallic implants e.g. steel can deteriorate as a result of *in vivo* corrosion, releasing by-products (ions, chemical compounds and particulate debris) that can cause adverse biological responses and reduce the biocompatibility of the material (70). The

rigidity of the metallic plates is often not ideal for the complex three-dimensional geometry of fracture sites such as those in the face and the miniature fixation screws required. Metallic plates can also be visual and palpable below the skin and cause problems with such imaging techniques as magnetic resonance imaging (MRI) scans (71).

Despite all the drawbacks, fixation with metal plates is still currently the most accepted method of joining fractured bones (70). These can be made from stainless steel, titanium alloys or cobalt-chromium alloys.

1.6.2 Poly(methyl methacrylate) (PMMA)

A typical acrylic bone cement composition contains a mixture of a liquid component and a powder component (14;25). The powder component consists of PMMA and benzoyl peroxide (BP) and the liquid component consists of methylmethacrylate monomer (MMA) and a tertiary amine, such as N,N-dimethyl-p-toluidine (DMPT) (Figure 1.3). Other additives can also be included, such as hydroquinone as inhibitors to prevent premature polymerisation under exposure to light/ elevated temperature, or barium sulphate as a contrast agent to allow the bone cement to be visible on radiographs. These two components, when mixed, undergo chemically induced free radical polymerisation using BP as initiator and DMPT as accelerator. The semi-liquid nature of the cement allows application *in situ* which then continues to harden in a short time (10 -15 min) (72) with adherence to surrounding tissue via micromechanical means. PMMA is relatively rigid and has a high T_g of 105°C (9). As such these materials are strong (see Table 1.1).
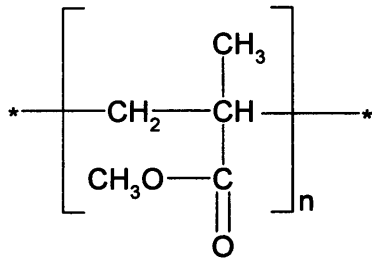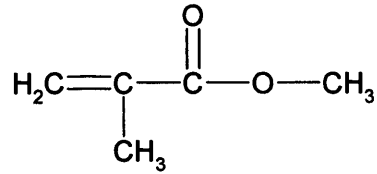
Poly(methyl methacrylate) (PMMA)   Methyl methacrylate (MMA)

Figure 1.3. Structures of poly(methyl methacrylate) (PMMA) and methyl methacrylate (MMA).

PMMA, however, suffers the drawback of not being degradable and can often lead to problems of stress shielding and wear. The latter could result in fragmentation that may elicit long term inflammatory response upon formation of particulates (66). Furthermore, being non-interactive with body cells, they can act as barriers to new bone ingrowth and can limit blood flow (73). High temperatures achieved with curing large volumes of PMMA cement in the body (124°C has been observed in some circumstances) can also cause necrosis of surrounding tissue (66;72;74). It has been suggested that in order to minimise the risk of bone necrosis, the cement mantle for prosthesis fixation should only be 2-4 mm thick (25).

Most polymeric bone cements currently on the market are based on PMMA (26). They are commonly used as an aid in securing implants for total hip or knee replacement and are often preloaded with antibiotics (25). PMMA beads have also been impregnated with antibiotics before being surgically packed into wound cavities for treatment of chronic osteomyelitis (75).

1.6.3 Poly(α-hydroxy esters)

The earliest and most prevalent biodegradable orthopaedic fixation devices that have been commercialised are made from poly(lactic acid) (PLA), poly(glycolic acid) (PGA), and their copolymers poly(D,L-lactic-co-glycolic acid) (D,L-PLGA) (11). These linear aliphatic polyesters are available in different compositions and molecular weights that allow their degradation rates and mechanical properties to be controlled (76). They are, however, not normally injectable. In addition, the poly(α-hydroxy esters) are largely degraded by bulk erosion. This means that water gets into the polymer faster than the rate at which the polymer turns into a soluble material. This can result in a sudden and dramatic decrease in the mechanical properties of the polymer, and in the pH of the surrounding tissue resulting in adverse reactions during the repair process (1). Although the materials have been approved as biocompatible (1;69), inflammatory reactions have been reported upon degradation of L-PLA and PGA (1). Long-term *in vivo* studies have also shown that the by-products of PLGA degradation often lead to local tissue irritation and necrosis (77).

In terms of their drug-releasing properties, there are other problems. For example, PLGA microparticles have been formulated to release transforming growth factor β1 (TGF-β1), bone morphogenetic protein 2 (BMP-2), and osteogenic peptides (59;78). These loaded polymeric microparticles were prepared by a double-emulsion, solvent extraction technique [(water-in-oil)-in water]. The process basically involved mixing of an aqueous drug solution into an organic solvent containing the polymer and then mixing this emulsion with an aqueous solution to form a water-in-oil-in-water emulsion. The microparticles were formed by evaporating off the solvents resulting in the polymer

coating the bioactive molecules in the centre. The production of a drug delivery system using this method is not easy, and only provides a limited range of particle size which depends on factors such as the presence of surfactants in the emulsion, and hence could provide only limited control of drug release rates. Besides the use of organic solvents can cause denaturation when protein drugs are to be encapsulated (79).

Furthermore, the drug release profile of PLGA copolymer is often such that a burst phase is followed by a slow or negligible release of the drug before a final drug dumping period due to bulk erosion of the polymer, causing possible exceedingly high rate of drug release (80). The drastic pH reduction inside the PLGA matrix, which can be as low as pH 2 *in vivo*, can additionally compromise the stability of encapsulated drugs such as peptides or proteins (47).

1.6.3.1 poly(lactic acid) (PLA)

The basic monomeric unit of poly(lactide) or poly(lactic acid) (PLA) is lactic acid. PLA can be synthesised by ring-opening polymerisation of the cyclic dimer lactide in a moisture-free atmosphere under heat (105-185 °C) and use of catalyst (76) (Figure 1.4).
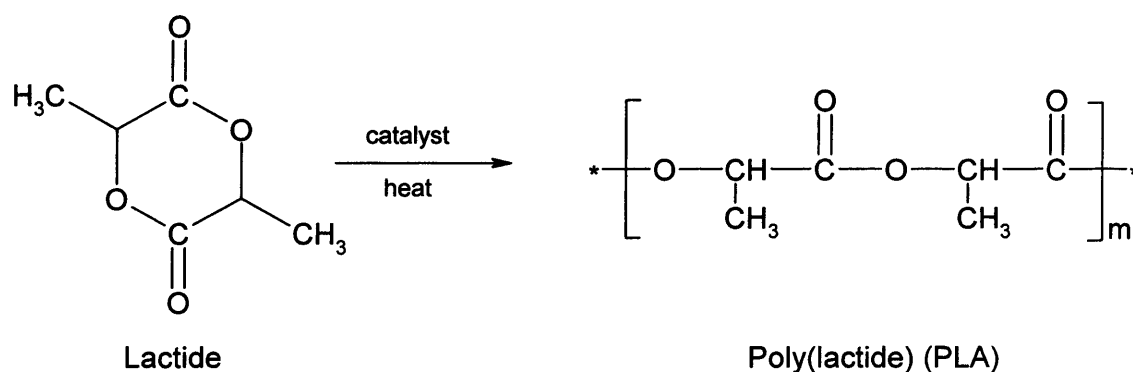
Figure 1.4. Synthesis of poly(lactide) or poly(lactic acid) (PLA)

Lactic acid, and its cyclic dimer, lactide, is a chiral molecule, existing in two optical isomers, D (+) and L (-) (53). The L isomer is the naturally occurring biological metabolite, while D,L-lactide is synthesised from D-lactide and L-lactide. Three stereo forms of PLA can therefore exist: poly-L-lactic acid (L-PLA), poly-D-lactic acid (D-PLA), and poly-D,L-lactic acid (D,L-PLA). L-PLA is semi-crystalline (~37 % crystalline) and like PGA, it has a high modulus that makes it useful for load-bearing applications. It has a T_m of 175-178 °C and a T_g of 60-65 °C (11). Degradation of L-PLA can take more than 2 years to be completely resorbed depending on the size and type of implant (40;81). One study has found that total resorption of L-PLA bone plate and screws had not taken place after 5.7 years of implantation in patients with zygomatic bone fractures (40). D,L-PLA, on the other hand, is amorphous as both isomeric forms of lactic acid are randomly distributed and consequently the polymer is unable to arrange into an organised structure (11). Although D,L-PLA has a lower modulus, it has a faster degradation time (12-16 months) (81). The Tg of D,L-PLA is 50- 60 °C (9;81).

PLA degrades into water-soluble monomers of lactic acid via hydrolysis of the ester linkage, and also undergoes enzymatic hydrolysis when its molecular weight becomes lower than ~10,000 g/mol (55). The lactic acid eventually becomes incorporated in the tricarboxylic acid cycle (Krebs cycle) and is excreted by the lungs as carbon dioxide and water (9). Degradation rate is progressively arrested with an increase in molecular size (35).

Homopolymers of L-PLA are mainly used clinically because the L isomer of lactic acid is preferentially metabolised in the body (1). PLA polymers are widely used in the medical arena as degradable suture and screws under different brand names (11).

Bioabsorbable fixation plates and screws manufactured from D,L-PLA have also been used clinically (71)

Efforts have been made to modulate the degradation kinetics of poly(α-hydroxy esters). D,L-PLA has been endcapped with acrylates in an attempt to produce a crosslinkable formulation or reacted with different co-initiators in order to produce oligomers of controllable molecular weights (82;83). As bulk erosion in polyesters occurs due to the relative hydrophilicity of the polymer backbone, it was postulated that the amount of water uptake could be influenced by incorporating hydrophobic units into the polymer backbone. A very recent study by Xu *et al* (84) developed a poly(α-hydroxy ester) that appears to exhibit surface erosion behaviour. Alkanediols of increasing hydrocarbon chain length were first terminated with oligo(L-lactoyl) moieties (10-40 units at each end). These lactic acid-alkanediol-lactic acid oligomers were then polymerised with each other by reacting with hydrophobic diacid dichlorides. The resultant polyesters exhibited different thermal behaviour from pure L-PLA. After an initial degradation period of 14 days similar to the pure L-PLA, these polyesters exhibited almost steady and linear mass loss profiles consistent with surface erosion behaviour over 6 weeks. Release studies of a water-soluble dye as a model drug from these polyester microspheres also showed linear release profiles. The polyesters were, however, all viscous solids or solid materials and were therefore not injectable. High temperature for the formation of lactoyl-terminated alkanediols (200 °C) was also necessary for good product yields.

1.6.3.2   poly(glycolic acid) (PGA)

The synthetic monomeric unit of poly(glycolide) or poly(glycolic acid) (PGA) is glycolic acid. PGA is synthesised from the ring-opening polymerisation of the cyclic

dimer glycolide in a moisture-free process under heat and use of catalyst (Figure 1.5). A typical polymerisation using stannous octoate as a catalyst takes place at ~175 °C for 2 to 6 hours (1). PGA is semi-crystalline (45-55 %) with a high T_m (220-225 °C) and a T_g just below or around body temperature of 35-40 °C (53). Unlike PLA and other polyesters, PGA is not soluble in most common organic solvents due to its high degree of crystallinity, except in highly fluorinated organic solvents (1). Sutures of PGA lose about 50 % of their strength after two weeks and 100 % at four weeks (11). The degradation time for full resorption of PGA could be between 6 and 12 months (81).
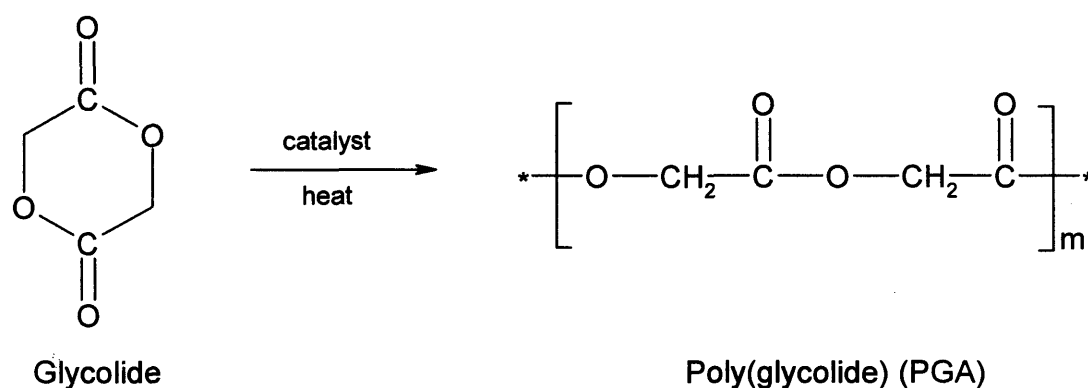
Figure 1.5. Synthesis of poly(glycolide) or poly(glycolic acid) (PGA)

Apart from hydrolytic degradation, PGA is additionally broken down by non-specific esterases and carboxy peptidases *in vivo* to produce water-soluble glycolic acid. This can then be excreted in the urine or undergo further enzymatic conversion and reaction before eventually entering the tricarboxylic acid cycle (Krebs cycle) (9).

PGA has been used as biodegradable sutures and is commercialised under the name Dexon® (9).

1.6.3.3 Poly(lactic acid-co-glycolic acid) (PLGA)

In order to combine and extend the range of properties conferred by their homopolymers, co-polymers of glycolide with both L-lactide and D,L-lactide are commonly synthesised (Figure 1.6).
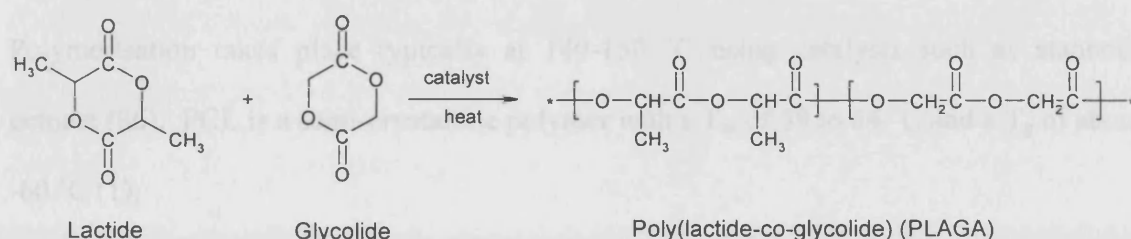
Figure 1.6. Synthesis of poly(lactide-co-glycolide) or poly(lactic acid-co-glycolic acid) (PLGA).

Co-polymerisation reduces the crystallinity of the overall polymer structure and hence most co-polymers are completely amorphous with faster degradation time (53). The degradation times of PLGA to full resorption differ depending on the molar ratio of lactic acid to glycolic acid and can be unpredictable as a result of the variability in the sequencing of the monomer units (9). The degradation time for an amorphous 50:50 D,L-PLGA could be 1 to 2 months (81), or for an amorphous 85:15 D,L-PLGA this could be 5 to 6 months (11). It was known that decreasing the molecular weight of PLGA increases its rate of degradation.

The long degradation time of the homopolymers (L-PLA and PGA) makes them unsuitable for short-term applications, whereas the co-polymer PLGA is the material of choice for relatively short-term drug delivery (85). PLGA has been commercially used for

peptide delivery (e.g. Zoladex™) and for anticancer treatment (Decapeptyl™)(47). It is also used as biodegradable sutures (Vicryl® and Polyglactin®) (9)

1.6.4 Poly-ε-caprolactone (PCL)

Poly(ε-caprolactone) (PCL) is an aliphatic polyester which is synthesised by the ring-opening polymerisation of the cyclic monomer ε-caprolactone (Figure 1.7). Polymerisation takes place typically at 140-150 °C using catalysts such as stannous octoate (86). PCL is a semi-crystalline polymer with a T_m of 59 to 64 °C and a T_g of about -60 °C (1).
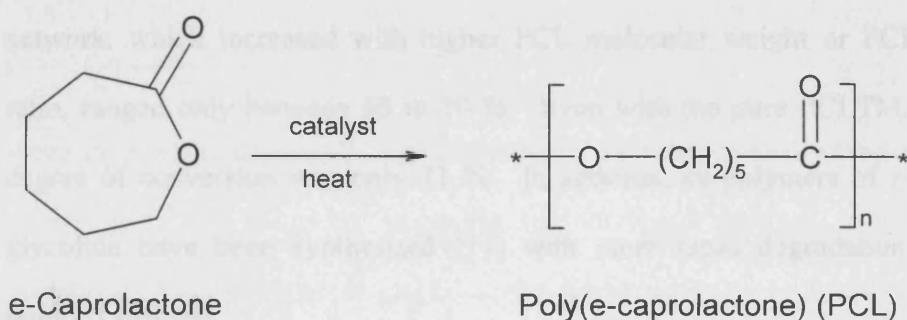
Figure 1.7. Synthesis of poly(ε-caprolactone) (PCL).

PCL is non-toxic and biocompatible. *In vivo* degradation of PCL into caproic acid begins with random hydrolytic chain scission of the ester linkages, manifested by a reduction in the viscosity and molecular weight of the polymer until the number-average molecular weight (Mn) has decreased to approximately 5000 g/mol. The second phase of polymer degradation is then characterised by a decrease in the rate of chain scission and the onset of weight loss, implant fragmentation and intracellular degradation (71). PCL

degrades at a slow rate, and a homopolymer can take up to two to three years to break down fully (1).

Although PCL is strong, the slow degradation rate has limited its applications. In view of this, one study has combined PCL with PPF that has lower strength as a drawback but higher degradation rate (17). In this study, di(propylene fumarate)-dimethacrylate (DPFDMA) was mixed with very low molecular weight trimethacrylated PCL (PCLTMA) and the injectable mixture was photo-polymerised using 10 minutes of blue light exposure. The polymerisation shrinkage ranged from 5.1 to 6.4 % and was much lower than that of PMMA (10.2 %). Nevertheless, the degree of double bond conversion of the polymer network, which increased with higher PCL molecular weight or PCLTMA: DPFDMA ratio, ranged only between 60 to 70 %. Even with the pure PCLTMA formulation, the degree of conversion was only 72 %. In addition, co-polymers of ε-caprolactone with glycolide have been synthesised (11) with more rapid degradation rates albeit with reduced stiffness.

Because of its slow degradation rate, PCL has only been used for long term applications, for example, it has been developed as a one-year contraceptive delivery device (Capronor™) (87). The caprolactone-glycolide co-polymer has been used as a suture under the trade name 'MONOCRYL ®' (1), and has also been studied as nerve guidance channels to bridge the gap created in the peripheral nerve after injury (88).

1.6.5 Natural polymers

Collagen, a naturally derived polymer, is commercially used as a skin substitute and as nerve guidance channels but has also been developed as a scaffold for bone tissue engineering (44;89). Collagens have been widely utilised as carrier materials to constitute

the delivery systems for BMP (42). Nevertheless, it has the problems of poor handling

properties and of having no inherent mechanical properties (90). Also the potential risks

of implanting collagen from animal sources, such as unexpected immune reactions and

disease transfer e.g. spongiform encephalopathies, are of major concern. Furthermore,

unlike synthetic polymers, their chemical constituents cannot be varied to give tailor-made

properties for particular end applications.

1.6.6 Ceramics

Inorganic degradable bone materials are also available on the market; these are

based on hydroxyapatite (HA, $Ca_{10}(PO_4)_6(OH)_2$) and β-tricalcium phosphate (β-TCP,

$Ca_3(PO_4)_2$) and / or various other calcium phosphates (CaP) (13;91). These are easily

made injectable as a ceramic paste, or as particles that can be incorporated into a cellulose

carrier gel (13). The major advantage of CaP based materials is that, being similar in

elemental composition to the inorganic component of bone (i.e. hydroxy carbonate apatite),

they can chemically interact and bond with bone, as well as being more biocompatible and

osteoconductive than polymeric materials (42;92-94). Degradation of β-TCP occurs by

osteoclastic activity (91). The degradation products of calcium (Ca^{2+}) and phosphate

(HPO_4^{2-} and PO_4^{3-}) ions are resorbed as part of the normal ion pool in the body. HA, on

the other hand, degrades extremely slowly (over decades). Composites of β-TCP and HA

have been synthesised to increase the degradation rate of the latter (91).

The newer calcium phosphate cements (CPC) are made of an aqueous solution and

one or several CaP(s). When mixed the CaP(s) dissolves and precipitates into a less

soluble CaP. During this precipitation, the CaP crystals grow and become entangled,

conferring a mechanical rigidity to the cement (91). Significant limiting factors for these

CPC materials, however, include their brittleness and difficulties in maintaining mechanical properties whilst controlling setting and degradation rates (95;96). With the latter a balance has to be made between fast setting to ensure stability in the body but slow initial set to provide the clinician with a working time in which to mix the formulation. These limiting factors make CPC unsuitable as load-bearing implants and limit their use in orthopaedics.

HA has been used as a filler for bone defects (e.g. Endobon $^{®}$) and as an implant in load-free anatomic sites (e.g. nasal septal bone and middle ear). It has also been used as a coating on metallic orthopaedic and dental implants to promote their fixation in bone. In the latter the metal carries the load while the surrounding bone bonds to HA (97). β-TCP has been extensively used as a bone substitute either as granules or blocks (e.g. chronOS$^{®}$).

1.7   Products under development

Only a limited number of resorbable injectable polymers that may be used as bone replacement materials have to date been investigated. Examples include poly(ether-esters) (98-100), poly(anhydrides) (41;101-103), and poly(propylene fumarate) (65;73;104;105). In several studies the end groups of these fluid polymers were converted into reactive acrylate or methacrylate crosslinking moieties in order to provide a means to convert them into solids after injection. These injectable adhesive materials offer a simpler bone fixture procedure than solid polymeric or metal screws (13) and can bond to bone via micromechanical attachment. The polymer degradation products are naturally removable but unfortunately the polymers produced to date are all of limited strength and low modulus (1;13;100;106).

1.7.1 Poly(ether-esters)

Many methods have been used to produce polymers with both ether and ester linkages in their main chains (55). These poly(ether-esters) are chiefly prepared by (i) ring-opening polymerisation of cyclic ester-ethers such as 1,4-dioxane-2-one. The resultant poly(dioxanone) is composed of alternating ether and ester in the structure (Figure 1.8 a). Poly(ether-esters) are also commonly prepared by (ii) ring-opening polymerisation of cyclic ester such as lactide, glycolide or ε-caprolactone initiated by polyether, or by polycondensation of telechelic polyester with telechelic polyether. These give block copolymers of polyether and polyester (Figure 1.8 b).

Although polyesters are not generally injectable, through using biocompatible polyethers as initiators for ring opening polymerisation of cyclic ester, fluid and relatively short chain poly(ether- co- ester)s can be produced (100). On the other hand, insertion of ester linkages allow the system to be biodegradable, whereas pure poly(ethers) are normally not. For example, the commercially used Poloxamer hydrogels [poly(ethylene glycol-b-propylene glycol-b-ethylene glycol)] are not biodegradable and dissolve *in vivo* within a few days (79;98). Of all ethers, poly(ethylene glycol) (PEG) has been used most commonly to co-polymerise with esters in an effort to increase polyester biocompatibility (68) and to modulate the mechanical and degradation properties in relation to the pure polyester and polyether alone (88).

(a)   (b)   +

p-Dioxanone   Lactide   PEG

synthesis   synthesis

Poly(dioxanone)   Poly(lactic acid-PEG-lactic acid)
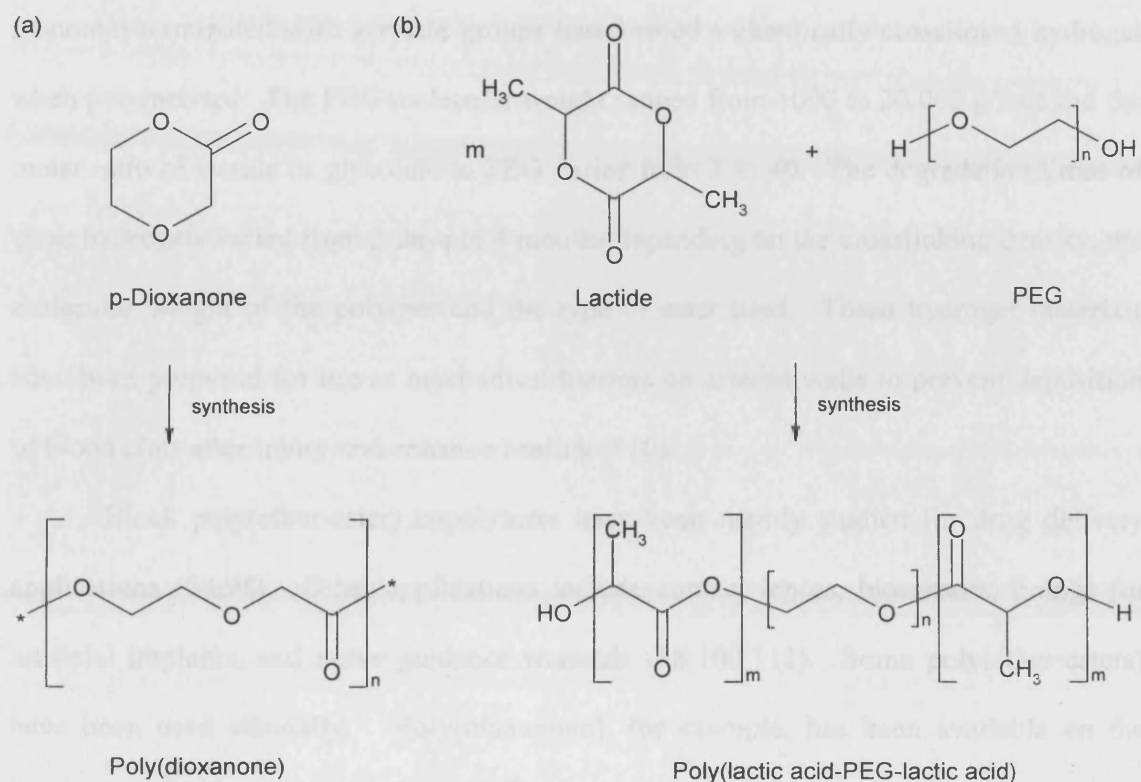
Figure 1.8. Synthesis of example poly(ether esters): (a) poly(dioxanone); (b) poly(lactic acid-PEG-lactic acid). PEG stands for poly(ethylene glycol).

The poly(ethers) (A) and poly(esters) (B) in these polymers usually form a triblock structure either of ABA (58;107) or BAB type (98). As the ether used is normally PEG, these materials are highly hydrophilic (i.e. hydrogels) that absorb large amounts of water and swell to produce materials whose physical characteristics resemble those of soft tissue with good permeability. These temperature-sensitive hydrogels are soluble in water at or below room temperature but become physically crosslinked by sol-gel phase transition *in vivo* and degrade over a period of 4-6 weeks (98).

In several studies, endcapping of the poly(ether-esters) with acrylates allowed them to form crosslinkable systems with increased mechanical strength and reduced swelling (88;99;108;109). Sawhney *et al* (99) yielded a water–soluble ester-PEG-ester

monomer terminated with acrylate groups that formed a chemically crosslinked hydrogel when polymerised. The PEG molecular weight ranged from 1000 to 20,000 g/mol and the molar ratio of lactide or glycolide to PEG varied from 2 to 40. The degradation times of these hydrogels varied from 2 days to 4 months depending on the crosslinking density, the molecular weight of the polymer and the type of ester used. These hydrogel materials have been proposed for use as mechanical barriers on arterial walls to prevent deposition of blood clots after injury and enhance healing (110).

Block poly(ether-ester) copolymers have been mainly studied for drug delivery applications (58;98). Other applications include contact lenses, biosensors, linings for artificial implants, and nerve guidance channels (88;100;111). Some poly(ether-esters) have been used clinically. Poly(dioxanone), for example, has been available on the market as a biodegradable suture (PDS®) and pin (Johnson & Johnson Orthopedics) (11). A PLGA-PEG-PLGA hydrogel, with PEG of a molecular weight of 1000 g/mol and a D,L-lactide/glycolide molar ratio of 3, has been traded under the name ReGel® and has been formulated to release protein drugs over a period of 1 to 6 weeks (48).

1.7.2 Polyanhydrides

Poly(anhydrides) are synthesised by the dehydration of a dicarboxylic acid or a variety of aromatic and aliphatic dicarboxylic acids via melt condensation (18;112). The dicarboxylic acid monomers are first converted to form acetyl terminated anhydride prepolymers of low molecular weight using reflux in excess acetic anhydride. These prepolymers are then polymerised at elevated temperature (e.g. 150-200 °C) under vacuum with a nitrogen sweep to yield high molecular weight polymers. Figure 1.9 shows the

general structure of anhydride, polyanhydride and some of the most extensively investigated polyanhydrides.

Polyanhydrides contain one of the most reactive functional groups available for degradation on the basis of passive hydrolysis, providing fast degradation and accelerated drug release which can be useful for short term drug delivery applications (51). Because of their water insoluble, hydrophobic nature, they degrade by surface erosion and hydrolyse via their labile anhydride bonds to dicarboxylic acid monomers in aqueous medium (51). This type of degradation mechanism can be advantageous as both material loss and drug release can be linear with time without the sudden dose dumping effect as observed with the bulk-eroding PLGA devices.
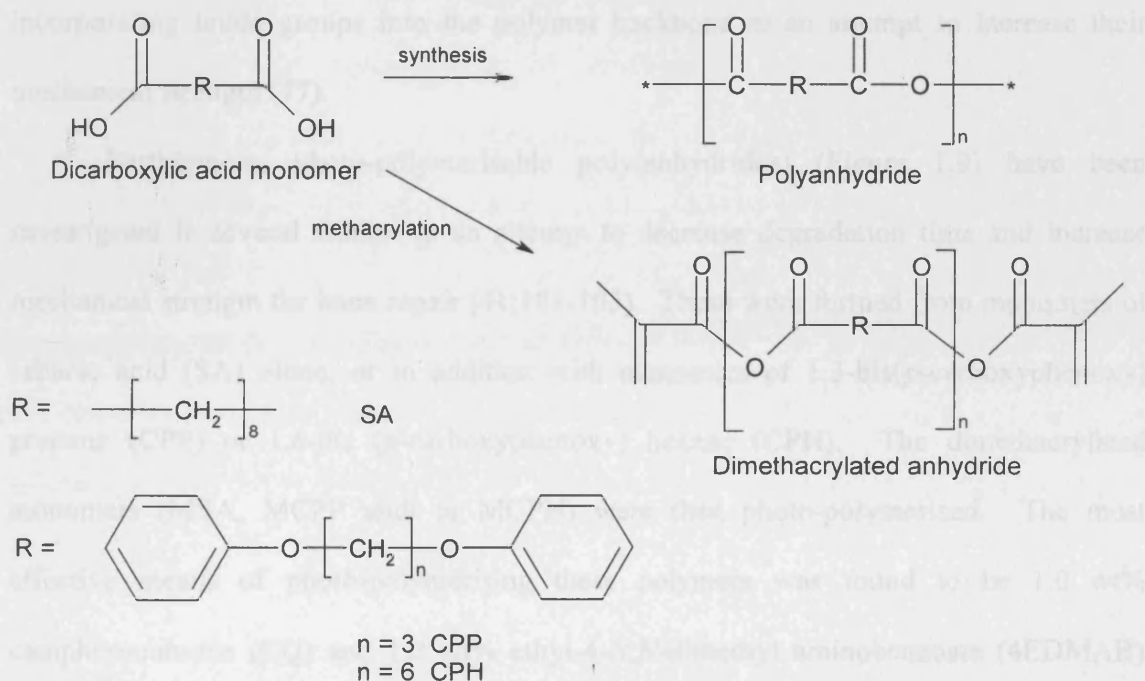
Figure 1.9. **General structure of dicarboxylic acid, polyanhydride, and dimethacrylated polyanhydride. SA is the anhydride monomer of sebacic acid, CPP is 1,3-bis(*p*-carboxyphenoxy) propane and CPH is 1,6-bis (*p*-carboxyphenoxy) hexane.**

The degradation times of polyanhydrides vary from days to years depending on the degree of hydrophobicity of the monomer units. Degraded aliphatic monomers such as sebacic acid are likely to participate in the β-oxidation pathway, yielding acetyl-co-A which can be used in other biosynthetic pathways. Degraded aromatic monomers are eliminated without further metabolic transformation (112). The *in vitro* and *in vivo* biocompatibility of these polymers, as manifested by minimal inflammatory responses with no fibrous capsule formation and no toxicity, has been demonstrated (1;110). The reactivity of the anhydride groups, however, can give polymers that are difficult to purify and with potentially poor shelf – life (113).

Polyanhydrides have limited mechanical properties that restrict their use in load-bearing applications (1)(see Table 1.1). Linear polyanhydrides have been modified by incorporating imide groups into the polymer backbone in an attempt to increase their mechanical strength (77).

Furthermore, photo-polymerisable poly(anhydrides) (Figure 1.9) have been investigated in several studies in an attempt to decrease degradation time and increase mechanical strength for bone repair (41;101-103). These were formed from monomers of sebacic acid (SA) alone, or in addition with monomers of 1,3-bis(p-carboxyphenoxy) propane (CPP) or 1,6-bis (p-carboxyphenoxy) hexane (CPH). The dimethacrylated monomers (MSA, MCPP and/ or MCPH) were then photo-polymerised. The most effective means of photo-polymerising these polymers was found to be 1.0 wt% camphoroquinone (CQ) and 1.0 wt% ethyl-4-N,N-dimethyl aminobenzoate (4EDMAB) with 150 mW/ cm^2 of blue light (103). The degradation rates of these polymers could be controlled, spanning ~2 days to ~1 year, through changing the MSA/ MCPH ratio in the structure (41;103). Through crosslinking, the degradation rate of poly(MSA) was found to

76

decrease by more than two-fold compared to poly(SA), whilst the modulus of poly(MSA) increased by an order of magnitude compared to that of poly(SA) (41)(Table 1.1). To further modulate the degradation rates and volume shrinkage, these crosslinkable polyanhydrides have also been polymerised with other linear polymers (e.g. poly(CPP-CPH) within them in order to form a semi-interpenetrating network.

Currently the main use of polyanhydrides is in the area of controlled drug delivery (112). Some types of polyanhydrides have been approved for clinical use. These include Gliadel^{TM} implant [P(CPP-SA)] for the treatment of brain tumours and Septacin^{TM} implant [poly(erucic acid dimer-sebacic acid), P(EAD-SA)] for the treatment of chronic bone infections (112) .

1.7.3 Poly(propylene fumarate) (PPF)

Poly(propylene fumarate) is an unsaturated linear polyester formed by copolymerisation of fumaric acid and propylene glycol (24) (Figure 1.10a).

Many methods have been proposed for the synthesis of PPF but they generally use temperatures ranging from 145- 160 °C and reduced pressure with or without a catalyst. Examples include (i) transesterification of diethyl fumarate and propylene glycol (59;73); (ii) transesterification of oligomer synthesised from fumaryl chloride and propylene glycol (66;68;114); (iii) direct esterification of fumaric acid and propylene glycol catalysed by an acid (23;115).
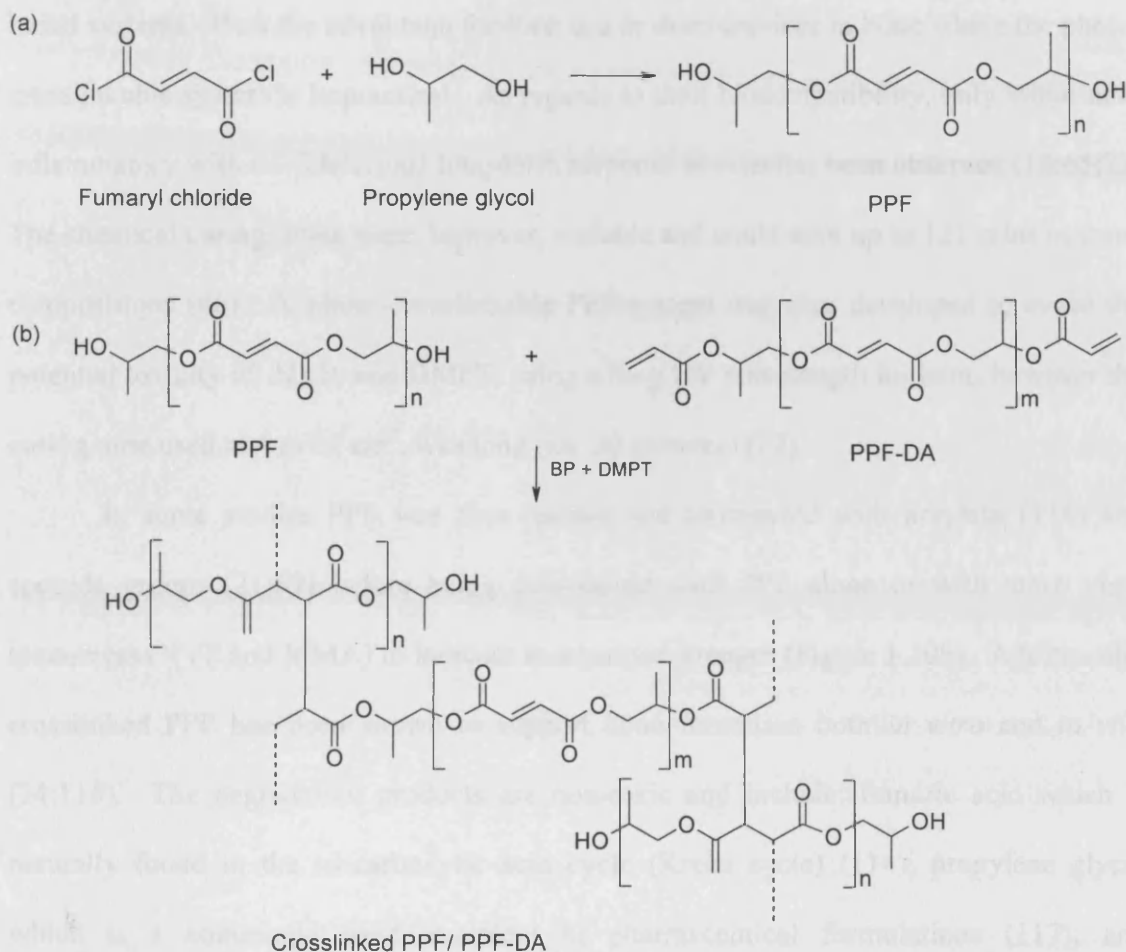
Figure 1.10. (a) Formation of poly(propylene fumarate) (PPF) from fumaryl chloride and propylene glycol. (b) Crosslinking of PPF and diacrylated PPF (PPF-DA) using chemical initiators benzoyl peroxide (BP) and dimethyl-ρ-toluidine (DMPT), adapted from (114).

The repeating units in the PPF structure contain one unsaturated double bond which allows for covalent crosslinking and two ester groups that enable hydrolytic degradation into fumaric acid and propylene glycol (114). It is injectable, and can be crosslinked *in situ* with either (meth)acrylate or *N*-vinylpyrrolidone (NVP) using benzoyl peroxide (BP) as an initiator and *N,N*-dimethyl-ρ-toluidine (DMPT) as an accelerator (66;73;104). This chemical-initiated polymerisation employed by most injectable PPF-

based systems offers the advantage for their use in deep crevices in bone where the photo-crosslinkable system is impractical. As regards to their biocompatibility, only initial mild inflammatory with no deleterious long-term response *in vivo* has been observed (13;65;73). The chemical curing times were, however, variable and could take up to 121 mins in some compositions (66). A photo-crosslinkable PPF-system was also developed to avoid the potential toxicity of NVP and DMPT, using a long UV wavelength initiator, however the curing time used at 4 mW/ cm^2, was long (i.e. 30 minutes) (22).

In some studies PPF was first reacted and terminated with acrylate (114) and epoxide groups (21;69) before being crosslinked with PPF alone or with more vinyl monomers (NVP and MMA) to increase mechanical strength (Figure 1.10b). Additionally crosslinked PPF has been shown to support bone formation both *in vitro* and *in vivo* (24;116). The degradation products are non-toxic and include: fumaric acid which is naturally found in the tri-carboxylic acid cycle (Krebs cycle) (114); propylene glycol which is a commonly used excipient in pharmaceutical formulations (117); and poly(acrylic acid-co-fumaric acid) which is excretable from the body (114). If NVP is used as a crosslinking agent, however, the poly(vinyl pyrrolidone) (PVP) crosslinks in the crosslinked PPF networks are not-degradable (114).

PPF is a relatively hydrophobic material and water absorption into the polymer is slow (24). PPF undergoes bulk degradation and degradation time is dependent on polymer structures as well as other components but is on the order of several months (1). For example, after 12 weeks of degradation in phosphate buffered saline a PPF/ β-TCP composite lost about 58 % of its original weight, compared to 75 % weight loss for an unfilled PPF polymer(118).

The mechanical properties of PPF vary greatly depending on the synthetic method and the crosslinking agents used. One study (68) used PEG-dimethacrylate as a crosslinking agent to form PPF polymer networks with good compressive modulus close to that of human trabecular bone, however, the modulus decreased quickly in the wet state due to the hydrophilic PEG. Mechanical properties have been improved by incorporating ceramic particles such as β-TCP (66;68). For example the compressive moduli for composites containing PPF/ NVP incorporated with 33 % β-TCP were found to range between 23 and 265 MPa depending on the NVP and BP levels (66). A decrease in NVP or an increase in BP created a more densely crosslinked network and enhanced the mechanical properties of PPF-based material. Because of the good initial mechanical properties shown in PPF formulations, they have mainly been studied as biodegradable bone cements, although they have also been developed to deliver bioactive molecules to bone (20) and to create degradable scaffolds for bone tissue engineering (24).

An example of the latter two functions was demonstrated in a study by Hedberg *et al* (59). They incorporated an osteogenic peptide into PLGA/PEG microparticles, which were then added to a mixture of PPF, PPF-DA (as crosslinking agent) and sodium chloride (as leachable porogen) with the composite being subsequently polymerised using BP and DMPT. The release of the peptide from the resultant scaffold was between 53 to 86 % over 4 weeks, and was shown to be controllable through varying (i) the loading of the peptide within the PLGA/PEG microparticles, (ii) the percentage of PEG within the microparticles, (iii) the loading of the microparticles within the polymer matrix, and (iv) the initial loading of sodium chloride. In a more recent study conducted by Hedberg *et al* (24), they compared the *in vitro* degradation of PLGA/ PEG microparticle-loaded PPF scaffolds to the unloaded PPF scaffolds, and found that none of the variables investigated

i.e. (ii) to (iv) had any effects on degradation over 26 weeks. It was therefore concluded that microparticle carriers can be incorporated into PPF for local delivery of bioactive agent without altering the expected degradation rate of the normal, unloaded polymer.

1.7.4 Other biodegradable polymers

1.7.4.1 Poly(orthoesters)

The basic structure of poly(ortho esters) is shown in Figure 1.11 (a). They are highly hydrophobic materials, and because the amount of water available to react with the hydrolytically labile ortho ester linkage is limited, they are very stable under physiological conditions (119). As they degrade by surface erosion, these materials have been considered to be potentials for drug delivery applications (120). They have, however, seen limited use because of their lack of variability in degradation kinetics (84). In view of this, lactide segments have been incorporated as part of the polymer structure. These lactide segments, when degraded to produce carboxylic acids, act as catalysts to control hydrolysis of the acid-labile ortho ester linkages in the polymer backbone (1;119).
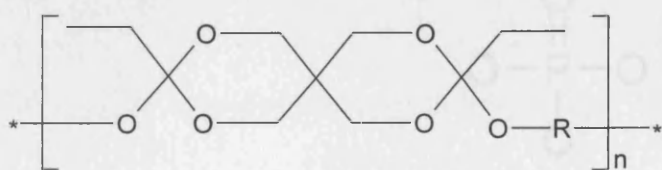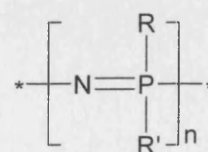
(a) Poly(ortho ester)   (b) Poly(phosphazene)

Figure 1.11. General structure of (a) poly(ortho esters) and (b) poly(phosphazenes).

1.7.4.2 Polyphosphazenes

The general structure of this class of polymers is shown in Figure 1.11 (b). These polymers contain alternating nitrogen and phosphorous with no carbon atoms in their backbone structure. The biodegradability of these polymers lies in the addition of side groups (R and R') after the backbone synthesis, such as amino acid esters, lactate, or imidazolyl units. Hydrolysis of the polymer then leads to free side group units, phosphate and ammonia.

1.7.5 Phosphate glasses

Phosphate-based glasses represent another important class of biomaterials being developed for bone and soft tissue engineering applications. The basic building blocks of phosphate-based glasses are the orthophosphate (PO_4^{3-}) tetrahedra (Figure 1.12); these are joined together through P-O-P linkages, forming linear and/or cyclic structures in a three-dimensional or chain like structural network. Metal oxides such as calcium oxide (CaO) and sodium oxide (Na_2O) are commonly incorporated into the glass structure as network modifiers.

$$O-\overset{\overset{\displaystyle O}{\|}}{\underset{\underset{\displaystyle O}{|}}{P}}-O$$
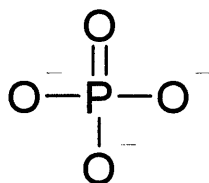
Figure 1.12. An orthophosphate tetrahedral (PO_4^{3-}).

These glasses are soluble and their degradation rates can be tailor-made to suit the end application via alteration of the glass composition (121-124). For example, Ahmed *et*

82

al (121) studied a ternary glass system consisting of $CaO-Na_2O-P_2O_5$ in bulk form and indicated that their dissolution rate was approximately inversely proportional to the CaO content within the glass. In addition these glasses were able to be processed into fibres allowing their potential use as fibre reinforcement materials in biodegradable fracture fixation devices (125). As their constituent atoms are found in the inorganic mineral phase of bone, these glasses are biocompatible i.e. they are not cytotoxic (126) and cause only minimal *in vivo* inflammatory response (127). Nevertheless, use of these glasses has sometimes been restricted by their high dissolution rates (from a couple of hours) as well as their brittle nature. One study (128) incorporated iron oxide (Fe_2O_3) to produce a quaternary glass system. The dissolution rates were decreased through increasing the CaO and Fe_2O_3 mol% content and / or increasing the diameter size of the glass fibres. The degradation rates were reduced by a couple of orders of magnitude. Cell attachment and proliferation were also achieved. These glass fibres were therefore proposed as cell delivery vehicles. Soluble phosphate glasses can be used not only for guided tissue regeneration, but can also be used for localised release of specific ions, for example, platinum for cancer treatment or silver for treating bacterially infected tissue (124;129).

1.8   The new polymer in this study

The above problems experienced in commercialised products or products currently under development demonstrate the need for new materials for drug delivery and bone tissue engineering applications. One approach to overcome problems is the incorporation of two or more of the above products to produce a hybrid/ composite material. Another commonly used approach is to synthesise new injectable and biodegradable polymers with

tailor-made chemical structures that target the desired material properties for the end applications (130;131). Structures of the new polymers are often based on the polymers already synthesised or investigated. Through systemically changing the chemical constituents within the polymer structure, incremental differences in their physical and chemical properties can be made, producing a library of a particular type of polymer with a wide selection of material properties.

The basic components of the oligomeric monomers to be synthesised and investigated in this research project included (i) a polyether: poly(propylene glycol) (PPG), (ii) an ester: D,L-lactide or glycolide and (iii) a crosslinkable end group: methacrylate.

Use of the polyether as a catalyst for ring opening lactide polymerisation enabled preparation of fluid oligomers with a wide range of molecular weights. In several previous studies fluid poly(ether co ester) oligomers, mostly for drug delivery systems, have been produced (58;79;99). These poly(ether co esters) were, however, normally highly hydrophilic because the ether used was polyethylene glycol (PEG). In this study the use of PPG was anticipated to produce more hydrophobic backbones to provide a means of reducing water sorption rates. This would affect mechanisms of degradation and drug release rates. It was speculated that through increasing hydrophobicity the polymers generated might degrade via a surface erosion mechanism. This could be advantageous for a combined bone tissue engineering / repair and controlled drug delivery system (132). Being biocompatible and non-toxic, PPG has been evaluated as potential lubricous coatings for various medical products (100). When of low molecular weight, these polyethers can be eliminated from the body by excretion (114).

Biodegradation was facilitated by the lactoyl or glycoyl moieties in the new polymer, which provided hydrolytically unstable linkages in the backbone. The *in vitro*

and *in vivo* degradation of oligomeric lactide or glycolide is well understood and the degradation products are natural metabolites that are readily eliminated by the body (1;15). D,L-lactide was used in this study because its amorphous nature enabled more rapid degradation than possible with L-lactide. In the latter, the degradation time of semi-crystalline homopolymer devices can be greater than two years making L-lactide less suitable for a combined bone tissue and drug delivery system (40).

The methacrylate (MA) end groups provided a ready mechanism for the monomers to polymerise and crosslink in the body using either light or chemical cure means. These end group methacrylate crosslinking functionalities have a long history in biomedical applications such as dental restorative materials and bone cements (133;134). Though they may polymerise more slowly, methacrylates can form highly cross-linked networks, producing a stronger, more hydrophobic polymer with higher T_g values than acrylates (135). Such end groups should also be more reactive to radicals and easier to polymerise than fumarate groups as in PPF which are more sterically hindered (114). Using difunctional methacrylates, improved mechanical properties and durability (41;136) as well as better water sorption characteristics (137) suitable for a bone replacement and drug delivery material may be obtained. Furthermore, many studies have found that methacrylates have a less cytotoxic effect than corresponding acrylates (138-140). Methacrylate rather than acrylate end groups were therefore attached to the new monomers in this study.
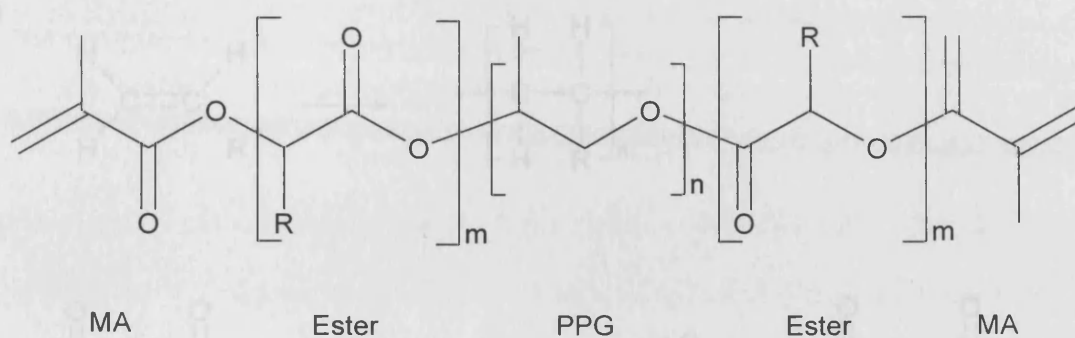
R = CH₃ Lactic acid
or   H   Glycolic acid

Figure 1.13. Structure of the new monomer in this project: poly(ester-co-PPG) dimethacrylate.

The synthesised product of these three components (Figure 1.13) was termed as 'an oligomeric monomer' or simply 'a monomer' in this project rather than 'an oligomer' because it formed the basic structural unit for the photo-polymerisation reaction in a later, separate process to form the final, crosslinked polymer.

1.9   Synthesis of polymers

1.9.1 Polymerisation process

Synthesis of polymers was first classified into two main groups by Carothers (8): addition polymerisation and condensation polymerisation. An addition polymer (a) contains the same atoms in its repeating unit as the monomer, whereas a condensation polymer (b) contains fewer atoms within the polymer repeat unit because of formation of by-products during the polymerisation process (Figure 1.14).

(a)

(b)
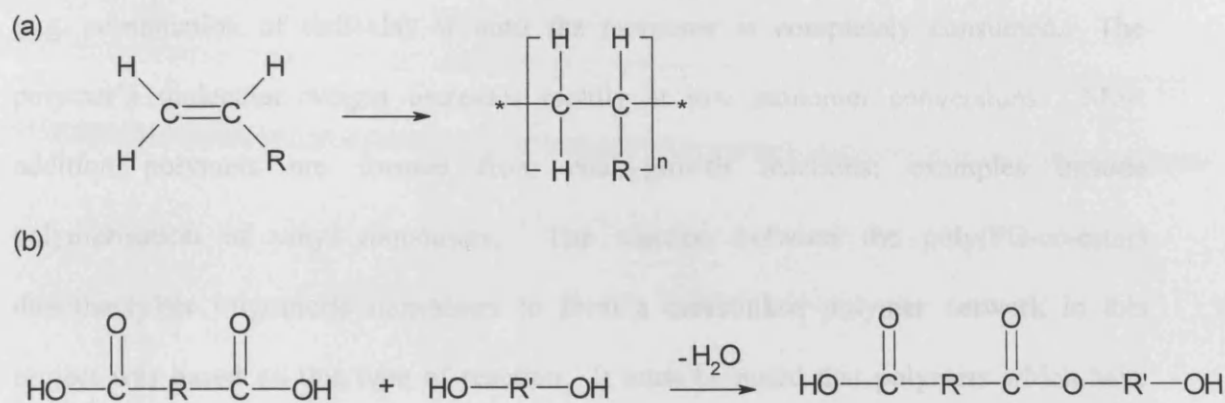
Figure 1.14. Synthesis of polymer through (a) an addition polymerisation or (b) a condensation polymerisation.

Polymerisation reactions are now commonly characterised according to the polymerisation mechanism (8;141;142). One reaction is step-growth polymerisation, in which the polymer chains are built up in a step-wise manner by the random fusion of monomer molecules to form dimers, trimers, and higher species as the reaction progresses. Any two molecular units having the necessary energy of activation and correct functionality and orientation can react. The polymer's molecular weight increases slowly with rapid monomer consumption and continues until the concentration of reactive end groups becomes too low for the reaction to proceed at a significant rate. Most condensation polymers are formed from step-growth reactions; examples include polyesters and polyamides. The reaction of PPG with ester linkages in this project was based on this type of reaction.

Another type of reaction is called chain-growth polymerisation, in which the polymer chain lengths are increased by the successive linking of monomer molecules to the end of a growing chain. This requires initiation, for example, a free radical, to begin chain growth, which propagates until some termination reaction renders the chain inactive

(e.g. combination of radicals) or until the monomer is completely consumed. The polymer's molecular weight increases rapidly at low monomer conversions. Most addition polymers are formed from chain-growth reactions; examples include polymerisation of vinyl monomers. The reaction between the poly(PG-co-ester) dimethacrylate oligomeric monomers to form a crosslinked polymer network in this project was based on this type of reaction. It must be noted that polymers which have identical repeating units but are formed by different polymerisation processes may differ in their physical and mechanical properties due to the variations in molecular weight, end groups, stereochemistry and possible chain branching. Mixed modes of step-growth and chain-growth polymerisation can also occur.

1.9.2 Synthetic criteria

When synthesising a polymer the following criteria need to be considered;

1. Monomer selection

2. Initiator selection

3. Synthetic conditions

4. Presence of additives

These factors will affect the physical and chemical properties of a polymer such as (9;11):

1. Hydrophilicity

2. Crystallinity

3. Melt and glass transition temperatures

4. Molecular weight

5. Molecular orientation/ tacticity

6. End groups

7. Sequence distribution (random vs. block)

8. Presence of residual monomer or additives

These properties of the polymer in turn affect the performance of the material including its biodegradation, mechanical properties, setting rate, biocompatibility etc.

1.9.2.1 Monomer selection

The structures of the polymers depend greatly on the monomers used for the synthesis and can affect the physical properties of the resultant product such as T_g and T_m. The T_g and T_m of a polymer can in turn affect its degradation and mechanical properties at a particular temperature (9). The use of different types of poly(α-hydroxy esters) for synthesis is one example. Both glycolide and L-lactide homopolymers are semi-crystalline, but copolymers of L-lactide and glycolide exhibit some crystallinity only when either monomer is present over 70 mol%. Below this percentage, the regularity of the polymer chain is disrupted by the other monomer. Co-polymers of D,L-lactide and glycolide are amorphous when D,L-lactide is the major component (11). The crystalline regions of a semi-crystalline polymer act as crosslinks giving the polymer higher mechanical properties as compared to an amorphous analog. The semi-crystalline L-PLA has a modulus about 25 % higher than the amorphous D,L-PLA. Therefore for load-bearing applications it would be preferable to choose a more semi-crystalline polymer than a totally amorphous one. Increasing molecular weight or branching of a polymer will also augment the degree of crystallisation in the structures (143) and cause an increase in the melting temperature (9). When a semi-crystalline polymer is heated beyond its T_m point it may be shaped into rods or molded parts.

Furthermore, use of monomers with large and polar groups would cause intra- and inter-molecular interactions in a polymer structure and subsequently decrease the flexibility of the chains and increase the T_g value (144). A polymer that has a T_g around body temperature may be much more ductile when implanted than it appears to be at room temperature.

On the other hand, polymers which are branched are normally more compact than those which are linear and therefore exhibit lower viscosity. High molecular weight polymers that are highly viscous will undergo slower degradation than those with lower molecular weight and lower viscosity (9), but will have higher mechanical properties. The effect of monomer choice on degradation will be discussed further in section 1.10.1.

1.9.2.2 Initiator selection

Initiators and catalysts are often added in polymer synthesis. For example, in the ring-opening polymerisation of lactides, stannous octoate [Sn (II) 2-ethylhexanoate, $Sn(Oct)_2$] has been frequently used as one of the most effective catalysts to produce polyesters (55;145-147). This catalyst is preferred because it is commercially available, is soluble in common organic solvents and cyclic ester monomers (148), and has been approved by the FDA (82). It also gives high reaction yields for the synthesis and low degrees of ester racemisation even at high temperatures (82;146;149). The cytotoxicity (150) and difficulty in removal of this catalyst after reaction (146), however, have limited its use in many cases. Efforts have been made to develop highly active catalysts that contain low toxicity metals. Iron compounds (55), for examples, can be found in the body and are considered to be less harmful than most other metal compounds. One study (150) has found that high reaction yields and similar molecular weights in the copolymerisation

of glycolide and L-lactide can be achieved using iron (III) acetylacetonate or iron (III) ethanolate instead of $Sn(Oct)_2$. Stolt *et al* also investigated the polymerisation of L-lactide using monocarboxylic iron derivatives such as iron acetate, and obtained high molecular weight L-PLA with high yield (55). High polymerisation temperatures (170-210 °C), however, were required with these iron catalysts and some ester racemisation of the product resulted. Lithium chloride, another biocompatible catalyst, has also been used for the ring opening polymerisation of lactide in the presence of hydroxyl-containing compounds such as ethylene glycol but racemisation still occurred (55).

In recent years much interest has been devoted to metal-free ring-opening polymerisation of cyclic monomers. Goraltchouk *et al* (88) used phosphoric acid (H_3PO_4) to catalyse the ring opening polymerisation of cyclic L-lactide by PEG diol in order to produce lactide-PEG-lactide oligomers. High yields (>95 %) and nearly complete reaction between lactide and PEG were achieved allowing the product to be used without the need for purification. Similarly Myers *et al* (151) used nucleophilic phosphines as organic transesterification catalysts in combination with an alcoholic initiator for the controlled ring-opening polymerization of lactide. PLA of narrowly dispersed and predictable molecular weights were produced.

1.9.2.3 Synthetic conditions

Synthetic conditions are also important. For example, in step-growth polymerisation, heat is often required to activate the catalyst or to melt the reactants in order to allow their necessary intimate contact for reaction to occur. In ring-opening polymerisation of polymers, a thermodynamic equilibrium normally exists between the polymerisation reaction and the reverse reaction that will result in monomer formation.

Exceedingly high synthetic temperature can drive the equilibrium to depolymerisation resulting in monomer formation and lowering the polymer molecular weight (150). Conversely when the reaction temperature is less than the melting point of the semi-crystalline PGA and L-PLA (~225 and ~175 °C respectively), crystallisation of the polymerising polymer occurs resulting in solid-state polymerisation and very high molecular weight polymers (76). Another study (152) has found that increasing the reaction temperature from 180 to 200 °C increased the racemisation reaction of L-lactic acid to D-lactic acid during the polymerisation of L-lactic acid molecules and consequently decreased the product crystallinity by ~40 mol%. The increase in the reaction temperatures also caused some thermal degradation reactions in the polymerisation mixtures forming PLA of lower average molecular weight.

The types of reactants involved and their concentrations should also be carefully considered. Korhonen *et al* (82) has found that the ratio of L-lactide to a co-initiator controls the molecular weight of the reacted products with higher molecular weights being obtained at lower concentrations of the co-initiator. Faster polymerisation of the lactide molecules was also achieved when a co-initiator was added in comparison with $Sn(Oct)_2$ alone. Moreover, the presence of moisture can reduce the efficiency of the synthetic process due to the hydrolytic sensitivity of the polymer bonds causing a reduction of the polymer molecular weight and altering the resulting polymer properties. Therefore pressure is often reduced in synthesis.

1.9.2.4 Presence of additives

Possible adverse local and systemic reactions could arise if unreacted additives such as residual catalysts and polymerisation initiators, unreacted monomers, residual

solvents or plasticizers are released into the blood stream as the polymer degrades. These agents could be cytotoxic in high concentration (9). One study has found that CQ and DMPT, which are commonly used to initiate photo-polymerisation, generated reactive oxygen species *in vitro* that could possibly cause cytotoxicity issues (153). These residual radical-generating initiators could also pose problems when the material is to be encapsulated with cells, proteins and DNA (154). For polyesters, the presence of water can act as a plasticizer and lower the T_g and subsequently the mechanical and degradation properties of the polymer (11). Similarly the presence of excess monomers may act as plasticizers and also catalyse the hydrolysis of the material resulting in alteration of their properties (11).

One solution for the avoidance of unreacted monomers, residual catalysts, initiators or solvents in the final polymer product has been the use of supercritical carbon dioxide ($SC\text{-}CO_2$) as a solvent for polymerisation (155). $SC\text{-}CO_2$ is non-toxic and solvent removal concerns after polymerisation are alleviated because it could easily be separated from the polymer by depressurisation back into a gas, leaving a dry polymer product. This polymer product could additionally be of high purity as $SC\text{-}CO_2$ may extract any unreacted species and impurities from the polymer solution. Being the liquid phase, $SC\text{-}CO_2$ also has the ability to plasticize the forming polymer phase. This is because swelling of the polymer phase, which occurs as CO_2 is absorbed, reduces the number of entanglements between polymer chains and decreases the viscosity of the solution. As a result the diffusion of the monomer into and through the polymer phase to the site of reaction is enhanced. Use of $SC\text{-}CO_2$ for the polymerisation of D,L-lactide and glycolide (155) as well as of ε-caprolactone (156) have been reported.

1.9.3 Photo-polymerisation and Crosslinking

Termination of monomers/ oligomers with a single reactive vinyl group enables upon light, chemical or thermal initiation, formation of long linear polymers with pendant chains (formed by the monomeric or oligomeric units) similar to a comb-like structure. If the monomers/ oligomers are terminated with vinyl groups at both ends, the linear polymer chain can become crosslinked to a second chain / chains through the second double bond on the other end forming a complex network of interlinking polymer blocks (Figure 1.15).
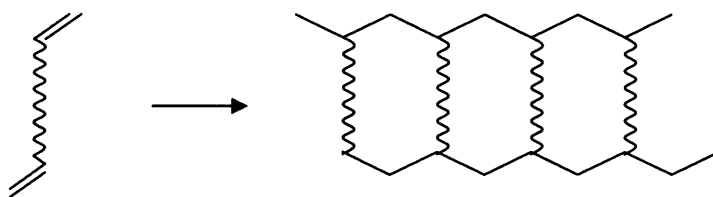
Figure 1.15. A monomer with one vinyl group at each end; when polymerised with other similar monomers, both double bonds react with the others to form a densely crosslinked polymer network.

The free radicals required to initiate polymerisation and crosslinking are normally produced using chemical compounds (chemical initiators) or light–sensitive compounds (photoinitiators) that interact with visible or ultraviolet (UV) light.

The use of light to cure polymers has been practised extensively in dentistry to form sealant and dental restorations *in situ* (111). The advantages of photo-initiated polymerisation are vast including spatial and temporal control over polymerisation and fast curing rates (over a time period of a few seconds to several minutes) at physiological temperatures (39;111). In addition, one study (157) has compared polymerisation of PPF/ PPF-DA using both chemical- and photo-initiator systems and found that the latter

increased the compressive modulus of the polymer network by three-fold due to a higher double bond conversion and crosslinking density.

A photoinitiator has high absorption at a specific wavelength of light and upon light exposure, produces radical initiating species either by (i) bond cleavage at C-C, C-Cl, C-O or C-S bonds; these photoinitiators are normally aromatic carbonyl compounds such as the UV initiator 2,2-dimethoxy-2-phenyl acetophenone (DMPA), or by (ii) undergoing hydrogen abstraction from an H-donor molecule (e.g. N,N-dimethyl-p-toluidine, DMPT) to generate radicals; these photoinitiators are aromatic ketones such as camphoroquinone (CQ) (Figure 1.16). The efficiency of the photoinitiators to initiate polymerisation depends on several factors such as oxygen inhibition, initiator concentration, light intensity, light penetration, and time of light exposure. For example, it has been found that increasing the initiator concentration caused an increase in both the polymerisation rates and maximum conversion of a photo-crosslinkable polyanhydride, but varying the light intensity only had minimal effect on these parameters (41;101).

(a)

(b)

(c)

R = CH₃   R' = H   or

R = H   R' = CH₃
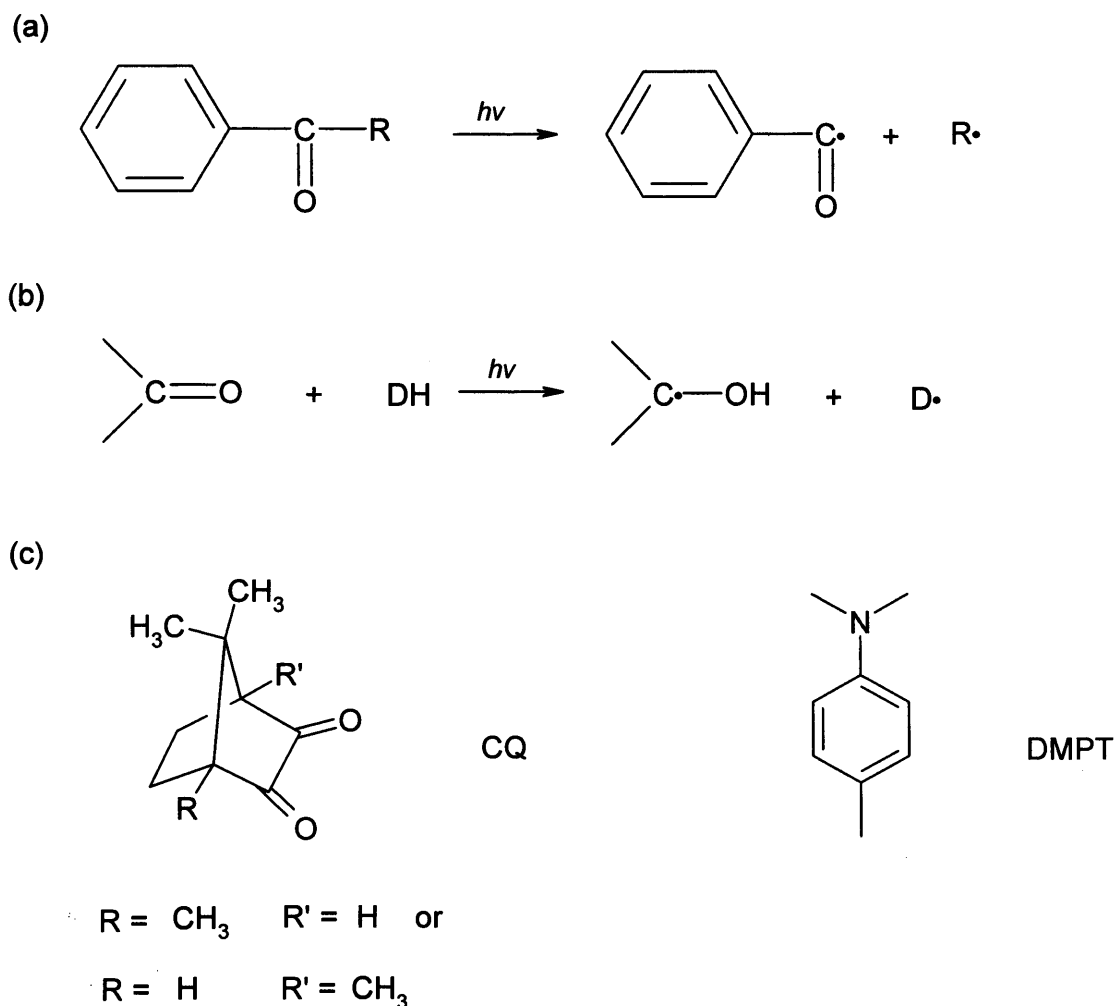
Figure 1.16. Photoinitiators that promote radical photo-polymerisation. (a) Formation of initiating radicals by photocleavage of the photoinitiator. (b) Formation of initiating radicals via hydrogen abstraction of the photoinitiator from the H-donor (DH). (c) Structures of the photoinitiator, camphoroquinone (CQ), with its H-donor, *N,N*-dimethy-*p*-toluidine (DMPT), used in this project

One of the most widely used initiators in modern light-cured methacrylate systems is CQ with a reducing agent. Unlike the UV initiators which attenuate the polymerising light dramatically, this system allows deeper penetration of the visible (blue) light because of the tendency of CQ to quickly photobleach (101;103). Indeed UV methacrylate curing has been superseded in the dental surgery by use of safer, high-intensity blue lights of

narrow wavelength range from quartz tungsten halogen lights and more recently also by use of light emitting diodes and lasers (158). Use of higher intensity of light may increase reaction rate and if the material is additionally to be used as a controlled drug release device, the use of higher wavelength can also prevent damage of drugs capable of UV absorption.

In an attempt to minimise the potential cytotoxic problems associated with residual photoinitiators and the light attenuation problems during polymerisation of thick samples, initiator-free photo-polymerisations are being developed. Rydholm *et al* (154) has recently developed a degradable thiol-acrylate monomer that was capable of polymerising upon exposure to UV light (365 nm), with or without added photo-initiators, forming polymer with thicknesses exceeding 10 cm. This reaction occurred between multifunctional thiol monomers (with four S-H groups) and PLA-PEG-PLA diacrylate monomers and involved both step-growth and chain-growth reactions.
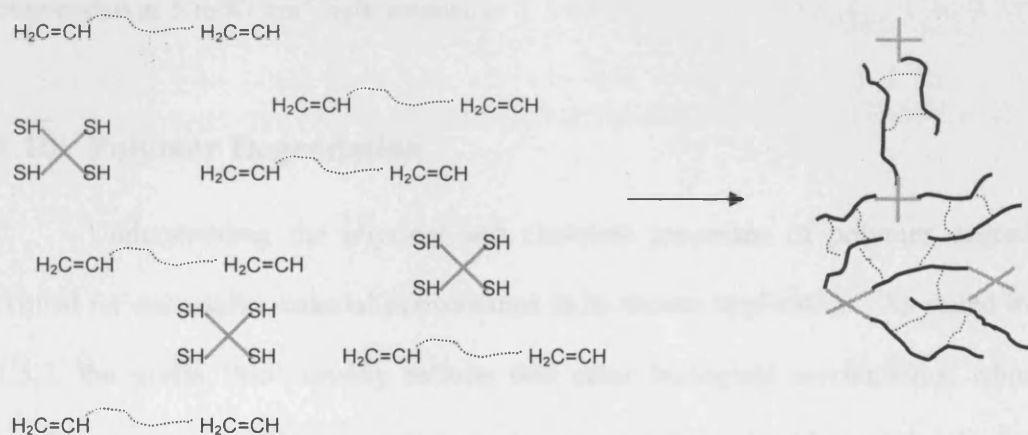
Figure 1.17. Polymerisation of multifunctional thiol monomers and diacrylate monomers to form a crosslinked polymer network. Modified from (154).

In this reaction a photo-initiated thiolate ion first reacts with an acrylate group to form a carbon-based radical, which can then react with another thiol group to form a thiol-acrylate molecule and regenerate another thiolate ion, and this step-growth process repeats. At the same time other acrylate groups can also react with the carbon-based radicals, resulting in chain propagation similar to the chain-growth polymerisation of pure acrylates. The resulting polymer network is one with each S-H group being covalently crosslinked with the polyacrylate blocks (Figure 1.17). The structure of the network can be controlled by varying the ratio of thiol to acrylate groups. The group found that with the presence of tetrathiol monomers and an UV initiator, 95 % acrylate polymerisation could be achieved with 60 s of UV light exposure, compared to the 90 s needed in the absence of any thiol monomers. When tetrathiol monomers (15 mol%) were used with no UV initiator, the system could still achieve 75 % acrylate conversion in 14 minutes, and in ~4 minutes when the light intensity was increased from 5 to 50 mW/ cm^2. The acrylate monomers without any addition of thiol monomers or UV initiator needed 27 minutes to reach a 75 % conversion at 5 mW/ cm^2 light intensity.

1.10 Polymer Degradation

Understanding the physical and chemical processes of polymer degradation is critical for successful material performance in its chosen application. As stated in Section 1.5.2, the prefix 'bio' usually reflects that other biological mechanisms, which could involve enzymes, cells, tissues or organs, may contribute, besides passive hydrolysis, to the kinetics of the degradation process. For example, the hydrolysis of poly(α-hydroxy acids) has been shown to be enhanced by an enzymatic mechanism *in vivo* (9;55).

In the literature, degradation is often used interchangeably with erosion, another term used to describe the breakdown of polymer. Different definitions, however, exist between these two commonly used terminologies.

Biodegradation is defined by Williams (159) as 'breakdown of a material mediated by a biological system', whereas bioerosion means 'removal of matter from the surface of a biomaterial following implantation in the body without regard to the specific mechanism involved'.

On the other hand, Gopferich (160) has defined polymer degradation as 'the process of polymer chain scission by the cleavage of bonds between the monomers in the polymer backbone', whilst polymer erosion is 'the sum of all processes that can lead to the loss of mass from a polymer matrix' . These processes can be biological, chemical or physical, resulting in mass loss that can be due to the loss of monomers, oligomers or pieces of non-degraded polymer.

Although biodegradable and bioerodible polymers have been defined to imply breakdown of polymeric devices to form fragments or degradation products which can subsequently move away from their site of action, these terms do not necessarily imply that the breakdown products are being eliminated from the body. Hence this generates another commonly quoted term for degradation of polymer- bioresorption. This has been used by Vert (29) to describe polymeric materials whose degradation by-products have been shown to be totally eliminated out of the body through natural pathways i.e. either by kidney filtration or via metabolism.

1.10.1 Chemical Degradation

Solubilisation of intact polymers, for example, as a result of pH changes of the surrounding solution can lead to erosion (143). Most polymers, however, are water insoluble, and require the process of degradation prior to erosion (51). This results in a size reduction of the polymer chains that eventually renders them water-soluble. Degradation can be characterised by a number of ways such as loss of molecular weight or loss of mechanical strength (53). A polymer can have a large reduction in both molecular weight and mechanical strength e.g. a polyester, before the molecular chains are reduced to a size which allows them to freely diffuse out of the polymer matrix and result in mass reduction of the sample i.e. erosion. Only scant information is available on the critical molecular weight for water solubility of polymer degradation products but it has been mentioned that for poly(α-hydroxy esters) the numbers range from 1500 to 5000 Da (161).

There are four common modes of polymer degradation: photo-, mechanical-, thermal- and chemical degradation (160). Photo-degradation can occur during exposure of polymers to UV or gamma radiation. Mechanical degradation can occur during polymer processing and handling, or when placed under stress *in vivo*. Thermal degradation can also occur when polymers are exposed to high temperatures e.g. during polymer processing. Chemical degradation of a polymer is usually accomplished by addition of chemical functional groups to the polymers to provide hydrolytically unstable linkages in the backbone. The most common chemical functional groups used are esters, anhydrides, orthoesters and amides.

The rate of chemical degradation depends primarily on two parameters: the diffusivity of water into the polymer matrix and the rate of chain scission of the polymer

backbones (24;162). These parameters are in turn affected by an array of factors. These include the polymer composition, the crosslinking density of the polymer network, possible autocatalysis by acidic degradation products inside a matrix, the removal of degradation products out of the polymer network, device dimensions such as size, shape and surface area to volume, and presence of other excipients such as protolytic drugs (162-164). The following discusses the effects of these factors.

1.10.1.1 Bond lability

The type of bonds in the structure determines how susceptible the polymer backbone is to hydrolytic attack. Anhydride bonds are the most hydrolytically unstable when compared with esters, amides, and ethers (53). The rate of hydrolysis of a bond can be altered by changing the pH of the dissolution medium, the presence of ions or the chemical environment of the bond (160). For example, the hydrolysis of acetic anhydride can be catalysed by acetate and formate ions, and the reactivity of ester can be increased by introducing electronegative substituents in the α-position of the ester.

1.10.1.2 Crystallinity

The rate of water sorption can be affected by the degree of crystallinity (9). The crystalline L-PLA retards water sorption and degrades more slowly than the amorphous racemic D,L-PLA. The degradation time of the semi-crystalline L-PLA is on the order of 3 to 5 years, compared to the 12 to 16 months of the amorphous D,L-PLA (11). Co-polymers of PLA and PGA are less crystalline than the homopolymers and thus degrade more rapidly. The effect of crystallinity has been observed for other polymers. It has been reported that the amorphous parts of the polyanhydride, poly(SA), degrade faster than the crystalline regions (51).

1.10.1.3 Chemical constituents (hydrophobicity)

Factors such as hydrophobicity and crosslinking determine the access of water to the labile bond. Monomers that contain hydrophobic moieties will lower the water uptake in the resultant polymer matrix. Degradation rate has been shown to alter upon changing the overall hydrophobicity of the polymer network (102). For example, MCPH, with its two phenyl rings and long hydrocarbon backbone is a more hydrophobic anhydride monomer than MSA and as a result, the rate of erosion of poly(MCPH) is much slower (~1 year) than that of poly(MSA) (~50 hr) (41;103).

Similarly, highly crosslinked hydrophobic dimethacrylated polyanhydrides degrade through a more controllable surface erosion mechanism whilst the loosely crosslinked hydrophilic dimethacrylated PLA-PEG-PLA hydrogels undergo bulk erosion (154). Hollinger and Battistone (9) state that the rate at which PLGA co-polymers degrade *in vivo* is affected by both the molar ratio of lactic acid to glycolic acid and the sequence distribution of the lactic acid and glycolic acid units along the structure. Lactic acid hydrolysis is comparably slower than that of glycolic acid because methyl groups on the former protect the carbonyl carbons from tissue fluid. Consequently, increasing lactic acid or decreasing glycolic acid constituents will decrease the degradation rate of a PLGA polymer. Sawhney *et al* (99) has observed that in their PEG-co-ester diacrylate polymers, degradation rates could be varied by changing the length and composition of the ester segments. Decreasing the crosslinking density of PPF networks has also been shown to increase the *in vitro* material degradation (163).

1.10.1.4 Chemical constituents (molecular weight))

Higher molecular weight causes an increase in the T_g of a polymer and slows the degradation process because glassy polymers degrade slower than rubbery ones (160). In addition, higher molecular weight increases polymer chain length with more bonds that need to be cleaved in order to generate water soluble degradation products.

1.10.1.5 pH and solubility

The pH of the surrounding environment and the solubility of the degradation products can affect the degradation of a polymer. For example, degradation of polyanhydrides is faster in a basic medium than in an acidic medium because (i) hydrolysis of the anhydride bond is base catalysed and (ii) the degradation products i.e. carboxylic acids, exist in more ionised form at high pH and thus solubilise more easily into the surrounding medium allowing their better diffusion (51). Aliphatic polyanhydrides, which are composed of longer-chain, less water soluble monomers, degrade slower than those composed of shorter and more water soluble monomers (165). The presence of acidic degradation products within a polymer matrix can also reduce the local pH and accelerate degradation of the remaining intact polymer through autocatalysis (15). PGA and PLA implants upon degradation, release acidic by-products which can accelerate the hydrolytic process over time. This is because the outward diffusion of high molecular weight degradation products is slow and the concentration of carboxylic end groups inside the material increases with time (161). The faster degradation inside the polymer centre compared to its surface eventually disintegrates the device when the osmotic pressure builds up inside the matrix due to the accumulation of degradation products (162). One study has shown that when PPF was incorporated without β-TCP,

degradation was accelerated leading to rapid decrease in mechanical properties (65). They

speculated that the presence of calcium ions from the β-TCP would associate with the

negatively charged entities on the PPF backbone and act as a local buffer.

1.10.1.6 Device dimensions

As the surface area per unit volume of a polymer device increases, the likelihood

for hydrolytic attack increases. A porous implant will generally therefore degrade more

rapidly than a dense implant. Additionally PGA (Dexon®) sutures can take 60 to 120

days to be absorbed (9), whereas PGA in the form of thicker rods of lower surface area to

unit volume can take between 336 (as a subcutaneous implant) to 588 days (bone fixation)

to be absorbed in vivo (15). Furthermore, if the device is of small size, soluble

degradation products can escape before they are totally degraded. In large size devices

only degradation products located close to the surface are released while those located

inside the device can remain entrapped and undergo greater chain cleavage. The location

of the polymer device is also important. If it were placed in a highly vascular area, its

degradation rate would be more rapid.

1.10.2 Erosion

The earliest and simplest classification of erosion mechanisms are surface

(heterogenous) and bulk (homogeneous) erosion (160). It has been hypothesised that the

erosion kinetics depends on two major processes (162): the diffusion of water into the

polymer bulk and the degradation rate of the polymer backbone.

Bulk erosion occurs when the diffusion of water into the polymer is faster than the

degradation of polymer bonds (162). As a result, water cannot be absorbed quickly

enough on the surface and can reach the inner polymer bulk. Degradation occurs all over the cross section of the polymer matrix, and there is no constant erosion velocity (51;162). Instead the polymers do not erode for long periods of time after which erosion sets in spontaneously (Figure 1.18 b).
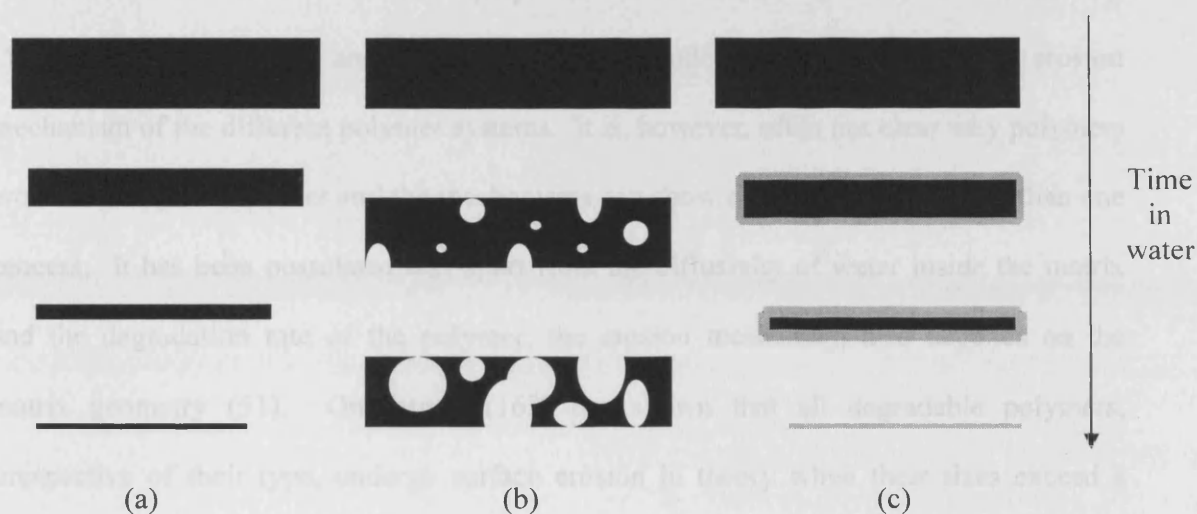
Figure 1.18. Schematic diagram of (a) surface erosion, (b) bulk erosion, and (c) surface erosion front formation.

Surface erosion, on the other hand, occurs when degradation of the polymer bonds is faster than the diffusion of water into the material (Figure 1.18 a). Any water influx will be consumed by the hydrolysis of bonds on the polymer surface and will thus be prevented from diffusing into the bulk. Degradation processes are then strictly confined to the matrix surface, the structural integrity is maintained throughout the erosion and the mass loss tends to proceed at constant velocity (166). It has been said that surface eroding polymers are largely materials containing functional groups with short hydrolysis half lives (162).

In addition, it has been postulated that since degradation of the anhydride bond by hydrolysis occurs much faster than does the dissolution of the hydrolysed products, this leads to the formation of two distinct erosion zones (167), with erosion originating at the surface and moving to the centre of the polymer samples (Figure 1.18 c).

Erosion mechanisms of polymers have been researched extensively (51;161;162;164;166;167) and attempts have been made to understand the exact erosion mechanism of the different polymer systems. It is, however, often not clear why polymers erode one way or the other and the mechanisms can show characteristics of more than one process. It has been postulated that apart from the diffusivity of water inside the matrix and the degradation rate of the polymer, the erosion mechanism also depends on the matrix geometry (51). One study (162) has shown that all degradable polymers, irrespective of their type, undergo surface erosion in theory when their sizes exceed a certain critical dimension ($L_{critical}$) specific to each polymer. Polyanhydrides were found to be surface eroding down to a size of approximately $L_{critical} \sim 100$ µm whereas poly(α-hydroxy esters) matrices need to be larger than $L_{critical} \sim 10$ cm to be surface eroding. Small polymer matrices can undergo surface erosion only when the diffusivity of water in the polymer matrix is low or the reactivity of polymer bonds with respect to hydrolysis is high.

It must be stressed that processes other than degradation can contribute to erosion, for example, cracks formed during early degradation on the surface of polymer matrix discs have led to the loss of pieces of non-degraded material due to mechanical instabilities. Additionally parts of fragile and brittle materials on the matrix surface may wear off under the weak mechanical forces that are applied during *in vitro* degradation experiments (51).

1.11 Aims and Objectives

This project was divided into three parts: synthesis and chemical analysis of the monomers, characterisation of polymer properties, and modification with drugs or ceramic/ glass particles. The monomers were synthesised as ABA triblock molecules with a methacrylate group at each end. The central B block was PPG with an average molecular weight of 425, 1000 or 2000 g/mol. The side A blocks were D, L-lactic acid or glycolic acid moieties. The reactant molar ratio of PPG to the ester was varied from 1 to 2, 1 to 4 and 1 to 8. It was found, however, that only the PPG-co-lactide methacrylates (and not the glycolide materials) could be obtained as stable fluids via the methods employed. The remainder of the project was thus based on the characterisation and modification of the lactide based monomers. Previous studies on any poly(ether-esters) concentrated mainly on use of PEG as the ether or acrylate group to endcap the monomers (58;79;98-100). It was also difficult to find detailed kinetic studies for injectable degradable polymers that provided any understanding of how various monomer variables affect photo-polymerisation rates. In this investigation the light curing polymerisation kinetics of the monomers was therefore studied using a combination of Raman and time-based FTIR methods.   Degradation and drug release studies were then followed in order to gain an understanding of the properties of these PPG-co-lactide methacrylate polymers.   The project was finally extended to fabrication of one of the polymers with filler materials to create composites. These filler materials included the ternary phosphate glass (based on the P_2O_5-CaO-Na_2O formula) particles which have only been, to our knowledge, added to PCL (67) and PLA (168). The other filler material included a mixture of β-TCP and monocalcium phosphate monohydrate (MCPM), which react with water to form brushite.

Use of a reactive filler of this type has never been, to our knowledge, examined in a degradable polymer. In all studies the formulations were fabricated according to a factorial experimental design. This allows the effects of various variables (which could be between two and four in number) to be investigated with minimal number of samples. Factorial designs have previously been used to investigate the effect of various variables on the release of bioactive agent (59), degradation (24), and crosslinking characteristics (66) of polymers, although in these studies only graphical comparison was used and no mathematical interpretation was attempted to analyse the data. In this project, the results were analysed by visually comparing the figures and also, provided the data fitted the factorial analysis rationale, mathematically (see Section 2.8.1, Chapter 2). The latter was useful in providing a quantitative value of the effect, and extent, of the different parameters with respect to time of the experiment.

1.11.1 Aims

The aim of this project is to develop a new series of poly(ester-co-ether) methacrylate polymers of systematically changing chemical structure to produce materials with incremental differences in properties for various bone tissue engineering and drug delivery applications. The properties considered include injectability, polymerisability, mechanical properties, degradation rates and drug release rates. These polymers can potentially act (i) as fixation devices or implants for damaged surrounding tissue, (ii) as biodegradable cements that give slow mechanical transfer to newly formed bone, (iii) as scaffolds for cellular migration, proliferation, and differentiation, and (iv) as localised delivery vehicles for controlled and sustained release of drugs and osteoinductive molecules.

1.11.2 Objectives

The objectives of the project were as follows:

1. Synthesis of fluid PPG-co-lactide / glycolide oligomers at different molar ratios of PPG to ester using a factorial experimental design and parallel synthesis equipment.

2. Endcapping of these oligomers with methacrylate groups to give polymerisable monomers.

3. Structural characterisation of the synthesised products, using Fourier transform infra-red (FT-IR) spectroscopy, Raman spectroscopy and nuclear magnetic resonance spectroscopy (NMR), to determine the reacted compositions of PPG to ester ratios, the efficiency of PPG hydroxyl groups reacted, and the percentage of final methacrylate termination.

4. Photo-polymerisation kinetics study of the methacrylate monomers at 37 °C using a combination of time-based FT-IR and Raman spectroscopic techniques. The formulations studied were fabricated according to a factorial analysis, using different levels of PPG to ester ratios, photo-initiator concentrations and blue light exposure times.

5. Degradation and mechanical study of the methacrylate polymer discs in pH-adjusted deionised water at 37 °C using gravimetrical, pH, FT-IR and dynamic mechanical analyses. Factorial analysis was again used and the polymer discs were fabricated using different levels of PPG to ester ratios and photo-initiator concentrations.

6. Drug release study of the above methacrylate polymer discs, incorporating three different drugs at different concentrations. The three drugs have varying solubility

in water and monomers, and drug release was studied using ultraviolet (UV) spectroscopy.

7. Modification of the methacrylate polymers via addition of calcium phosphate and ternary phosphate glass particles in order to further modulate their properties (degradation rates, modulus, pH, porosity).   Raman mapping was used to determine the dispersion of the filler particles in the polymers and ion chromatography was used to determine the rates and species of ion release from the composite discs.

2 Analytical Techniques

2.1   Analytical Techniques

Several analytical techniques were used to elucidate structural information and characterise the physical and chemical properties of the synthesised polymeric specimens. The principles of the techniques will be discussed in this chapter. These include attenuated total reflectance Fourier transform infra-red (ATR FT-IR) spectroscopy, Raman spectroscopy, nuclear magnetic resonance (NMR), ultraviolet/ visible (UV/vis) spectroscopy, dynamic mechanical analysis (DMA) and ion chromatography (IC). This chapter will also discuss the principles of factorial analysis used for experimental design in this study.

2.2   Fourier Transform Infra-red (FT-IR) Spectroscopy

Infra-red spectroscopy is one of the most widely used methods for studying polymer chemical structure (169;170). It can be used to identify stereoisomers or monomer sequence distributions, and to study polymer reactions such as degradation or crosslinking. FT-IR spectroscopy was used in this study (i) to identify the monomers and by-products from each synthetic stage and (ii) to determine the rate of polymerisation of the monomers.

The infra-red region of the electromagnetic spectrum can be divided into three regions: (i) near infrared (12800-4000 cm^{-1}), (ii) mid infrared (4000-200 cm^{-1}), and (iii) far infrared (200-10 cm^{-1}). Most IR spectrophotometers detect in the mid-IR region as it provides the greatest information in the elucidation of molecular structure. The energy of an electromagnetic light beam (Energy) is directly proportional to its frequency f (Hz) (or

wavenumber υ (cm^{-1},) since $f = c\upsilon$) and inversely proportional to its wavelength (nm, λ) as indicated by the Planck's equation (see Equation 2.1).

$$Energy = hf = hc\upsilon = h \times \frac{c}{\lambda} \qquad\qquad 2.1$$

Where h is the Planck's constant and c is the velocity of light.

2.2.1 Theory of infra red absorption

Absorption of IR radiation causes transitions in the vibrational and rotational states associated with the ground electronic state of a molecule (Figure 2.1). Bonds in a molecule behave like springs, oscillating at a particular frequency. The distance between the atoms in a chemical bond i.e. the bond length is determined by a balancing of forces: attractive forces between the nuclei and the electrons, and repulsive forces between the two nuclei and their electron clouds. When light is shone on a molecule, energy is absorbed to increase the amplitude of the vibrations. This causes the bonds to stretch (change in bond length) or bend (change in bond angles). This interaction between light and a molecule is only observable in FTIR spectra if the change in the amplitude of vibration is accompanied by a net change in the dipole moment (μ) i.e. the dipole moment at one extreme of a vibration must be different from that at the other extreme of the vibration (Figure 2.2). Light is only absorbed when the energy supplied by the frequency of the radiation matches exactly that required for a transition of the molecule from the bottom vibrational state to an excited state (171).
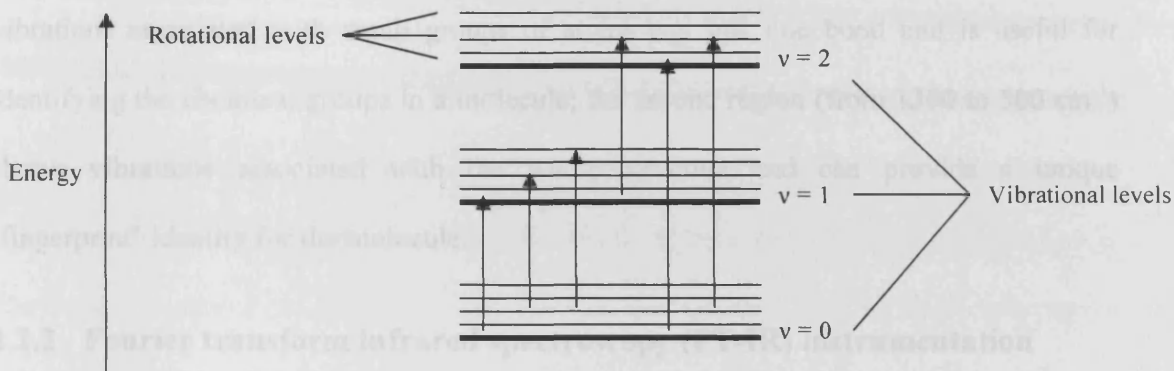
Figure 2.1. Energy level diagram of vibrational-rotational transitions that occur during infrared absorption.
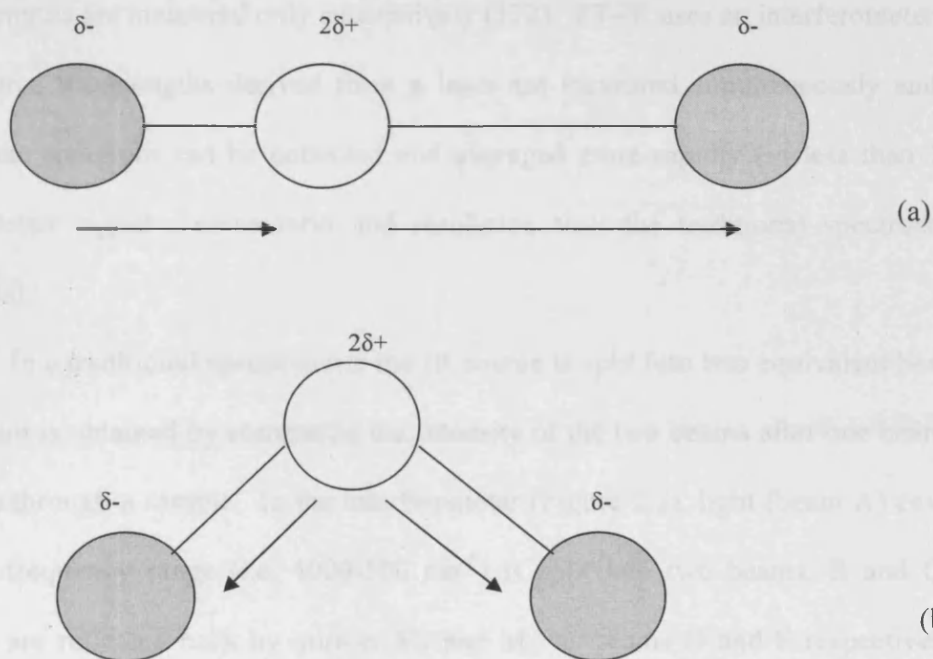
Figure 2.2. Two main types of IR active molecular vibrations resulting in a change in the overall dipole moment ($\Delta\mu \neq 0$): (a) asymmetrical stretch and (b) bending

Peaks at various wavenumbers on a FT-IR spectrum can be assigned to chemical groups because each bond or group of atoms has different vibrational energies. A FTIR

spectrum can be divided into two regions: the first region (from 4000 to 1300 cm^{-1}) shows vibrations associated with small groups of atoms e.g. just one bond and is useful for identifying the chemical groups in a molecule; the second region (from 1300 to 500 cm^{-1}) shows vibrations associated with the whole structure and can provide a unique 'fingerprint' identity for the molecule.

2.2.2 Fourier transform infrared spectroscopy (FT-IR) instrumentation

An IR instrument is composed of an IR source, a spectrometer and a detector. Traditionally IR spectra were taken using a dispersive spectrometer, in which slits and prisms or grating are used to disperse the IR radiation monochromatically and all source wavelengths are measured only successively (172). FT-IR uses an interferometer in which all source wavelengths derived from a laser are measured simultaneously and hence a complete spectrum can be collected and averaged more rapidly (in less than 1 minute) with better signal : noise ratio and resolution than the traditional spectrometer (2-3 minutes).

In a traditional spectrometer the IR source is split into two equivalent beams and a spectrum is obtained by comparing the intensity of the two beams after one beam is made to pass through a sample. In the interferometer (Figure 2.3), light (beam A) covering the whole frequency range (i.e. 4000-500 cm^{-1}) is split into two beams, B and C. These beams are reflected back by mirrors M_1 and M_2, as beams D and E respectively, which recombine to form a single beam F that passes through the sample to the detector. If the distances between the beam splitter and the mirrors M_1 and M_2 are identical, beam F will be the same as beam A. If mirror M_1 is set to move along the light path, the distance traversed by beams B and D will be different to that traversed by C and E. The time to

travel the various distances will depend upon the wavelength of light. The different wavelength components of beam D and E will arrive back at the beam splitter for recombination at different times. The same components of these two beams will interfere with one another either constructively or destructively such that the intensity of beam F will vary with time as a function of the optical path differences of beam B + D and C + E. The pattern produced, the interferogram, will then be converted by Fourier transformation using a computer in the system into a plot of absorbance vs. wavelength (171).
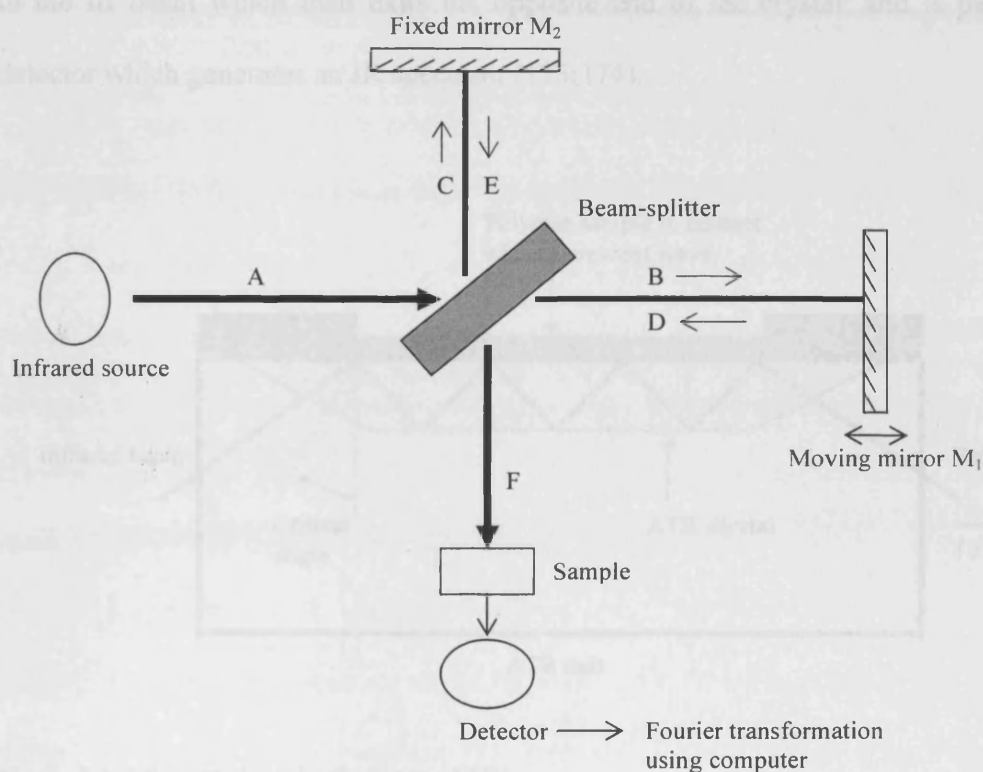
Figure 2.3. A Fourier transform spectrometer.

2.2.3   Attenuated total reflectance (ATR) infrared spectroscopy

ATR occurs when an IR beam is directed onto an optically dense crystal with a high refractive index at an angle greater than the critical angle. The beam penetrates through the crystal into a sample (with a lower refractive index) that is held in contact with the crystal, before being reflected internally (Figure 2.4). The resultant evanescent wave that is reflected protrudes only a few microns (0.5 µm – 5 µm) beyond the crystal surface and into the sample. Its intensity is attenuated or altered by the sample when the sample absorbs energy. The attenuated energy from each evanescent wave is passed back to the IR beam which then exits the opposite end of the crystal; and is passed to the detector which generates an IR spectrum (173;174).
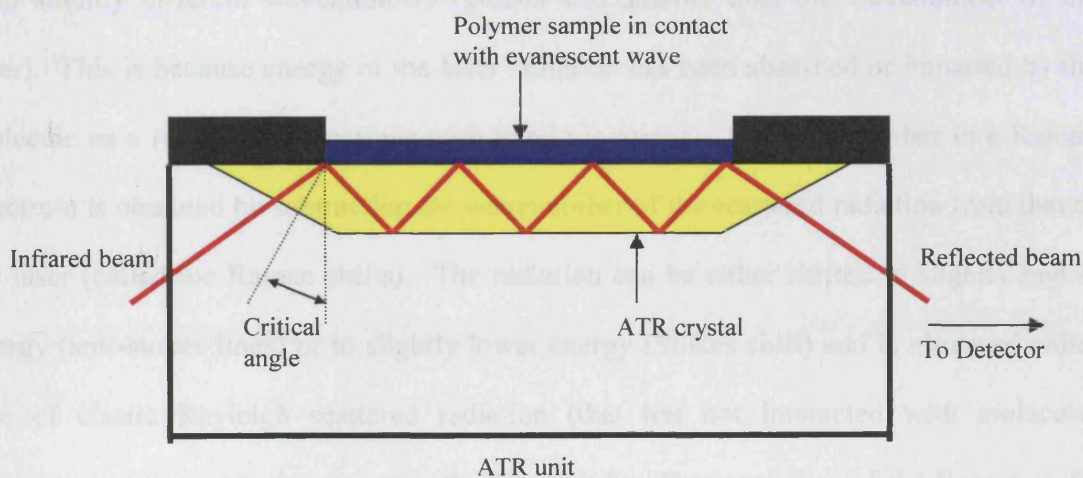
Figure 2.4. Attenuated total reflectance (ATR)

2.3   Raman Spectroscopy

Raman is similar to IR spectroscopy in that it can be used to investigate polymer structure based on vibrational modes of the molecule. Raman was used in this study to provide complementary information to FT-IR on monomer structures and to determine the final extent of monomer polymerisation.

FT-Raman spectroscopy uses laser light from the near IR region (wavenumber of between 12800 and 5000 cm^{-1}). The technique examines wavenumber changes in laser radiation scattered by molecules.

2.3.1   Theory of Raman effects

As laser radiation hits a molecule, a proportion of the deflected photons emerge with slightly different wavenumbers (greater and smaller than the wavenumber of the laser). This is because energy of the laser radiation has been absorbed or imparted by the molecule as a result of interactions with bond vibrations. The wavenumber in a Raman spectrum is obtained by subtracting the wavenumber of the scattered radiation from that of the laser (called the Raman shifts). The radiation can be either shifted to slightly higher energy (anti-stokes lines) or to slightly lower energy (Stokes shift) and is observed either side of elastic Rayleigh scattered radiation (that has not interacted with molecular vibrations) at the excitation wavelength (Figure 2.5). The intensities of the Raman shifts are generally 1000 times less than the intensity of the Rayleigh scattering, and hence intense light sources such as laser light are needed. FT Raman usually uses a near IR laser which emits radiation at 9395 cm^{-1} (175).
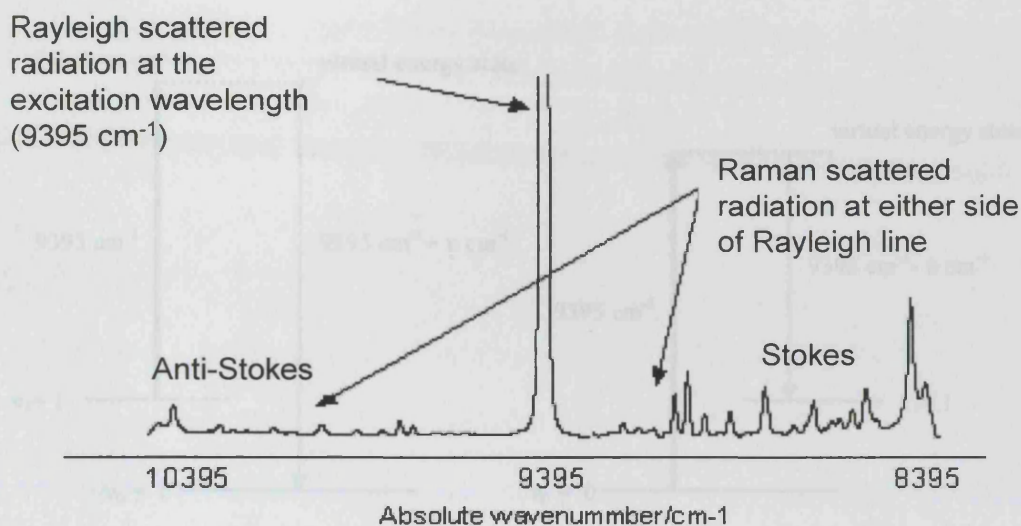
Figure 2.5. Rayleigh and Raman scattering. In Raman spectroscopy, the stronger Stokes spectrum is used and the Raman spectrum is obtained by subtracting the wavenumbers of the scattered radiation from the laser wavenumber (9395 cm^{-1}). Modified from (175).

Anti-Stokes shifts occur when the laser radiation interacts with molecules in the first vibration state and promotes them to short-lived virtual states 9395 cm^{-1} above the first vibrational state (Figure 2.6a). The unstable molecules with such high energy level then decay, and the scattered radiation is detected at a wavenumber equal to the laser wavenumber (9395 cm^{-1}) plus the wavenumber of the original vibrational state.

Stokes shifts, on the other hand, originate from the ground vibrational state but molecules relax to the first vibrational states, hence the energy of the scattered Raman radiation in this case corresponds to the laser wavenumber (9395 cm^{-1}) minus the vibrational wavenumber (Figure 2.6b).

The Stokes spectrum is a mirror image of the anti-Stokes spectrum and is usually determined in Raman spectroscopy as it is comparatively stronger than the anti-Stokes spectrum.

virtual energy state

virtual energy state

9395 cm^{-1}

9395 cm^{-1} + υ cm^{-1}

9395 cm^{-1} - υ cm^{-1}

9395 cm^{-1}

$v_1 = 1$

$v_1 = 1$

$v_0 = 0$

$v_0 = 0$

(a)

(b)
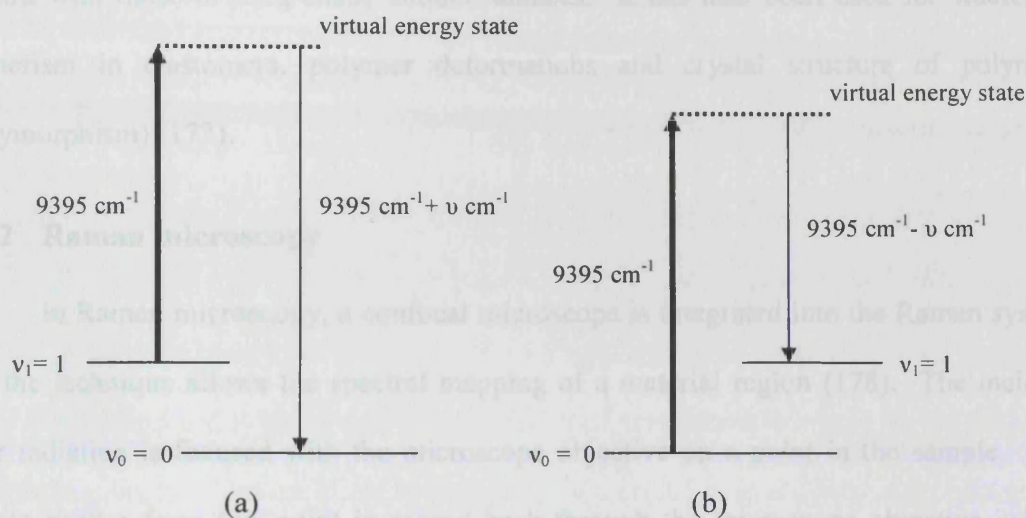
Figure 2.6. Anti-Stokes (a) and Stokes (b) shifts of Raman effects.

Unlike IR, different selection rules apply to the Raman effect. Whereas IR absorption occurs only if there is a change in the dipole moment during the vibration, a change in polarisability is required for Raman scattering to be observed, that is, the electron cloud of the molecule must be more readily deformed in one extreme of the vibration than in the other (176). A particular chemical group will give rise to peak(s) at the same wavenumber(s) in both Raman and FT-IR spectra. In a molecule with a centre of symmetry, those vibrations symmetrical about the centre of symmetry are active in the Raman and inactive in the IR; those vibrations which are unsymmetrical are inactive in the Raman and usually active in the IR. Hence, peaks that absorb weakly in the mid-FTIR region will absorb strongly in the Raman region and vice versa. The two techniques therefore provide complementary information to each other.

As Raman is most responsive to symmetrical stretching in carbon-carbon bonds, it has been applied primarily to conformational studies of polymer chains by comparing

spectra with those of long-chain 'model' alkanes. It has also been used for studies of isomerism in elastomers, polymer deformations and crystal structure of polymers (polymorphism) (177).

2.3.2 Raman microscopy

In Raman microscopy, a confocal microscope is integrated into the Raman system and the technique allows the spectral mapping of a material region (178). The incident laser radiation is focused with the microscope objective on a point in the sample. The Raman scatter from this point is passed back through the microscope objective, which focuses the scattered photons on a pinhole aperture. The Raman signal is then picked up by the detector. Any Raman scatter from points outside of the focal point is refracted by the microscope objective to be out of focus at the pinhole aperture, and is therefore not transmitted to the detector. Thus the resulting Raman spectrum contains Raman signal almost exclusively from a point (the focal point of the laser) within the bulk of the sample. The microscopy often uses fibreoptics to allow radiation to be pinpointed and is equipped with a motorised translational stage. By scanning the surface of a sample in a grid pattern over a designated region, a Raman spectrum can be acquired for each grid area (on a micrometer scale) generating a chemical image map of the region in the interior of the sample. This technique is particularly useful for characterising the distribution of components in a polymer mixture such as homogeneity of a blend.

2.4   Nuclear Magnetic Resonance Spectroscopy (NMR)

Nuclear magnetic resonance (NMR) is a powerful technique for polymer structure elucidation. Structural characteristics of oligomer structures including chain ends can be accurately ascertained using NMR techniques (179;180). Through determination of sequence distributions, NMR has also been used to determine bond lability during degradation of a polymer (181). NMR was used in this study to derive the exact structures of the monomers and to determine the efficiency of the ester attachment to the PPG and the methacrylation of the molecule as well as the total molecular weights of the monomers.

Structural information on a polymer molecule is provided by three parameters in NMR: (i) chemical shift values (δ), which are characteristic of particular groups of equivalent protons; (ii) line intensity, which indicates the number of equivalent protons responsible for the NMR signal; and (iii) spin-spin coupling patterns, which indicates the number of protons in interacting groups (182-184).

2.4.1   Theory of nuclear magnetic resonance

Protons and neutrons of certain nuclei (^{1}H, ^{13}C, ^{19}F, ^{31}P) possess a magnetically active property called spin which comes in multiples of 1/2 and can be + or -. The NMR phenomenon is based on transitions between the energy states of this spin when these nuclei are immersed in a static magnetic field (B_0) and exposed to a second oscillating magnetic field (B_1). Only non zero nuclear spin can produce NMR signals. Two types of NMR are commonly used - ^{1}H-NMR and ^{13}C-NMR, both with spins of 1/2. In this study ^{1}H-NMR was used.

The resonance frequency depends upon both the applied field strength (B_0) and the nature of the proton in question. When the proton is placed in an external magnetic field

(B_0), its spin can take up either of two orientations rather like a magnet: a low energy orientation (N_1) aligned with the applied field or a high energy orientation (N_2) opposed to the applied field. The transition between the two energy states of proton spin occurs via absorption of a photon with matching energy (resonant frequency). In NMR, the frequency of the photon is in the radio frequency (RF) range which for ^{1}H-NMR is between 60 and 800 MHz. The initial populations of equivalent protons occupying the high or low energy levels are distributed according to the Boltzmann Distribution Law; the lower level will contain slightly more nuclei than the higher level. An NMR signal arises from the difference between the energy absorbed by the spins which make a transition from the lower energy state to the higher energy state, and the energy emitted by the spins which simultaneously make a transition from the higher energy state to the lower energy state. The signal is proportional to the population difference between the states.

In NMR, the energy difference between the ground and excited state is not large and hence ΔN, the difference between the number of protons in the low energy and high energy states is very small. The net energy absorption by the population of low energy protons in a sample is therefore low when compared with IR and ultraviolet / visible spectroscopy. NMR is therefore a relatively insensitive technique. Higher field NMR spectrometers (e.g. 200- 750 MHz) are used to improve sensitivity. This is because the greater the field strength, the greater is the energy difference between N_1 and N_2, and the higher the radiation frequency (i.e. shorter wavelength with larger amount of energy) is required to bring about resonance. A strong magnetic field (i.e. a stronger magnet) increases the attraction between the field and the spin alignment and so more energy is needed for the transition to occur (Figure 2.7).
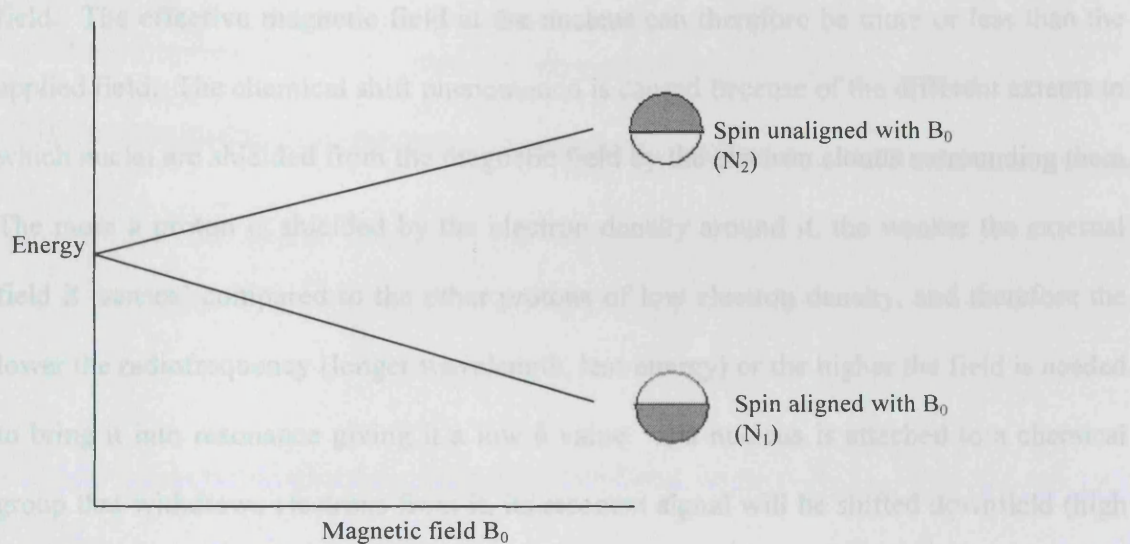
Figure 2.7. Energy level diagram between the two transition states of the spin of a proton.

2.4.2 Chemical shift

Protons of different types in a molecule absorb energy at different frequencies depending on their molecular (and hence magnetic) environments and the signals are described as having a chemical shift from some standard frequency. This chemical shift (δ) is determined by measuring the difference of the frequency of the sample peak (υ_s) from some internal standard (e.g. tetramethysilane, $Si(CH_3)_4$) (υ_{TMS}), and then dividing this by the operating frequency of the radiowaves (Hz) to obtain a field-independent number. This chemical shift, (measured in ppm), of a particular group of protons will be the same whatever NMR spectrometer is used.

All protons are not identical as they are surrounded by nonbonding and bonding/ valence electrons. When an atom is placed in a magnetic field, its electrons circulate about the direction of the applied field within their sigma and pi molecular orbitals, creating a local magnetic field (ρB_0) at the nucleus which opposes the externally applied

field. The effective magnetic field at the nucleus can therefore be more or less than the

applied field. The chemical shift phenomenon is caused because of the different extents to

which nuclei are shielded from the magnetic field by the electron clouds surrounding them.

The more a proton is shielded by the electron density around it, the weaker the external

field it 'senses' compared to the other protons of low electron density, and therefore the

lower the radiofrequency (longer wavelength, less energy) or the higher the field is needed

to bring it into resonance giving it a low δ value. If a nucleus is attached to a chemical

group that withdraws electrons from it, its resonant signal will be shifted downfield (high

δ). Equivalent nuclei are those that experience the same magnetic environment or

chemical shift; non-equivalent nuclei are those with different environment or chemical

shifts.

2.4.3   Spin-spin coupling

The magnetic environment of a nucleus is also affected by the spin of nearby non-

equivalent nuclei that are less than or equal to three bond lengths away. The result of this

spin-spin coupling is that the NMR signal produced is split into groups of related peaks,

called doublets, triplets, multiplets etc. In ^{1}H-NMR the number of peaks formed in a split

signal is given by the spin-spin coupling rule (n+1) where n is the number of protons on

the neighbouring atom. The distance between two split absorption peaks (measure in Hz)

is called the J coupling constant or the spin-spin splitting constant and is a measure of the

magnetic interaction between two nuclei.

2.4.4 Intensity of NMR signal

The absorption of each signal is proportional to the number of protons coming into resonance at the frequency of the signal; therefore the relative area under each signal gives information on the number of a given type of protons being detected in the molecule. It is noted that an absorption signal is defined as the family of peaks centred at a particular chemical shift.

2.4.5 Sample preparation and instrumentation

The sample to be investigated is dissolved in a deuterium solvent such as deuterated chloroform ($CDCl_3$) or in tetrachloromethane (CCl_4) and can contain $Si(CH_3)_4$ as a reference substance. The solution is placed in a 5 mm glass NMR tube, which is placed between two electrical (RF) coils at right-angles to each other and at the centre of an extremely powerful electromagnet giving a very high magnetic field (B_0). One coil transmits a strong pulse of radio-frequency waves (B_1) from an oscillator and the other acts as a detector. At an appropriate frequency and magnetic field strength, the protons absorb energy from the transmitter coil and induce signals in the detector coil. An NMR spectrum may be produced by increasing the magnetic field strength and keeping constant the frequency of the transmitted radio-waves, or by increasing the frequency of the transmitted radio-waves and keeping constant the magnetic field strength.

2.5 Ultraviolet-Visible Spectroscopy

Ultraviolet-visible (UV/ vis) absorption spectroscopy is used for the detection and quantitative measurement of chromophores that undergo electronic transitions. Being a very sensitive technique, it has been used to detect residual monomers, inhibitors,

antioxidants etc. in polymers (185), chromophore-containing units in co-polymer composition analysis (186) and end group identification in polymers (177). The technique is also commonly used for quantitative analysis of drug release from polymers (56;58;60;187). In this study, UV/vis spectroscopy was used to quantify the release of three different drugs from the polymers synthesised.

2.5.1 Theory of ultraviolet-visible spectroscopy

The UV/vis region spans between 190 and 750 nm in the electromagnetic spectrum. The technique is based on the absorption of UV/vis light resulting in the excitation of a valence electron from its ground state orbital to a higher energy state orbital, such that the electron cloud holding the atoms together redistributes itself and the orbitals occupied by bonding electrons no longer overlap (188). Three main types of electrons can be involved: lone pair (n), sigma (σ) and pi (π) electrons and their possible electronic transitions are shown in Figure 2.8.
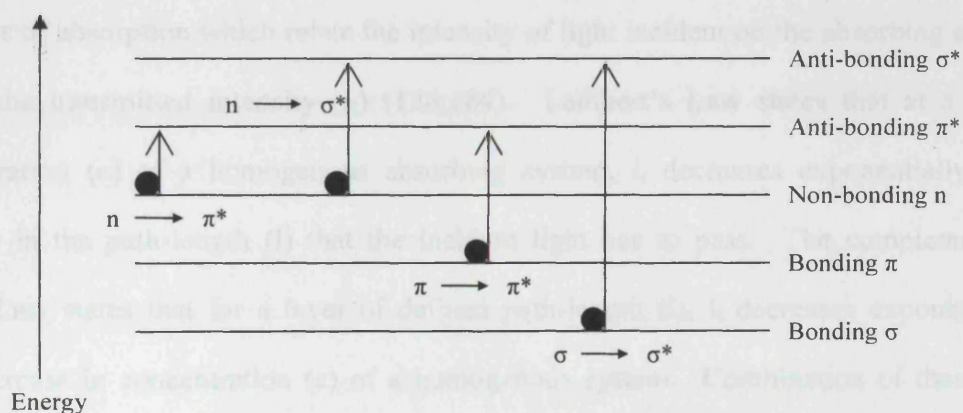
Figure 2.8. Energy level of different orbitals and possible electronic transitions in UV absorption.

The energy required for $\sigma \rightarrow \sigma^*$ transition is large and usually only occur in the far UV region (below 150 nm, higher energy). The $n \rightarrow \sigma^*$ transition occurs in the range 150 – 250 nm but its incidence is low. Most studies are therefore based on transitions of $n \rightarrow \pi^*$ or $\pi \rightarrow \pi^*$ since the energy required for these transitions fall in the UV region of the spectrum. Absorption of light of a suitable wavelength can promote vibrational and rotational transitions in additional to electronic transitions, consequently the total quantities of energy absorbed in the excited molecules vary extensively such that the spectrum appears as a continuous band.

2.5.2 The Beer–Lambert Law

When light passes through a homogenous sample, a portion of incident light (I_o) is reflected (I_r), a portion is absorbed by the sample (I_a) and the remainder is transmitted (I_t). In order to measure the amount of light absorbed, the effect of light reflection is eliminated by use of a blank solution (containing pure solvent). The extent of light absorption by an absorbing system at a given monochromatic wavelength is governed by two laws of absorption which relate the intensity of light incident on the absorbing system (I_o) to the transmitted intensity (I_t) (176;184). Lambert's Law states that at a given concentration (c) of a homogenous absorbing system, I_t decreases exponentially with increase in the path-length (l) that the incident light has to pass. The complementary Beer's Law states that for a layer of defined path-length (l), I_t decreases exponentially with increase in concentration (c) of a homogenous system. Combination of these two observations gives the Beer-Lambert Law as defined in Equation 2.2.

$$A = \log\left(\frac{I_0}{I_t}\right) = kcl \qquad\qquad 2.2$$

Where A is the logarithmic of I_0 / I_t and is called the absorbance and k is the absorptivity of the system. Absorbance is therefore directly proportional to the concentration of the absorbing system and the path-length. When c has the units of mol dm^{-3}, k is called the molar extinction coefficient i.e. ε ($dm^3mol^{-1}cm^{-1}$) and represents the absorption of a one molar solution in a cell of 1 cm path-length. When c is expressed in % m/v, k is called the specific extinction coefficient i.e. A (1 %, 1 cm) and is the absorbance of a 1 %w/v solution in a cell of 1 cm path-length. The extinction coefficient at any given wavelength is constant and is an inherent characteristic of the absorbing species.

Because molecular transitions in UV absorptions have high ε values (> 1000); the technique is therefore very sensitive for quantitative analysis. On the other hand, ε values in IR spectroscopy are smaller (<100) because the transition is small with only vibrational and rotational modes so the technique is primarily used for qualitative analysis.

2.5.3 Instrumentation

In a typical UV spectrometer (Figure 2.9), light from a deuterium (for UV light, 190 -360nm) or Tungsten lamp (for visible light, 360 – 1000 nm) is focussed onto an entrance slit of the monochromator. The light is reflected by mirrors onto a diffraction grating which splits the light into its wavelength components. The monochromatic light containing a single wavelength (as selected by the exit slit) then passes through a chopper, which sends the light along two paths: one passing through the reference cell (I_0) and one passing through the sample cell (I_t). Both light beams are then focussed onto a single detector that alternately records their intensities and hence the absorbance (171).
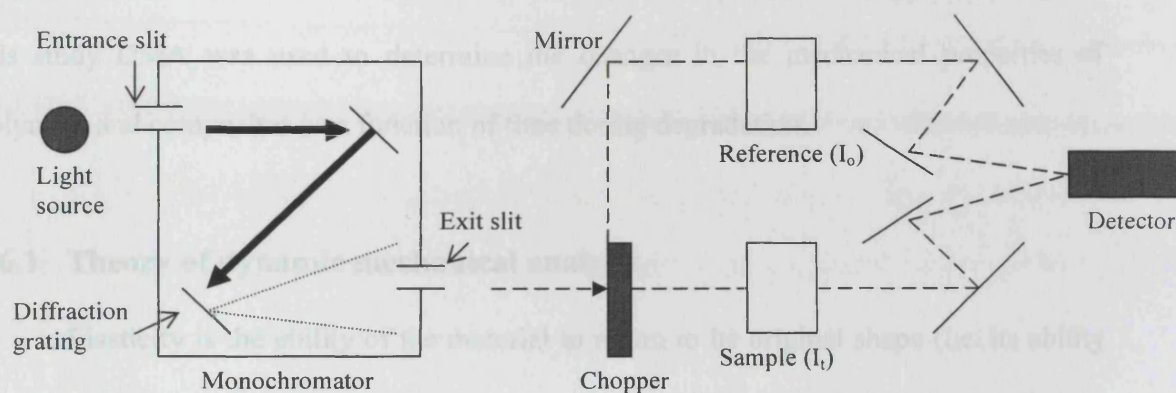
Figure 2.9. A typical UV/ visible spectrometer.

2.6   Dynamic Mechanical Analysis

Dynamic mechanical analysis (DMA) is a technique used to characterise the thermal and rheological (mechanical) properties of materials such as polymers, based on their viscoelastic nature (189). It is most commonly used for measuring stiffness (the resistance of a material to deformation i.e. modulus) of a material by applying an oscillating stress to the material and measuring the resulting displacement in strain (amount by which a material is deformed), and also for determining the damping properties of the material by measuring the time lag in the displacement compared to the applied stress.

Viscoelastic materials such as polymers exist in two distinct states, a glass state (high modulus) at low temperatures and a rubbery state (low modulus) at higher temperatures. DMA can therefore be used to determine the transition temperature between these two states (called glass transition temperature, T_g) by scanning the temperature and observing the change in modulus. As T_g of a polymer changes with

polymerisation level, DMA can also be used to determine the extent of polymer curing. In this study DMA was used to determine the changes in the mechanical properties of polymers and composites as a function of time during degradation.

2.6.1   Theory of dynamic mechanical analysis

Elasticity is the ability of the material to return to its original shape (i.e. its ability to store energy). A fully elastic material (e.g. a spring) recovers completely after an applied stress is removed. Elasticity (as defined by the elastic modulus, E) is governed by Hooke's Law and is obtained by dividing applied stress (σ) by strain (ε) as shown by Equation 2.3 (189).

$$E = \frac{\sigma}{\varepsilon}$$ 2.3

Viscosity is the resistance of a material to flow (i.e. its ability to dissipate energy). A fully viscous material (e.g. a liquid) will not recover once extended. Viscosity (η in Pa.s), which is governed by Newton's Law, is obtained by dividing stress by strain rate as in Equation 2.4 (189).

$$\eta = \frac{\sigma}{d\varepsilon/dt}$$ 2.4

Thus elastic (solid) materials store applied energy and use this to recover from the deformation induced by the applied stress, whilst viscous (liquid) materials dissipate applied energy as heat and hence are unable to recover their structure. Most materials possess behaviour that is partially elastic and partially viscous. In a DMA experiment, a sinusoidal oscillating stress (i.e. load/ area) is applied to a material, which then deforms

(strain) in a similar sinusoidal oscillating manner with respect to time, provided that the material stays within its linear viscoelastic region (190). Four parameters are measured: material temperature, load (or stress), probe position (or strain), and time (phase angle, δ).

Figure 2.10 shows the relationship between the applied stress and the measured strain on a material (191). When the material responds to the applied wave perfectly elastically, an in-phase, storage or elastic response is produced with a phase angle δ being equal to 0; on the other hand a viscous material produces an out of phase, loss or viscous response with a phase angle δ of 90°. Viscoelastic materials will produce a response between these two extremes, whereby the measured strain will lag behind the applied stress by a phase angle δ ranging between 0 and 90 °.

For any one point on the stress curve in a viscoelastic material, the stress applied is described by Equation 2.5.

$$\sigma = \sigma_o \sin\left(\omega t + \delta\right) \qquad\qquad 2.5$$

Where σ is the stress at time t, σ_0 is the maximum stress, ω is the frequency of oscillation and δ is the phase lag (see Figure 2.10(iii)). The resultant strain response at anytime can therefore be described by Equation 2.6.

$$\varepsilon = \varepsilon_o \sin \omega t \qquad\qquad 2.6$$

Where ε is the strain at anytime t and ε_0 is the strain at the maximum stress. Using trigonometry Equation 2.5 can be represented as Equation 2.7.

$$\sigma = \sigma_o \sin\left(\omega t\right)\cos\delta + \sigma_o \cos\left(\omega t\right)\sin\delta \qquad\qquad 2.7$$

The complex modulus of a material (E*), which is a measure of the overall resistance to deformation, is given by Equation 2.8. Substituting Equations 2.6 and 2.7

into 2.8 allows E* to be separated into an in-phase modulus (E') and an out-of-phase

modulus (E'') as described by Equations 2.9 to 2.11.

$$E^* = E' + iE'' = \frac{\sigma}{\varepsilon}$$

2.8

$$\frac{\sigma}{\varepsilon} = \frac{\sigma_o}{\varepsilon_o} \cos \delta + \frac{\sigma_o}{\varepsilon_o} \sin \delta \left(\frac{\cos \omega t}{\sin \omega t} \right)$$

2.9

$$E' = \frac{\sigma_o}{\varepsilon_o} \cos \delta$$

2.10

$$E'' = \frac{\sigma_o}{\varepsilon_o} \sin \delta$$

2.11

The in-phase storage (real or elastic) modulus E' is a measure of the elastic

component portion of the material (i.e. the stored energy) under the testing conditions of

temperature, load and frequency. The out-of-phase loss (imaginary or viscous) modulus

E'' is a measure of the viscous component of the material (i.e. energy lost to heat). The

ratio of the two moduli (E''/ E'), called the tan delta (δ), is the tan of the phase angle δ

(called damping) and is a measure of the amount of deformational energy dispersed as

heat during each cycle (Equation 2.12).

$$\delta = \frac{E''}{E'}$$

2.12

The DMA method used for this project is called a dynamic stress scan, in which

the dynamic and static stresses are linearly programmed up or down over time while the

frequency and temperature are held constant. Compressive stress was used and the stress-

dependent behaviour was characterised by monitoring changes in strain and phase.
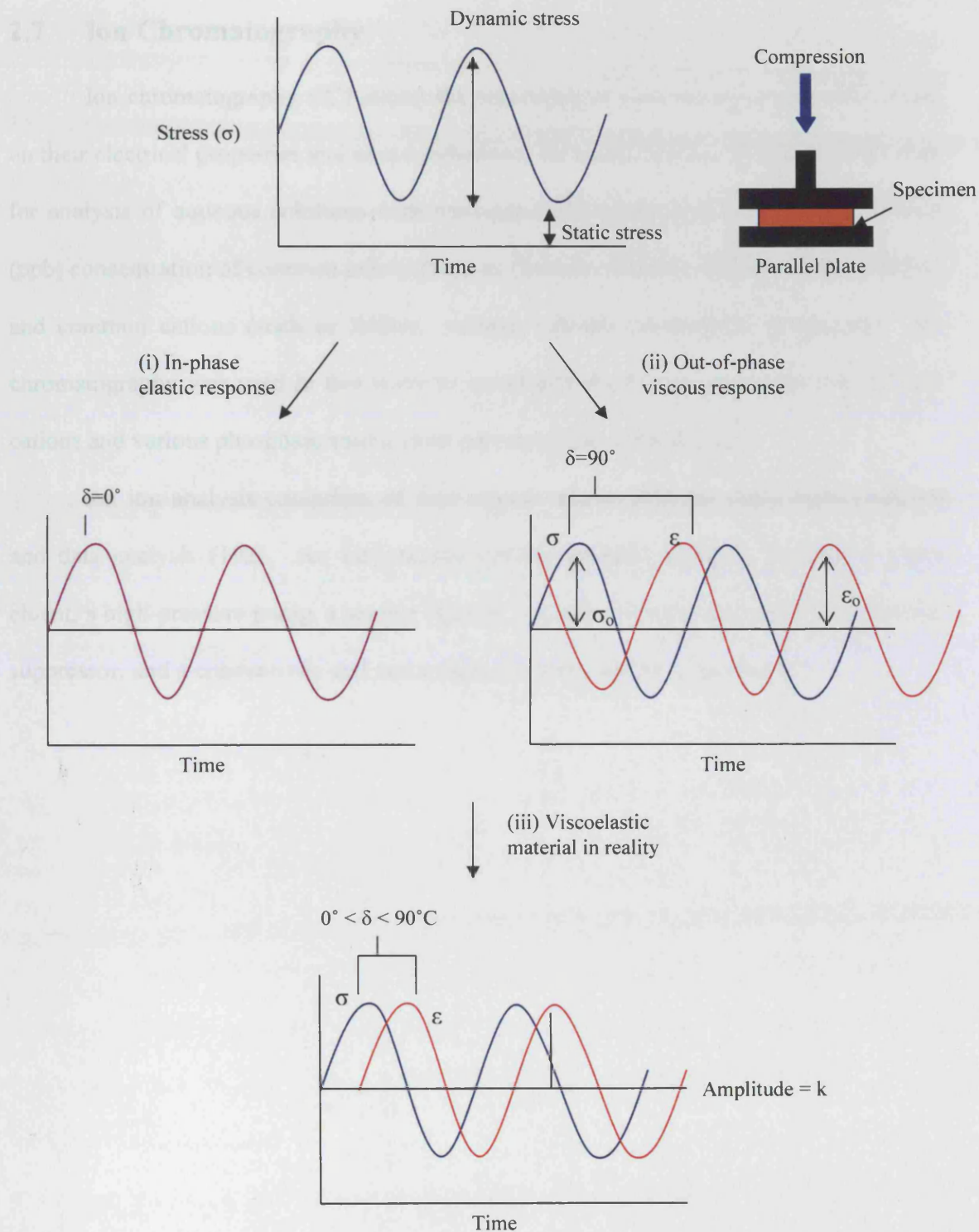
Figure 2.10. Relationship between applied stress (σ) and measured strain (ε) in a dynamic stress scan in (i) a fully elastic material; (ii) a fully viscous material; and (iii) in viscoelastic material. From the phase angle produced (δ) and the amplitude at peak k, the storage and loss moduli and the damping property of the material can be determined.

2.7   Ion Chromatography

Ion chromatography (IC) allows the separation of ions and polar molecules based on their electrical properties and uses conductivity for quantification. It is commonly used for analysis of aqueous solutions with parts-per-million (ppm) or even parts-per-billion (ppb) concentration of common anions (such as fluoride, chloride, nitrite, nitrate, sulphate) and common cations (such as lithium, sodium, calcium, ammonium, potassium). Ion chromatography was used in this study to investigate the release of sodium and calcium cations and various phosphate anions from polymer-glass composites.

An ion analysis comprises of four stages: eluent delivery, separation, detection and data analysis (192). An ion chromatography analyser typically contains a liquid eluent, a high-pressure pump, a sample injector, a guard and separator column, a chemical suppressor, and a conductivity cell and a data collection system (Figure 2.11).
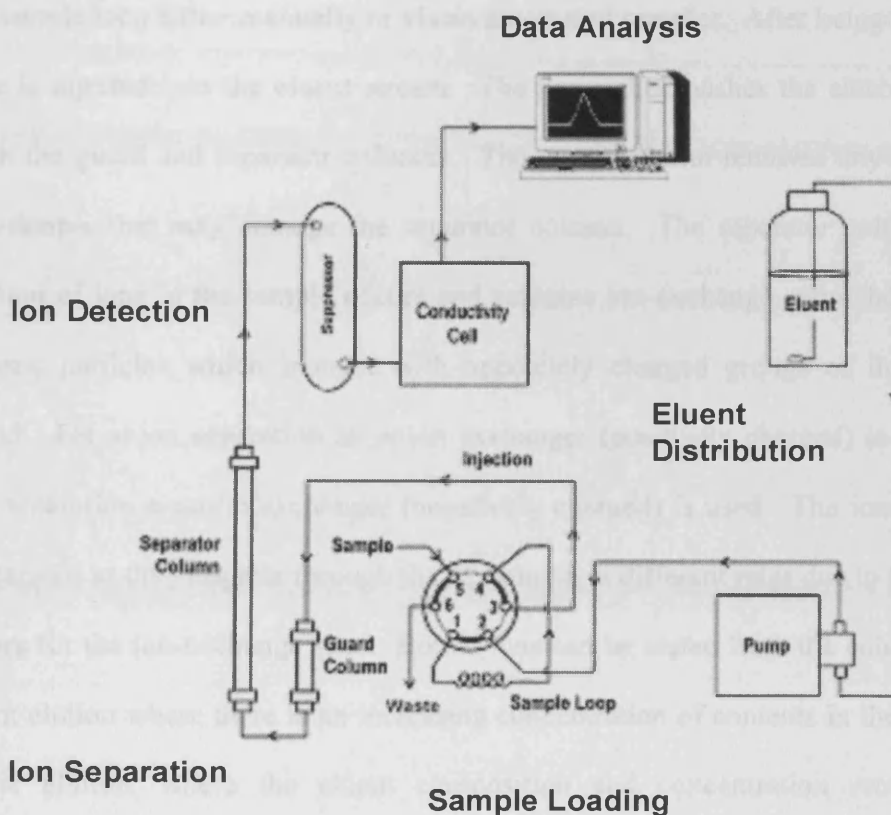
Figure 2.11. An ion chromatography analyser. Modified from (192)

2.7.1 Ion exchange

Prior to running samples, the ion chromatography system is calibrated using standard solutions. These solutions contain known amounts of a single ion, or a combination of several ions under investigation and are run through the system. By comparing the data obtained from a sample to those obtained from the standards, sample ions could be identified and quantified.

The eluent is a liquid used to separate the sample ions and to carry the sample through the ion chromatography system. The eluent is firstly distributed throughout the chromatography system before running samples. An unknown sample liquid is loaded

into a sample loop either manually or via an automated sampler. After being triggered, the sample is injected into the eluent stream. The pump then pushes the eluent and sample through the guard and separator columns. The guard column removes any contaminants in the sample that may damage the separator column. The separator column is where separation of ions in the sample occurs and contains ion-exchange resins bonded to inert polymeric particles which interact with oppositely charged groups of the ions to be detected. For anion separation an anion exchanger (positively charged) is used and for cation separation a cation exchanger (negatively charged) is used. The ions in a sample are separated as they migrate through the IC column at different rates due to their different affinities for the ion-exchange sites. Bound ions can be eluted from the column either by gradient elution where there is an increasing concentration of contents in the eluent or by isocratic elution, where the eluent composition and concentration remain constant throughout the run.

2.7.2 Ion detection

As the eluent and sample ions leave the column they are pumped through a suppressor, which consists of an ion-exchange column or membrane. The suppressor is used to selectively suppress the conductivity of the eluent thereby allowing measurement of conductivity due only to the sample ions that exit the column. As these sample ions emerge from the suppressor, a conductivity cell measures their electrical conductance and produces a signal based on a chemical or physical property of the ion. The voltage signal is then transmitted to a data collection system. The data collection system identifies the ions based on retention time, and quantifies each ion by integrating the peak area or peak height. The data is displayed as a chromatogram, and by comparing the sample peaks

with those produced from standard calibration solutions, the concentration of each ion is automatically determined.

2.8   Factorial Analysis

Several studies in this project were based on a factorial experimental design to investigate the effects of various variables (which could be between two and four in number) on the measured outcome whilst minimising the number of samples for the experiments. The following section explains the layout of a factorial experiment and its mathematical interpretation.

2.8.1   Factorial design

A typical factorial design used in this study is as follows: for each variable, high (F= +1), intermediate (F= 0) and low values (F= -1) in the ratio of 4: 2: 1 (or as close as possible) are chosen. The combinations of these variables for each formulation are determined according to the factorial design (Table 2.1), which varies the F levels of the variables systemically. In total, for an experiment involving three or four variables, nine different formulations are tested with the 'intermediate' sample repeated in sample ten. An outcome is measured for these ten samples. The samples C1 and C10 have all variable values at the 'intermediate' levels (F = 0), and the remaining eight samples, C2 to C8, have only the low or high variable values with corresponding F terms of -1 or +1. Each high or low value of each variable is used in half of these eight samples (see Table 2.1). On averaging a given set of four samples F will be +1 or -1 for one variable only. F terms for all other variables (and the effects of their different values) will cancel (F = 0). For

example, samples C2 to C5 all have F for the first variable being equal to +1 but two each

of +1 and -1 for variable 2, 3 and 4. By comparing the average outcome for samples C2 to

C5 with that for C6 to C9, the effect of variable 1 alone can be obtained. Similarly,

comparing the average outcome for samples C2, C5, C7 and C9 with that for C3, C4, C6

and C8 gives the effect of variable 2, and so on.

Table 2.1. Sample combinations for a factorial experimental design involving three to four variables. Each variable contains three levels with F term being +1 for high, 0 for intermediate and -1 for low values.

Sample formulation	Variable 1	Variable 2	Variable 3	Variable 4
C1	0	0	0	0
C2	+1	+1	-1	-1
C3	+1	-1	+1	-1
C4	+1	-1	-1	+1
C5	+1	+1	+1	+1
C6	-1	-1	-1	-1
C7	-1	+1	-1	+1
C8	-1	-1	+1	+1
C9	-1	+1	+1	-1
C10	0	0	0	0

2.8.2 Mathematical interpretation

Where the results of the experiment follow the factorial analysis reasoning,

interpretation of the results could be compared mathematically using the following

rationale.

The rates of reactions and levels of components in a reaction at equilibrium are generally proportional to the concentrations of components to some power, b_i. This gives Equation 2.13 and in logarithmic form, Equation 2.14.

$$Q = k \times V_1^{b_1} \times V_2^{b_2} \times V_3^{b_3} \times V_4^{b_4} \qquad\qquad 2.13$$

$$\ln Q = \ln k + \sum_{i=1}^{4} b_i \ln V_i \qquad\qquad 2.14$$

Where Q is a measured outcome at a given time and V_i the value of a variable i in the experiment. It is therefore reasonable to assume that the measured outcome (in the following studies e.g. polymerisation fraction, % drug release) at a given time for all the samples will be given by an analogous factorial design equation of the form

$$\ln Q_c = B_0 + \sum_{i=1}^{4} B_i F_i + \sum_{j=2}^{4} B_{1,j} F_1 F_j \qquad\qquad 2.15$$

Where c represents the sample number and i or j represents the variable number. All F terms equal -1 or +1, for samples C2 to C9 and zero for samples C1 and C10 and refer to whether each variable has its low, intermediate or high value in the sample (see Table 2.1). Using the methods below the eight B parameters are obtainable using samples C2 to C9.

B_0 is an average value of the natural logarithm of the measured outcome (e.g. polymerisation fraction) for samples C2 to C9. It can be calculated using excel and the Equation 2.16.

$$B_0 = \frac{1}{8} \sum_{C=2}^{9} \ln Q_c \qquad\qquad 2.16$$

In most studies in this project, the values chosen for low, intermediate and high levels for each variable were all in (or close to) the ratio of 1:2:4. If Equation 2.14 is therefore valid for all data, then exp B_0 calculated using samples C2 to C9 will equal the results for sample C1 and its repetition C10. This was not the case for every experiment done in this project and therefore interpretation of the results in this case was done by graphical methods only.

The design of the experiment enables effects of each variable 1 to 4 on the measured outcome (e.g. polymerisation fraction) to be calculated using Excel and Equation 2.17.

$$B_i = \frac{1}{8}\sum_{C=2}^{9} F_i \ln Q_c \qquad\qquad 2.17$$

In this particular study, exp B_i will be the amount by which the measured outcome is multiplied by, when the value of variable i is doubled from its low to intermediate or intermediate to high value.

Any interaction effects between pairs of variables can also be calculated using Equation 2.18.

$$B_{1,j} = \frac{1}{8}\sum_{C=2}^{9} F_1 F_j \ln Q_c \qquad\qquad 2.18$$

In this study $B_{1,2}$ is a measure of the interaction effect between variables 1 and 2 (or 3 and 4), $B_{1,3}$, variables 1 and 3 (or 2 and 4) and $B_{1,4}$, variables 1 and 4 (or 2 and 3). If variable 1 has the most effect on the measured outcome under investigation, then the interaction is most likely with this variable (rather than the parings in the brackets). If

there are significant interaction terms for a set of data, and it cannot be elucidated by logic which pairings are important, then a further set of eight samples is required for a factorial design involving four variables. For example, in the factorial experiment for determining the effects of four variables on polymerisation fraction, only two variables were found to have any significant effects and the pairings of which variables to be involved in an interaction effect could be easily deducted. Exp $B_{i,j}$ is the amount that the measured outcome must be multiplied or divided by if the values of variables i and j are both doubled or one doubled and the other halved respectively.

3 Synthesis and Polymerisation Kinetics of Monomers

3.1   Background

Fluid, and therefore injectable polymers, have the advantage that they can be moulded into a bone void of any shape and size before curing *in vivo* into a solid that is adhesive to the immediate surroundings.   These materials offer a minimally invasive surgical technique for insertion into the body and could potentially be cured using either a light or chemical initiated free radical polymerisation process.   The chemical cure method may be more convenient for use in deep fractures occurring in some bones but light curing is potentially easier to control and less prone to surface oxygen inhibition problems and moisture effects with thin samples (193).   In the latter the liquid polymer can be easily introduced into the body through needle injections and can be photocured with fibre optic cables using arthroscopic techniques (39) .

Injectable biodegradable polymers that have been investigated include poly(ether-esters) (99;100), poly(anhydrides) (41;101;102), and poly(propylene fumarate) (73;104;105;194).   In several studies attachment of acrylate or methacrylate groups on the chain ends of these monomers enabled them to crosslink and set with light or chemical cure activation.   These injectable polymers are, however, generally of low modulus in comparison with bone (1;13).   It is also difficult to find detailed kinetic investigations for injectable degradable polymers that provide any understanding of how various monomer variables affect polymerisation rates.

The work of this chapter was to synthesise new monomers consisting of ABA poly(ester –co- propylene glycol –co ester) tri-block oligomers with methacrylate group at each end.   Two sets of the monomers of systematically changing ester/ PPG molar ratio were produced: one set containing D,L-lactide as the A block and the other containing

glycolide. The aim of this work was to produce more hydrophobic monomers than mentioned above that provide greater control over water sorption rates and thereby degradation and drug release rates as well as mechanical properties. These will be presented in later chapters but the following will concentrate on chemical characterisation of the monomers and their polymerisation.

Firstly a combination of FTIR, Raman and NMR were used to identify the products and confirm success of the syntheses; detailed structural characteristics of the monomers were elucidated as this information will be useful in understanding the physical properties of the polymers in later chapters.

Secondly a combination of Raman and FTIR techniques was used to quantify light curing polymerisation kinetics of the monomers. In many of the degradable (meth) acrylate formulations so far developed, low power ultra violet (UV) irradiation with 2 to 12 minutes light exposure have been used for curing (100;108;195;196). For these materials to be used as injectable clinical bone materials much shorter light exposure times which can fully cure polymer layers would be desirable (197). Incomplete polymerisation would lead to concern, over release upon degradation, of more toxic double bond-containing components. If the material is additionally to be used as a controlled drug release reservoir, drug damage by UV exposure or "burst release" (198) due to slow polymerisation could occur. In this work a blue dental light was therefore used to cure the polymers. The blue light emits radiation in the range of 420-490 nm, which is where CQ absorbs most (λ_{max} = 470 nm) (199). Factorial analysis was used to quantify simultaneously the effects of initiator concentration, light exposure time and monomer structure on polymerisation kinetics.

3.2   Materials and methods

3.2.1   Variation of monomer structure

In order to limit the number of oligomeric monomers that needed to be produced in each set whilst allowing assessment of the effects of changing chemical structures on material properties, a three-level factorial design varying two parameters for the synthesis - the PPG molecular weight and the length of ester linkage - was employed. The high, low and intermediate values for each parameter and the five resultant systematically changing ABA tri-block poly(PG-co-ester) dimethacrylate monomers are presented in Table 3.1.

Table 3.1 (a) Variable levels for the monomer synthesis and (b) monomers synthesised.

(a)

	n for PPG [1]	m for ester linkage
Low level (-)	7	2
Intermediate level (0)	17	4
High level (+)	34	8

[1] The PPG molecular weight for $n = 7$ is 425; for $n = 17$ is 1000; and for $n = 34$ is 2000 g/ mol.

(b)

Monomer Code[2]	PPG M_w[3] (g/ mol)	Lactide or Glycolide / PPG (mol/mol)
P34L8DMA / P34G8DMA	2000 (+)	8 (+)
P34L2DMA / P34G2DMA	2000 (+)	2 (-)
P17L4DMA / P17G4DMA	1000 (0)	4 (0)
P7L8DMA / P7G8DMA	425 (-)	8 (+)
P7L2DMA / P7G2DMA	425 (-)	2 (-)

[2] The number after 'P' denotes the propylene glycol units (n) and the number after 'L' or 'G' denotes the length of lactide or glycolide linkage in lactic or glycolide acid units on either side of the PPG (m).
[3] Provided by Sigma Aldrich

In order to distinguish the monomers, the intermediates are coded as PnLm or PnGm, where the subscript n denotes the propylene glycol units, and m denotes the lactide (L) or glycolide (G) chain length on either side of the PPG block, in lactic / glycolic acid units. The final products are coded as PnLmDMA or PnGmDMA, where DMA stands for dimethacrylates.

3.2.2 Synthesis of poly(propylene glycol-co-ester) dimethacrylate monomers

The ABA triblock poly(PG-co-ester) dimethacrylate monomer was synthesised using a parallel synthesis equipment (Radley®) (200) in a two-step reaction as illustrated in Figure 3.1.

For the synthesis of poly(PG-co-lactide) dimethacrylate monomers, approximately 10 to 40 g PPG (molecular weight of 425 and 2000 or 1000 g/mol) was reacted with D,L-lactide (molar ratios of 2 and 8 or 4) under vacuum at 150 °C in a nitrogen atmosphere for 6 hours, using stannous octoate (0.05 % (gram per gram) of PPG) as a catalyst. The resultant poly(PG-co-lactide) co-oligomer was purified by dissolving in propan-2-ol and filtering to remove any unreacted solid lactide.

In the methacrylate termination reaction, the co-oligomer was dried and dissolved in dichloromethane at a concentration of 0.20 mol/l. After cooling to 0 °C, triethylamine (TEA) and methacryloyl chloride (MAC) were added at a ratio of 4 mol/mol of the poly(PG-co-lactide) co-oligomers, with the MAC being added dropwise after adding in TEA. This co-oligomer to TEA and MAC molar ratio was found to be the optimal level for full methacrylate oligomer reaction in both our own preliminary studies and those by Xie *et al* (201). The reaction mixture was stirred for 24 hours at room temperature. The mixture was then filtered and washed with 100 ml acetone three times to remove

triethylamine hydrochloride. The acetone was removed by rotary evaporation and the

dried mixture extracted with 100 ml hexane three times in order to obtain the final product,

poly(PG-co-lactide) dimethacrylate. In this hexane extraction, partial fractionation was

achieved as two layers were obtained- products with lactide to PPG reaction molar ratios

of equal to or less than 4 were extracted into the top filtrate layer whereas others remained

as sediments in the bottom layer. The appropriate layer was collected, condensed via

rotary evaporation, and dried under vacuum overnight.
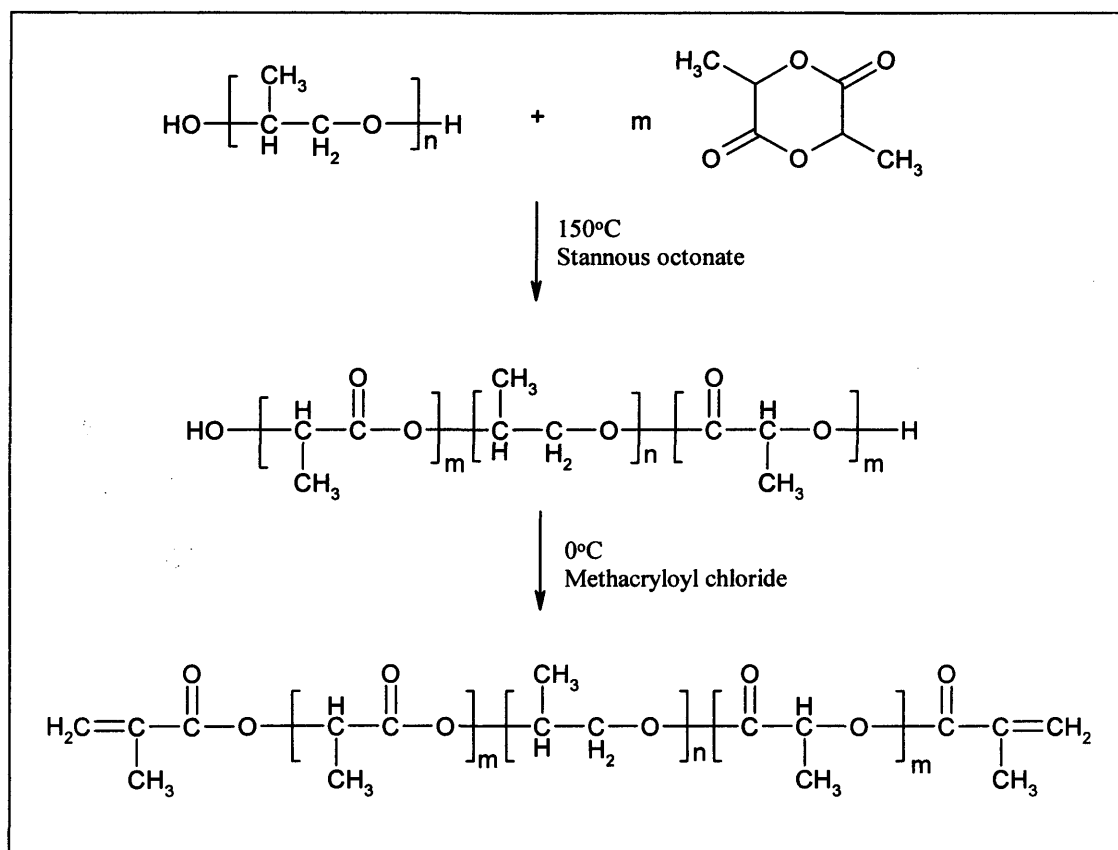
Figure 3.1. Synthesis scheme for poly(PG-co-lactide) dimethacrylate co-oligomeric monomers.

For the synthesis of poly(PG-co-glycolide) dimethacrylate monomers, the synthetic procedures were the same as described above with the exception that a temperature of 180 °C was used for the polymerisation of glycolide to PPG.

The intermediate and overall reaction yields were calculated using Equation 3.1 and 3.2.

$$Y_I \text{ or } Y_E \text{ (\%)} = \frac{G_{obt}}{G_{exp}} \times 100 \qquad\qquad 3.1$$

$$Y_O \text{ (\%)} = \frac{Y_I \times Y_E}{100} \qquad\qquad 3.2$$

Where Y_I and Y_E and Y_O are the reaction yields of the intermediate products (PnLm or PnGm), end products (PnLmDMA or PnGmDMA) and of the overall synthesis, respectively; G_{obt} and G_{exp} are the obtained and expected mass of product.

Throughout the project two batches of all five monomers were synthesised for the poly(PG-co-lactide) dimethacrylates, which were assigned the following lot numbers: (i) 180803 and (ii) 091104. These monomers were subsequently used for further investigation of the polymer properties which will be discussed in later chapters. Only one batch of the poly(PG-co-glycolide) dimethacrylate monomers were produced and were not used for further study.

The structures and compositions of the poly(PG-co-ester) dimethacrylate monomers were identified by FT-IR, Raman and ^{1}H-NMR spectroscopy.

3.2.3 Raman and FITR Monomer Spectra

Attenuated Total Reflectance Fourier Transform Infra-Red (ATR-FTIR) and

Raman spectra of the PPG oligomers, the intermediate poly(PG-co-ester) co-oligomers

and the end poly(PG-co-ester) dimethacrylate monomers were obtained using a Perkin

Elmer series 2000 FTIR/ Raman spectrometer. Peak assignments were made by

comparing spectra of the starting materials, intermediates, final products and literature.

3.2.3.1 Quantitative analysis of FTIR peak heights

According to Beer's Law, the absorbance of each chemical group should be

proportional to its concentration in the layer of the sample that is in contact with the ATR

diamond. Attempts were therefore made to determine quantitative relationships between

the fraction of the ester and methacrylate units in the monomer and the FTIR absorbance

of a peak representative of each chemical group. From the reaction scheme, the expected

ratio of PG : ester in each intermediate product is $n/2$: m (see Figure 3.1). The fraction of

units that are ester (a_{LA} for lactide and a_{GL} for glycolide) in each intermediate product was

calculated using Equation 3.3.

$$a_{LA} = \frac{m}{\left[\dfrac{n}{2} + m\right]} \quad \text{or} \quad a_{GL} = \frac{m}{\left[\dfrac{n}{2} + m\right]} \qquad\qquad 3.3$$

The fraction of units that are methacrylates (a_{MA}) in each end product was calculated using

Equation 3.4.

$$a_{MA} = \frac{1}{\left[\dfrac{n}{2} + m + 1\right]} \qquad\qquad 3.4$$

The 1744 cm^{-1} peak in the intermediate product spectra and the 1640 cm^{-1} peak in the end product spectra are representative of the ester and methacrylate groups in the monomers respectively. The heights of these peaks above background (i.e. 1800 cm^{-1}) were determined and plotted against a_{LA} or a_{GL} and a_{MA}. Linear regression of the plots was calculated. Any samples deviating significantly from a straight line would be suggestive of incomplete reaction.

3.2.3.2. Quantitative analysis of Raman peak heights

From the reaction scheme (Figure 3.1), the ratio of peak heights above background intensity I, at 1765 and 1640 cm^{-1} due to the polyester and methacrylate respectively should be proportional to *m* if one methacrylate group attaches to both ends of the co-oligomer. The ratios of these two peak heights above background in the end product spectra were plotted against the number of *m* units in the final monomers and the linear regression determined. Any samples deviating significantly from a straight line would be suggestive of inconsistent methacrylate termination level between the samples.

3.2.4 Monomer ^{1}H-Nuclear Magnetic Resonance (NMR) Spectra

One dimensional ^{1}H-Nuclear Magnetic Resonance (NMR) spectra were obtained at 25 °C on a Varian *Unity plus* 500 MHz instrument using 5 mm o.d. tubes with deuterated chloroform ($CDCl_3$) as solvent. The ^{1}H-NMR spectra of PPG oligomers, intermediate poly(PG-co-ester) co-oligomers and end poly(PG-co-ester) dimethacrylate monomers were obtained. Peak assignments were determined by comparison with spectra for the corresponding starting materials, and/ or use of standard literature values in journals (82;100;201;202). Several parameters were determined from the ^{1}H-NMR spectra using

151

relevant peaks including: (i) the average length of the ester chains, m, in each monomer; (ii) the total lactide (LA) or glycolide (GL) groups per propylene glycol (PG) unit; (iii) the number of end LA_e or GL_e per PG unit; and (iv) the number of methacrylate (MA) groups per PG unit (see Section 3.3.1.4d & 3.3.2.4d). The total molecular weights of the monomers could then be calculated using the above information.

3.2.5 Polymerisation kinetics studies

The five poly(PG-co-lactide) dimethacrylates (monomer batch number 180803) were used in order to study the polymerisability and setting of the monomers. Four variables, which could affect the reaction kinetics, were examined based on a factorial experimental design. These variables were (i) PPG n level (i.e. 34, 17, 7); (ii) lactide linkage m level (i.e. 8, 4, 2); (iii) time of UV light exposure (i.e. 240 s, 120 s, 60 s) and (iv) CQ and DMPT concentration (i.e. 2, 1, 0.5 wt%). According to the factorial design (see Table 2.1 in Chapter 2), 0.5 or 2 wt % of both CQ and DMPT were added to the four monomers produced using PPG 425 or 2000 g/mol and lactide 2 or 8 mol/mol PPG; and 1 wt% of both CQ and DMPT were added to the single PPG 1000 g/mol and lactide 4 mol/mol PPG based "intermediate" formulation. The combinations of the ten formulations, with the intermediate formulation being a duplicate, are presented in Table 3.2.

In order to aid dispersion of the initiators, 10 wt% of hydroxyethyl methacrylate (HEMA) was included in each sample. The appropriate ratios of poly(PG-co-lactide) dimethacrylate monomer, CQ, DMPT and HEMA, were mixed thoroughly for each formulation in a darkened room and kept in an amber glass prior to use.

Table 3.2. Combinations of the ten formulations investigated for reaction kinetic studies. Note that according to the factorial design (Table 2.1 Chapter 2), there are two identical formulations for the intermediate formulation with P17L4DMA.

Monomer code	Photoinitiator concentration (wt%)	Light exposure time (sec)
P34L8DMA	0.5	60
P34L8DMA	2	240
P34L2DMA	0.5	240
P34L2DMA	2	60
P17L4DMA	1	120
P17L4DMA	1	120
P7L8DMA	0.5	240
P7L8DMA	2	60
P7L2DMA	0.5	60
P7L2DMA	2	240

After gaining a Raman spectrum, each monomer mix was placed in a ring of 8 mm diameter and 1 mm depth positioned centrally on the Golden Gate™ heated diamond ATR top-plate (Specac) in the FTIR spectrometer. The temperature was kept at 37 °C to mimic normal body condition, using a 3000 Series™ high stability temperature controller with RS232 control (Specac). The top surface of the sample was then sealed with acetate sheet to prevent oxygen inhibition of polymerisation. FTIR spectra of the lower few microns of the sample in contact with the diamond were obtained. The 'Timebase software' from Perkin Elmer was used to monitor the spectral changes in the sample continuously. Resolution was set at 4 cm^{-1} and wavenumber range between 500 and 4000 cm^{-1}. Number of scans was fixed at 8, which means an average absorbance spectrum for the sample was acquired every 46.2 seconds. The total run time was set between 30 and 55 minutes, generating approximately 39 to 71 spectra for the samples. At 2 minutes after start of

spectral collection, the eight formulations containing PPG 425 or 2000 g/mol and LA 2 or

8 mol/mol PPG were exposed to blue light [*Coltolus* dental light curing gun, 400 mW/cm^2,

Coltene®] for either 60 or 240 seconds (see Table 3.2). The 'intermediate' formulation

had 120 seconds of light exposure. The monomer mix was then covered with an inverted

box until the run was finished. The polymerised disc was finally detached from the ATR

unit and after a further 24 hours a Raman spectrum obtained. Three repeat runs were

performed for each sample to assess data reproducibility.

The final extent of polymerisation for each sample was determined by comparing

Raman spectra of the 24-hour samples with their corresponding spectra prior to

polymerisation. In addition, by combining Raman and FTIR results the level of reaction

as a function of time was calculated (for details see Section 3.3.3).

3.3 Results

3.3.1 Poly(PG-co-lactide) dimethacrylate monomers

3.3.1.1. Monomer synthesis of poly(PG-co-lactide) dimethacrylate monomers

Table 3.3 shows the appearance and fluidity of the five monomers and the

percentage reaction yields of the two different batches synthesised. Initially all five

monomers were fluid in nature and therefore injectable as required; the longer the lactide

chain length, the more viscous the monomer. Those prepared with lactide to PPG ratios of

8 were the most viscous and were found to gel in short time with storage at 4 °C. Reaction

yields varied from batch to batch synthesis but were all consistently greater when the ratio

of lactide to PPG was low. The intermediate yield ranged between 75 to 99 %. The

overall yield from the two-step reaction scheme ranged between 22 to 90 %.

Table 3.3. Appearance, viscosity and intermediate and overall reaction yield of poly(PG-co-lactide) dimethacrylate monomers of different batches synthesised

Monomer code	Monomer appearance	Viscosity	Reaction yield %			
			Lot no: 180803		Lot no. 091104	
			Interme-diate	Overall	Interme-diate	Overall
P34L8DMA	Pale yellow liquid	Viscous	93	65	78	40
P34L2DMA	Yellow liquid	Fluid	99	90	97	77
P17L4DMA	Yellow-orange liquid	Fluid	99	58	96	22
P7L8DMA	Yellow liquid	Highly viscous	98	73	76	52
P7L2DMA	Yellow-orange liquid	Fluid	99	86	96	72

3.3.1.2. FT-IR of poly(PG-co-lactide) dimethacrylate monomers

(a) Peak assignments

Figure 3.2 shows example FTIR spectra of a PPG (i.e. P7), a poly(PG-co-lactide)

co-oligomer (i.e. P7L2) and a poly(PG-co-lactide) dimethacrylate (i.e. P7L2DMA). The

FTIR spectra are consistent with the reaction scheme (Figure 3.1). The PPG FTIR spectra

(Figure 3.2) give, as expected, absorption peaks at 1452 cm^{-1} and 1372 cm^{-1} due to C-H

stretches, and an absorption peak at 1088 cm^{-1} due to C-O stretches. In the FTIR spectra

of poly(PG-co-lactide) and poly(PG-co-lactide) dimethacrylate these peaks remain but

there are additional strong peaks at 1745 cm^{-1} and 1184 cm^{-1} due to, respectively, the C=O

and C-O groups of the oligo-lactide. The lack of corresponding cyclic lactide peaks (e.g.

C-O in benzoic ester) at 1248 cm^{-1} and 1145 cm^{-1} indicate that this has been fully reacted

or extracted during purification of the intermediate products. The OH absorption band at

3446 cm^{-1} of PPG and poly(PG-co-lactide) disappears in the FTIR spectrum of the

monomer on methacrylation. In the latter, the peaks at 1640 cm^{-1} and 1155 cm^{-1} are

attributed to C=C stretches and C-H bends of the methacrylate groups of the monomer,

respectively. Main FTIR peak assignments are summarised in Table 3.4.
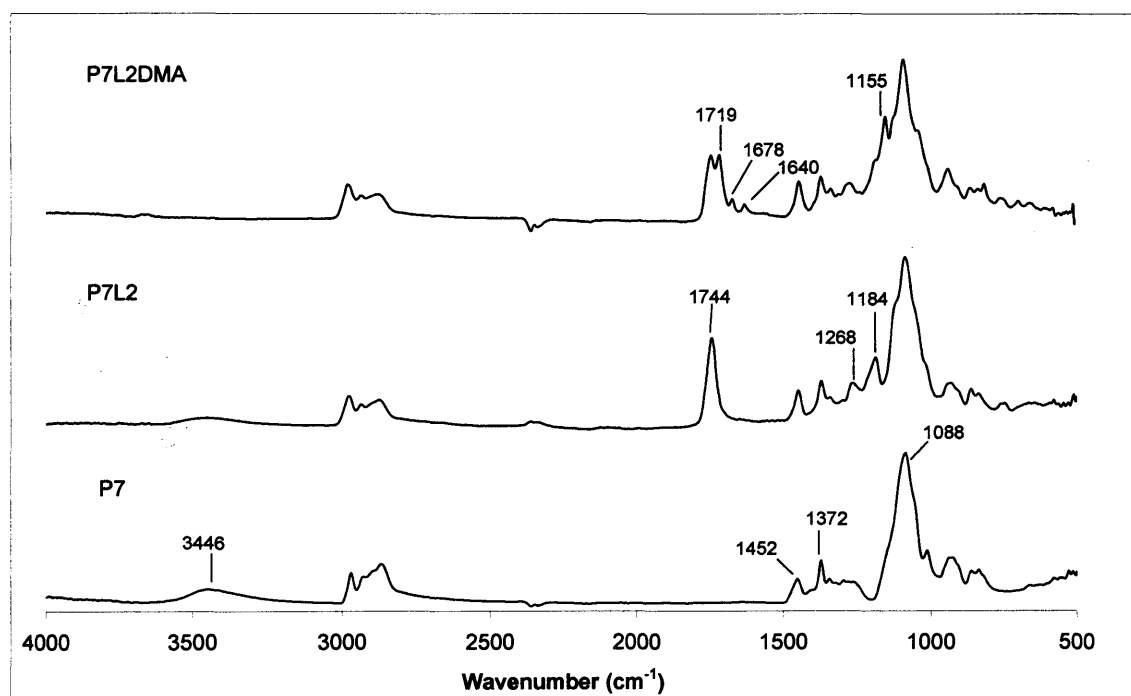
Figure 3.2. FTIR spectra of a PPG (molecular weight 425 i.e. P7), a poly(PG-co-lactide) co-oligomer (i.e. P7L2) and a poly(PG-co-lactide) dimethacrylate (i.e. P7L2DMA).

Table 3.4. PPG, poly(PG-co-lactide) and poly(PG-co-lactide) dimethacrylate FTIR peak assignments.

Wavenumber (cm^{-1})	Strength*	Assignment	Chemical group
PPG spectrum			
3446	m	O-H stretch	PPG hydroxyl OH
1452	m	C-H scissor	PPG methylene -CH$_2$-
1372	m	C-H bend	PPG methyl -CH$_3$
1088	s	C-O-C asymmetrical stretch	PPG ether C-O-C
Poly(PG-co-LA) spectrum			
1744	s	C=O stretch	Lactoyl ester –(O=)C-O-R
1268	m	C-O stretch	Lactoyl ester –(O=)C-O-R
1184	m	C-O stretch	Lactoyl ester –(O=)C-O-R
Poly(PG-co-LA) dimethacrylate spectrum			
1719	m	C=O stretch	Methacrylate carbonyl C=O
1678	w	C=O stretch	Methacrylate carbonyl C=O
1640	w	C=C stretch	Methacrylate olefin RHC=CH$_2$
1155	m	C-H bend	Methacrylate methyl –CH$_3$

*s= strong, m= medium and w= weak
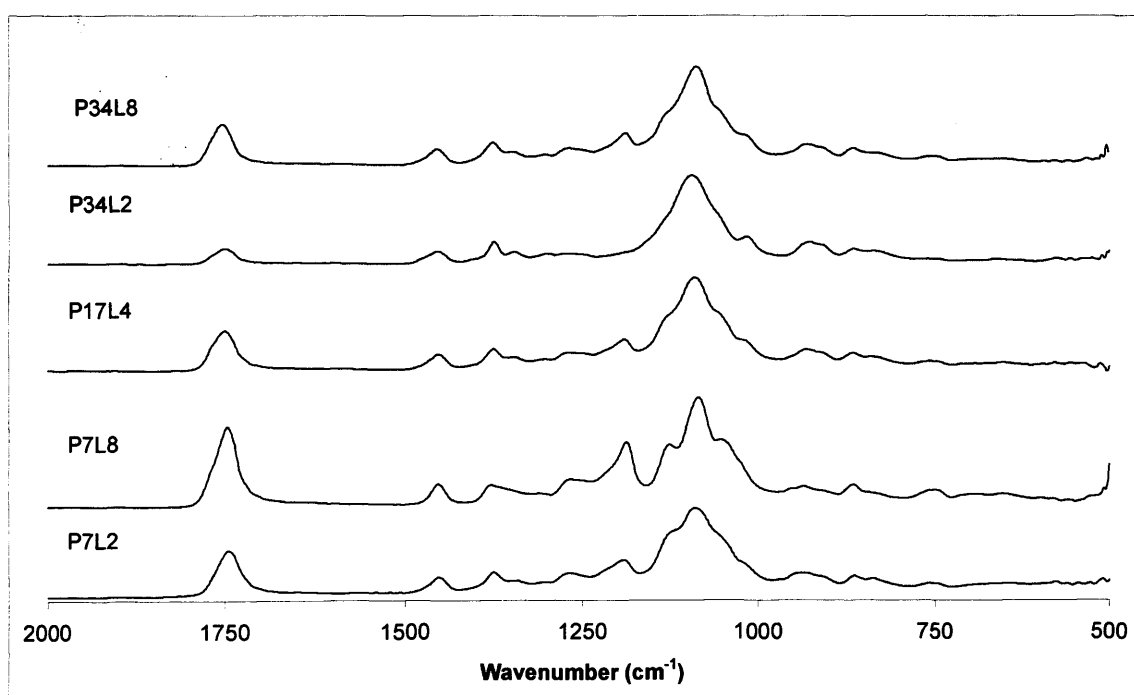
Figure 3.3. FTIR spectra of poly(PG-co-lactide) co-oligomeric monomers (Lot no. 180803).

Figure 3.4. **FTIR spectra of poly(PG-co-lactide) dimethacrylate co-oligomeric monomers (Lot no. 180803).**

(b) Quantitative analysis of peak heights

Figure 3.3 and Figure 3.4 show the FTIR spectra of the five co-oligomeric monomers after the intermediate and final synthetic stages respectively. With ATR FTIR spectroscopy, the lower surface (at the magnitude of a few microns depth) of samples in contact with the ATR FTIR diamond is analysed. Any absorbance above background due to chemical groups (assuming no interaction effects) is expected to be proportional to their concentrations in the molecules in close contact with the diamond. The areas for the lactoyl peaks relative to those for the PPG in both the intermediate and final spectra can be seen as proportional to the PPG n / LA m ratios in the monomer structure. Monomers with a higher proportion of n relative to m units (i.e. P34L2: $n/2m$= 8.5) have a relatively much bigger PPG peak (1088 cm^{-1}) than the lactoyl peaks (1744 cm^{-1} and 1184 cm^{-1}).

Those with comparable proportions of n and m in their structures (i.e. P7L2, P17L4 and

P34L8: $n/2m$ = 1.8, 2.1 and 2.1, respectively) show similar ratios of PPG peak areas

relative to lactoyl peak areas. The monomer P7L8 ($n/2m$= 0.4) have both prominent PPG

and lactoyl peaks in the spectrum. As regards to the methacrylate peaks, P7L2DMA and

P34L8DMA are expected and observed (see Figure 3.4) to have the largest and smallest

1640 cm^{-1} peaks respectively.

Table 3.5 shows the equations and the linear regression co-efficients obtained for

the absorbance (A_v) of 1744 cm^{-1} and 1640 cm^{-1} peaks, above background levels at 1800

cm^{-1}, with respect to the fraction of lactoyl (a_{LA}) and methacrylate (a_{MA}) units in the

intermediate and end products respectively, for each batch synthesised.

Table 3.5. The absorbance of the 1744 cm^{-1} and the 1640 cm^{-1} peaks (above background levels at 1800 cm^{-1}) with respect to the fraction of lactoyl (a_{LA}) and methacrylate (a_{MA}) units in the intermediate and final products respectively.

Batch number	From intermediate spectra		From end product spectra	
	Equation*	R^2 value	Equation	R^2 value
180803	$A_{1744} - A_{1800} = 0.76a_{LA}$	0.99	$A_{1640} - A_{1800} = 0.32a_{MA}$	0.96
091104	$A_{1744} - A_{1800} = 0.75a_{LA}$	0.97	$A_{1640} - A_{1800} = 0.28a_{MA}$	0.93

*A_v is the absorbance at wavenumber v.

The comparable equations for the two batches with their high R^2 values indicate

reproducibility of the first synthetic stage and can be used to estimate the relative ratios of

lactide to PPG when FTIR absorbance of the 1744 cm^{-1} peak above background is known.

The greater variability in the equations obtained during the final stage of the synthesis

indicate variations in the efficiency of methacrylation of the monomers, which would be

determined in more detail later using NMR.

3.3.1.3. Raman of poly(PG-co-lactide) dimethacrylate monomers

(a) Peak assignments

Raman spectroscopy provides complementary structural information to FTIR.

Figure 3.5 shows example Raman spectra of a PPG (i.e. P7), a poly(PG-co-lactide) co-

oligomer (i.e. P7L2) and a poly(PG-co-lactide) dimethacrylate (i.e. P7L2DMA). The

spectra confirm the presence of the chemical groups and give several strong peaks that are

indistinct or weak on the equivalent FTIR spectra. These include peaks at 3110 cm^{-1} and

1407 cm^{-1} (both C-H stretches attached to C=C), 1719 cm^{-1} and 1678 cm^{-1} (both C=O

stretches), and 1640cm^{-1} (C=C stretch). The three main peaks at $\sim 3000 \text{ cm}^{-1}$ also

correspond to C-H stretches. The peak at $\sim 2875 \text{ cm}^{-1}$ is attributed to the methylene (CH$_2$)

groups of PPG; the number per unit volume of these groups decreases in the intermediate

and end product samples (with increasing ratios of lactide to PPG) resulting in a reduced

intensity of this peak relative to the other two C-H peaks in the latter two spectra. The

peaks at 2975 and 2940 cm^{-1} are attributed to the methyl (CH$_3$) and methine (R$_3$CH)

groups of the molecule respectively whose relative concentrations will vary little with

reaction (see Figure 3.1). The greater intensity and separation of the 1640 cm^{-1} Raman

peak makes it more sensitive to levels of methacrylate than FTIR and is therefore useful

for quantifying monomer content and polymerisation extents (see later in Section 3.3.3.1).
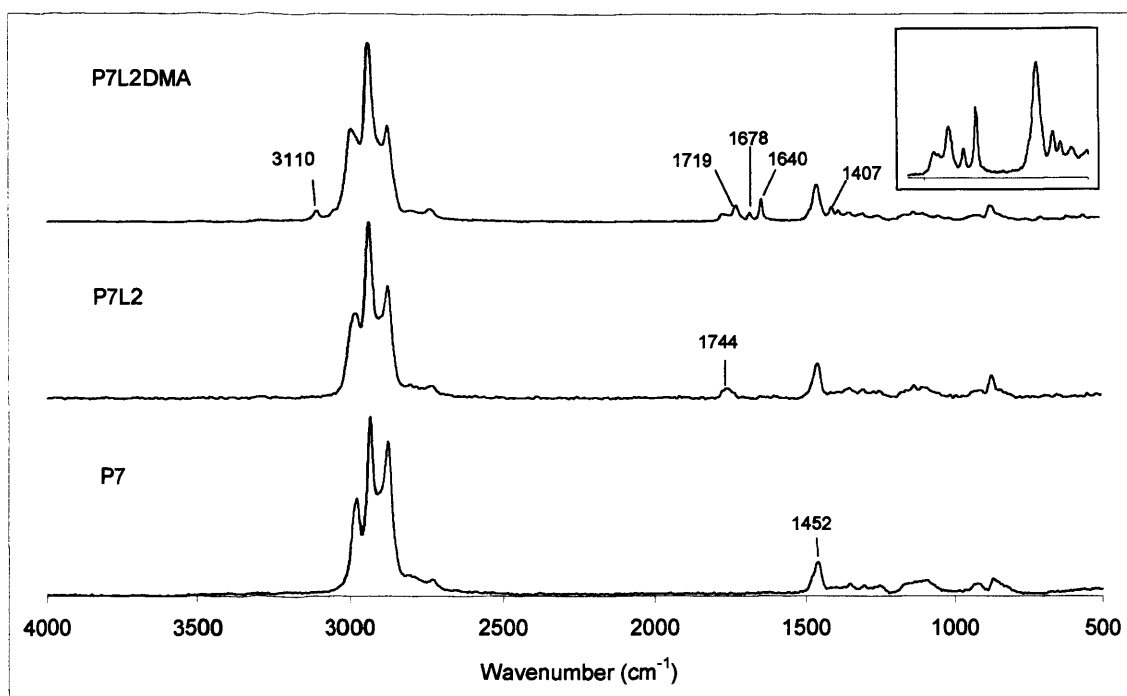
Figure 3.5. FT-Raman spectra of a PPG (molecular weight 425 i.e. P7), a poly(PG-co-lactide) co-oligomer (i.e. P7L2) and a poly(PG-co-lactide) dimethacrylate (i.e. P7L2DMA). The inset shows an amplification of the P7L2DMA spectrum in the region between 1300 and 1850 cm^{-1}.

(b) Quantitative analysis of Raman peaks

Raman spectra of the five monomers after background subtraction are shown in Figure 3.6. Unlike ATR FTIR spectra, the intensity of Raman spectra can vary significantly with time due to laser variations but relative peak heights should remain constant. In this case, quantitative analysis must use relative peak heights. In Figure 3.6 the spectra are normalised by the peak at 2940 cm^{-1}. Relative to this C-H peak the shorter monomers, which contain more end methacrylate groups per unit volume in a specimen, have the strongest methacrylate peaks. The monomer P7L2DMA, which has the highest methacrylate to PPG plus lactoyl group ratio (i.e. 2 methacrylate groups to 11 of $n + 2m$ groups), exhibits the highest intensity of the relative methacrylate peak. For P7L8DMA, P17L4DMA and P34L2DMA monomers, the ratios of the number of methacrylate groups

161

to that of PPG plus lactoyl groups are 2 to 23, 2 to 25 and 2 to 38, respectively. As such, these monomers show intermediate relative methacrylate peak strengths. The monomer P34L8DMA has 2 methacrylate groups relative to 50 groups of PPG plus lactoyl moieties, and peak intensity for the methacrylate peak is therefore the weakest.
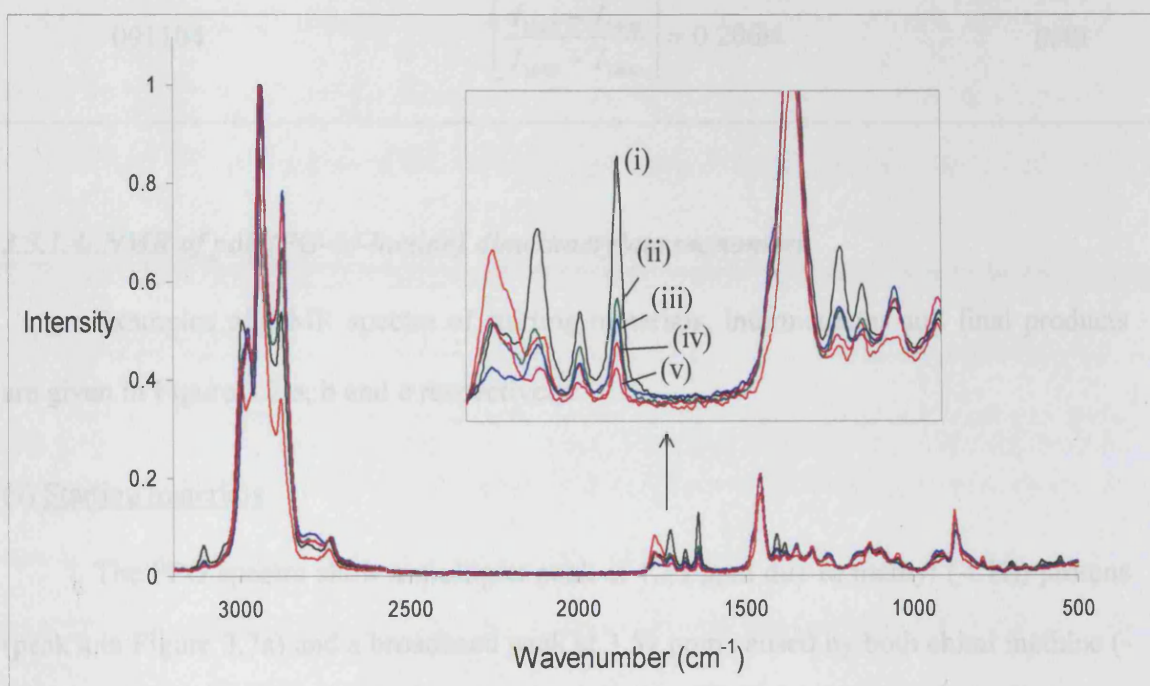
Figure 3.6. FT-Raman spectra of poly(PG-co-lactide) dimethacrylate co-oligomeric monomers: (i) P7L2DMA, (ii) P17L4DMA, (iii) P34L2DMA, (iv) P7L8DMA & (v) P34L8DMA.

Table 3.6 shows the results of the linear regression plots of the relative ratios of the peak heights I at 1765 cm^{-1} (lactoyl C=O) and 1640 cm^{-1} (methacrylate C=C) above background intensity against m. The low R^2 value especially in the 091104 batch indicates that not all monomers were attached with two methacrylate groups and there was a greater variation of methacrylate attachment between the different monomers, as will be confirmed later in NMR analysis.

Table 3.6. **Linear regression of the relative ratios of 1765 cm^{-1} and 1640 cm^{-1} peak heights above background intensity against m units in the monomer products.**

Batch number	From final Raman spectra	
	Equation	R^2 value
180803	$\left[\dfrac{I_{1765} - I_{1800}}{I_{1640} - I_{1800}}\right] = 0.243m$	0.91
091104	$\left[\dfrac{I_{1765} - I_{1800}}{I_{1640} - I_{1800}}\right] = 0.206m$	0.49

3.3.1.4. NMR of poly(PG-co-lactide) dimethacrylate monomers

Examples of NMR spectra of starting materials, intermediates and final products are given in Figure 3.7 a, b and c respectively.

(a) Starting materials

.. The PPG spectra show a multiplet peak at 1.13 ppm due to methyl (-CH$_3$) protons (peak a in Figure 3.7a) and a broadened peak at 3.54 ppm caused by both chiral methine (-CH-) and methylene (-CH$_2$) protons (peak b). Unreacted cyclic lactide has a doublet at 1.68 ppm and a quartet at 5.04 ppm with peak areas in the expected ratios for attached CH$_3$ and CH groups (spectrum not given).

(b) Intermediate products

In the poly(PG-co-lactide) spectra, the original PPG peaks are slightly shifted in shape due to reaction of the terminal OH groups (compare peaks a and b with a' and b'). There are also new peaks at 1.54 ppm (c' in Figure 3.7b) arising from the presence of linear oligo - lactide CH$_3$ groups. The terminal OH groups give broad bands at ~2.80 ppm

(peak f'). Multiplets at 5.11 ppm (d') and 4.35 ppm (e') can be assigned to linear oligo-

lactide CH protons in the chains and adjacent to the terminal OH group respectively. The

peaks at 1.68 ppm due to the CH_3 protons of any residue cyclic D,L-lactide (peak c) are

very small. It must be noted that assignment of each individual signal to individual

proton(s) in each lactic acid unit in the oligolactic acid chain was difficult to achieve for

two reasons (180): (i) because D,L-lactide was used, enantiomers of lactic acid (e.g. LL,

DD or LD, DL), which are diastereomerically different, led to complicated splitting of the

signals ;and (ii) the different stereoisomers of each PG and lactoyl unit could cause

overlapping of the resonances.

(c) Final products

All final dimethacrylate ^{1}H-NMR spectra exhibit three additional peaks to those

observed for the intermediates (see Figure 3.7c). Those at 5.64 and 6.21 ppm (peak h")

can be assigned to olefinic protons i.e. protons beside the C=C bonds and at 1.95 ppm to

methyl (-CH_3) protons (peak g") of methacrylate groups that are attached to lactide. In

addition, the broad OH peak at 2.80 ppm on the poly(PG-co-lactide) spectrum disappears

in the final product spectra. There are additionally smaller olefinic peaks at 5.51 and 6.07

ppm and a methyl peak at 1.93 ppm in the spectra. The ratio of intensities for these peaks

relative to the main methacrylate peaks increase as m decreases and more PPG OH groups

remain unreacted in the intermediate stage. These peaks have therefore been assigned to

methacrylate groups attached directly to a PPG block. Further evidence for the validity of

this assignment will be given in Section 3.3.1.4 d.
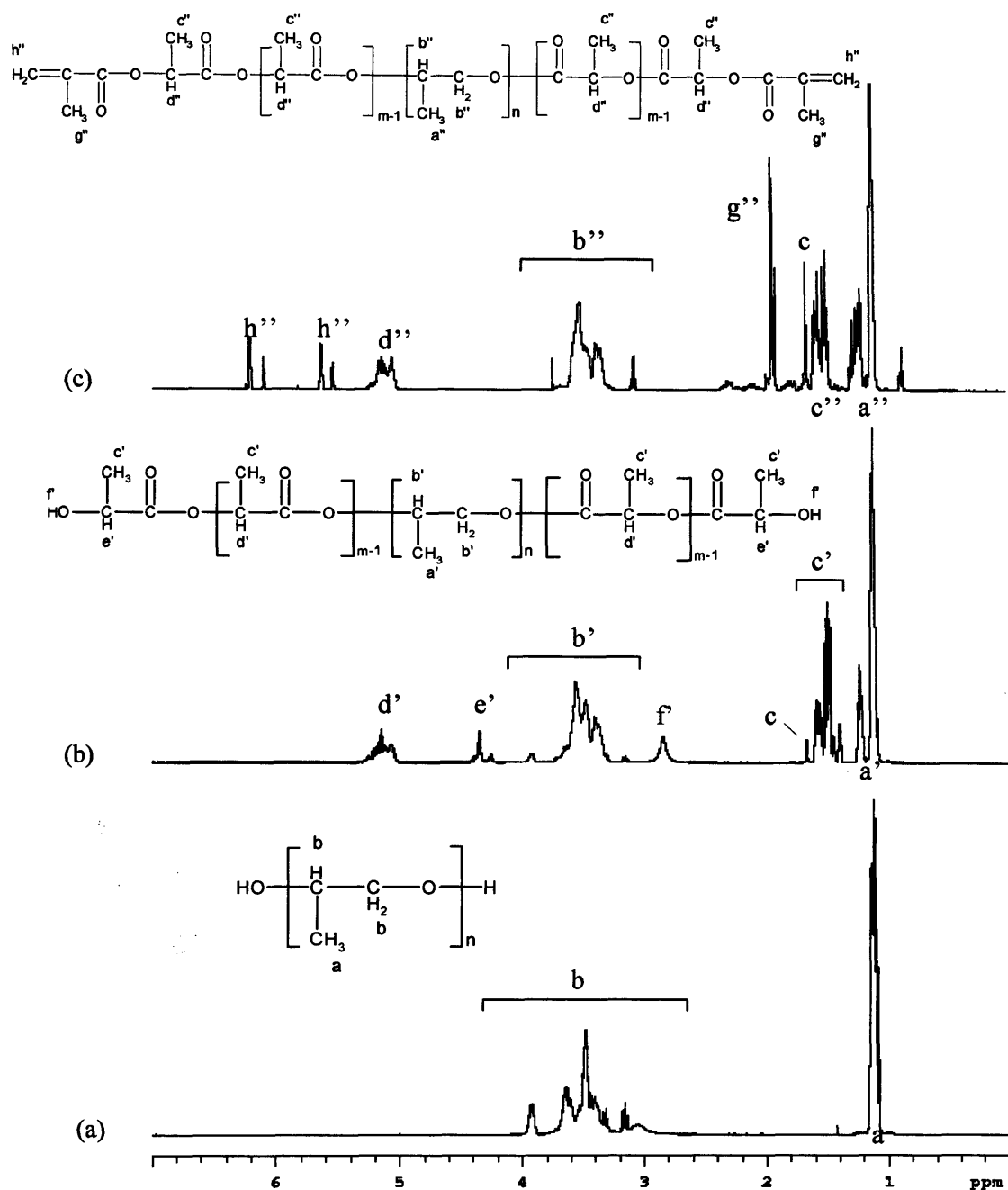
Figure 3.7. ^{1}H NMR spectra of (a) a PPG (molecular weight 425 i.e. P7), (b) a poly(PG-co-lactide) co-oligomer (i.e. P7L2) and (c) a poly(PG-co-lactide) dimethacrylate (i.e. P7L2DMA).

(d) NMR calculations

From the ^{1}H-NMR spectra more details on the exact structural composition of the monomers could be elucidated. These include the average m length of each monomer, the molar ratios of total lactide to PG in the intermediate reaction stage, the number of PPG OH groups reacted, and the efficiency of lactic acid and methacrylate endcapping in the intermediate and final reaction respectively.

The average length of the lactide chains in lactic acid units m for each monomer was estimated using the peak areas (P) of the two lactide multiplet CH peaks, d' and e' (in Figure 3.7) and Equation 3.5.

$$m_{calc} = \frac{[P_{d'} + P_{e'}]}{P_{e'}} \qquad\qquad 3.5$$

The molar ratios of total lactide to PG (LA_{tot}) for each monomer was calculated using the peak areas (P) of the intermediate lactide multiplet CH_3 peak, c' and PPG CH_3 peak, a' (in Figure 3.7) and Equation 3.6.

$$LA_{tot} = \frac{P_{c'}}{P_{a'}} \qquad\qquad 3.6$$

The number of end lactic acid (LA_e) and methacrylate (MA) groups per PG unit were calculated using Equations 3.7 and 3.8 respectively.

$$LA_e = \frac{P_{e'} \times 3}{P_{a'}} \qquad\qquad 3.7$$

$$MA = \frac{P_{h''} \times 3}{P_{a''}} \qquad\qquad 3.8$$

The total molecular weight of each monomer was calculated using Equation 3.9.

$$M_{mw} = PPG_{mw} + \left(LA_{tot} \times \frac{PPG_{mw}}{PG_{mw}} \times LA_{mw} \right) + \left(MA \times \frac{PPG_{mw}}{PG_{mw}} \times MA_{mw} \right) \qquad 3.9$$

where M_{mw}, PPG_{mw}, PG_{mw}, LA_{mw} and MA_{mw} are the molecular weight of the synthesised monomer, PPG, PG (i.e. 58 g/mol), lactic acid (i.e. 72 g/mol) and methacrylate (i.e. 85 g/mol), respectively.

The calculated lactoyl chain lengths (m_{calc}), molar ratios of lactide to PG (LA_{tot}), LA_e and MA end units per PG unit and monomer molecular weights for the two batches are presented in Table 3.7 (ii) and (iii). These values were compared with the expected values (estimated from PPG molecular weight and reactant lactide to PPG mass ratios) in Table 3.7 (i).

With full reaction of all the PPG OH groups and cyclic lactide the calculated m should equal the expected value. The results show that the calculated m was slightly smaller or larger than the expected value indicating that respectively, not all the cyclic lactide or PPG OH groups reacted during the synthesis. This was also observed with the calculated total lactide per PG unit which was on average, of the five monomers, 90 % and 70 % of the expected from the reactant ratios for the two batches, indicating not all cyclic lactide in the reaction mixture was reacted. The ratio of calculated LA_e to estimated OH end on the original PPG (presented as percentages) increased as the reactant molar ratio of lactide to PPG increased indicating that only when the lactide level was high were all the PPG ends attached to a degradable lactoyl group. This observation was in accord with the estimated fraction of OH groups that might remain unreacted using probabilities. When a molecule of PPG reacts with m molecules of cyclic lactide the first step must involve loss

Table 3.7. Lactoyl chain lengths (m), ratios of lactide (both total and end group) and methacrylate (MA) to propylene glycol (PG) and molecular weights of the five monomers measured from different batches synthesised and compared to the expected values. (The percentage of OH groups that would be expected (from simple probabilities) to be reacted after the first reaction stage, x_{exp}, is also given)

(i) Expected values

Code	Expected m	Expected LA_{tot}/PG (mol/mol)[1]	OH end groups / PG (mol/mol)[2]	Expected % OH groups reacted x_{exp}[3]	Expected total molecular weight (g/mol)[1]
P34L8DMA	8	0.46	0.059	99	3322
P34L2DMA	2	0.12	0.059	50	2458
P17L4DMA	4	0.46	0.12	88	1746
P7L8DMA	8	2.18	0.29	99	1747
P7L2DMA	2	0.55	0.29	50	883

[1] Calculated from PPG Mw and the molar ratio of lactide to PPG in the reactant mixture
[2] Calculated from the PPG Mw
[3] Calculated using Equation 3.10

(ii) Batch lot no. 180803

Code	m_{calc}	LA_{tot} / PG mol/mol	%	End groups / PG LA$_e$ (mol/mol)	%	MA (mol/mol)	%	Total molecular weight (g/mol)
P34L8DMA	6.9	0.44	95	0.056	95	0.024	40	3161
P34L2DMA	3.3	0.11	95	0.040	68	0.048	81	2413
P17L4DMA	4.7	0.43	92	0.085	72	0.096	81	1671
P7L8DMA	8.2	1.72	79	0.23	82	0.18	65	1449
P7L2DMA	3.4	0.50	92	0.17	59	0.25	88	845

NB. % = percentages as compared to the expected values in Table 3.7(i)

(iii) Batch lot no. 091104

Code	m_{calc}	LA_{tot} / PG (mol/mol)	%	End groups / PG LA$_e$ (mol/mol)	%	MA (mol/mol)	%	Total molecular weight (g/mol)
P34L8DMA	5.3	0.30	65	0.050	86	0.036	61	2848
P34L2DMA	3.3	0.085	73	0.038	65	0.043	74	2338
P17L4DMA	4.4	0.43	92	0.085	72	0.10	85	1675
P7L8DMA	6.8	1.56	72	0.21	72	0.14	48	1335
P7L2DMA	4.3	0.46	84	0.10	36	0.17	60	772

NB. % = percentages as compared to the expected values in Table 3.7(i)

of a hydroxyl group. When a second lactide molecule is then attached, assuming for simplicity that the reactivity of both ends after the first step are equally reactive, there is a 1/ 2 chance that a PPG OH group remains. With a third cyclic lactide molecule attachment this reduces to 1/4 chance. In general, with m cyclic lactide molecules attached (m_{pred}), the probability of a remaining PPG hydroxyl group will be 1/ 2^{m-1}. The fraction of PPG OH reacted in a mixture would therefore be expected (x_{exp}) to be given by Equation 3.10.

$$x_{exp} = \left(1 - \frac{1}{2^{m_{pred}-1}}\right)$$

3.10

These are given in Table 3.7 (i). The trend seen with x_{exp} for the five monomers is in close agreement with the percentages obtained for LA_e from the syntheses (see Table 3.7 ii and iii). In other words, increasing lactide to PPG reactant molar ratios increased the probability of a successful reaction collision of a PPG OH group in the mixture and the formation of a complete ABA triblock poly(PG-co-lactide) molecule.

The percentages obtained by comparing the number of MA groups per PG with the number of original OH groups per PG indicated the efficiency of full chain end methacrylation in the final reaction. They were found to be comparable only when the ratio of lactide to PPG was 4 or 2. The methacrylate attachment efficiencies, on average of the monomers P34L2DMA, P17L4DMA and P7L2DMA, were 83 % and 73 % for batch no. 180803 and 091104 respectively. On average of the monomers P34L8DMA and P7L8DMA from both batches, only ~50% of the ends of the final products were endcapped with methacrylates when the lactide to PPG molar ratio was 8.

The fluid nature of the poly(PG-co-lactide) dimethacrylate monomers produced with relatively controllable lactide to PPG ratio and methacrylate attachment suggest that they are a promising candidate set of monomers for further study

3.3.2 Poly(PG-co-glycolide) dimethacrylate monomers

3.3.2.1. Monomer synthesis of poly(PG-co-glycolide) dimethacrylate monomers

Table 3.8 shows the appearance and fluidity of the five poly(PG-co-glycolide) dimethacrylate monomers and their percentage reaction yields. As with the poly(PG-co-lactide) dimethacrylates, all monomers were initially fluid with increasing viscosity on increasing PPG: glycolide molar ratios. Intermediate reaction yields were higher when the ratio of glycolide to PPG was low and decreased significantly in the P7G8 monomer. Two products were obtained from the extraction of the intermediate reaction: the fluid poly(PG-co-glycolide) and white hard solids. IR spectrum (not shown) of the latter suggested it was largely pure polyglycolide. It was observed that increasing amounts of these white solids were obtained when the glycolide : PPG ratio increased especially in P7G8. The P7G8DMA monomer could not be readily synthesised as a result of the particularly low yield of the intermediate product. The overall yield from the two-step reaction scheme for the poly(PG-co-glycolide) dimethacrylates was at least two to three times lower than that of the poly(PG-co-lactide) dimethacrylates. With the exception of P34G2DMA, the overall yield ranged only between 12 to 30 %. Raman spectra of the poly(PG-co-glycolide) dimethacrylate monomers could not be obtained due to the low yields of the monomers. It must also be noted that in our preliminary studies exploring different reaction temperatures and times for the synthesis of poly(PG-co-glycolide), a

temperature of 180°C in the intermediate reaction was found to provide slightly better

reaction yield than 130°C and 150°C (by 10 %) whilst increasing the reaction times from 6

to 24 hours did not show any significant improvement in yield.

Table 3.8. Appearance, viscosity and intermediate and overall reaction yield of poly(PG-co-glycolide) dimethacrylate co-oligomeric monomers.

Monomer code	Monomer appearance	Viscosity	Reaction yield %	
			Intermediate	Overall
P34G8DMA	Pale yellow liquid	Viscous	66	17
P34G2DMA	Pale yellow liquid	Fluid	97	80
P17G4DMA	Pale yellow liquid	Fluid	74	12
P7G8DMA[1]	Pale yellow liquid	Viscous	6	*
P7G2DMA	Yellow liquid	Fluid	99	30

[1] P7G8DMA was not synthesised

3.3.2.2. FT-IR of poly(PG-co-glycolide) dimethacrylate monomers

(a) Peak assignments

Figure 3.8 shows example FTIR spectra of a PPG (i.e. P17), a poly(PG-co-glycolide) co-oligomer (i.e. P17L4) and a poly(PG-co-glycolide) dimethacrylate (i.e. P17G4DMA). The FTIR spectra exhibit peaks comparable with those obtained for the lactide monomer synthesis (see Section 3.3.1.2 a and Table 3.4), indicating the attachment of the glycolide ester to the PPG and the subsequent methacrylation to give the monomer. In the FTIR spectra of poly(PG-co-glycolide) intermediates, two extra peaks were present

which were not found in the poly(PG-co-lactide) spectra. These include peaks at 1422

cm^{-1} and 1156 cm^{-1} which are attributed to CH_2 groups of the oligo-glycolide chains of the

products.
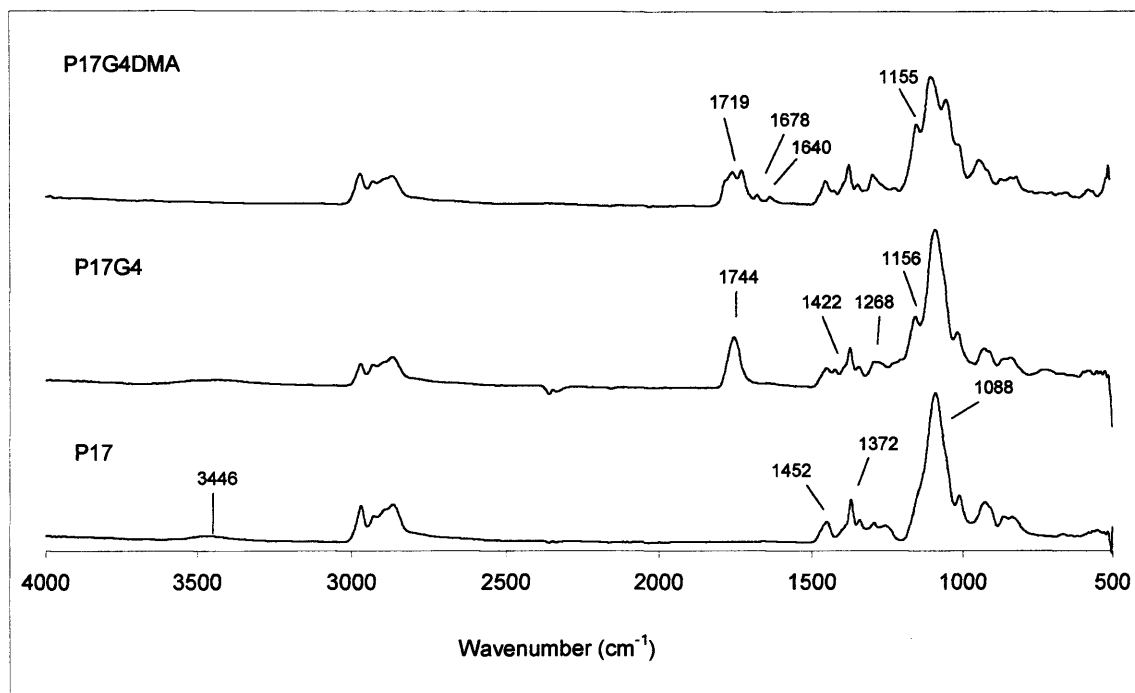
Figure 3.8. FTIR spectra of a PPG (molecular weight 1000 i.e. P17), a poly(PG-co-glycolide) co-oligomer (i.e. P17L4) and a poly(PG-co-glycolide) dimethacrylate (i.e. P17G4DMA).

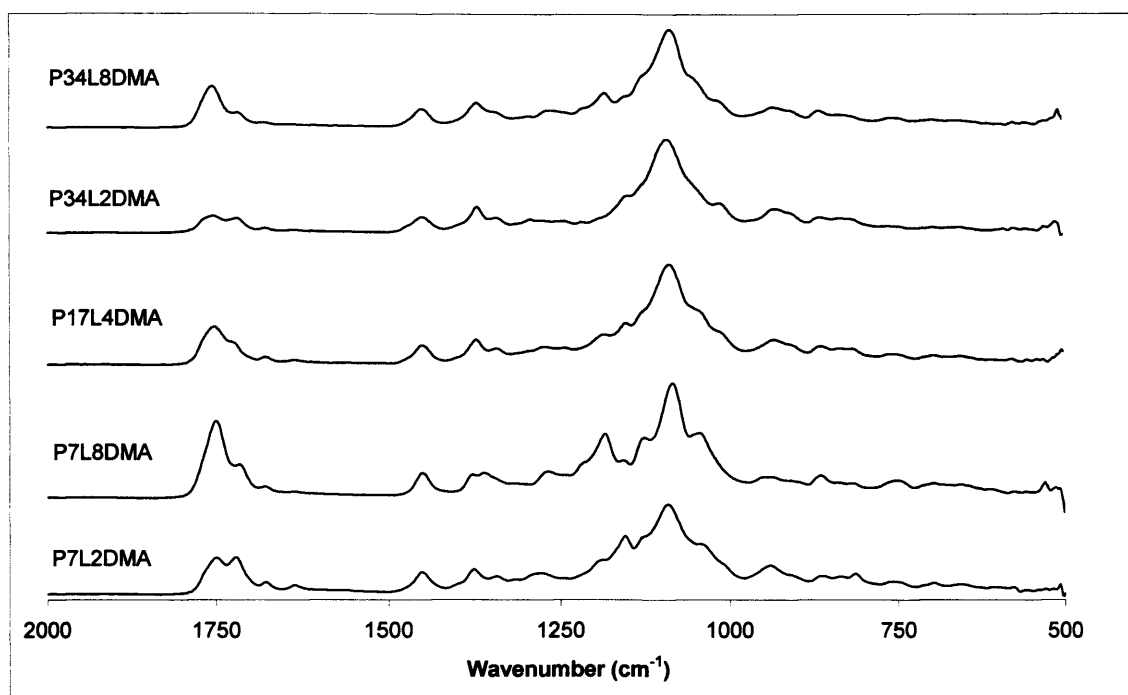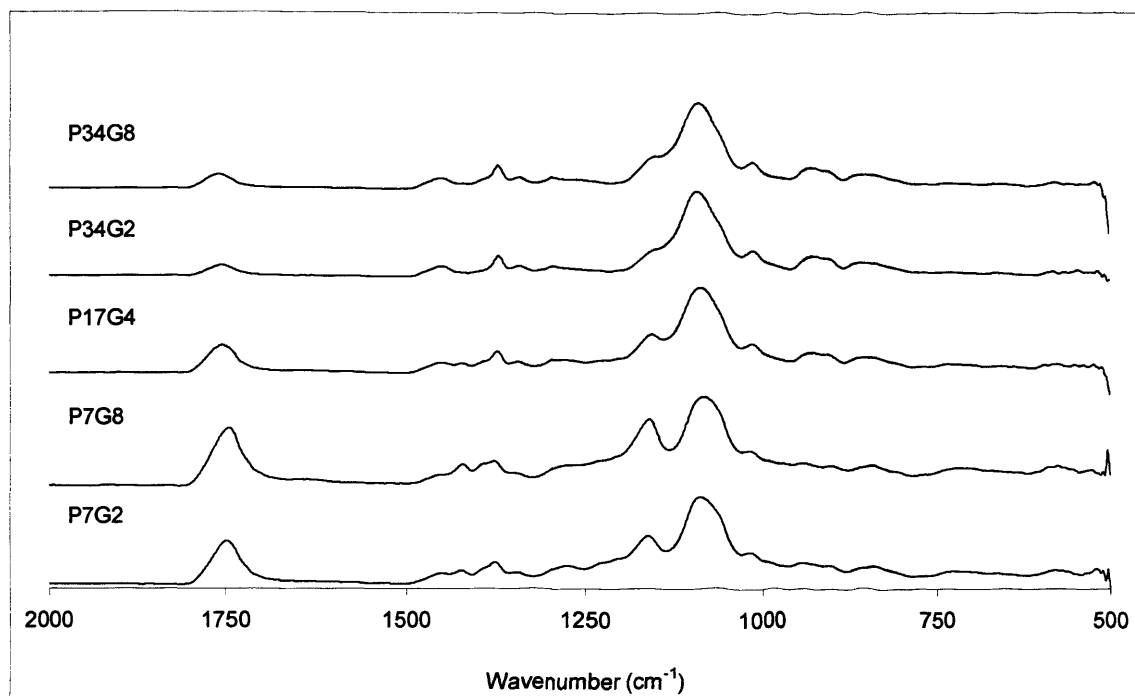Figure 3.9. FTIR spectra of poly(PG-co-glycolide) co-oligomeric monomers
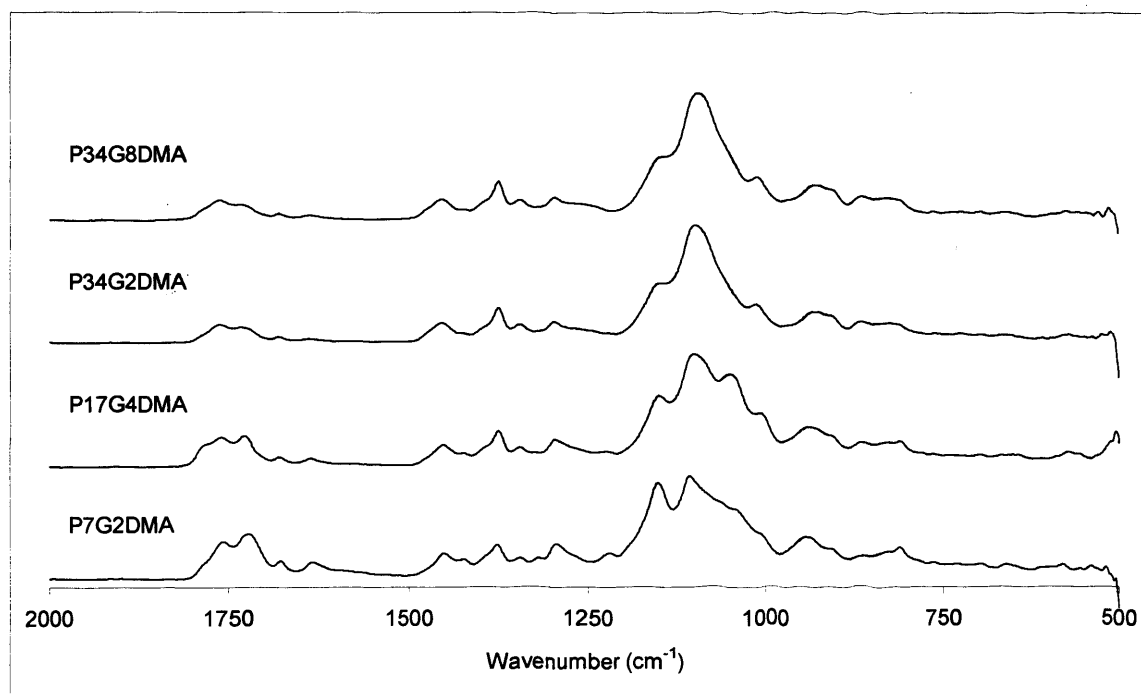
Figure 3.10. FTIR spectra of poly(PG-co-glycolide) dimethacrylate co-oligomeric monomers

173

(b) Quantitative analysis of peak heights

Figure 3.9 and Figure 3.10 show the FTIR spectra of the five co-oligomeric monomers during the intermediate and final synthetic stages respectively. As described for the lactide monomers, the areas for the glycoyl peaks relative to those for the PPG in both spectra are expected to be proportional to the PPG n / GL m ratios in the monomer structure. Comparing the spectra, monomers with a higher proportion of n relative to m units (i.e. P34G2) were found to have relatively much bigger PPG peaks (1088 cm^{-1}) than glycoyl peaks (1744 cm^{-1} and 1156 cm^{-1}). The monomer P7G8 has prominent PPG and glycoyl peaks in the spectrum. It was observed that the P34G8 monomer, with comparable proportions of n and m as P7G2 and P17G4, exhibited a smaller glycoyl peak than expected, indicating that shorter glycoyl m chains were attached than expected. Like the poly(PG-co-lactide) dimethacrylates, P7G2DMA and P34G8DMA are observed (see Figure 3.10) to have the largest and smallest methacrylate peaks respectively.

The equations and the linear regression coefficients obtained for absorbance (A_v) of the 1744 cm^{-1} and 1640 cm^{-1} peaks above background levels at 1800 cm^{-1}, with respect to the fraction of glycoyl (a_{GL}) and methacrylate (a_{MA}) units in the intermediate and final products respectively, were as follows:

From the intermediate spectra

$$A_{1744} - A_{1800} = 0.562a_{GL} \qquad R^2 = 0.77$$

From the final product spectra

$$A_{1640} - A_{1800} = 0.290a_{MA} \qquad R^2 = 0.81$$

The relatively low R^2 values indicate discrepant lengths of the glycolide m chains attached and variable methacrylation efficiency of the monomers. This will be studied in more detail in Section 3.3.2.4 using NMR.

3.3.2.4. NMR of poly(PG-co-glycolide) dimethacrylate monomers

Examples of NMR spectra of starting materials, intermediates and final products are given in Figure 3.11 a, b and c respectively. It must be noted that the NMR spectrum of the P7G8 monomer was not obtained.

(a) Starting materials

NMR peaks of the PPG spectra (Figure 3.11a) were assigned and described in Section 3.3.1.4 a. Unreacted cyclic glycolide has a singlet at 4.96 ppm due to its CH_2 groups (spectrum not shown).

(b) Intermediate products

In the poly(PG-co-glycolide) spectra, the peaks between 4.68 and 5.09 ppm (j' in Figure 3.11b) can be assigned to linear oligo-glycolide CH_2 groups and the peak at 4.28 ppm (i') is due to the glycoyl CH_2 protons adjacent to the terminal OH group. There is an upfield peak at 4.14 ppm next to peak i' which is attributed to terminal OH-linked CH_2 protons of unreacted PPG ends. The peak at 4.96 ppm due to the CH_2 protons of any residue unextracted cyclic glycolide is negligible.
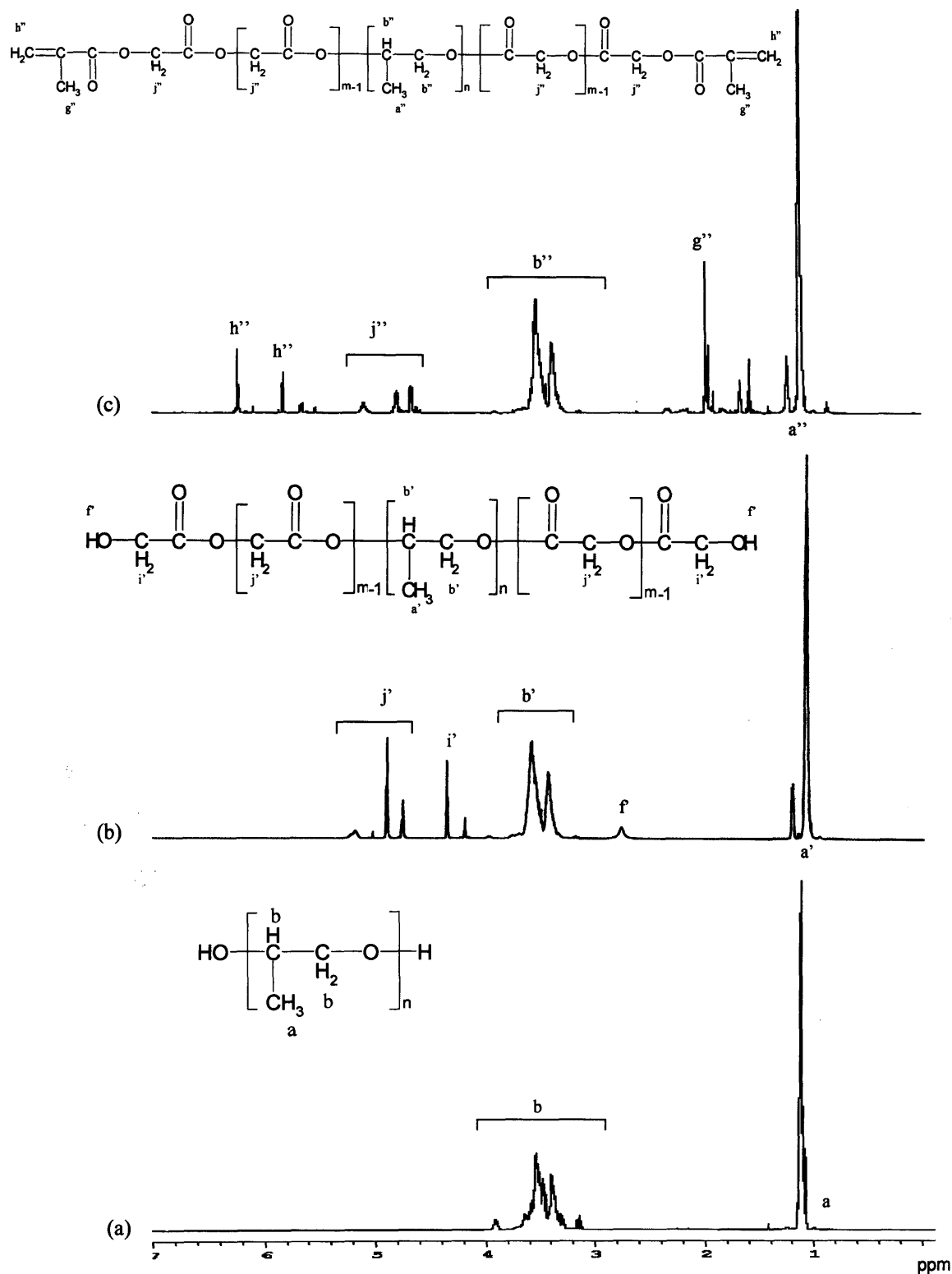
Figure 3.11. ¹H NMR spectra of (a) a PPG (molecular weight 1000 i.e. P17), (b) a poly(PG-co-glycolide) co-oligomer (i.e. P17G4) and (c) a poly(PG-co-glycolide) dimethacrylate (i.e. P17G4DMA).

(c) Final products

In all final dimethacrylate ^{1}H-NMR spectra, additional peaks due to methacrylation of the monomers were seen (see Figure 3.11c). As described for poly(PG-co-lactide) dimethacrylates, those at 5.64 and 6.21 ppm (peak h") are due to olefinic protons and at 1.95 ppm to methyl (-CH$_3$) protons (peak g") of methacrylate groups that are attached to glycolide. There are again smaller olefinic peaks at 5.51 and 6.07 ppm and a methyl peak at 1.93 ppm due to methacrylate groups attached directly to a PPG block. The intensity of these additional methacrylate peaks increases in P7G2DMA and P34G2DMA.

(d) NMR calculations

From the ^{1}H-NMR spectra the exact structural composition of the monomers was elucidated. These include the average length of glycolide m of the monomers, the fraction of glycolide attached to the PPG in the intermediate reaction stage, the number of PPG OH groups reacted and the efficiency of methacrylate endcapping in the final reaction.

The average length of glycolide chains, in glycolic acid units m, for each monomer was estimated using the peak areas (P) of the two glycolide CH$_2$ peaks, i' and j' (in Figure 3.11) and Equation 3.11.

$$m_{calc} = \frac{\left[P_{i'} + P_{j'}\right]}{P_{i'}}$$

3.11

The molar ratios of total glycolide to PG for each monomer (GL$_{tot}$) was calculated using the peak areas (P) of the intermediate glycolide CH$_2$ peaks, i' and j', and PPG CH$_3$ peak, a' (in Figure 3.11) and Equation 3.12.

$$GL_{tot} = \frac{\left(P_{i'} + P_{j'}\right)}{P_{a'}} \times \frac{2}{3}$$ 3.12

The number of end glycolic acid (GL_e) and methacrylate (MA) groups per PG unit were calculated using Equations 3.13 and 3.8 respectively.

$$GL_e = \frac{P_{i'}}{P_{a'}} \times \frac{2}{3}$$ 3.13

The total molecular weight of each monomer was calculated using Equation 3.14.

$$M_{mw} = PPG_{mw} + \left(GL_{tot} \times \frac{PPG_{mw}}{PG_{mw}} \times GL_{mw}\right) + \left(MA \times \frac{PPG_{mw}}{PG_{mw}} \times MA_{mw}\right)$$ 3.14

Where M_{mw}, PPG_{mw}, PG_{mw}, GL_{mw} and MA_{mw} are the molecular weight of the synthesised monomer, PPG, PG (i.e. 58 g/mol), glycolic acid (i.e. 58 g/mol) and methacrylate (i.e. 85 g/mol), respectively.

The calculated glycolic acid chain lengths (m_{calc}), molar ratios of glycolide to PG (GL_{tot}) and GL_e and MA end units per PG unit and monomer molecular weights for the monomers are presented in Table 3.9ii, with the expected values presented in Table 3.9i.

Table 3.9. Glycolide (GL) chain lengths (m), ratios of GL (both total and end group) and methacrylate (MA) to propylene glycol (PG) and molecular weights of the four monomers measured and compared to the expected values.

(i) Expected values

Code	Expected m	Expected GL_{tot}/PG (mol/mol)[1]	OH end groups / PG (mol/mol)[2]	Expected % OH groups reacted X_{exp}[3]	Expected total molecular weight (g/mol)[1]
P34L8DMA	8	0.46	0.059	99	3098
P34L2DMA	2	0.12	0.059	50	2402
P17L4DMA	4	0.46	0.12	88	1634
P7L2DMA	2	0.55	0.29	50	827

[1] Calculated from PPG Mw and the molar ratio of glycolide to PPG in the reactant mixture
[2] Calculated from the PPG Mw
[3] Calculated using Equation 3.10

(ii) Measured values

| Code | m_{calc} | GL_{tot} / PG | | End groups / PG | | | | Total molecular weight (g/ mol) |
		mol/mol	%	GL_e (mol/mol)	%	MA (mol/mol)	%	
P34G8DMA	4.4	0.15	32	0.033	57	0.037	63	2403
P34G2DMA	4.0	0.11	98	0.028	49	0.036	62	2333
P17G4DMA	4.9	0.35	76	0.072	61	0.103	87	1505
P7G2DMA	4.0	0.62	113	0.156	55	0.168	59	792

NB. % = percentages as compared to the expected values in Table 3.9(i)

The results show that unlike poly(PG-co-lactide) monomers, the calculated m of the four poly(PG-co-glycolide) monomers did not vary systematically with increasing reactant glycolide : PPG ratios. The calculated total glycolide (GL_{tot}) per PG unit was only 32 % in P34G8DMA, and the glycolide m length only half that expected. Higher percentages were obtained with P7G2DMA and P34G2DMA but both these had twice the glycolide m length expected. The ratio of calculated GL_e to OH end groups on the

original PPG (presented as percentages) also did not vary significantly between monomers indicating that increasing glycolide level had no effect on increasing the probability of a reaction collision of a PPG OH group with a glycolide molecule as was found with the poly(PG-co-lactide) monomers in previous section (3.3.1.4 d).

The number of methacrylate (MA) groups per PG was compared with the number of original OH groups per PG. The P17G4DMA monomer had a methacrylation efficiency of 87 %. In all other monomers, however, only about 60 % of the intermediate product ends were endcapped with methacrylate groups after the second reaction step.

Due to the low reaction yield of the poly(PG-co-glycolide) monomers and the difficulty in attaching controllable lengths of glycolide moieties onto the PPG blocks to form monomers of systematically changing structures, this set of monomers was not investigated further.

3.3.3 Polymerisation kinetic studies of poly(PG-co-lactide) dimethacrylate monomers

3.3.3.1. Final extent of polymerisation

Figure 3.12 shows example Raman spectra of P7L2DMA containing 10 wt% HEMA and 2 wt% CQ and DMPT, as a monomer and as a polymer disc after 240 s of light exposure. The methacrylate peaks at 3110 cm^{1} and 1407 cm^{-1} (both due to H-C=C), 1719 cm^{-1} (due to C=O) and 1640 cm^{-1} (due to C=C) practically disappear in the post-cure spectrum as expected for full monomer polymerisation.
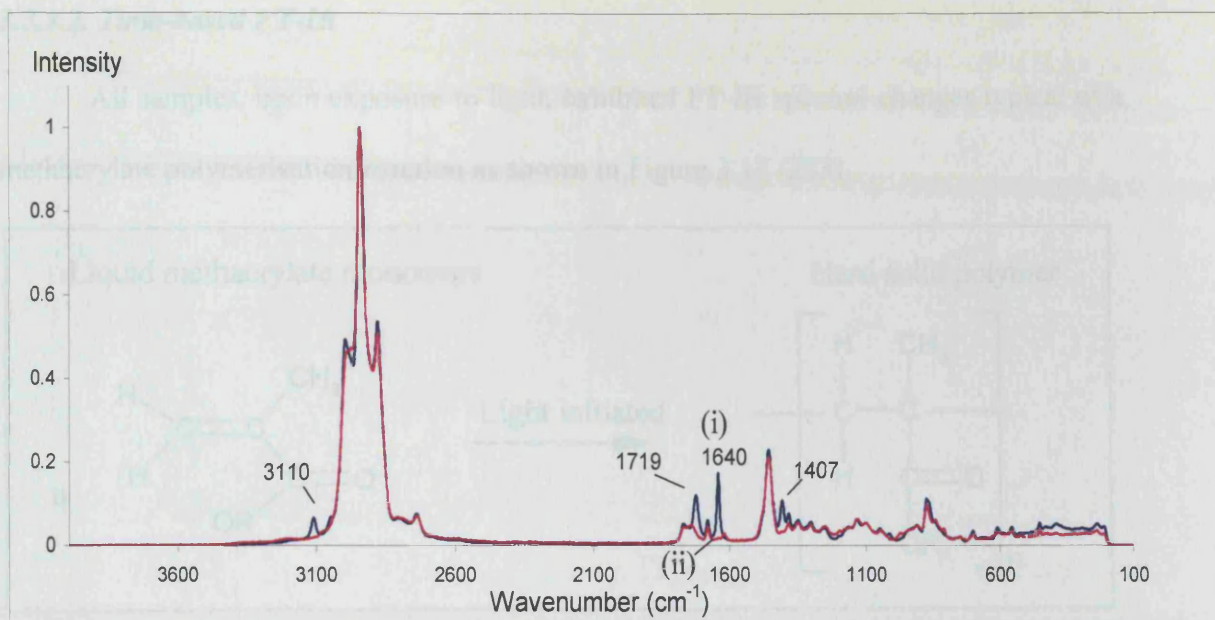
Figure 3.12. FT-Raman spectra of P7L2DMA with 10 % HEMA and 2 % CQ and DMPT (i) before and (ii) after exposure to 240 sec of UV light.

For each sample, the pre- and post-cure Raman spectra were baseline corrected and normalised using a peak that was not significantly affected by the polymerisation process (i.e. 2940 cm^{-1}). Since the 1640 cm^{-1} peak was the most intense and well separated from others, its height above background divided by that before light exposure was used to quantify final polymerisation percentages. The pre- (H_0) and post-polymerisation (H_f) peak height at 1640 cm^{-1} was obtained and the final fraction (%) of methacrylate groups polymerised for each sample (Q_f) calculated using Equation 3.15.

$$Q_f = \frac{H_0 - H_f}{H_0} \times 100 \qquad\qquad 3.15$$

The final polymerisation percentages at 24 hours for all samples are presented in Table 3.11.

___

3.3.3.2. Time-based FT-IR

All samples, upon exposure to light, exhibited FT-IR spectral changes typical of a

methacrylate polymerisation reaction as shown in Figure 3.13 (203).
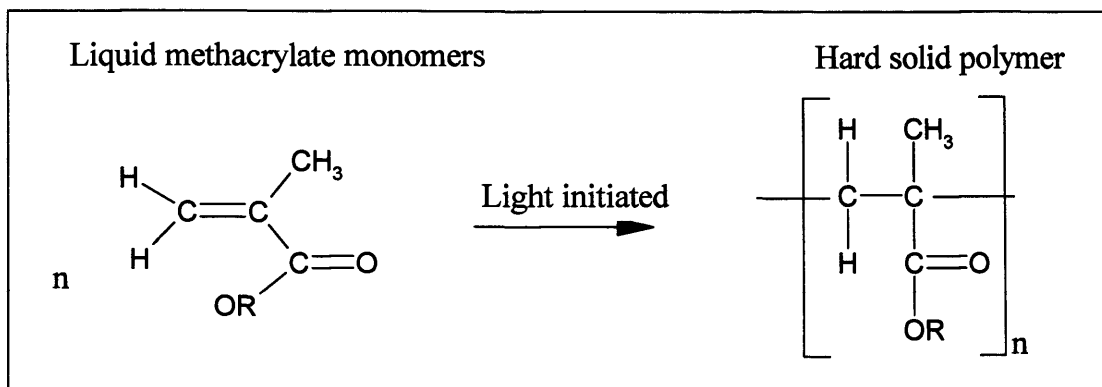
Figure 3.13. The methacrylate polymerisation reaction

Figure 3.14 (a) shows example FTIR spectra of P7L2DMA with 10 wt% HEMA

and 2 wt% CQ and DMPT before, during and after light exposure. The spectral changes

included absorbance loss at 1640 cm^{-1} and 1155 cm^{-1}. Additionally there are changes in

the C=O peak at 1730 cm^{-1} and a shift in the double C-O peak near 1300 cm^{-1} to lower

wavenumbers. The absorbance change as a function of time at any wavelength will be

proportional to the rate of reaction (203). To assess the wavenumbers at which greatest

absorbance changes occurred during the polymerisation reactions, difference spectra were

obtained using 'Spectrum software' from Perkin Elmer. In such plots (e.g. Figure 3.14b)

absorbance at each wavenumber in the 90 s spectra (before light exposure) was subtracted

from values in later time spectra. Difference spectral peak and trough assignments are

presented in Table 3.10. It can be seen that in this study the C=O shift caused greater

absorbance change than the C-O shift. In the unpolymerised state this C=O group is

conjugated with the C=C bond and on curing this conjugation is lost (144). As a result the

electrons were no longer delocalised, the bond became stronger, and the C=O peak shifted

to a higher wavenumber in the polymerised state.
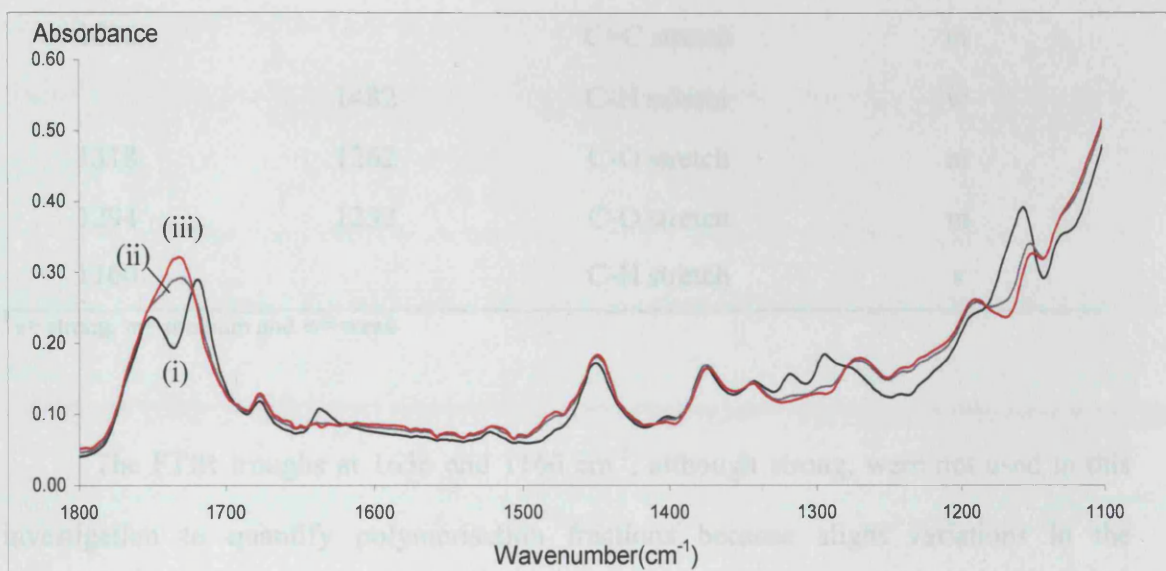
(a)
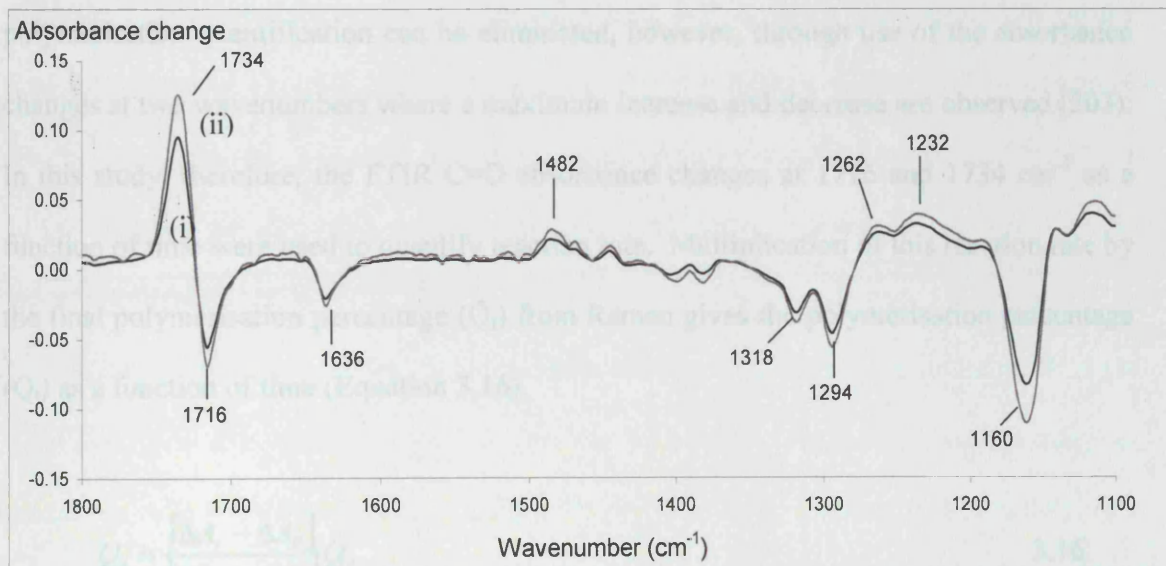
(b)

Figure 3.14. (a) FTIR spectra of P7L2DMA with 10 % HEMA and 2 % CQ and DMPT at (i) 90, (ii) 180 and (iii) 1800 s (light exposure from 120 to 360 s); (b) Absorbance change between (i) 90 and 180 s, and (ii) 90 and 1800 s

Table 3.10. Difference spectra peak and trough assignments for methacrylate polymerisation.

Wavenumber (cm^{-1})		Assignment	Strength [1]
Trough	*Peak*		
1716	1734	C=O stretch	s
1636		C=C stretch	m
	1482	C-H scissor	w
1318	1262	C-O stretch	m
1294	1232	C-O stretch	m
1160		C-H stretch	s

[1] s= strong, m= medium and w= weak

The FTIR troughs at 1636 and 1160 cm^{-1}, although strong, were not used in this investigation to quantify polymerisation fractions because slight variations in the background absorbance can cause large errors. Any background variation in monomer polymerisation quantification can be eliminated, however, through use of the absorbance changes at two wavenumbers where a maximum increase and decrease are observed (203). In this study, therefore, the FTIR C=O absorbance changes at 1716 and 1734 cm^{-1} as a function of time were used to quantify reaction rate. Multiplication of this reaction rate by the final polymerisation percentage (Q$_f$) from Raman gives the polymerisation percentage (Q$_t$) as a function of time (Equation 3.16).

$$Q_t = \frac{[\Delta A_t - \Delta A_0]}{[\Delta A_f - \Delta A_0]} Q_f$$

3.16

Where ΔA_t, ΔA_0, ΔA_f are the difference in absorbance at 1736 and 1716 cm^{-1}, respectively, at time t, initially and finally (extrapolated).

Polymerisation fractions as a function of time for formulations containing PPG of

2000, 425 and 1000 g/mol are provided in Figure 3.15, Figure 3.16 and Figure 3.17

respectively. The average standard deviation was 6 % of the polymerisation fraction

during the first 60 s after light exposure but then declined to an average value below 1 %.

Table 3.11 presents the polymerisation fractions at different times after light exposure for

all samples.

In addition, the results were also fitted to the factorial equations 2.15 to 2.18 (see

Section 2.8.2, Chapter 2). ExpBi values from the factorial analysis as a function of time

from the beginning of light exposure are presented in Figure 3.18. The close overlapping

of results for the two duplicate intermediate formulations (see Figure 3.17) indicate good

reproducibility of the data. Values of exp B_0 (see Figure 3.17 and Equation 2.16, Section

2.8.2, Chapter 2) and polymerisation percentages for the intermediate formulations are in

reasonable agreement as expected if Equation 2.15 is valid for all samples. The results

could therefore be explained by visually comparing the figures and using B values from

the factorial analysis. The latter was useful in providing a quantitative value of the effect

of the different variables investigated with respect to time of experiment. In Figure 3.18,

B1 to B4 indicate the level of the effects of the variables investigated, including PPG n

length, lactide m length, time of light exposure and photoinitiator concentrations; B1,2 (or

3,4); B1,3 (or 2,4) and B1,4 (or 2,3) are the interaction effects between the pairs of

variables. Exp Bi is the amount by which the polymerisation fraction (i) is multiplied by

when the value of the variable is doubled from its low to intermediate or intermediate to

high value; or (ii) is multiplied or divided by when the two variables in an interaction

effect are both doubled or one doubled and the other halved respectively.

Table 3.11. Percentage of monomer polymerisation at different times since light exposure and final monomer conversions at 24 hours. Note that there are two identical samples for the intermediate formulations with P17L4DMA. (Numbers have been highlighted in red when there is a significant effect of initiator concentration or exposure time on the rate of polymerisation of a given monomer)

Monomer code	Initiator conc. (wt%)	Exposure time (s)	Double bond conversion (%)			
			60 s	110 s	900 s	24 hrs
P34L8DMA	0.5	60	53	73	84	90
	2	240	40	72	98	99
P34L2DMA	0.5	240	39	72	99	99
	2	60	37	64	80	94
P17L4DMA	1	120	48	84	94	96
	1	120	44	83	96	97
P7L8DMA	0.5	240	65	90	98	98
	2	60	67	91	98	100
P7L2DMA	0.5	60	77	96	98	98
	2	240	65	95	99	99
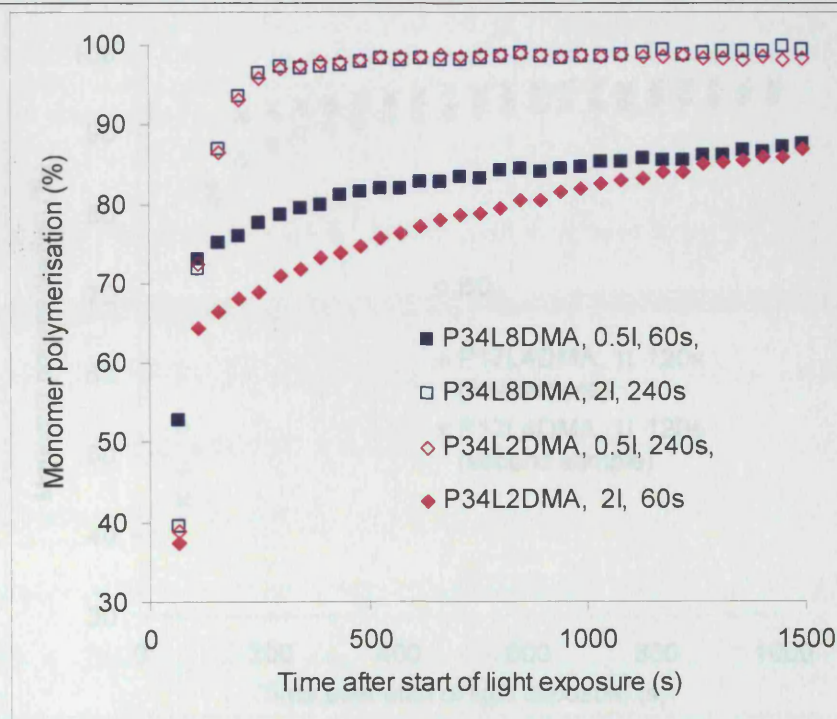
Figure 3.15. Polymerisation as a function of time for monomers prepared using PPG 2000g/mol, containing 0.5 or 2.0 wt% initiators with light exposure times of 60 or 240s.
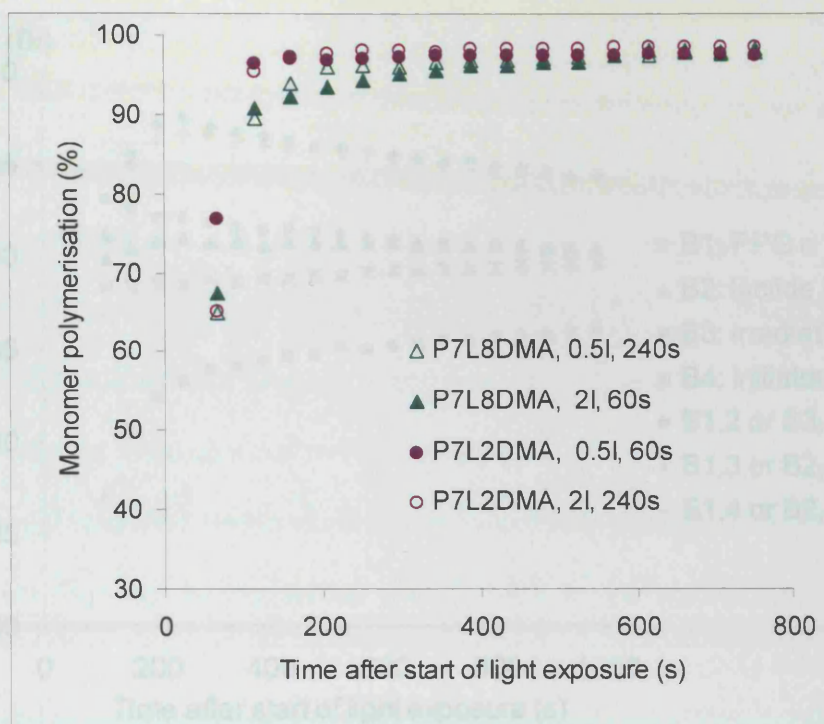
Figure 3.16. Polymerisation as a function of time for monomers prepared using PPG 425g/mol, containing 0.5 or 2.0 wt% initiators with light exposure times of 60 or 240s.
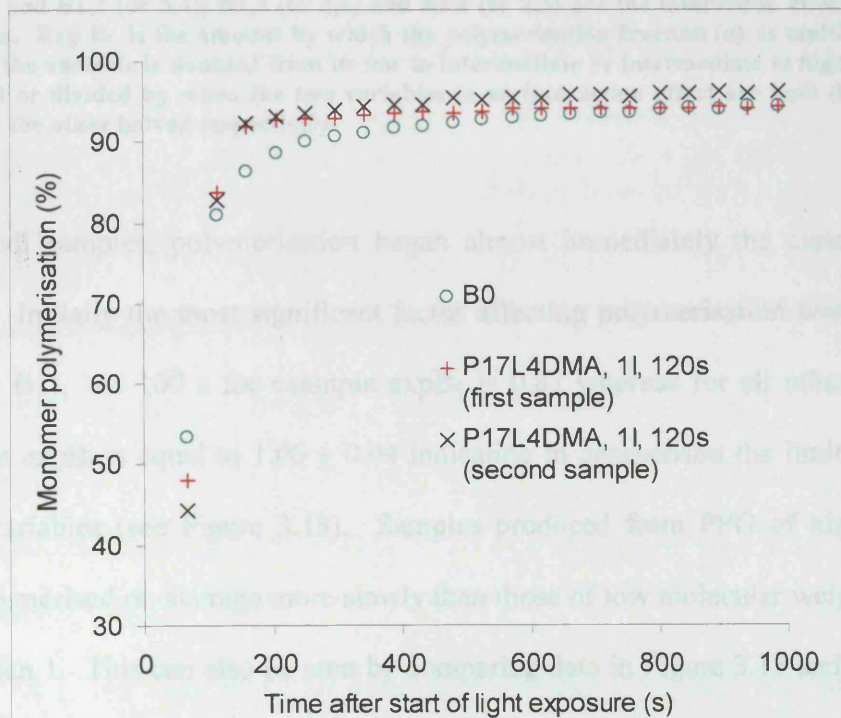
Figure 3.17. B0 values (see Equation 2.16, Chapter 2), and polymerisation as a function of time for monomers prepared using PPG 1000 g/mol, containing 1 wt% initiators with light exposure times of 120 s.
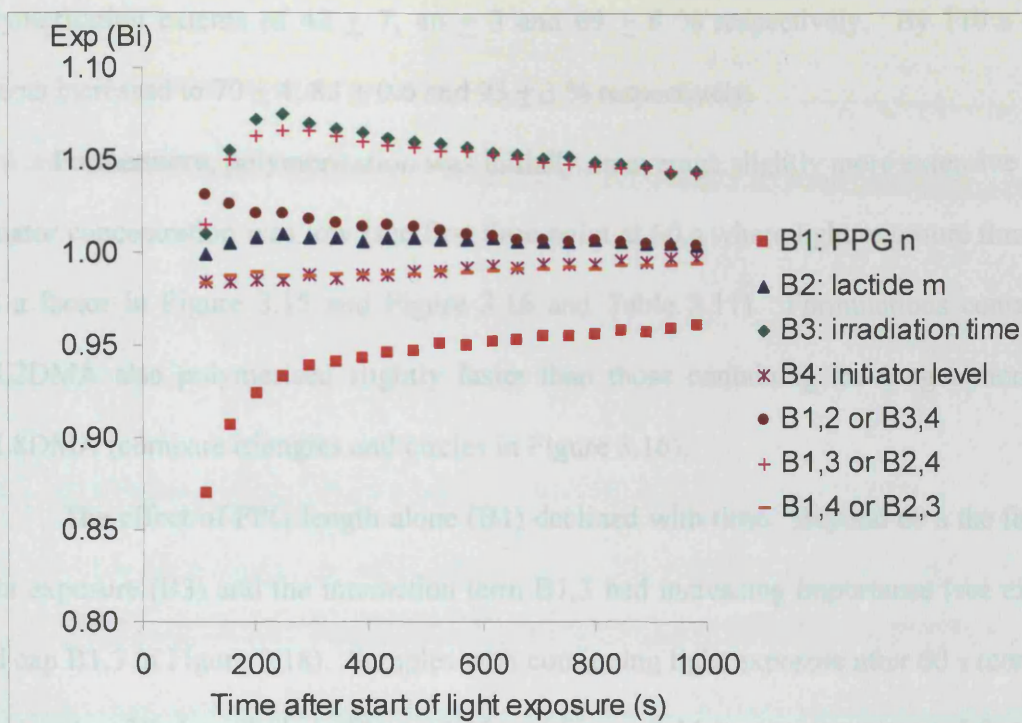
Figure 3.18. Variation of exp B parameters (Equations 2.17-2.18, Chapter 2) for polymerisation fractions with respect to time after the start of light exposure. B1 to B4 are the effects of the variables investigated and B1,2 (or 3,4); B1,3 (or 2,4) and B1,4 (or 2,3) are the interaction effects between the two variables. Exp B_i is the amount by which the polymerisation fraction (a) is multiplied by when the value of the variable is doubled from its low to intermediate or intermediate to high value ; or (b) is multiplied or divided by when the two variables in an interaction effect are both doubled or one doubled and the other halved respectively.

In all samples, polymerisation began almost immediately the curing light was turned on. Initially the most significant factor affecting polymerisation was PPG length (parameter B1). At 100 s for example $expB_1$ is 0.87 whereas for all other factors and interactions $expB_i$ is equal to 1.00 ± 0.04 indicating in comparison the limited effects of all other variables (see Figure 3.18). Samples produced from PPG of high molecular weight polymerised on average more slowly than those of low molecular weight as exp B_1 was less than 1. This can also be seen by comparing data in Figure 3.15 and Figure 3.16. At 60 s, samples prepared using PPG 2000, 1000 and 425 g/mol had average

188

polymerisation extents of 42 ± 7, 46 ± 3 and 69 ± 6 % respectively. By 110 s these extents increased to 70 ± 4, 83 ± 0.6 and 93 ± 3 % respectively.

Furthermore, polymerisation was initially on average slightly more extensive if the initiator concentration was low (see first time point at 60 s where light exposure time was not a factor in Figure 3.15 and Figure 3.16 and Table 3.11). Formulations containing P7L2DMA also polymerised slightly faster than those containing the longer monomer P7L8DMA (compare triangles and circles in Figure 3.16).

The effect of PPG length alone (B1) declined with time. Beyond 60 s the time of light exposure (B3) and the interaction term B1,3 had increasing importance (see exp B3 and exp B1,3 in Figure 3.18). Samples with continuing light exposure after 60 s (compare filled and unfilled symbols in Figure 3.15 and Figure 3.16) on average reacted faster. If the PPG length was long, polymerisation was particularly enhanced by increased light exposure time causing complexity of data interpretation and the non zero B1,3 interaction term. By 240 s exp B3 = exp B1,3 = $(\exp B1)^{-1}$. This means that from this time the level of polymerisation for samples with PPG 2000 and short exposure time are equal to exp B0 multiplied by $(\exp B1)^{3}$ (see factorial equation 2.15, Chapter 2). By 15 minutes (i.e. 900 s), polymerisation fractions for these samples were equal to 82 ± 3 %. All other combinations of samples (i.e. PPG 425 & short exposure time; PPG 425 & long exposure time; and PPG 2000 & long exposure time), however, had polymerisation fractions equal, effectively, to exp B0 divided by exp B1. With these samples polymerisation fraction was 98 ± 0.4 % by 15 minutes.

By 24 hours, only those formulations with both PPG 2000 and short exposure times had more than 5 % monomer remaining. The intermediate samples prepared with P17L4DMA and using 120 s light exposure had 4 % monomer at 24 hours and all other

samples had 2 % monomer or less remaining (see Table 3.11). The final fully

polymerised polymers varied between highly flexible rubbers when the monomers were

long and more rigid rubbers when they were short.

3.4   Discussion

3.4.1   Synthesis of poly(PG-co-lactide) dimethacrylate monomers

In this investigation, a series of five ABA triblock poly(lactide-co-PG-co-lactide)

monomers endcapped with methacrylate groups have been synthesised and their structures

elucidated qualitatively and quantitatively using FT-IR, Raman and NMR. The results

showed that provided the ratio of lactide to PPG was kept below eight, fluid ABA

copolymers with an average oligo(lactide) chain length as expected from the relative

reactant ratios, could be produced using PPG of molecular weight 425 to 2000 g/mol. The

overall reaction yields of fluid monomer were high when the lactide level was low but

decreased at higher lactide to PPG ratios (Table 3.3). One possible explanation was the

fractionation stage in the methacrylation reaction. During the extraction of the

methacrylated products in hexane, those with reacted lactide to PPG reaction molar ratios

of ≤ 4 were mainly extracted into the top filtrate layer whereas others should remain as

sediments in the bottom layer. The monomer P17L4DMA had the lowest reaction yield as

its extraction was at the fractionated point between the two phases. About 10 and 30 % of

cyclic lactide remained unreacted with the PPG in the two batches. As would be expected

from reaction probabilities as the molar ratio of lactide to PPG increased so did the

percentage of PPG OH group reaction.

The efficiency of end-capping with methacrylate groups was also high when the ratio of lactide to PPG was low (Table 3.7) and comparable with that obtained previously with similar molecular weight poly(ethylene glycol-co-lactide) methacrylate oligomers (88). In repeat reaction batches gaining full chain end methacrylation was found to be a persistent problem when the lactide to PPG molar ratio was 8. As will be shown in the following chapters the variability in the percentage of methacrylation between the monomers or between the same monomer of different batches significantly affects the properties of the polymers.

Relative peak areas in both FTIR and Raman intermediate and final product spectra varied in a manner consistent with the ratios of PG to lactoyl or methacrylate groups in the five different products quantified via NMR. This is useful as in subsequent batches the structures of the monomers can be assessed quickly using the equations obtained from the FTIR and Raman only.

3.4.2 Synthesis of poly(PG-co-glycolide) dimethacrylate monomers

The synthesis of the five ABA triblock poly(glycolide-co-PG-co-glycolide) dimethacrylate was less successful in respect that the oligo(glycolide) chain length could not be controlled by varying the PPG to glycolide reactant ratios and that the yields were low. The overall yields of fluid monomer were particularly low for high glycolide to PPG ratios and were much lower than the poly(PG-co-lactide) dimethacrylates (Table 3.8). The high yields of the white solid by-products obtained particularly when PPG: glycolide ratio was high and the non-controllable glycolide m lengths of the monomers indicate that esterification between glycolide molecules tended to occur in the reaction rather than with the OH groups of the PPG molecules.

191
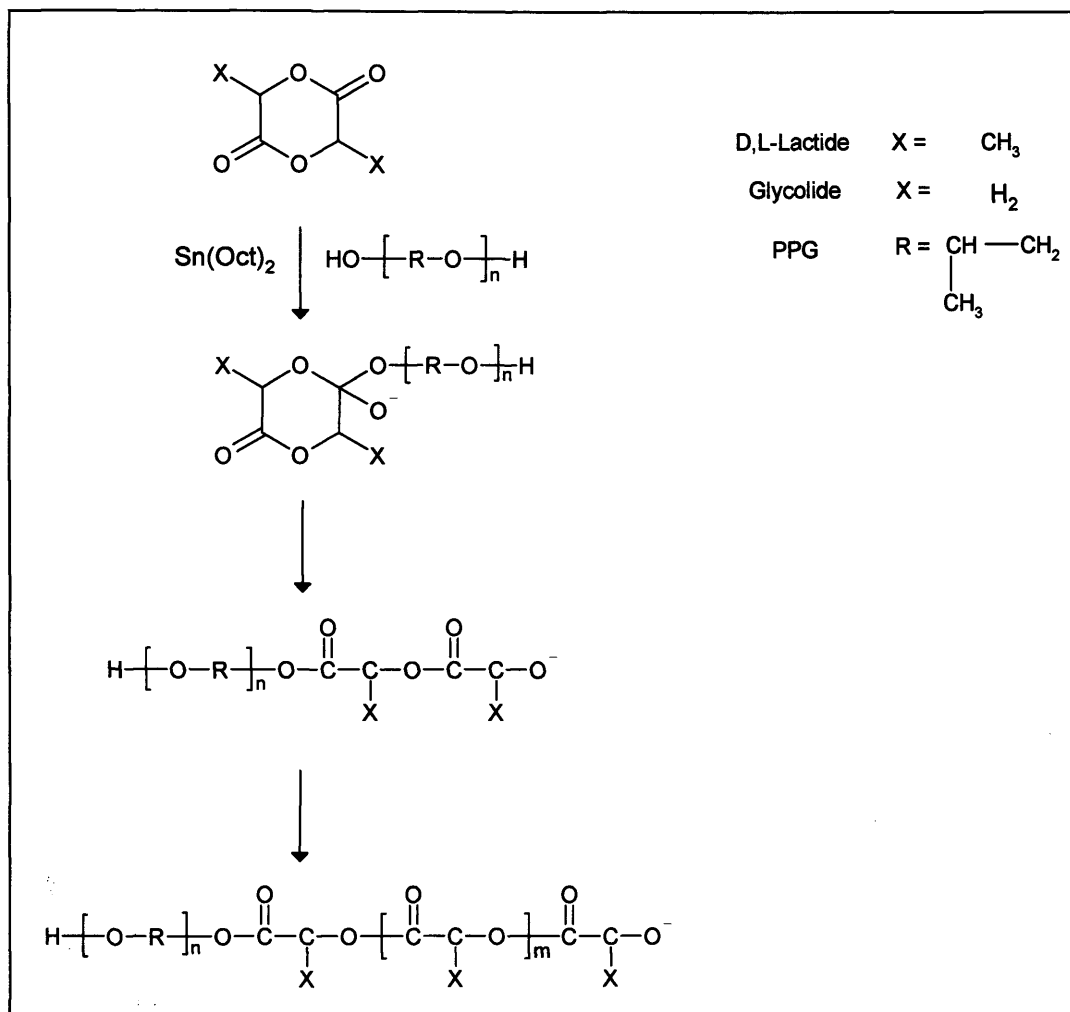
Figure 3.19. Synthetic reaction mechanism of poly(PG-co-ester)

As shown in this and previous studies (98-100;107;108), the ABA type poly(ester-ether-ester) block monomer can be synthesised by using PPG diols as ring opening polymerisation initiation sites with the aid of stannous octoate [Sn(Oct)$_2$] as catalyst (Figure 3.19). The electronegative oxygen atom in the carbonyl group of the cyclic ester polarises the bond and makes the carbon atom an electrophile susceptible to attack from the nucleophilic OH group at each end of the PPG molecule. The resultant nucleophilic addition to the carbonyl group is then followed by acyl-oxygen cleavage which

subsequently leads to propagation through alkoxide ion chain ends (204). The propagation is stopped when chain transfer with another alcohol molecule causes the ends to be terminated with hydroxyl groups. Two lactic or glycolic acid units are added onto the growing chain each time as each cyclic ester is a dimer. With the presence of $Sn(Oct)_2$ this catalyst first reacts with the hydroxyl groups of the PPG to form a tin alkoxide that subsequently acts as an actual initiator (145;147). Ring-opening of the cyclic ester can also occur in the presence of $Sn(Oct)_2$ only as the initiator.

The low efficiency of attachment of the glycolide molecules onto PPG could be due to a combination of factors. It was possible that some PPG molecules might not initiate PLG chain growth from both hydroxyl ends as a result of their different reactivities. According to the structure in Figure 3.1, PPG has a primary and a secondary alcohol group on its chain ends. The secondary hydroxyl group of the PPG has a lower initiation activity than the primary hydroxyl group. One study (82) has experimented on the reaction between D,L-lactide and alcohols with different numbers of hydroxyl groups, and at different alcohol/ lactide molar ratios. It was found that the percentage of reacted initiating OH groups using polyglycerine-06 (alcohol: lactide molar ratio= 1:20), which contains 6 secondary hydroxyl groups and 2 primary hydroxyl groups, was only 50 %. This was compared, for similar molar ratios of alcohol to lactide, to 85 % achieved using pentaerythritol (containing 4 primary hydroxyl groups), and 95-100 % using 1,4-butanediol. The average PLA chain length formed with the polyglycerine-06 was longer than expected. It was also found that increasing the molar ratios of lactide to polyglycerine-06 increased the percentage of reacted OH groups on the latter.

Furthermore, the likelihood of polyester homopolymerisation could increase significantly in the poly(PG-co-glycolide) synthesis due to the lack of methyl groups in

the glycolide structures. This caused less steric interference in the reaction between two glycolide molecules, and as a result, polymerisation of the ring-opened glycolides to themselves was preferred to their attachment to the methyl-containing PPG backbone. Homopolymerisation of polyglycolide was more significant when the ratio of glycolide to PPG was high. A further possibility is that as the reaction temperature used was less than the melting point of polyglycolide (~225°C), crystallisation of the polymerising polyglycolide could occur resulting in what is known as solid state polymerisation (76). This solid state polymerisation did not occur in poly(PG-co-lactide) synthesis as D,L-lactide, used in this study, is amorphous. Increasing the reaction temperature beyond 180 °C to exceed the melting point of polyglycolide to prevent solid state polymerisation and to increase PPG and glycolide reaction was prohibited due to the temperature control limitation in the parallel synthesis equipment.

The poor yields of poly(PG-co-glycolide) dimethacrylate monomers meant that they could not be used in further studies. The polymerisation kinetic study in the following section and the characterisation of the physical and mechanical properties in subsequent chapters will therefore be based on the ABA triblock poly(PG-co-lactide) dimethacrylate monomers only.

3.4.3 Methacrylate polymerisation of poly(PG-co-lactide) dimethacrylate monomers

The reaction kinetics of photopolymerisation of the poly(PG-co-lactide) dimethacrylate monomers was monitored by a combination of time-based ATR-FTIR and Raman methods. FTIR has previously been used to quantify polymerisation levels of methacrylate monomers in many studies (203;205;206) but sensitivity of this technique to

residual monomer is poor when conversion is high because the methacrylate C=C peak used is weak, not well separated from other peaks (particularly that due to water) and can have a high background level that is difficult to estimate accurately. Raman spectroscopy was therefore used to quantify final levels of cure in this experiment. Raman spectra of monomers, however, can take several minutes to generate, making the technique unsuitable for fast setting kinetics quantification. In this aspect the problem was overcome through combining an ATR FTIR methacrylate polymerisation kinetics quantification method (203) with the Raman data.

The monomers started to polymerise immediately on light exposure (Figure 3.15 to Figure 3.17). The polymerisation rate increased rapidly to a maximum and then decreased slowly as light was removed or the monomer was consumed. With all the monomers in this study 60 s light exposure gave final levels of methacrylate conversion of greater than 90 % (Table 3.11). At early times, PPG length had the most significant effect on polymerisation rate with samples of high n level polymerising more slowly than those of low n. The monomer P7L2DMA with low initiator concentration was the fastest polymerising formulation with over 96 % reaction by 120 s when the exposure time was 60 s. If the monomer length or initiator concentration was raised, on average, the lower-surface rate of reaction declined. At later times the effect of light exposure time, as a single factor or as an interaction effect with the PPG length factor, became prominent (Figure 3.18). With slower polymerising formulations i.e. long PPG length, increased time of light exposure could improve overall polymerisation rate.

The methacrylate polymerisation process involves light activated initiation and free radical propagation steps (142;207).

Initiation: Initiator → 2R˙

                       R˙ + M → M₁˙

Propagation: M₁˙ + M → M₂˙

                       Mₓ˙ + M → M˙₍ₓ₊₁₎

Termination: Mₓ˙ + Mᵧ˙ → M₍ₓ₊ᵧ₎
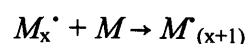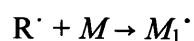
In the initiation step, each initiator molecule is decomposed, upon light exposure, to yield two initiator radicals (2R˙), each of which in turn reacts with a monomer molecule (M) to give a new monomer radical M_1˙. In the propagation step this new monomer radical is added onto another monomer molecule to form a new radical M_2˙, which in turn adds to another M to form another new radical and through many repetitions of this step, the free radical chain grows M˙₍ₓ₊₁₎. Termination occurs when two such macroradicals couple together ($M_{(x+y)}$).

When the light source is removed, the reaction rate rapidly declines as free radicals combine via the termination step and their concentration decreases (203). The polymerisation rate, R_p, during light exposure of a monomethacrylate under steady state conditions is initially given by an expression of the form as shown in Equation 3.17 (208).

$$R_p = \left(\frac{k_p}{2^{0.5} k_t^{0.5}} \right) R_i^{0.5} [M]$$ 3.17

Where k_p and k_t are rate constants for the propagation and termination steps, [M] the monomer concentration and R_i the rate of initiation. The rate of reaction of dimethacrylates will have a similar mechanism and expression but with additional steps

and terms due to chain branching (209). The significant differences in the rate of polymerisation between monomers with different PPG length might be explained by monomer chain mobility (26;144). At the start, when all monomers were in free-flowing, liquid state, polymerisation was chemically controlled and was affected by the mobility of the monomer system. The propagation step of polymerisation (in which a monomer reacted with a polymeric free radical) was facilitated easily if PPG length was short and the monomer chains were more mobile. This means that as the monomer length decreased, their rate of diffusion (and therefore k_p) and methacrylate concentration increased, explaining the observed rise in polymerisation rate. The movements of the polymeric free radicals became more and more restricted as the crosslinked network grew. The rate of the termination step (where 2 polymeric free radicals reacted and stopped polymerisation) then became reduced. This effect was more pronounced with large molecules. This would explain why polymerisation in monomers with long PPG length continued at a slow rate after removal of the light source. With further development of the crosslinked network, the rate of polymerisation became diffusion limited to a point that further double bond conversion was impossible. It is observed therefore, as in the literature (101) and in this study, that polymerisation often stops priors to 100 % double bond conversion.

As the initiator concentration is raised, the rate of initiation (and therefore R_i) increases with the production of more free radicals and faster polymerisation is anticipated. The use of the FT-IR spectroscopy in this study, however, only analysed the lower few microns of the specimen in contact with the ATR FTIR diamond, and light was shone directly onto the top surface of the specimen. While the rate of initiation might be increased at the top surface of the specimen, the lower surface process could be delayed because less light could penetrate to the bottom of the sample (210). This explained why

low initiator concentration may have slightly increased the initial apparent rate of polymerisation (see first time point at 60 s where light exposure time was not a factor in Figure 3.15 and Figure 3.16 and Table 3.11). One study by Muggli *et al* (101) investigated the effect of initiator concentration and varying sample thickness on the polymerisation of a dimethacrylated polyanhydride [poly(MCPH)] using ATR-FTIR and found that the double bond conversion, using a blue light exposure at 150 mW/ cm^2, at the top (illuminated) surface of the sample was much faster than that at a depth of 1 mm into the sample. The light penetration, however, increased with increasing length of light exposure due to decaying and photobleaching capability of the CQ initiator. It is interesting to note that in this study the effect of initiator concentration on the polymerisation of poly(MSA) was also investigated. The sample was compressed as a thin film between polypropylene sheets and using FTIR it was found that increasing the CQ from 0.2 to 1 wt% increased the double bond conversion from 70 to 90 %, after 10 minute of blue light exposure at 150 mW/ cm^2.

In polymeric dental composites, which use multifunctional methacrylate monomers, maximum double bond conversions are normally only between 55 to 75 % (101). The levels of monomer polymerisation in this study were significantly greater than observed in dental composites under comparable conditions, which might be due to the low glass transition temperature of the initial monomers preventing vitrification that can limit final polymerisation (144). Vitrification often occurs in the room temperature polymerisation of inflexible dimethacrylate monomers, resulting in slowing down of the polymerisation reaction and incomplete conversion (144). The high level of conversion of the materials in all cases with this investigation suggests that the decrease in flexibility of the final polymers with reducing monomer molecular weight was likely to be due to an

increase in methacrylate group concentration and crosslinking rather than plasticization by any unconverted monomer. It has been stated that unreacted monomer can plasticize the polymer network making it more pliable and decreasing its mechanical properties (101).

In degradable systems rapid and complete conversion is required to allow immediate bonding to surrounding tissues after placement and to ensure that reactive and potentially toxic double bond-containing components are not released upon degradation. The degree of conversion can also affect the bulk physical properties of the resultant polymers such as mechanical strength. The results have proved that high levels of polymerisation can be achieved for all the monomers (>90 %) at 37 °C which is beneficial for injectable, rapid set formulations. When the monomers are short, clinically acceptable light exposure times of 60 s using blue light are sufficient for greater than 98 % conversion of 1 mm thick specimens, but for larger monomers longer times are required (240 s). A lower initiator concentration of 0.5 wt% is also sufficient and may be favourable compared to 2 wt% to reduce required times of light exposure for thicker specimens. The lower initiator concentration is also preferable because of the potential cytotoxic effects of initiators. It has been observed by Pagoria *et al* that visible light-irradiated CQ/ DMPT damaged DNA in a concentration-dependent manner (211). Through further investigations, such as mechanical properties or degradation and drug release rates, these polymers may potentially lead to a new favourable range of materials for various applications in bone tissue engineering and drug delivery.

The disadvantages of photocuring include limitations on sample size and depth (only a few millimetres) due to light attenuation by the initiator and the need to use fibre optic technology with non-open surgical sites. The technique, however, can be particularly useful in 'open' environments such as the oral cavity or during invasive

procedures such as surgery. In addition one study has shown the feasibility of transdermal photopolymerisation of a dimethacrylate polymer (212). UVA and visible light were able to penetrate skin up to 2 mm and more than 3.5 mm in thickness respectively. On exposure to UVA and visible lights the polymer at 1.5 mm skin deep was 80 % polymerised after 900 and 100 s respectively. The rapidly setting polymer in this study could therefore be delivered subcutaneously through a small diameter needle and then converted to a solid through transdermal exposure to light. Such an implant polymer system would be useful for tissue engineering and drug delivery applications.

4 Polymer Degradation

4.1   Background

In the last chapter, five fluid and therefore injectable poly(PG-co-lactide) dimethacrylate monomers were synthesised and their polymerisation rate and extent determined. In the following chapter physical, degradation and mechanical properties of these polymers will be discussed.

As has been previously described, degradable polymers have been utilised in many medical and biomedical applications. They have been used as resorbable plates and screws (27), as scaffolds for the growth and repair of tissue and organs (30) and as carriers for the delivery of drugs (34) to name just a few. The rationale is to use a degradable polymer that, after placement in the body, provides temporary support of the tissue function and then degrades at a rate comparable with regeneration of the damaged tissue, such that the load of function is gradually transferred back to the new tissue enabling better and faster restoration of natural tissue function. The degradation products should also be eliminable from the body safely without causing extensive immunological and inflammation response (13).

Limitations of biodegradable polymers to date, however, include their erratic degradation mechanisms or rates as well as their insufficient mechanical properties as needed for high load bearing applications (1;213). For example polymers such as PCL can take up to two years to fully degrade rendering it unsuitable for short-term applications (67), whilst commercially used PLA and PGL and their co-polymers degrade catastrophically (11). The photocrosslinkable (meth) acrylate end capped poly(ether-co-esters) produced to date primarily contain PEG (196), which because of their high hydrophilicity, can also degrade catastrophically in a similar manner to PLA (214;215). In

this type of bulk degradation mechanism water sorption causes a steady reduction in the bulk polymer molecular weight and acid build up without product release until the material suddenly collapses. This may lead to localised cytotoxic or irritant effects in the body and a sudden loss of functional support for the damaged tissue (1).

For a polymeric device, surface erosion is generally preferable, as in this type of degradation mechanism both material loss and release of any substances, such as drugs dispersed within prior to set, can be linear with time. The hydrophobic methacrylate end capped poly(hydrocarbon-co-anhydride)s (195) that have previously been produced for biomedical applications is one example of a surface eroding polymer, but the reactivity of the anhydride group makes purification of the polymers difficult and can lead to a potentially poor shelf-life (113). Understanding degradation mechanisms is important, because a polymer that is generally considered as surface eroding can become bulk eroding if the device is of small enough dimension. For example, PLA becomes surface eroding when the pH of the medium is raised to 13 so that surface bond degradation occurs more rapidly than bulk (214). Lowering pH to 2, however, was found to have no effect on PLA degradation. This has been attributed in part to release of degradation products being a rate limiting factor (214).

The aim of this study was therefore to investigate the degradation and mechanical properties of the five ABA poly(PG-co-lactide) dimethacrylate polymers in water.

4.2   Materials and Methods

4.2.1   Formulations studied

The five poly(PG-co-lactide) dimethacrylate monomers (batch number 180803) were used. Detailed structural characteristics, including the lactide chain lengths and methacrylation efficiency of these monomers can be found in Section 3.3.1, Chapter 3.

Table 4.1. Combinations of formulations investigated for degradation studies and their polymerisation extent (determined by Raman spectroscopy). Note that according to the factorial design (Table 2.1 Chapter 2), there are two identical formulations for the intermediate formulation with P17L4DMA.

Monomer code	Photoinitiator concentration (wt%)	Double bond conversion (%)
P34L8DMA	0.5	100
P34L8DMA	2	100
P34L2DMA	0.5	99
P34L2DMA	2	100
P17L4DMA	1	100
P17L4DMA	1	100
P7L8DMA	0.5	100
P7L8DMA	2	100
P7L2DMA	0.5	98
P7L2DMA	2	100

Polymer formulations were fabricated according to a factorial experimental design (see Table 2.1, Chapter 2). In this experiment, effects of three variables on degradation and mechanical properties of the polymers were assessed: (i) PPG n level (i.e. 34, 17, 7); (ii) lactide linkage m level (i.e. 8, 4, 2); and (iii) CQ and DMPT concentration (i.e. 2, 1, 0.5 wt%). According to the factorial design, 0.5 or 2 wt % of both CQ and DMPT were added to the four monomers produced using PPG 425 or 2000 g/mol and lactide 2 or 8

mol/mol PPG and 1 wt% to the single PPG 1000 g/mol and lactide 4 mol/mol PPG based

"intermediate" formulation. The combinations of the formulations are presented in Table

4.1. In total ten sample formulations were prepared with the monomer P17L4DMA being

a duplicate.

4.2.2 Sample preparation

For each formulation, the fluid monomer was mixed with the photoinitiators and

HEMA (10 wt% to aid dispersion). The resultant monomer mix was placed into steel ring

moulds of approximately 10 mm internal diameter and 2 mm depth. The top and bottom

surfaces were covered with acetate sheets before placing into a blue light box (*Unilux Ac,*

Kulzer, 1.67 mW/cm^2) for multiple simultaneous sample curing. The monomer mix was

illuminated for five minutes each side and after 24 hours the crosslinked specimen was

removed from the ring. Three specimens were made for each formulation. Raman spectra

(Perkin Elmer series 2000 FTIR/ Raman spectrometer) were obtained on the monomer

mix prior to illumination and on the crosslinked specimens after 24 hours. Using the

methacrylate C=C peak at 1640 cm^{-1} and Equation 3.15 (see Section 3.3.3.1, Chapter 3),

the final polymerisation percentages for the formulations were quantified by dividing the

post-cure peak height above its background by that of pre-cure. As can be seen from

Table 4.1, all formulations achieved at least 98 % of polymer cure.

4.2.3 Degradation studies

Each specimen was placed upright in the conical end of a sterilin tube allowing

contact with water on all sides. The specimen was immersed in 10 ml of deionised water

already adjusted to pH 7 using ammonium hydroxide solution, and the sterilin tube was

incubated at 37 °C. After 0.5, 1, 2, 4, 24, 48, and 72 hours and 1, 2, 4, 8 and 14 weeks, the specimens were removed and placed in fresh pH-adjusted deionised water after undergoing gravimetric and mechanical analyses. In all analyses mean results from the three specimens for each formulation at each time point were obtained and relative standard deviations (RSD) calculated by dividing the standard deviations (s) by the means ($\bar{x}$), as shown in the following equation:

$$RSD = \frac{s}{\bar{x}} \qquad\qquad 4.1$$

These relative standard deviations expressed the variability in the values measured relative to the magnitude of the calculated mean as a fraction or percentage. For example, if the absolute standard deviation is 2 and the mean is 10, the relative standard deviation is 2 divided by 10 and the variability is equal to 0.2 or 20 % of the mean.

4.2.3.1 Gravimetric and dimensional analysis

Prior to immersion in water, the initial mass and volume of all specimens were determined gravimetrically using a Mettler Teledo balance with a density kit to an accuracy of 0.0001 g and their heights and diameters measured using callipers to an accuracy of 0.001 mm. At all the above time points, each specimen was removed from the storage water; the external surface blotted dry with tissue paper and re-weighed.

The wet mass change of each specimen (ΔW) was calculated using Equation 4.2:

$$\Delta W(\%) = 100 * \frac{W_t - W_0}{W_0} \qquad\qquad 4.2$$

Where, W_t and W_0 respectively, are mass of the specimen at time t and initially.

The specimens were then weighed in water using a density kit, and their density (ρ_t) and volume (V_t) at time t calculated using Equation 4.3 and 4.4 respectively:

$$\rho_t = \rho_{water} * \frac{W_t}{W_t - M_t} \qquad\qquad 4.3$$

$$V_t = \frac{W_t}{\rho_t} \qquad\qquad 4.4$$

Where ρ is the density of specimen and ρ_{water} is the density of water (g/cm^3) at the operating temperature (°C); M is the mass of specimen measured in water (g) and V is the volume of the specimen (cm^3). The density and volume were converted to total change as percentages of initial values (time 0) using Equations 4.5 and 4.6 respectively.

$$\Delta\rho(\%) = 100 * \frac{\rho_t - \rho_0}{\rho_0} \qquad\qquad 4.5$$

$$\Delta V(\%) = 100 * \frac{V_t - V_0}{V_0} \qquad\qquad 4.6$$

4.2.3.2 pH measurements

At each time-point the pH of the storage solution was measured (Hanna Instruments, pH 211 Microprocessor pH meter) after removal of the specimen. To quantify relative rates of degradation, the concentration of acid was calculated from the pH and converted to cumulative moles of acid released in 10 ml storage solution, C_a per specimen using Equation 4.7 and 4.8 respectively.

$$pH = -\log[H^+] \qquad \text{i.e.} \qquad \left[H^+\right] = inverse\,\log_{10}(-pH) \qquad 4.7$$

$$C_a = \sum_0^t [H^+]_t\,/100 \qquad\qquad 4.8$$

Where $[H^+]$ is the molar hydrogen ion concentration (mol dm^{-3}), t is the time point and 100 is the conversion factor to obtain C_a as moles of acid released per specimen in 10 ml storage solution.

4.2.3.3 Final gravimetric and dimensional analysis

To determine final material mass loss at the end of 14 weeks, specimens were dried under vacuum to constant mass except those from P34L8DMA (which had fallen apart at this time) and their total percentage polymer mass loss, ΔW_P, and water content, calculated by comparison with the initial dry and final wet mass respectively. The height and diameter of the specimens were re-measured using callipers.

The mass of degradation products per mole of acid released, W_{Pmol} (g/mol), was then calculated using Equation 4.9

$$W_{Pmol}\left(g\,/\,mol\right) = \frac{\Delta W_P \times W_0}{C_a}$$

4.9

4.2.3.4 FT-IR analysis of polymers and degradation products

IR spectroscopy has been proven to be a valid tool for investigating degradation of biodegradable polymers and assessing their degradation products (216). At each of the above degradation time points after removal of the specimens, the storage solutions were evaporated to dryness and ATR-FTIR spectra of the residues obtained. Degradation products were identified by comparing the FT-IR spectra with those for the polymers, PPG, polylactide and polymethacrylic acid.

4.2.3.5 Mechanical analysis

Two types of mechanical analyses were conducted on the specimens using a Perkin Elmer Dynamic Mechanical Analyser (DMA 7e, Perkin Elmer Instruments).

(a) Static modulus

Prior to immersion in water and at the end of the degradation study after drying, the dry specimens were tested to characterise their initial and final stress-dependent mechanical properties. By applying an increasing stress (σ) at a fixed rate and measuring the resultant strain (ε) it was possible to determine the stiffness of the specimen in the form of modulus (i.e. elastic modulus). In this test, a linearly increasing quasi-static stress was applied to the specimen on a parallel plate setup incorporating a 3 mm probe. The resultant deformation was recorded as a function of the applied stress. Before starting the run, the system was allowed to equilibrate at room temperature until the probe position became relatively stable. The sample height was then measured. An increasing static force from 10 mN ($\sigma = 1.4$ kPa) to 8000 mN ($\sigma = 1132$ kPa) was applied to the sample at a constant rate of 500 mN per minute (70.7 kPa/min). The resultant displacement in strain was plotted against the applied stress, and using software (Pyris TM version 5 software, Perkin-Elmer UK), the modulus (E) was calculated by dividing the stress (σ) by strain (ε) as shown in Equation 2.3 (Chapter 2). The moduli at 100 kPa stress level were determined for the polymers for comparative purposes. Three runs were made on each of the three specimens for each formulation.

(b) Dynamic modulus

At each of the above degradation time points after removal from storage water and having been blotted with tissue paper to remove excess water, the wet specimens were tested to monitor changes in their mechanical properties with time during degradation. A dynamic stress scan was used with a parallel plate setup incorporating a 3 mm probe, which applied a cyclically load onto the specimens. Specimens were tested dynamically

at a 1 % strain and a frequency of 1 Hz whilst maintaining a ratio of static to dynamic stress of 1.2. This low strain level was chosen so as not to cause any damage to the specimens during testing in order to test the same specimens as a function of degradation time. Testing was carried out at room temperature for 60 s, and the storage and loss moduli and tan delta recorded at 30 s of testing. One run was made on each of the three specimens for each formulation. The storage and loss moduli and tan delta (see Equation 2.10 to 2.12, Chapter 2) were each plotted versus the square root of time. The changes in the storage modulus ($\Delta E'$) of the polymers at 24 hr, 2, 4 and 14 weeks during degradation were also calculated using Equation 4.10.

$$\Delta E'(\%) = 100 * \frac{E'_t - E'_0}{E'_0} \qquad\qquad 4.10$$

Where, E'_t and E'_0 respectively, are storage modulus values at time t and initially.

4.3 Results

On analysis of the results it was found that the data could not be interpreted easily using Equations 2.15 to 2.18 from the factorial analysis mathematical explanation (Chapter 2). The degradation process in the polymers in this case was complicated by a mixture of influencing and interactive variables. For example in some polymers the extent of methacrylate end group termination deviated strongly from 100 % and this in turn would affect the level of crosslinking density and methacrylate block lengths and the subsequent complex degradation processes. In the following, therefore, the results were analysed based on comparison of individual polymers rather than attempting a full mathematical interpretation.

4.3.1   Sample appearance and dimensional change

All polymer specimens made had an average height of 1.92 $\pm$ 0.13 mm and diameter of 10.60 $\pm$ 0.23 mm prior to degradation. The specimens were re-measured at 14 weeks after having been vacuum-dried to constant weight. All polymer specimens except those of P34L8DMA retained their structural integrity, but with a diameter that is significantly (at 95 % level) reduced by, on average, 5.7 $\pm$ 0.6 % at the end of 14 weeks. All formulations with short PPG chains had in addition a significant decrease in height (on average 10.6 $\pm$ 3.2 % reduction).

(i)

(ii)

Before degradation   At 8 weeks   At 14 weeks
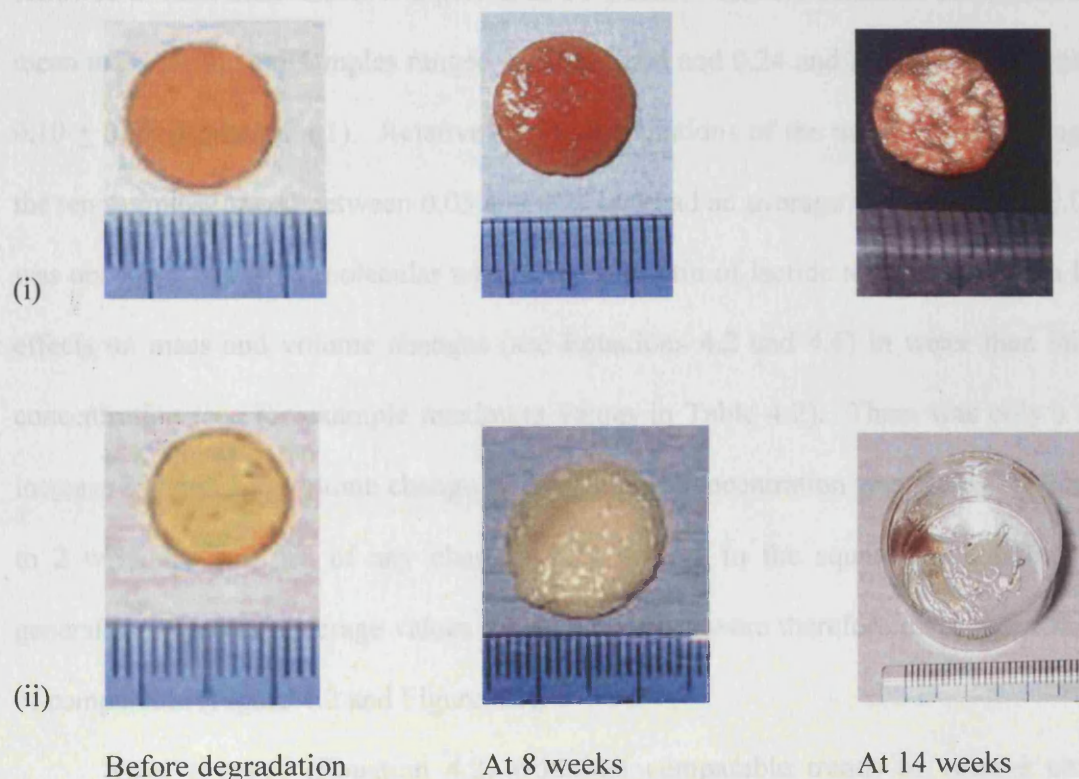
Figure 4.1. Appearance of the polymers before and after different times of degradation; (i) a fast-degrading polymer, P7L8DMA and (ii) initially slow-degrading but high-swelling and finally disintegrating polymer, P34L8DMA. The specimens were photographed at 8 weeks after having been blotted dry with tissue paper and at 14 weeks after having been vacuum-dried to constant weight.

Figure 4.1 shows the appearances of a fast-degrading specimen (i.e. P7L8DMA) and a slow-degrading specimen (i.e. P34L8DMA) before and after different times of the study. With both P34L8DMA polymers (containing 0.5 or 2 wt% initiators) the specimens swelled significantly to a maximum at 8 weeks and then disintegrated almost completely by 14 weeks.

4.3.2 Mass and volume change

The mass and volume of three 'wet' polymer specimens for each formulation were followed at time intervals over a period of 14 weeks. Relative standard deviations of the mean mass for the ten samples ranged between 0.04 and 0.24 and had an average value of 0.10 $\pm$ 0.07 (Equation 4.1). Relative standard deviations of the mean volume change for the ten samples ranged between 0.05 and 0.26 and had an average value of 0.10 $\pm$ 0.08. It was observed that PPG molecular weight and the ratio of lactide to PPG had much larger effects on mass and volume changes (see Equations 4.2 and 4.6) in water than initiator concentration (see for example maximum values in Table 4.2). There was only a small increase in mass and volume change as the initiator concentration was increased from 0.5 to 2 wt%; the profiles of any changes with respect to the square root of time were generally the same. Average values for each polymer were therefore determined for ease of comparison (Figure 4.2 and Figure 4.3).

Mass changes (Equation 4.2) exhibited comparable trends to volume changes (Equation 4.6) for all formulations with both, during the first 24 hours, increasing proportional to the square root of time as would be expected for diffusion controlled water sorption (compare Figure 4.2 & Figure 4.3). Polymers with longer lactide lengths,

P34L8DMA and P7L8DMA, absorbed water at a faster rate than the other samples in this

24 hour period (see Table 4.2). Following this initial period the polymers produced from

the longest monomer, P34L8DMA (with the lowest concentration of methacrylate groups),

continued to increase in both mass and volume before falling apart at 14 weeks. Changes

in mass and volume of all other formulations continued to increase for up to a week and

then either remained constant or declined slightly over the remaining time as erosion

dominated over water sorption. Maximum percentage swelling and mass change of

polymers from the intermediate length monomers (P34L2DMA, P17L4DMA and

P7L8DMA) were on average 22 ± 6 vol% and 19 ± 5 wt% and slightly higher when the

initiator concentration was raised (see Table 4.2). With the shorter monomer, P7L2DMA,

maximum mass and volume changes were only ~5%.

Figure 4.2. Average mass change in water as a function of the square root of time for the polymers. (Straight lines are best fit through either early (assuming an intercept of zero) or later time data).

Figure 4.3. Average volume change in water as a function of the square root of time for the polymers. (Straight lines are best fit through either early (assuming an intercept of zero) or later time data)

Table 4.2. Maximum mass and volume changes and average rates of mass and volume increase of the polymers during degradation in water.

Code	Initiator conc.	Max. mass increase	Max volume increase	Av. initial gradient of mass increase		Av. initial gradient of volume increase	
	wt%	wt%	vol%	$\text{wt\%/} \text{hr}^{0.5}$	R^2 value	$\text{vol\%/} \text{hr}^{0.5}$	R^2 value
P34L8DMA	0.5 2	139 194	155 216	2.92	0.97	3.53	0.98
P34L2DMA	0.5 2	17 23	20 26	2.16	0.82	1.94	0.86
P17L4DMA	1 1	15 15	16 16	1.27	0.89	1.04	0.92
P7L8DMA	0.5 2	19 26	22 34	2.72	0.96	2.80	0.97
P7L2DMA	0.5 2	4.8 4.9	5.4 5.5	1.01	0.97	1.27	0.99

4.3.3 Density change

Relative standard deviations of the mean density change for the ten samples ranged between 0.10 and 0.56 and had an average value of 0.38 ± 0.17. On increasing the initiator concentration from 0.5 to 2 wt%, there was only a small decrease in the mean % density change for each polymer (see Equation 4.5 and Table 4.3).
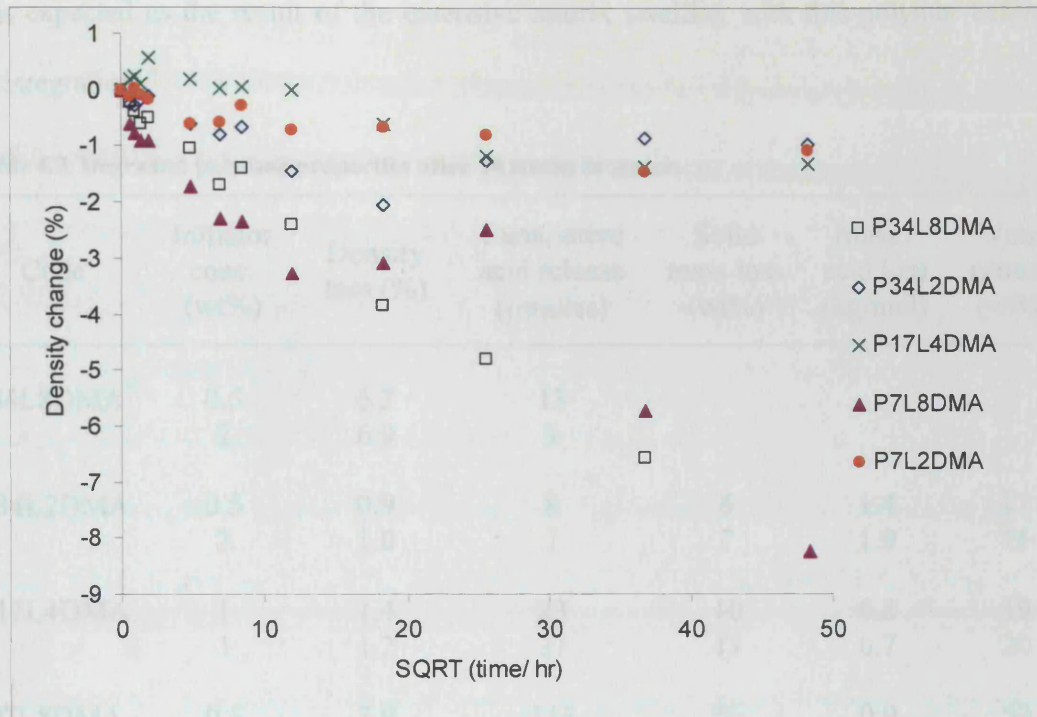
Figure 4.4. Average density change in water as a function of the square root of time for the polymers

Figure 4.4 shows the average values of mean % density change for each polymer plotted versus the square root of time. Densities for polymers produced from the short and intermediate length monomers, P7L2DMA, P17L4DMA and P34L2DMA were relatively constant throughout the 14 week period fluctuating by 2 % with an average final density decrease of 1.1 ± 0.2 %. Decrease in the polymer density could be caused by water, of slightly lower density ($1g/cm^3$) than the polymer, occupying holes / space in the material. Polymers with longer lactide segments, P7L8DMA and P34L8DMA, on the other hand, showed a constant decrease in density with the square root of time with a total decrease of 8.2 % at 14 weeks for P7L8DMA and 6.6 % at 8 weeks for P34L8DMA. With the P7L8DMA polymer, the slight reduction in volume and continual decrease in density with time indicated material erosion from the matrix. The large density decline in P34L8DMA

216

was expected as the result of the extensive matrix swelling with this polymer before its

disintegration.

Table 4.3. Degraded polymer properties after 14 weeks in water.

Code	Initiator conc. (wt%)	Density loss (%)	Cumulative acid release (μmoles)	Solid mass loss (wt%)	Mass / acid loss (kg/mol)	Water content (wt%)
P34L8DMA*	0.5	6.3	13			
	2	6.9	9			
P34L2DMA	0.5	0.9	8	6	1.4	11
	2	1.0	7	7	1.9	15
P17L4DMA	1	1.4	23	10	0.8	19
	1	1.2	27	11	0.7	20
P7L8DMA	0.5	7.9	114	56	0.9	53
	2	8.6	95	63	1.3	61
P7L2DMA	0.5	1.1	53	18	0.6	11
	2	1.0	44	19	0.8	14

* Final mass loss and water content could not be obtained for P34L8DMA due to polymer disintegration by 14 weeks.

4.3.4 Acid release

The pH of the storage solution was measured at each time point and converted to

cumulative moles of acid released per specimen (Equation 4.7 & 4.8) to quantify relative

rates of degradation in the polymers. Relative standard deviations of the mean cumulative

acid release for the ten samples for all the times points had an average value of 0.10 ± 0.07

and ranged between 0.03 and 0.16. Raising initiator concentration caused a measurable

but small decline in acid release for all polymers (see Table 4.3).

Differences in pH values and acid release with changing the monomer were,

however, much greater than occurred with initiator concentration so average values for

each are provided in Figure 4.5 and Figure 4.6 as a function of the square root of time respectively. The pH values dropped dramatically in the first 24 hours with all polymers to between pH 3 and 4 and either fluctuated around these values or continued to decline for the remaining period. The pH of polymers produced from short PPG, P7L8DMA and P7L2DMA, dropped to just below 3 after 1 and 8 weeks respectively.

Acid release was proportional to the square root of time for the full 14 weeks for polymers of P7L8DMA, P17L4DMA and P34L8DMA ($R^2 = 0.93 \pm 0.08$) but the gradient for the first sample (2.1 μmoles/ $hr^{0.5}$) was four and ten times that of the second and third in this series respectively. Acid release for P7L2DMA and P34L2DMA was initially comparable to that of P17L4DMA (0.5 μmoles/ $hr^{0.5}$) but after 1 week the gradient of acid release versus square root of time increased for P7L2DMA (1.2 μmoles/ $hr^{0.5}$) making it overall approximately proportional to time (hr) but decreased for P34L2DMA (0.03 μmoles/ $hr^{0.5}$). At 14 weeks, cumulative acid release decreased in the order P7L8DMA > P7L2DMA > P17L4DMA > P34L8DMA $\approx$ P34L2DMA (see Table 4.3).
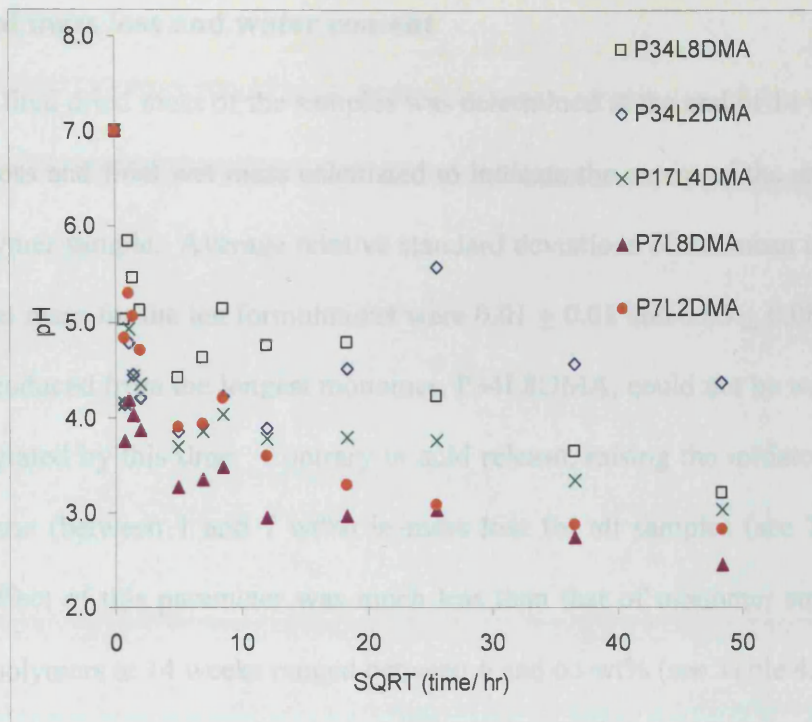
Figure 4.5. Average final pH of polymer storage water as a function of the square root of time
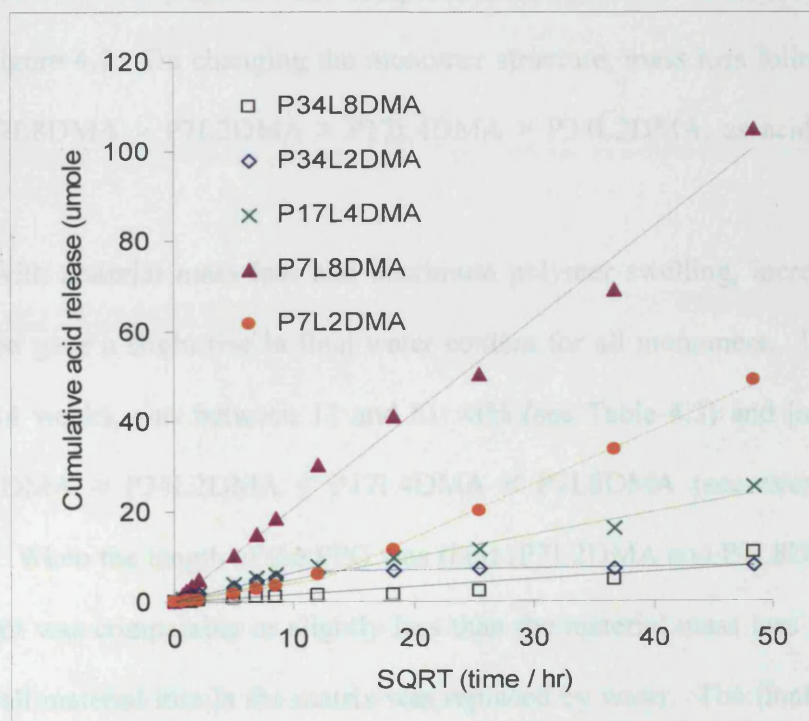
Figure 4.6. Average cumulative acid release per specimen as a function of the square root of time for the polymers. (Straight lines are best fit through either early (assuming an intercept of zero) or later time data)

4.3.5 Final mass loss and water content

The final dried mass of the samples was determined at the end of 14 weeks and the total mass loss and final wet mass calculated to indicate the extent of the erosion process of each polymer sample. Average relative standard deviations of the mean total mass loss and final wet mass for the ten formulations were 0.01 ± 0.01 and 0.05 ± 0.08 respectively. Polymers produced from the longest monomer, P34L8DMA, could not be weighed as they had disintegrated by this time. Contrary to acid release, raising the initiator level gave a slight increase (between 1 and 7 wt%) in mass loss for all samples (see Table 4.3) but again the effect of this parameter was much less than that of monomer structure. Mass loss of the polymers at 14 weeks ranged between 6 and 63 wt% (see Table 4.3) and was on average equal to 0.6 ± 0.2 wt% / μmole or 1.1 ± 0.4 kg / mole of acid release. Average values for the different polymers are compared with maximum mass increase and acid release in Figure 4.7. On changing the monomer structure, mass loss followed the same order i.e. P7L8DMA > P7L2DMA > P17L4DMA > P34L2DMA, as acid release at 14 weeks.

As with material mass loss and maximum polymer swelling, increasing initiator concentration gave a slight rise in final water content for all monomers. The final water content at 14 weeks, was between 11 and 61 wt% (see Table 4.3) and increased in the order P7L2DMA $\approx$ P34L2DMA < P17L4DMA < P7L8DMA (see average values in Figure 4.7). When the length of the PPG was short (P7L2DMA and P7L8DMA), the final water content was comparable or slightly less than the material mass loss indicating that most if not all material loss in the matrix was replaced by water. The final water content of these polymers, however, was much greater than the maximum mass increase, as the

latter was limited by dense crosslinking of the material at early times. For polymers with

longer PPG lengths (P34L2DMA), 14-week water content was greater than material loss

but less than the maximum mass increase (see Figure 4.7).
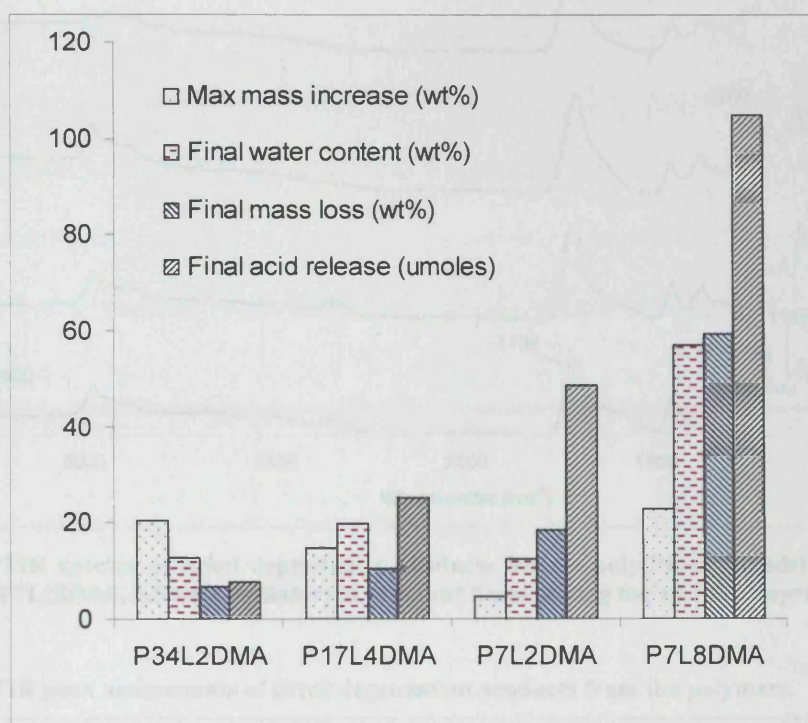
Figure 4.7. Average maximum mass increase and 14 week water content, mass loss and acid release of the four stable polymers

4.3.6   FT-IR spectra of degradation products

The amounts of residues in the storage solutions obtained after evaporation were

too small to assess gravimetrically but were sufficient to be analysed by FTIR.

Degradation products were identified by comparing the FT-IR spectra with those for the

polymers, PPG, polylactide and polymethacrylic acid. Examples of the polymer degraded

residues obtained at different times of degradation are shown in Figure 4.8 with peak

assignments presented in Table 4.4.
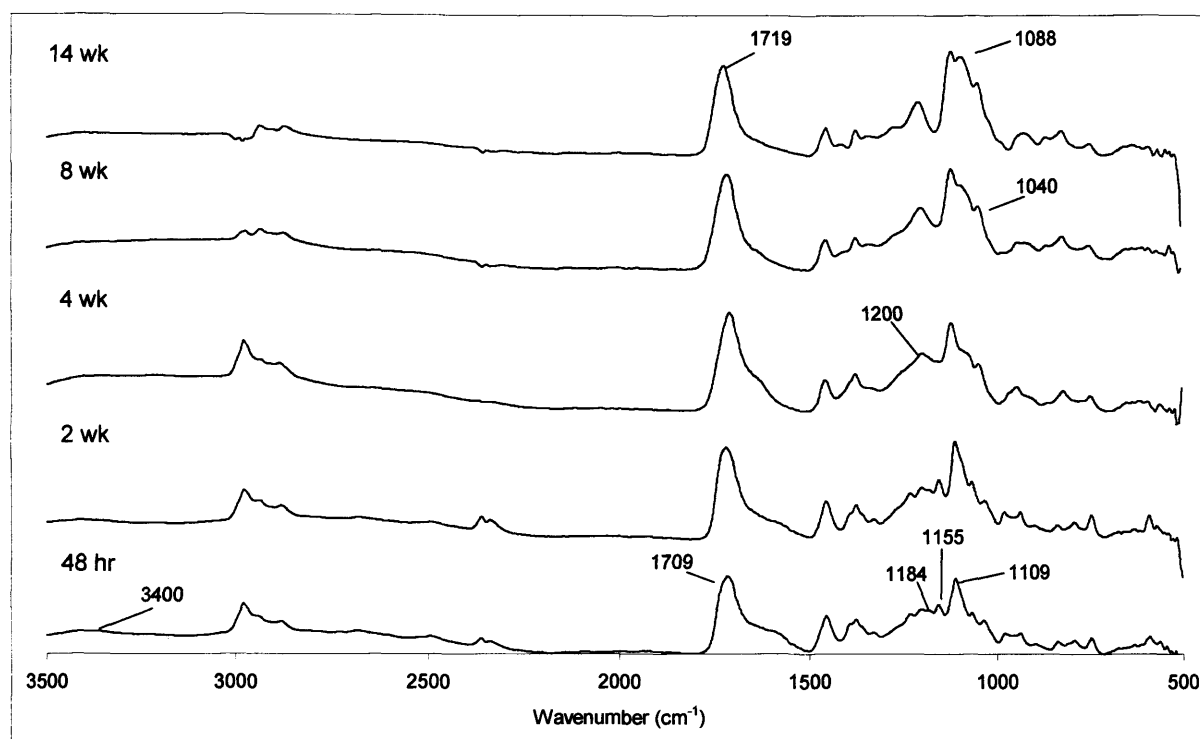
Figure 4.8. FTIR spectra of dried degradation products from a poly(PG-co-lactide) dimethacrylate polymer (i.e. P7L2DMA, 0.5 wt% initiator) at different times during the 14-week degradation study.

Table 4.4. FTIR peak assignments of dried degradation products from the polymers.

Wavenumber (cm^{-1})	Assignment	Chemical group
Early degraded product spectrum		
3400 to 3225	O-H stretch	Intermolecular bonded OH
1709	C=O stretch	Poly(methacrylic acid) carbonyl C=O
1184	C-O stretch	Lactoyl ester –(O=)C-O-R
1155	C-H bend	Poly(methacrylic acid) methyl –CH$_3$
1109	C-OH / C-O stretch	Ester –(O=)C-O-R
Late degraded product spectrum		
1719	C=O stretch	Poly(methacrylic acid) / Lactoyl carbonyl C=O
1200	C-O stretch	Lactoyl ester –(O=)C-O-R
1088	C-O-C asymmetrical stretch	PPG ether C-O-C
1040	C-O stretch	Lactoyl ester –(O=)C-O-R

For the second fastest degrading polymer, P7L2DMA, the residue FTIR spectra at early times suggested formation of mainly oligo(methacrylic acid) and lactic acid fragments. From 4 weeks the oligo(methacrylic acid) 1155 cm^{-1} peak became less prominent whilst the increasing oligo(lactic acid) 1200 and 1040 cm^{-1} peaks suggested increasing formation of the latter. At later times PPG peaks became clearer (1088 cm^{-1}) indicating release of poly(PG-co-lactic acid) fragments. The water insoluble PPG tended to remain within the polymeric matrix and was not released into the solutions until degradation was advanced. The FTIR degradation product spectra were comparable for all other polymers although the release of different components into the storage solutions occurred at different times dependent upon the rate of polymer degradation. For example, initial degradation products were not apparent from the slowest degrading P34L8DMA polymer until 4 weeks. By contrast PPG peaks were seen at much earlier times in the fastest degrading polymer P7L8DMA than with the other polymers. As this polymer contained longer lactide chains, the degraded oligo(lactic acid) peaks were also relatively more prominent in the degradation spectra than would be found in the polymers with short lactide chains. The latter observation also suggested that the lactide chains of the polymers during degradation were not fully hydrolysed before being released into solution.

4.3.7 Modulus

4.3.7.1 Static Modulus

Figure 4.9 (a) and (b) show the displacement in strain as a function of applied stress for the five dry polymers at different levels of initiator before and after 14 weeks of degradation respectively. Before degradation, the shortest polymer P7L2DMA had the least deformation with increasing applied stress and was the most rigid of all the polymers

(Figure 4.9a). The longest polymer P34L8DMA, by contrast, was the most flexible with the highest displacement in strain. All other polymers had rigidity between these two extremes. Within each polymer, those produced with a higher level of initiator had a bigger displacement in strain and were therefore relatively more flexible (compare filled and unfilled symbols in Figure 4.9a). After degradation in water and vacuum drying,, the polymers generally had a further displacement in strain indicating their increased flexibility. The compressive static modulus at 100 kPa stress level, calculated using Equation 2.3 (Chapter 2), was determined for the polymers at each initiator concentration to allow relative comparison between the samples (Figure 4.10).

Contrary to the above degradation results, raising initiator level had a large effect on the initial static modulus of the polymers (compare deep-coloured and thick-striped bars of each polymer in Figure 4.10). Initial static modulus in the polymers produced with 0.5 wt% initiator (between 308 and 3100 kPa) increased by one to three folds when compared to their counterparts with 2 wt% initiator (between 265 and 1149 kPa). For the final static modulus, however, there was no significant difference between the respective polymers containing the two initiator concentrations (compare light-coloured and thin-striped bars of each polymer in Figure 4.10). For constant initiator concentrations (both low and high) the initial moduli increased in the following order: P34L8DMA< P34L2DMA $\leq$ P7L8DMA < P7L2DMA (i.e. increasing with reducing chain length). The P17L4DMA polymer made with an intermediate initiator level had a modulus comparable to those of P7L8DMA and P34L2DMA at 0.5 wt% initiator level.

Results of initial and final moduli showed that on average, with 0.5 wt% initiator, there was a decrease in modulus after degradation. This decrease was as much as 37 % for P7L8DMA and 44 % for P7L2DMA. For the polymer P17L4DMA with 1 % initiator,

the modulus also decreased by 48 % after degradation. By contrast, after degradation there was on average an increase in the moduli for the polymers made with high initiator, being 114 % for P34L2DMA, and 61% for P7L2DMA.
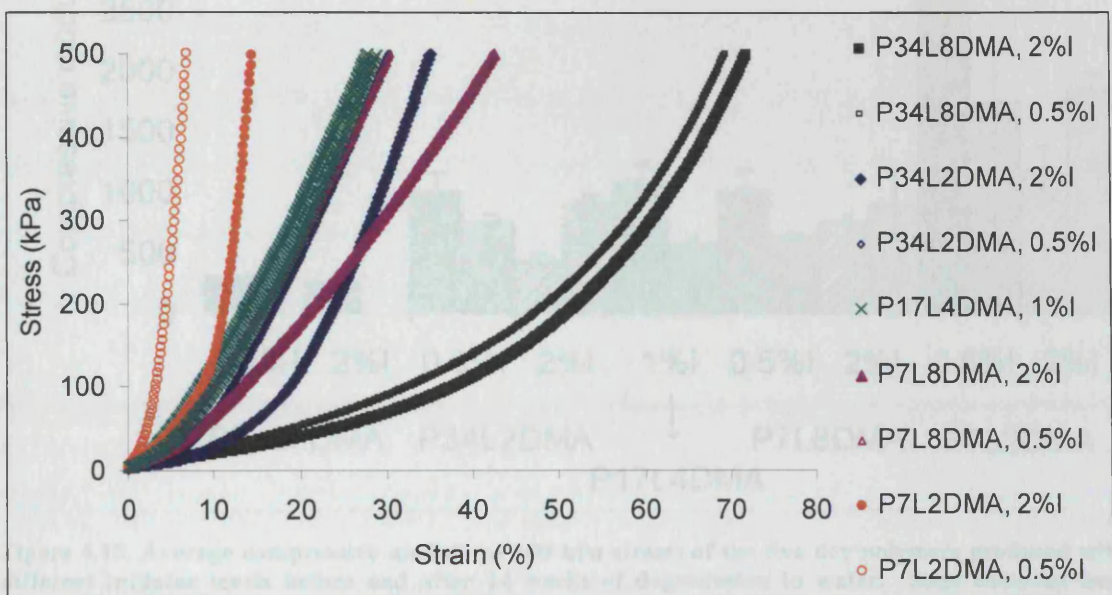
(a)
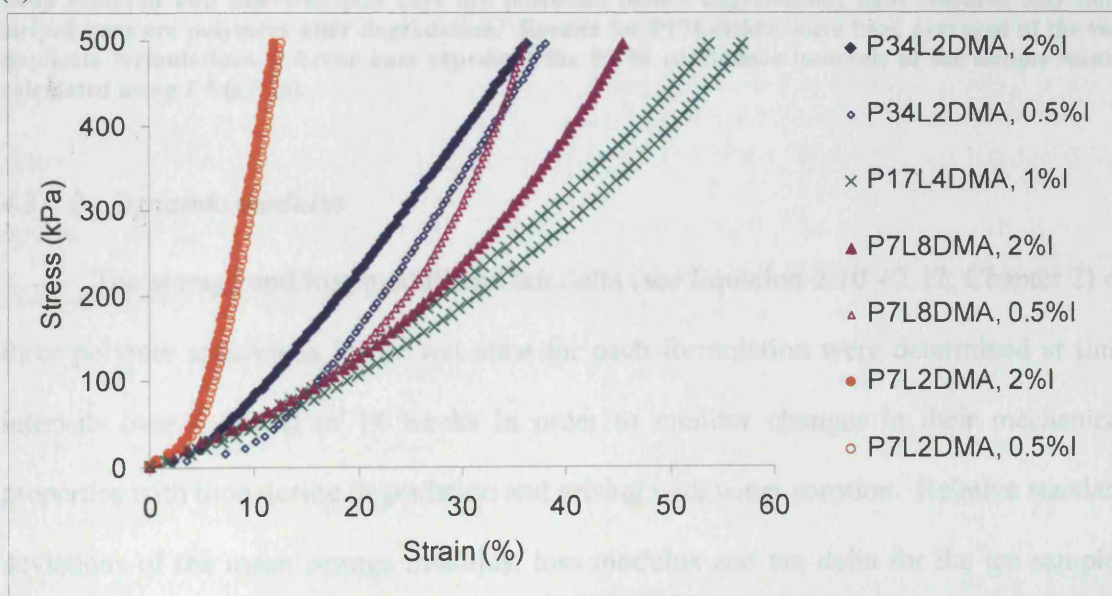
(b)

Figure 4.9. Stress-strain response curves for the five dry polymers produced with different initiator levels (a) before and (b) after 14 weeks of degradation in water. Unfilled symbols represent polymers at 0.5 wt% initiator level and filled symbols are polymers at 2 wt% initiator level. Results for P34L8DMA after 14 weeks could not be obtained as these polymers had disintegrated by this time.
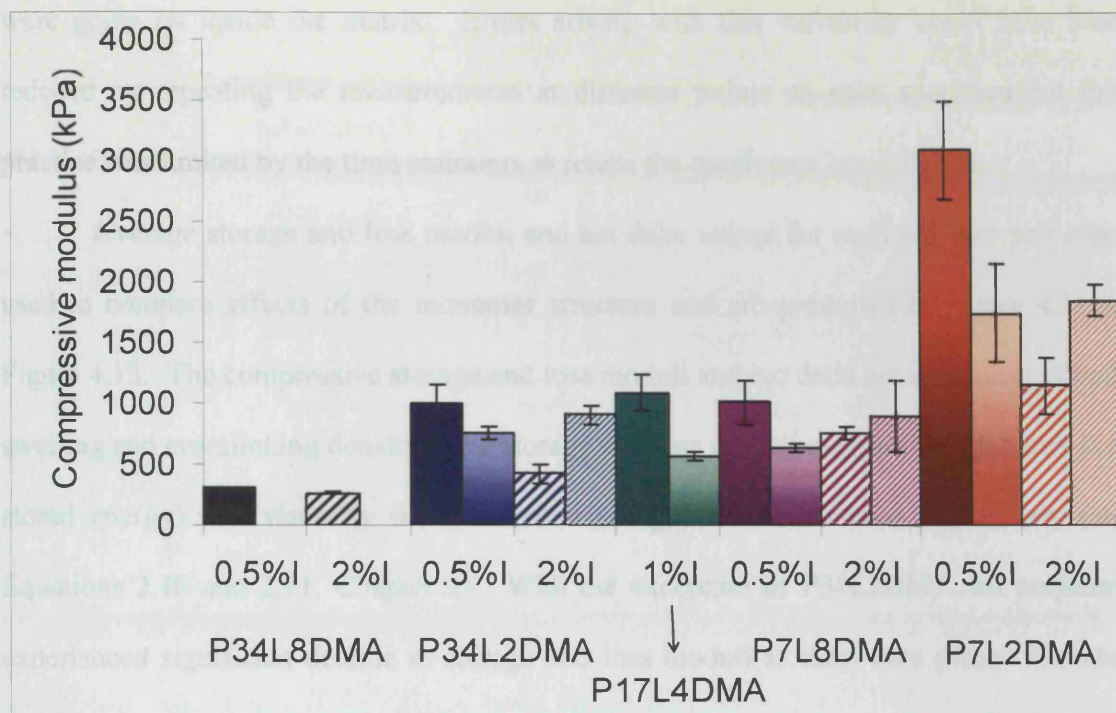
Figure 4.10. Average compressive moduli (at 100 kPa stress) of the five dry polymers produced with different initiator levels before and after 14 weeks of degradation in water. Solid coloured bars represent polymers at 0.5 wt% initiator level and striped bars represent those at 2 wt% initiator level. Deep coloured and heavy-striped bars are polymers before degradation; light coloured and thin-striped bars are polymers after degradation. Results for P17L4DMA have been averaged of the two duplicate formulations. Error bars represent the 95 % confidence intervals of the sample means calculated using 2 * (s / √n).

4.3.7.2 Dynamic modulus

The storage and loss moduli and tan delta (see Equation 2.10 - 2.12, Chapter 2) of three polymer specimens in the wet state for each formulation were determined at time intervals over a period of 14 weeks in order to monitor changes in their mechanical properties with time during degradation and arising with water sorption. Relative standard deviations of the mean storage modulus, loss modulus and tan delta for the ten samples had average values of 0.30 ± 0.35, 0.29 ± 0.30 and 0.16 ± 0.19, respectively. The variability of DMA measurements could be large in some cases as a result of the variable location of the measuring probe on the specimen and the complexity of processes that

were going on inside the matrix. Errors arising with this variability could have been reduced by repeating the measurements at different points on each specimen but this practice was limited by the time restraints to return the specimens into solution.

Average storage and loss moduli and tan delta values for each polymer pair were used to compare effects of the monomer structure and are presented in Figure 4.11 to Figure 4.13. The compressive storage and loss moduli and tan delta are a function of both swelling and crosslinking density. The storage and loss moduli measure the elasticity (i.e. stored energy) and viscosity (i.e. dissipated energy) of the material respectively (see Equations 2.10 and 2.11, Chapter 2). With the exception of P34L2DMA, all polymers experienced significant decline in storage and loss moduli as they were placed in water over the first 24 hours, after which their moduli either fluctuated or declined further over the remaining time. The storage and loss moduli of the shortest polymer, P7L2DMA, were much higher than the other polymers throughout the time period due to its higher degree of crosslinking and minimal water sorption and were on average at least 8 and 3 times higher than P7L8DMA respectively. The P34L8DMA, with its lower crosslinking and significant water sorption had the lowest storage and loss moduli which were on average 58 and 25 times less than P7L2DMA respectively.

Tan delta is a ratio of the loss modulus to the storage modulus (Equation 2.12, Chapter 2) and gives a measure of how well a material can absorb or lose the deformational energy. Polymers with high lactide, P34L8DMA and P7L8DMA, had initially higher tan delta values which particularly for P7L8DMA continued to increase with time indicating an increasing viscous nature of the material due to presence of large amounts of water. Tan delta for all other polymers with lower water sorption fluctuated between 0.1 and 0.4 and variations were within experimental errors (Figure 4.13).
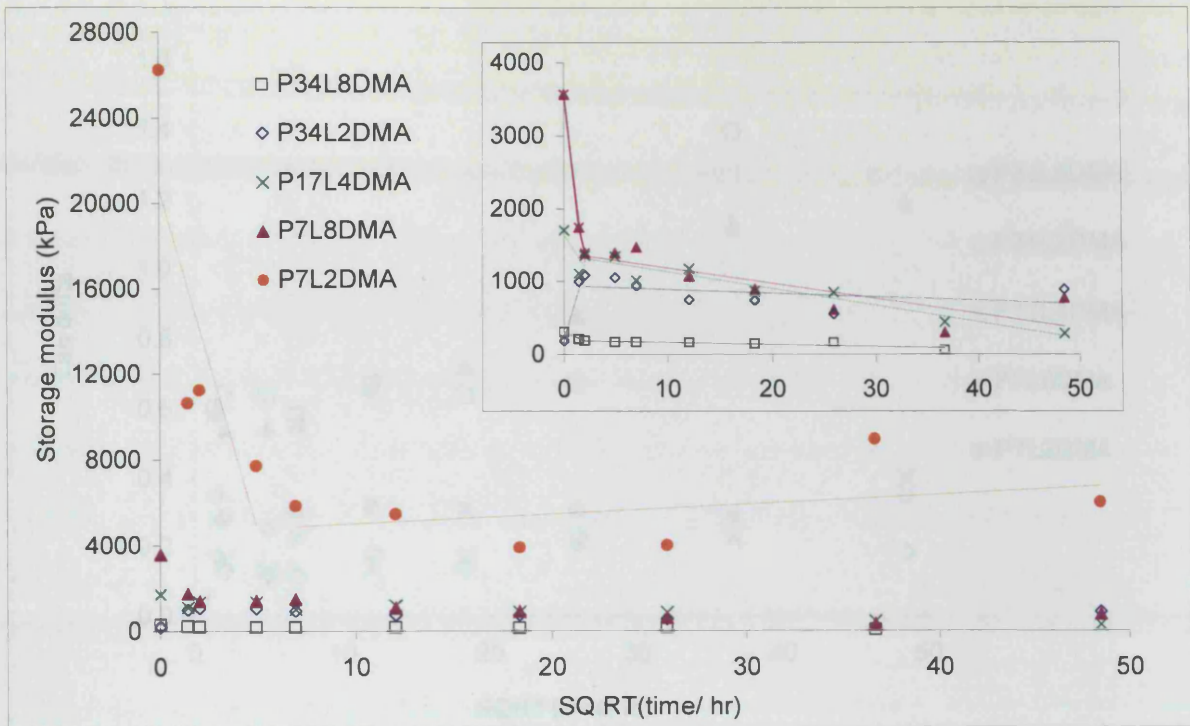
Figure 4.11. Average storage modulus in water as a function of the square root of time for the polymers. (Straight lines are best fit through early and later time data)
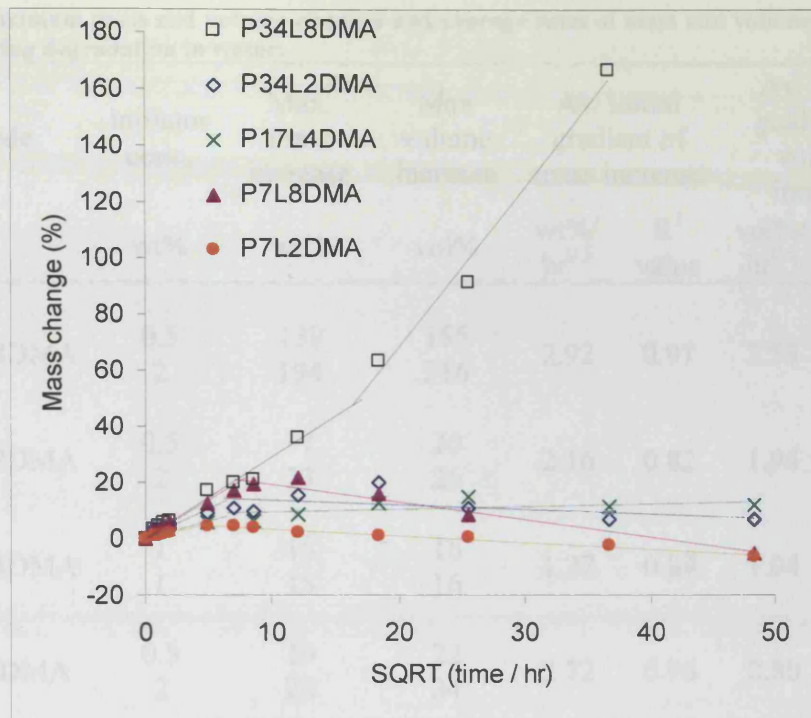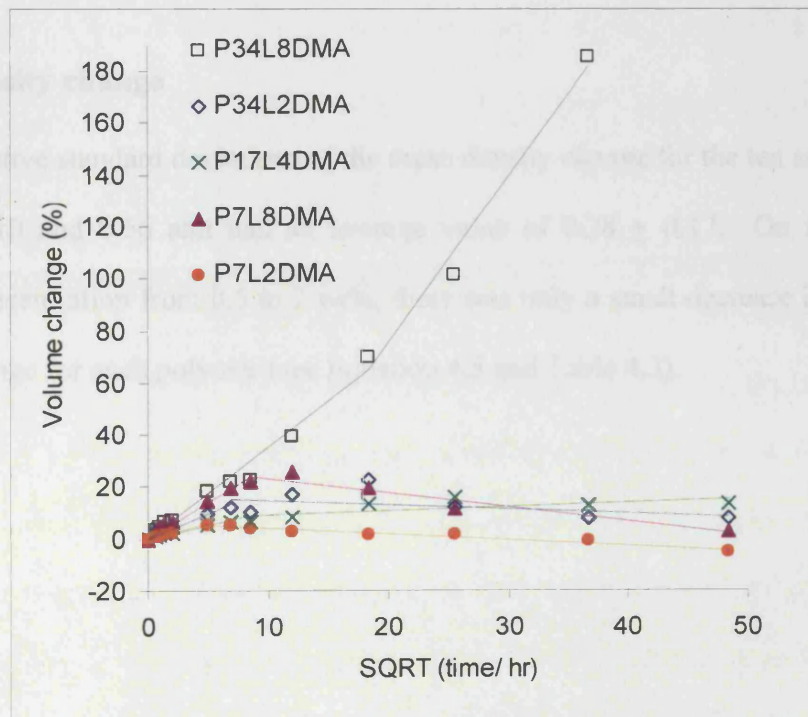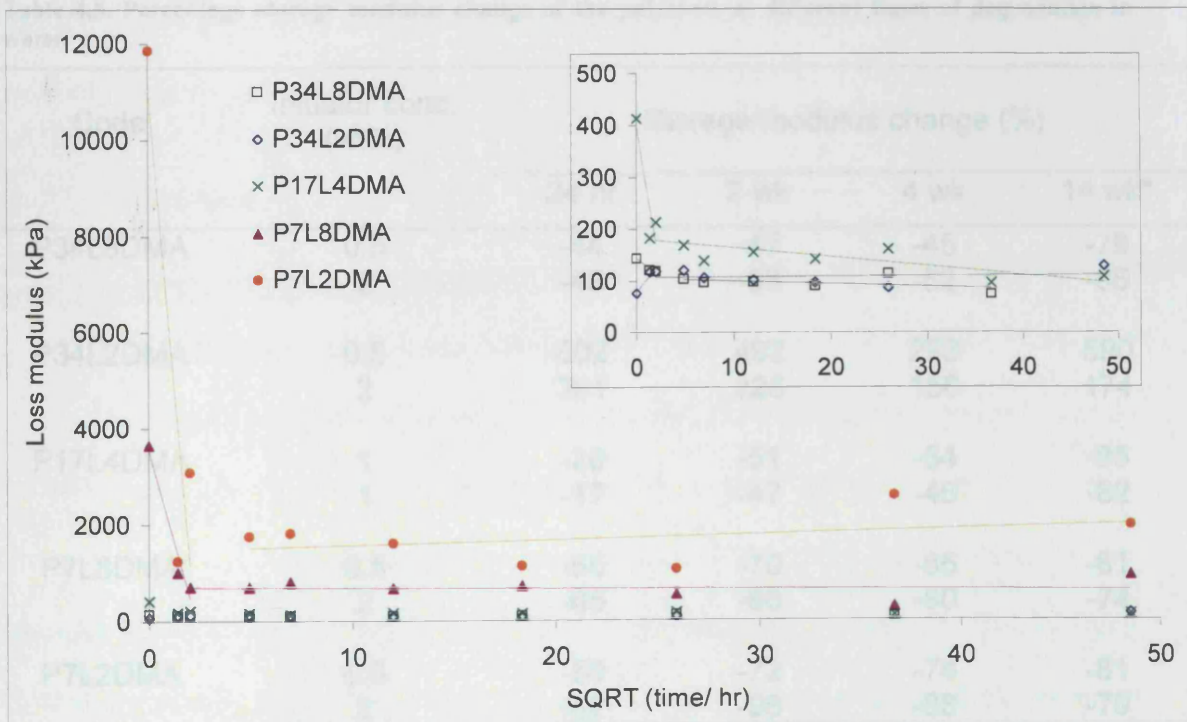

Figure 4.12. Average loss modulus in water as a function of the square root of time for the polymers. (Straight lines are best fit through early and later time data)
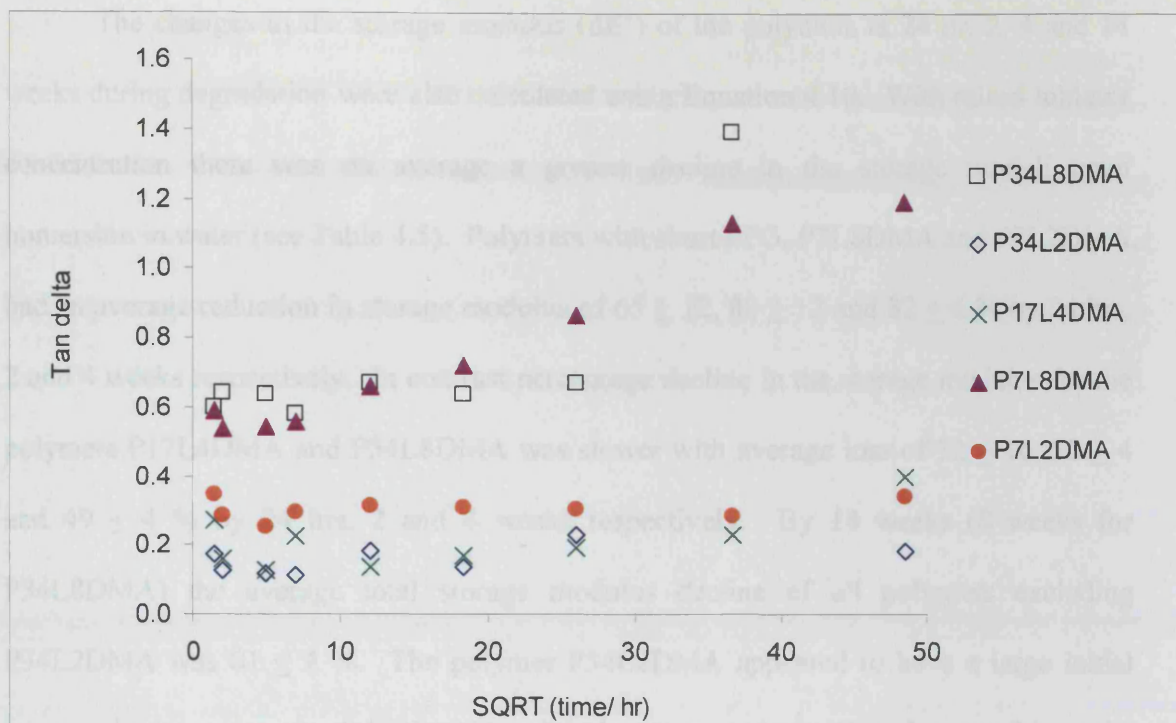
Figure 4.13. Average tan delta in water as a function of the square root of time for the polymers.

Table 4.5. Percentage storage modulus change of the polymers at different times of degradation in water.

Code	Initiator conc. (wt%)	Storage modulus change (%)			
		24 hr	2 wk	4 wk	14 wk*
P34L8DMA	0.5	-44	-47	-45	-79
	2	-48	-56	-52	-85
P34L2DMA	0.5	602	492	293	590
	2	381	226	156	174
P17L4DMA	1	-20	-51	-54	-85
	1	-17	-47	-46	-82
P7L8DMA	0.5	-55	-70	-85	-81
	2	-65	-80	-80	-74
P7L2DMA	0.5	-59	-72	-74	-81
	2	-82	-96	-88	-79

* The storage modulus change for P34L8DMA was recorded at 8 weeks instead of 14 weeks due to disintegration of the polymer.

The changes in the storage modulus ($\Delta E'$) of the polymers at 24 hr, 2, 4 and 14 weeks during degradation were also calculated using Equation 4.10. With raised initiator concentration there was on average a greater decline in the storage moduli upon immersion in water (see Table 4.5). Polymers with short PPG, P7L8DMA and P7L2DMA, had an average reduction in storage modulus of 65 ± 12, 80 ± 12 and 82 ± 6 % by 24 hrs, 2 and 4 weeks respectively. In contrast percentage decline in the storage modulus for the polymers P17L4DMA and P34L8DMA was slower with average loss of 32 ± 16, 50 ± 4 and 49 ± 4 % by 24 hrs, 2 and 4 weeks respectively. By 14 weeks (8 weeks for P34L8DMA) the average total storage modulus decline of all polymers excluding P34L2DMA was 81 ± 4 %. The polymer P34L2DMA appeared to have a large initial increase in the storage modulus but this might be an anomalous effect due possibly to the presence of plasticizing solvents (e.g. remnants from synthesis extraction or poorly polymerised segments). These were removed as the specimens were placed in water resulting in an apparent increase in the modulus.

4.4   Discussion

4.4.1   Water sorption

The initial materials in the degradation studies consist of fully polymerised polymethacrylate blocks whose length determines the number of degradable poly(lactide co PG) chains that crosslink them to other polymethacrylate blocks. When specimens, are placed in water they expand due to water sorption. Monomer length determines the distance between polymethacrylate blocks and the amount by which the polymer can expand to accommodate water without degradation. The monomer length increases in the following order: P34L8DMA> P34L2DMA> P17L4DMA $\approx$ P7L8DMA> P7L2DMA.

With the longest P34L8DMA the percentage of end group methacrylate termination is only 40 %, (see Section 3.3.1.4, Chapter 3) and therefore crosslinking is particularly low so this process causes swelling and by 14 weeks material disintegration despite low chemical bond hydrolysis. Decreasing the length of the monomer and increasing the percentage of methacrylate end termination (65– 88 % for the other polymers) raises the crosslink density such that with all other polymers, water sorption and disintegration is better controlled.

Monomer length

Crosslinking density
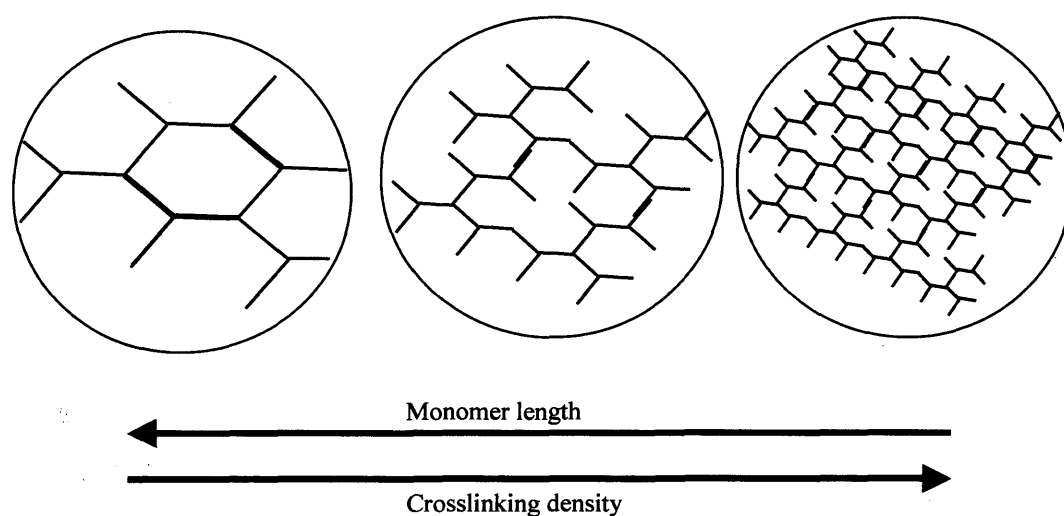
Figure 4.14. Illustration of different packing density of the polymers

As the monomer length is reduced, crosslinking density will increase and maximum swelling due to initial water sorption declines (Figure 4.14). Once maximum swelling is achieved samples from the intermediate and shorter length monomers largely maintain their volume as water sorption partially balances degradation product release (Figure 4.3). The water could fill pores generated by degradation product release or resulted from reduced crosslinking through hydrolysis allowing greater expansion of any remaining polymer.
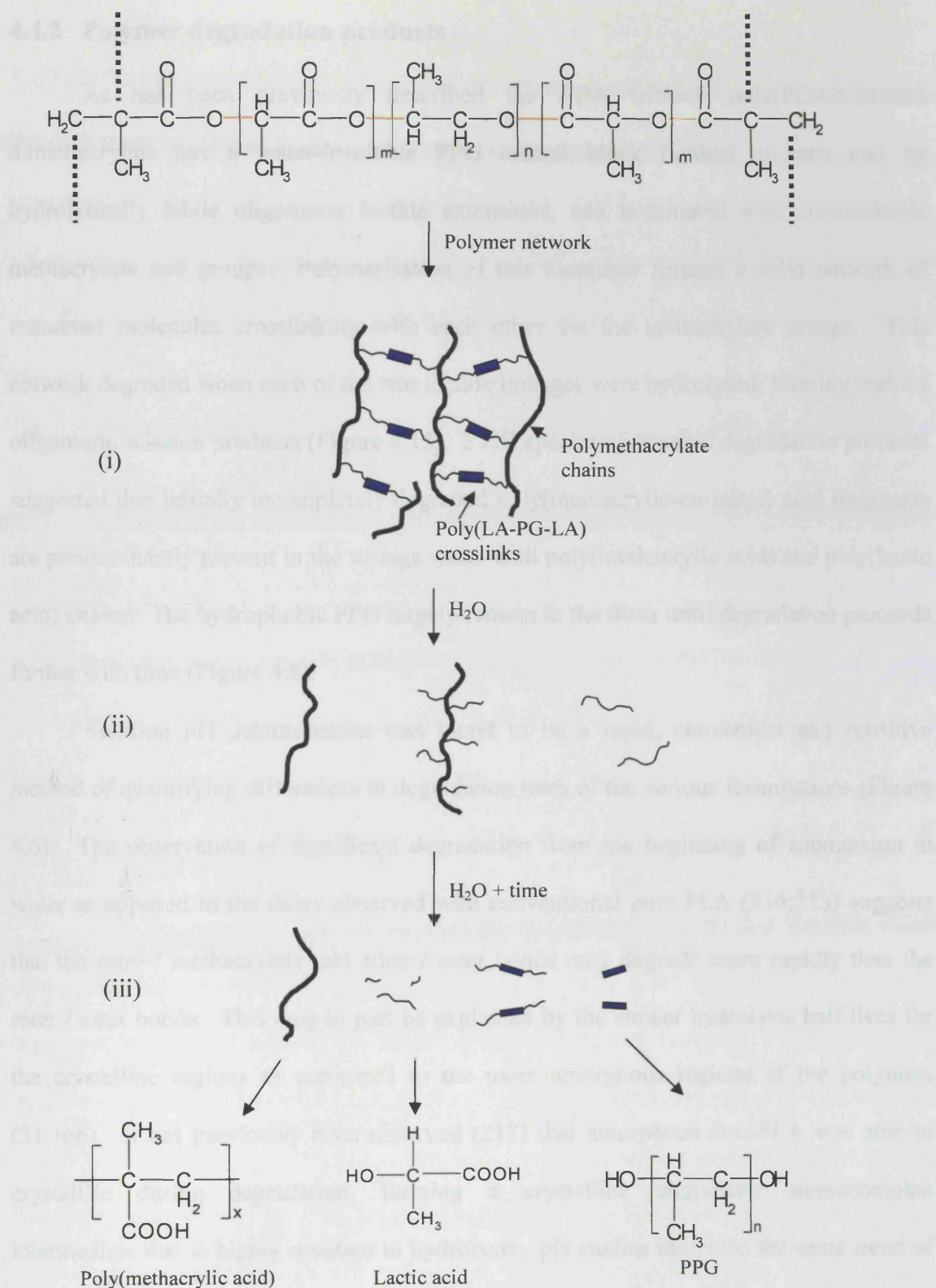
Figure 4.15. Illustration of the degradation scheme of a poly(PG-co-lactide) dimethacrylate; (i) as a polymerised network before degradation, (ii) initial degradation products, (iii) late degradation products after complete hydrolysis

4.4.2 Polymer degradation products

As has been previously described the ABA triblock poly(PG-co-lactide) dimethacrylate has a water-insoluble PPG central block flanked at each end by hydrolytically labile oligomeric lactide extensions, and terminated with crosslinkable methacrylate end groups. Polymerisation of this monomer formed a solid network of monomer molecules crosslinking with each other via the methacrylate groups. This network degraded when each of the two lactide linkages were hydrolysed, forming various oligomeric scission products (Figure 4.15). FTIR spectra of released degradation products suggested that initially incompletely degraded poly(methacrylic-co-lactic) acid fragments are predominantly present in the storage water with poly(methacrylic acid) and poly(lactic acid) chains. The hydrophobic PPG largely remain in the discs until degradation proceeds further with time (Figure 4.8).

Solution pH determination was found to be a rapid, convenient and sensitive method of quantifying differences in degradation rates of the various formulations (Figure 4.6). The observation of significant degradation from the beginning of submersion in water as opposed to the delay observed with conventional pure PLA (214;215) suggests that the ester / methacrylate and ether / ester bonds may degrade more rapidly than the ester / ester bonds. This may in part be explained by the slower hydrolysis half lives for the crystalline regions as compared to the more amorphous regions of the polymers (51;166). It has previously been observed (217) that amorphous D,L-PLA was able to crystallise during degradation, forming a crystalline oligomeric stereocomplex intermediate that is highly resistant to hydrolysis. pH studies indicated the same trend of 14-week degradation levels with changing monomer structure as seen in mass loss investigations (i.e. P7L8DMA > P7L2DMA > P17L4DMA > P34L2DMA) (Table 4.3).

Raising initiator concentration, however, decreased slightly the cumulative acid release but increased the level of mass loss. This may be explained if there is variability in the level of degradation of the released fragments. With linear polymers, decreasing the initiator concentration generally reduces the free radical level during polymerisation and subsequently raising the polymer chain length (209). Via similar reasoning decreased initiator concentration might be expected to raise methacrylate block length and the number of ether / ester or ester / methacrylate bonds that need to be broken before fragments can be released. This would delay and decrease the mass of product release at a given time but may also enable fuller hydrolysis of ester / ester bonds (and therefore formation of acid) prior to any material fragmentation. The calculated mass of fragments per mole of acid, was in all cases greater than expected for fully hydrolysed polymethacrylic and lactic acid giving further evidence (since PPG is not released until final stages of degradation) that early product release occurs mainly without full poly(lactide) degradation.

4.4.3 Polymer degradation rates

As with polymerisation studies (Chapter 3), initiator concentration has only minor effects on degradation rate in comparison with monomer compositions. The effects of monomer structure and time on rates of degradation are complex. Shortening the monomer length will raise the concentration of ester / methacrylate and ether / ester bonds per unit volume (Figure 4.14) but reduce water sorption leading to potentially opposing effects on degradation rate. The degradation mechanism is further complicated by the rate at which degradation products can diffuse out into the surrounding water and the varying material composition with time. Methacrylate block length variation with monomer

structure, which determines the number of ester / methacrylate bonds that must be broken

for poly(methacrylic acid) to be released, is additionally difficult to predict (209). The

fast initial degradation of the monomers produced using PPG 425 g/mol suggests,

however, that in these cases the methacrylate blocks are short. Subsequently the fewer

bonds that need be broken and the shorter degradation fragments produced mean that

diffusion of the degradation products out of the polymer matrix is much faster. This is

potentially advantageous as shorter polyelectrolytes can be removed from the body by

natural elimination (218).

Water sorption increases with increasing lactide length in the polymer and is

expected to increase degradation rate because of an increased diffusion medium for the

degradation fragments in the matrix as well as possible autocatalysis by the acidic

degraded carboxylic acid groups inside the matrix (214). Despite its high water sorption,

degradation of P34L8DMA is initially much slower than that of the other polymers. This

may, however, be an anomalous effect because of the low conversion of end groups to

methacrylate moieties causing the final structure of the polymer to be very different from

that of the more crosslinkable materials. The structure produced in this case would be

long linear polymers with comb-like degradable side chains. Swelling due to water

sorption would then not be restricted and the polymer could fall apart due to excessive

water uptake instead of full degradation of the ester / methacrylate bonds. The other

sample with a high lactide to PPG ratio, P7L8DMA, conversely exhibited the fastest

degradation rate. This fast rate could be due to a combination of a high concentration of

ether / ester and ester / methacrylate bonds and moderate initial rate of water sorption as

well as possibly short methacrylate blocks. Since cumulative acid release is linear with

the square root of time ($C_a = kt^{0.5}$), the reduction in reaction rate (dC_a / dt) with time (t)

with P7L8DMA suggests that diffusion of the degradation products from the specimens

could be a rate limiting step (Figure 4.6). Initially at the specimen surfaces this release

process would be fast but could then gradually slow as the reaction occurs deeper in the

PPG enriched remains of the specimen surface. With this material the high level of

degradation at 14 weeks (56-63 wt%) is mostly balanced by water sorption (Figure 4.7).

With P7L2DMA degradation is slower than P7L8DMA but linear with time which

for many applications can be beneficial (219). In this case final water content (11-14 wt%)

does not entirely balance the mass loss of 18-19 wt% and some slight material shrinkage

with degradation is detectable (Figure 4.7). With P7L2DMA the slow rate of water

sorption could however limit degradation to the material surfaces making bond hydrolysis

the rate determining step at all times.

P34L2DMA and P17L4DMA degrade initially at a comparable rate to P7L2DMA

possibly because greater maximum water sorption-induced expansion of the polymer

matrix balances lower ether / ester bond concentrations (Table 4.2). The maximum mass

loss at 14 weeks, however, for P34L2DMA and P17L4DMA is only 6 -7 and 10-11 wt%

respectively (Table 4.3) suggesting that the increased molecular weight of the

hydrophobic PPG left in the sample surfaces after initial surface degradation might inhibit

further product release thereby slowing degradation at later times. At 14 weeks with these

two samples final water content is greater than material mass loss so they are slightly

swollen (Figure 4.7).

4.4.4 Static modulus of polymers

The compressive static moduli, which are a measure of material stiffness or

rigidity, were determined on dry specimens of the formulations before and after 14 weeks

of degradation (Figure 4.10). Crosslinking with the shortest polymer P7L2DMA is initially the highest and hence has the highest modulus. On the other hand the modulus of the longer monomer-containing formulations is presumably low due to limited crosslinking. Additionally, on raising the initiator concentration a larger number of shorter less crosslinked chains could be produced further reducing modulus. With time in water, however, when a high initiator concentration is used, the smaller chains (or other plasticizing molecules such as remaining initiators) within such polymers might diffuse out more rapidly leaving behind any more densely crosslinked material and a dried structure of higher modulus (N.B. in the static tests the late samples had been dried). This would be consistent with the observed higher initial rate of mass loss from materials produced using high initiator level (Table 4.3). Conversely, with the samples produced with lower levels of initiator, greater degradation of the crosslinks before any material release occurs may be required. This could be consistent with the higher initial rate of acid release with low initiator levels despite slower mass loss (Table 4.3) but also provide an explanation as to how the remaining material can be of lower modulus than initially (Figure 4.10).

4.4.5 Dynamic modulus of polymers

The moduli of the 'wet' specimens during their placement in water were determined at different time points. At earlier time points the polymers display high initial storage modulus due to their relatively high degree of crosslinking and low level of swelling (Figure 4.11). As degradation proceeds the degradable poly(PG-co-lactide) segments within the matrix are hydrolysed and the network crosslinks are cleaved, leading to progressively lower crosslinking density. This together with a high degree of swelling

and an increase in water content, results in a decrease in storage modulus. Polymers with short PPG degrade faster and subsequently experience bigger decline in the modulus within the first 4 weeks of degradation as compared to the slower-degrading longer polymers (Table 4.5). As water is a plasticizer and can increase polymer flexibility, the slightly bigger drop in the moduli of the polymers on raising the initiator level is expected during degradation as polymers made with high initiator level have slightly larger water sorption.

5 Drug Release

5.1   Background

Another potential application for which biodegradable polymers can be of use is as a carrier for drug delivery; either as drug delivery system alone or as bifunctional medical device (14;75;220;221). The drug can be incorporated either in dissolved or dispersed form within the polymer matrix, which subsequently degrades in the body releasing the drug in a controlled manner (222;223). Several injectable drug delivery systems have been reported using various polymers. These range from thermosensitive PEG/ PLGA triblock hydrogels (58;98) to crosslinkable PPF/ VP cements (45) and other methacrylate systems (56;224). In all studies drug release rate has been mainly controlled either by varying molecular weight of the polymer (80;225) or the drug loading content (59;221;224).

Use of biodegradable polymers as drug delivery carriers is often limited due to interaction between polymer structures and drugs or incompatibility of the fabrication processes (53). For example polyanhydrides have been found to react with drugs containing free amino groups especially at high temperatures (143); whereas the widely studied PLGA may result in exceedingly high rates of drug release in the late period due to bulk erosion of the polymer (226). In some studies the drug has been incorporated into PLGA microparticles before blending it with a crosslinkable PPF polymer to protect it from the curing process (45;227).

In this study, three different drugs including chlorhexidine diacetate (CDA), ketoprofen and prednisolone were investigated for their release from the polymers. All three drugs have been previously studied in different polymer systems and investigated by UV/vis spectroscopy (56;58;60;187). Chlorhexidine is an antiseptic and antifungal agent

which has been widely used in dentistry especially for oral diseases (228). Ketoprofen is a non-steroidal anti-inflammatory drug commonly used for the treatment of arthritis and after orthopaedic surgery due to its analgesic and anti-inflammatory properties (229). Prednisolone is a steroidal anti-inflammatory agent and is also used for rheumatic disease and other inflammatory conditions. These three drugs exhibit different solubilities in water and behaviour in the monomers, and hence different release characteristics were expected. Each drug was blended homogenously with the varying monomers at three drug levels, and in addition for CDA, three particle size ranges, using a factorial experimental design. The drug-monomer mix was photo-polymerised into discs before placement in deionised water for gravimetric, pH and UV/vis spectroscopic studies. The aim of this study was therefore to assess the degradation properties of the drug-incorporated polymers and deduce information on the possible mechanisms by which the different drugs are released.

5.2   Materials and Methods

5.2.1 Polymers and drugs

The five poly(PG-co-lactide) dimethacrylate monomers with batch number 091104 were used.   Detailed structural characteristics, including the measured lactide chain lengths and methacrylation efficiency of these monomers can be found in Section 3.3.1, Chapter 3.

Three drugs were studied, including CDA, ketoprofen and prednisolone. All three drugs were received in the form of white powder. Each drug was incorporated into a set of monomers as described below. Ketoprofen and prednisolone were used as received

without further treatment. For CDA, the powders were ground and sieved to obtain three

ranges of particle size: (i) 107-150 μm, (ii) 76- 106 μm and (iii) 39-75 μm.

5.2.2 Formulations studied

For each set of specimens containing one of the three drugs being studied, polymer

formulations were fabricated according to a factorial experimental design (see Table 2.1,

Chapter 2). In this experiment, three variables were investigated: (i) PPG n level (i.e. 34,

17, 7); (ii) lactide linkage m level (i.e. 8, 4, 2); and (iii) drug level (i.e. 10, 5, 2.5 wt% of

total monomer mass). For polymer discs containing CDA, a forth variable, drug particle

size (i.e. median size 128.5, 91, 57 μm), was also investigated. According to the factorial

design, 2.5 or 10 wt% of drug particles were added to the four monomers produced using

PPG 425 or 2000 g/mol and lactide 2 or 8 mol/mol PPG, and 5 wt% to the single PPG

1000 g/mol and lactide 4 mol/mol PPG based "intermediate" formulation. The

combinations of the formulations are presented in Table 4.1. In total ten sample

formulations were prepared with the P17L4DMA being a duplicate.

Table 5.1. Combinations of the ten formulations investigated for drug release studies of each of the three drugs. Note that according to the factorial design (Table 2.1, Chapter 2), there are two identical formulations for the intermediate formulation with P17L4DMA.

Monomer code	Drug level (wt %)	Drug particle size (for CDA-containing specimens only) (μm)
P34L8DMA	2.5	39-75
P34L8DMA	10	107-150
P34L2DMA	2.5	107-150
P34L2DMA	10	39-75
P17L4DMA	5	76-106
P17L4DMA	5	76-106
P7L8DMA	2.5	107-150
P7L8DMA	10	39-75
P7L2DMA	2.5	39-75
P7L2DMA	10	107-150

5.2.3 Sample preparation

For each set of drug-containing specimens, the fluid monomer was mixed with CQ and DMPT (1 wt% each), HEMA (10 wt% to aid initiator dispersion) and appropriate level of the drug powder. The resultant monomer mix was placed into steel ring moulds of approximately 10 mm internal diameter and 2 mm depth. The top and bottom surfaces were covered with acetate sheets before placing into a blue light box (*Unilux Ac, Kulzer*, 1.67 mW/cm^2) for multiple simultaneous sample curing. The monomer mix was exposed to light for five minutes each side; this has been determined from polymerisation kinetic studies to give 98 % double-bond conversion (Table 4.1, Chapter 4). The crosslinked specimen was removed from the ring after 24 hours. Three specimens of each formulation were prepared. Polymer discs containing only P34L8DMA, P34L2DMA, P7L8DMA or P7L2DMA monomer were also fabricated with 1 wt% CQ and DMPT and 10 wt% HEMA

and polymerised as above. These discs were used as control samples for eliminating interfering absorbance in the assay of drug solutions using UV/vis spectroscopy (see Section 5.2.4.4 later).

5.2.4 Drug release studies

In all analyses described below mean results from the three specimens for each formulation were obtained and relative standard deviations calculated by dividing the standard deviations by the means (Equation 4.1, Chapter 4). These relative standard deviations expressed the percentage variability in the values measured relative to the magnitude of the calculated mean. The ketoprofen- and prednisolone-containing specimens were studied over a period of 18 weeks but the chlorhexidine-containing specimens were investigated up to 10 weeks only.

5.2.4.1 Gravimetric analysis

The initial mass of the specimens were measured using a Mettler Teledo balance with an accuracy of 0.0001g. Each specimen was then placed upright in the conical end of a sterilin tube allowing contact with water on all sides. The specimen was immersed in 10 ml of deionised water already adjusted to pH 7 using ammonium hydroxide solution, and the sterilin tube was incubated at 37 °C. After 0.5, 1, 2, 4, 24, 48, and 96 hours and 1, 2, 3, 4, 5, 6, 8, 10, 14 and 18 weeks, the specimens were removed, their external surface blotted dry with tissue paper and re-weighed. The specimens were then placed in new sterilin tubes containing fresh pH-adjusted deionised water. The wet mass of each specimen was converted into percentage change of the original mass using Equation 4.2 (Section 4.2.3.1, Chapter 4).

5.2.4.2 pH measurements

At each time-point the pH of the storage solution was measured (Hanna Instruments, pH 211 Microprocessor pH meter) after removal of the specimen. The concentration of acids was calculated from the pH and converted to cumulative moles of acid released in 10 ml storage solution (C_a) per specimen using Equation 4.7 and 4.8 respectively (Section 4.2.3.2, Chapter 4).

5.2.4.3 Final gravimetrical analysis

Final material mass loss at the end of the study period was obtained by drying the specimens under vacuum to constant mass and their total percentage mass loss, ΔW_D, and water content, calculated by comparison with the initial dry and final wet mass respectively. This total mass loss was contributed by both the polymer mass loss and drug release. Percentage mass loss due to polymer (ΔW_P) was calculated by deducting the mass loss due to drug release using Equation 5.1.

$$\Delta W_P \ (\%) = 100 \times \frac{W_D - C_D}{W_0} \qquad\qquad 5.1$$

Where W_D is the total specimen mass loss, W_0 is the initial specimen mass (i.e. at 0 hr) and C_D is the cumulative mass of drug released (see Equation 5.11, Section 5.2.4.4b).

The mass of polymer erosion per mole of acid released, W_{Pmol} (g/mol), was then calculated using Equation 4.9 (Section 4.2.3.3, Chapter 4).

5.2.4.4 Assay procedures

(a) Calibration curve

In order to determine the standard calibration curve of the drugs, a stock solution of 0.1 %w/w in deionised water was prepared for CDA and 0.01 %w/w for ketoprofen and

prednisolone. Using this stock solution, a series of calibration solutions for each drug at concentrations of 0.0005, 0.001, 0.002, 0.003, 0.004 and 0.005 %w/w were prepared. The Unicam UV 500 Thermospectronic® Spectrometer was used and the absorbance was set to zero in air prior to analysis. A 1 cm path quartz cell was filled with deionised water and a UV spectrum recorded between 200 and 400 nm at a spectral bandwidth of 1 nm. For each set of the calibration solutions, UV spectra were recorded and the 'deionised water' spectrum was subtracted from these spectra. The absorbance of each solution at the absorption maximum of the drug was recorded. This was 231 or 254 nm for CDA, 261nm for ketoprofen and 247 nm for prednisolone. A calibration curve of the drug was obtained by plotting the concentration versus absorbance and the gradient calculated through linear regression.

(b) Drug release

At each time point the sample storage solutions were diluted by an appropriate factor (between 0 and 10) with deionised water such that the measured absorbance fell within the linear calibration range. These diluted solutions were analysed by recording a UV spectrum between 200 and 400 nm and the 'deionised water' spectrum subtracted from these spectra. Corrected UV spectra from the storage solutions of the control specimens containing no drug were also obtained at the various time points. In order to eliminate absorbance due to other components in the solutions (e.g. residual monomers, initiators), the following mathematical analysis was used. Assuming that the components of the solutions do not react with one another, the absorbance A at a particular wavelength will be given by the sum of the absorbance for all the individual components (i.e. drug +

impurities). The ratio (K) of the absorbance at an absorption minimum and maximum is

constant for a substance and independent of concentration (Figure 5.1).
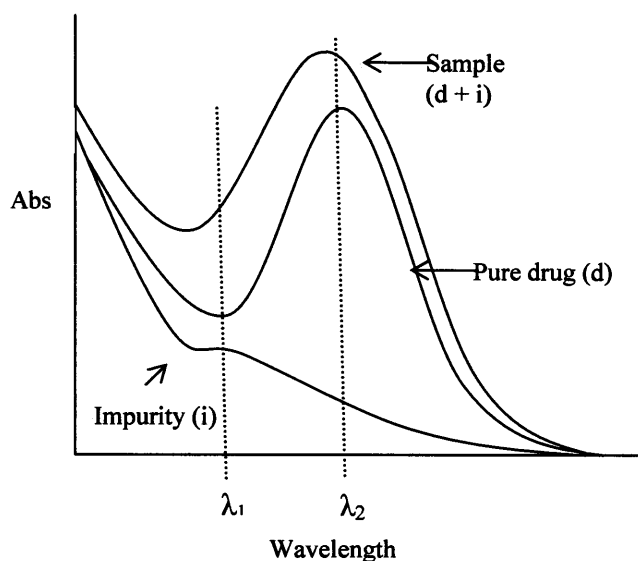
Figure 5.1. Schematic representation of sample, pure drug and impurity UV spectra.

The selected wavelengths λ_1 / λ_2 correspond respectively to the absorption

minimum / maximum of the drug. These were λ_{222} / λ_{254} for CDA, λ_{234} / λ_{261} for

ketoprofen and λ_{215} / λ_{247} for prednisolone. Mean values of K_1 and K_2 were obtained from

the impurity (i.e. control specimen containing no drug) and pure drug (i.e. calibration)

spectra respectively using Equations 5.2 and 5.3.

$$K_1 = \frac{A_{i,\lambda 1}}{A_{i,\lambda 2}}$$ 5.2

$$K_2 = \frac{A_{d,\lambda 1}}{A_{d,\lambda 2}}$$ 5.3

Where A_i and A_d are the absorbance due to the impurity and pure drug respectively at the

wavelengths λ_1 and λ_2. Table 5.2 presents the mean values of K_1 and K_2 calculated from,

all time points, the control specimens containing no drug (n= 48) and pure drug

(calibration)(n = 6) spectra respectively.

Table 5.2. Mean K_1 and K_2 values calculated from the control specimens containing no drug and pure drug (calibration) spectra using Equations 5.2 and 5.3 respectively. The +/- values are the 95 % confidence intervals of the sample means calculated by 2 * (s / √n).

	Prednisolone A215/ A247	Ketoprofen A234/ A261	Chlorhexidine diacetate A222/ A254
K1	3.87 ± 0.23	2.98 ± 0.20	3.85 ± 0.28
K2	0.33 ± 0.002	0.30 ± 0.04	0.90 ± 0.01

The absorbance of the drug-containing sample (A_s) at each wavelength is the sum

of that due to the impurity and drug component in the sample (Equations 5.4 to 5.7).

$$A_{s,\lambda 1} = A_{i,\lambda 1} + A_{d,\lambda 1}$$

$\qquad$ 5.4

Combining Equation 5.4 with 5.2 and 5.3 gives Equation 5.5:

$$A_{s,\lambda 1} = K_1 A_{i,\lambda 2} + K_2 A_{d,\lambda 2}$$

$\qquad$ 5.5

Rearranging gives

$$\frac{A_{s,\lambda 1}}{K_1} = A_{i,\lambda 2} + \frac{K_2}{K_1} A_{d,\lambda 2}$$

$\qquad$ 5.6

And

$$A_{s,\lambda 2} = A_{i,\lambda 2} + A_{d,\lambda 2}$$

$\qquad$ 5.7

Subtracting Equation 5.6 from 5.7 gives Equation 5.8:

$$A_{s,\lambda 2} - \frac{A_{s,\lambda 1}}{K_1} = A_{d,\lambda 2} \left(1 - \frac{K_2}{K_1} \right)$$

$\qquad$ 5.8

The absorbance due only to the drug component in the sample at λ_2 could then be calculated by rearranging Equation 5.8.

$$A_{d,\lambda 2} = \left(A_{s,\lambda 2} - \frac{A_{s,\lambda 1}}{K_1} \right) \div \left(1 - \frac{K_2}{K_1} \right)$$ 5.9

This absorbance value was converted into the amount of drug released (D, in grams) from the specimen using Equation 5.10. Cumulative amount of drug release (C_D in grams) at time t was calculated using Equation 5.11.

$$D = \left(\frac{A_{d,\lambda 2}}{g} \times u \right) wt\% \times V_s$$ 5.10

$$C_D = \sum_0^t D_t$$ 5.11

Where g is the gradient calculated from the calibration curve of the drug, u is the dilution factor and V_s is the storage solution volume (i.e. 10 ml). The cumulative amount of drug could then be converted into percentage release of the original drug mass in the specimen.

5.3   Results

5.3.1   Calibration curve and drug characteristics
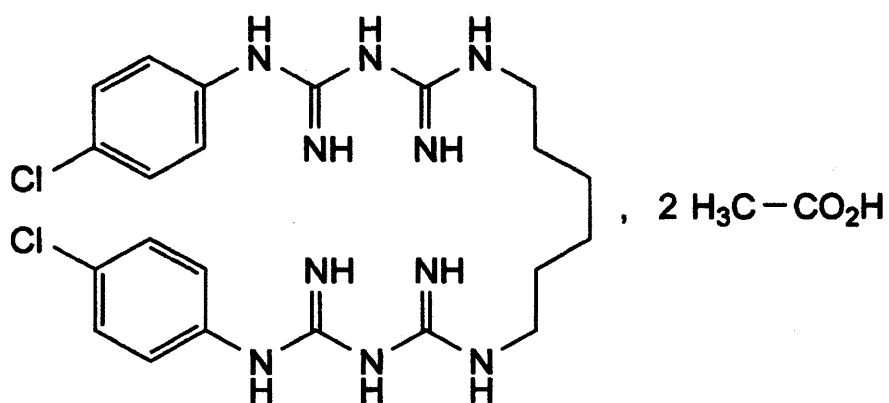
(a) Chlorhexidine diacetate $C_{22}H_{30}Cl_2N_{10}$. $2C_2H_4O_2$, Mw = 625.6

, $2\ H_3C-CO_2H$
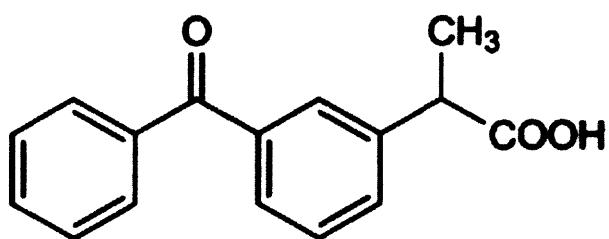
(b) Ketoprofen $C_{16}H_{14}O_3$,   Mw= 254.3
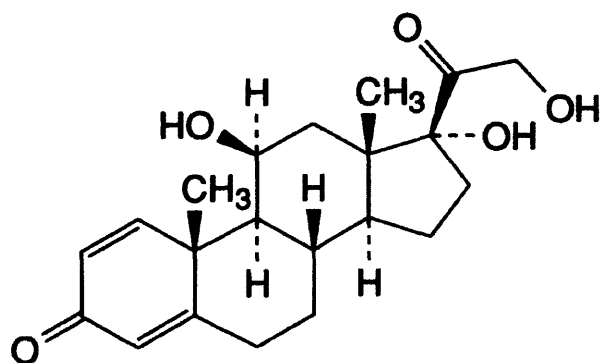
(c) Prednisolone $C_{21}H_{28}O_5$, Mw= 360.4

Figure 5.2. Structures of the three drugs, their molecular formula and mass

The structures of the three drugs are shown in Figure 5.2. The solubility of the drugs in water at 15 – 25 °C are as follows: 18 mg/ml for CDA, 0.1 mg/ml for ketoprofen and 0.1 – 1 mg/ml for prednisolone (230;231).

Figure 5.3 shows the appearance of example specimens for a polymer containing the drugs. Ketoprofen, being the least water-soluble drug, was soluble in the monomers giving a transparent appearance of the polymerised discs. CDA and prednisolone were both non-miscible with the monomers with the latter drug giving polymer samples that were less translucent. The various drug solubilities in water and monomer significantly affect their release characteristics from the polymer discs as will be shown in later sections.

(a)   (b)   (c)
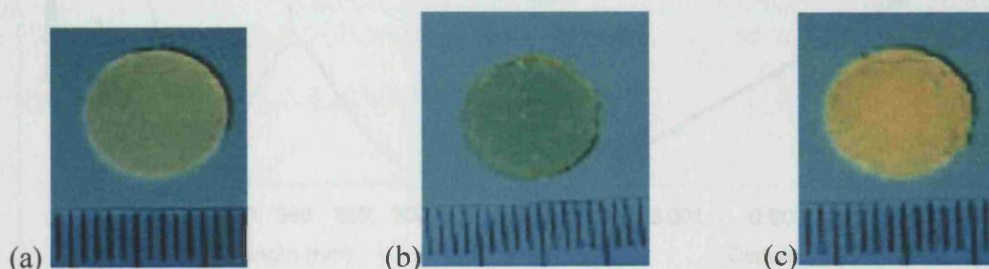
Figure 5.3. Appearance of the P34L2DMA polymer containing 2.5 wt% of (a) CDA, (b) ketoprofen and (c) prednisolone.

All three drugs possess conjugated double bonds and give detectable UV spectra with linear calibration curves in the concentration range investigated (Figure 5.4). CDA gives two absorption peaks; the peak at 254 nm was used as the absorption maximum for this study as it is further away from the possible reduced photometric performance of the instrument at short wavelengths and from the region where any degradation products from the polymer may absorb.
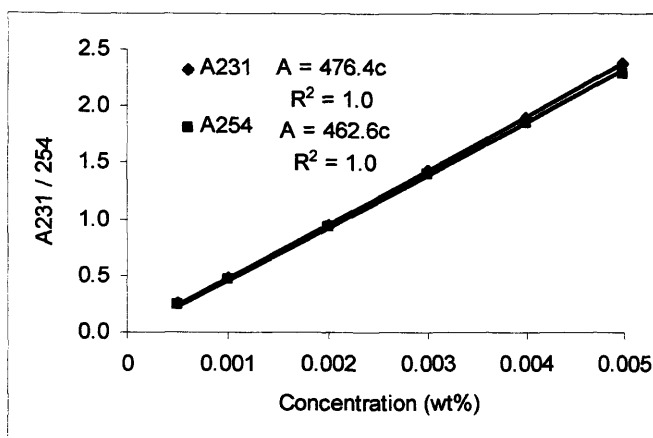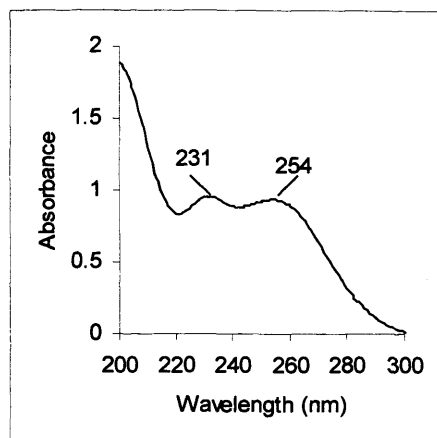
(a) Chlorhexidine diacetate
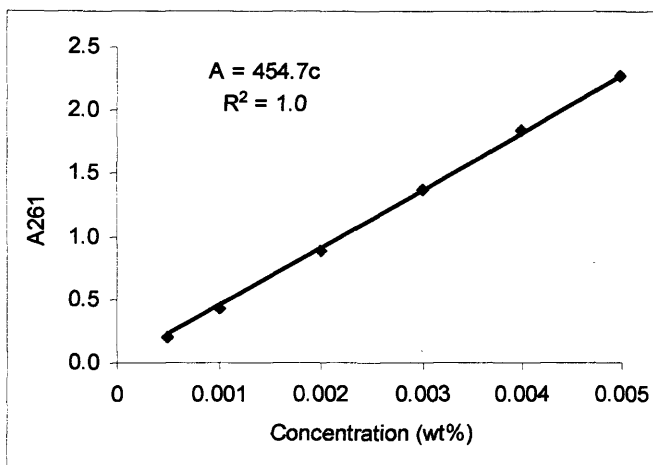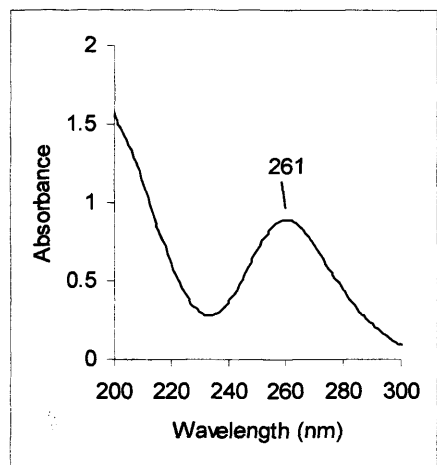
(b) Ketoprofen
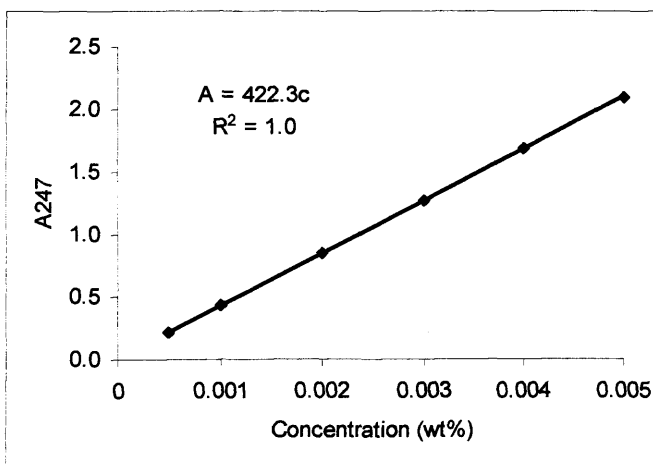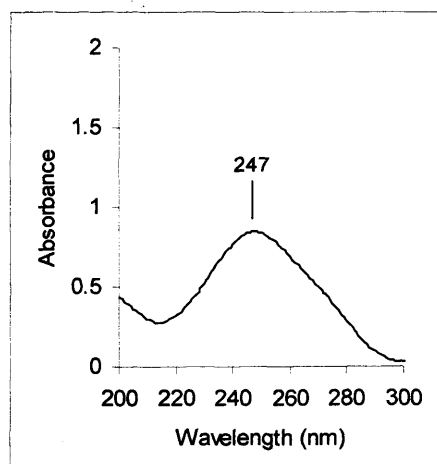
(c) Prednisolone

Figure 5.4. Typical UV spectra (0.002 wt%) and calibration curves of the three drugs.

5.3.2 Mass change

5.3.2.1 Chlorhexidine diacetate

The mass of three 'wet' polymer specimens of each sample were determined over a period of 10 weeks (see Equation 4.2, Chapter 4). Relative standard deviations of the mean mass change for the ten samples were on average 9 ± 2 %. Initially mass change with all polymers increased proportional to the square root of time as diffusion-controlled water sorption dominated over drug release or polymer erosion (Figure 5.5). Changing drug particle size had no apparent effect on the early mass change of the polymers (compare big and small symbols in Figure 5.5). The polymer P7L8DMA absorbed water at a much faster rate than the other samples. The other longer length polymers, P34L8DMA and P34L2DMA, absorbed water at similar rates but slower than that of P7L8DMA. Water sorption of these polymers was, however, almost twice as fast as with P17L4DMA and P7L2DMA (see Table 5.3). After this initial period mass increase with P7L8DMA levelled off whilst changes in mass of all other samples declined over the remaining period with the exception of P34L8DMA containing 2.5 wt% drug. In this latter sample mass continued to increase proportionally with the square root of time. Maximum percentage mass change from polymers with long lactide segments, P34L8DMA and P7L8DMA, containing 2.5 wt% drug were 63 and 68 wt% respectively and were higher than their 10 wt% drug containing counterparts (17 and 47 wt% respectively). Maximum mass increases in P34L2DMA for the 10 and 2.5 wt% drug levels were 32 and 20 wt% respectively with the 10 wt% drug level then having a faster decline in mass than the 2.5 %. With the shortest P7L2DMA polymer, mass changes between the two drug levels were comparable throughout the time period and had an average maximum mass change of 5.6 wt% only.
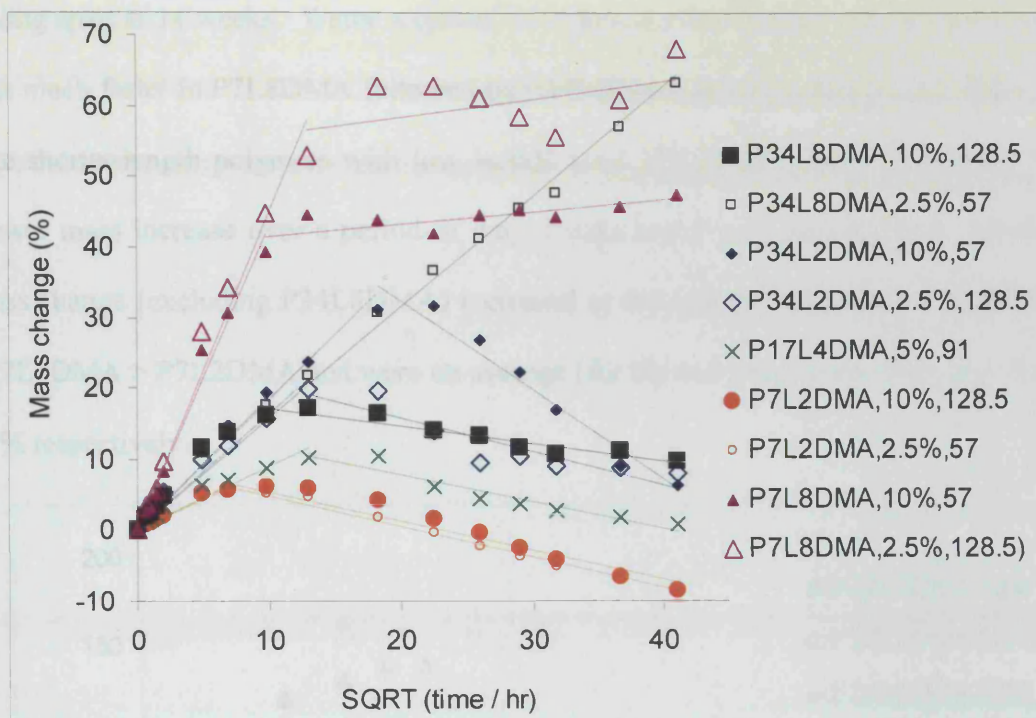
Figure 5.5. Mass change in water as a function of the square root of time for the polymers containing the drug chlorhexidine diacetate. Filled and unfilled symbols represent 10 and 2.5 wt% drug levels in the polymer. Big and small symbols represent larger (median size 128.5 μm) and smaller (median size 57 μm) drug particles respectively. Results were averaged for the two duplicate formulations of the P17L4DMA samples.

5.3.2.2   Ketoprofen

For polymers containing the drug ketoprofen, the mass of 'wet' specimens was determined in triplicate for each sample over 18 weeks (Equation 4.2, Chapter 4). Relative standard deviations of the mean mass change for the ten samples were on average 9 ± 2 %. Unlike CDA the mass changes of the two drug levels for each polymer were comparable throughout the whole time period (compare filled and unfilled symbols in Figure 5.6). Mass change in all polymers increased proportionally to a maximum before declining linearly with the square root of time except P34L8DMA (Figure 5.6). In this polymer, mass increase continued with the specimens containing 10 wt% drug eventually

falling apart at 14 weeks. Water sorption in the initial mass increase period (over 2 weeks) was much faster in P7L8DMA followed by P34L8DMA and P34L2DMA (see Table 5.4). The shorter-length polymers with low lactide level, P7L2DMA and P17L4DMA, had a slower mass increase over a period of only 2 days and 1 week respectively. Maximum mass change (excluding P34L8DMA) increased in the order P7L8DMA > P34L2DMA > P17L4DMA > P7L2DMA and were on average (for the two drug levels) 146, 19, 10 and 4 wt% respectively.
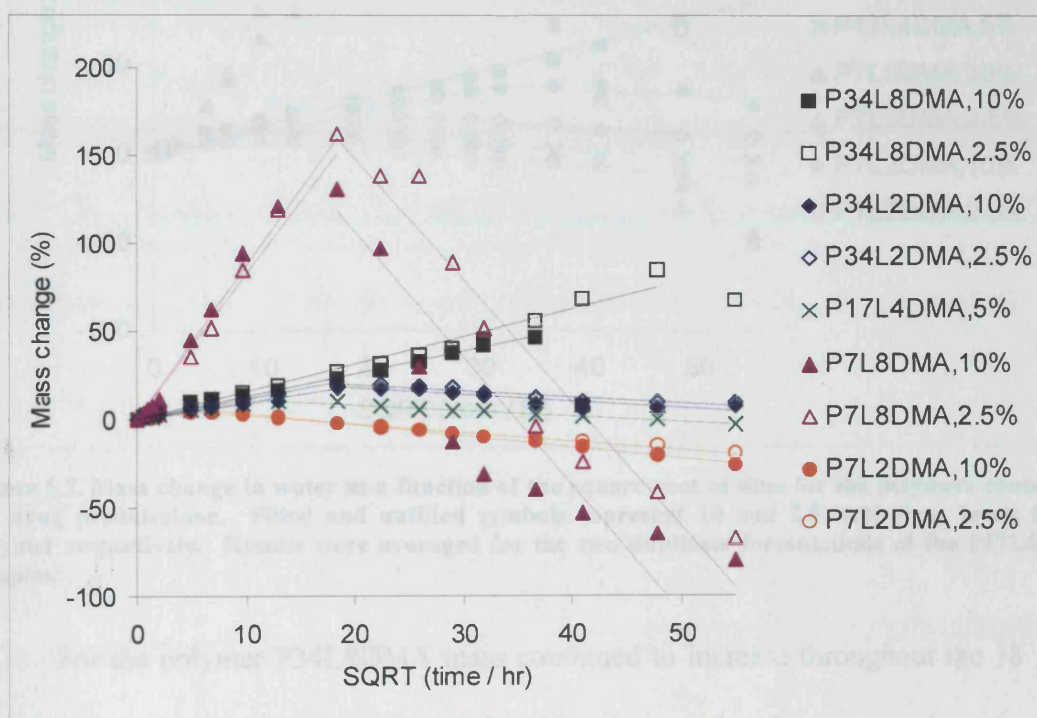
Figure 5.6. Mass change in water as a function of the square root of time for the polymers containing the drug ketoprofen. Filled and unfilled symbols represent 10 and 2.5 wt% drug levels in the polymer respectively. Results were averaged for the two duplicate formulations of the P17L4DMA samples.

5.3.2.3 *Prednisolone*

As with ketoprofen, polymers containing the drug prednisolone were studied in triplicate over 18 weeks (Equation 4.2, Chapter 4). Relative standard deviations of the

mean mass change for the ten samples were on average 9 ± 3 %. Again for all polymers except P34L8DMA there was an initial mass increase period followed by a decline when drug release and polymer erosion dominated over water sorption (Figure 5.7).
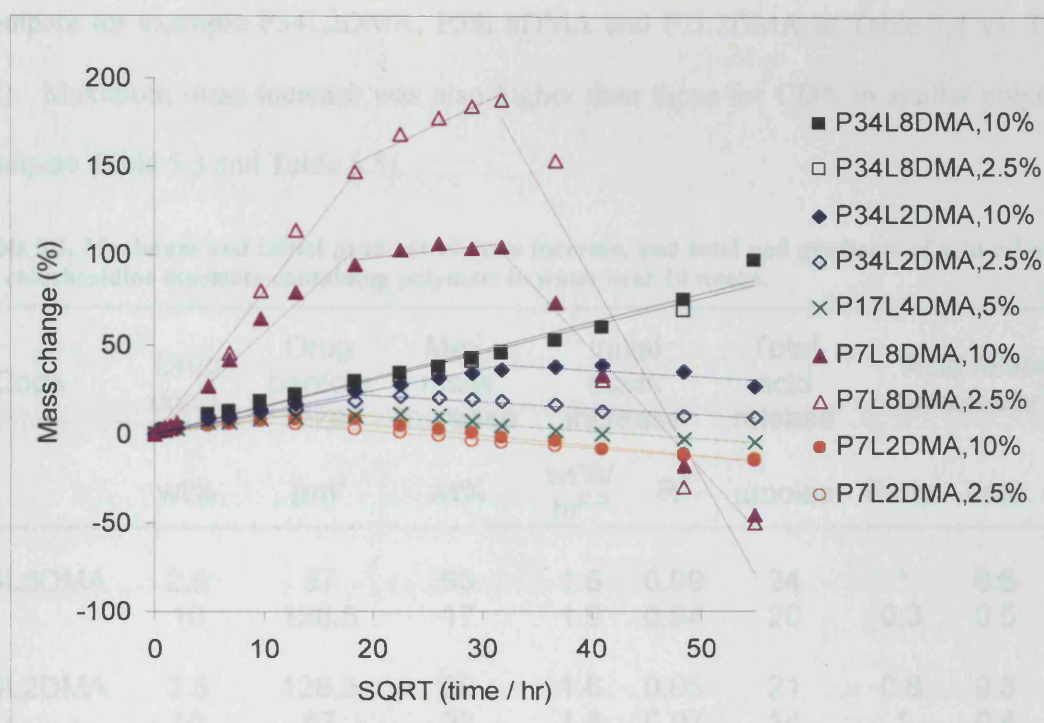
Figure 5.7. Mass change in water as a function of the square root of time for the polymers containing the drug prednisolone. Filled and unfilled symbols represent 10 and 2.5 wt% drug levels in the polymer respectively. Results were averaged for the two duplicate formulations of the P17L4DMA samples.

For the polymer P34L8DMA mass continued to increase throughout the 18 week period. Increasing the drug level from 2.5 to 10 wt% in each polymer caused on average a small increase in the gradient of mass change in the initial period (see Table 5.5). Polymers attached with longer lactide segments, P34L8DMA and P7L8DMA, absorbed water at a faster rate than the other samples in this initial period (see Table 5.5). There was then a plateau region for the P7L8DMA polymer before a decline. Maximum mass change increased in the order P7L8DMA > P34L8DMA > P34L2DMA > P17L4DMA > P7L2DMA. The shortest P7L2DMA polymer had, on average of the two drug levels, a

mass increase of 7 wt% only. Although initial gradients of mass increase were similar, maximum mass increases for prednisolone were in general higher than those for ketoprofen for a given polymer and could be twice as high at the 10 wt% drug level (compare for example P34L2DMA, P34L8DMA and P7L2DMA in Table 5.4 vs. Table 5.5). Maximum mass increase was also higher than those for CDA in similar polymers (compare Table 5.3 and Table 5.5).

Table 5.3. Maximum and initial gradient of mass increase, and total and gradients of acid release of the chlorhexidine diacetate-containing polymers in water over 10 weeks.

Code	Drug conc.	Drug particle size	Max. mass increase	Initial mass increase		Total acid release	Acid release (μmoles/hr$^{0.5}$)		
	wt%	μm^{ii}	wt%	wt%/ hr$^{0.5}$	R^2	μmoles	Early^i	Late	Av. R^2
P34L8DMA	2.5	57	63	1.6	0.99	24	*	0.6	0.99
	10	128.5	17	1.9	0.94	20	0.3	0.5	0.91
P34L2DMA	2.5	128.5	20	1.6	0.95	21	0.8	0.3	0.99
	10	57	32	1.8	0.97	14	*	0.4	0.99
P17L4DMA	5	91	11	0.9	0.90	33	*	0.8	0.99
P7L8DMA	2.5	128.5	68	4.5	0.98	64	3.3	1.3	1.00
	10	57	47	4.3	0.98	43	2.4	0.8	0.96
P7L2DMA	2.5	57	5	0.9	0.86	60	*	1.5	1.00
	10	128.5	6	0.9	0.96	61	3.3	1.4	0.98

^{i} Those marked with a * has no burst release phase; duration of this early phase for P34L8DMA: 0-4days; for P34L2DMA: 0-2wks; for P7L2DMA and P7L8DMA; 0-4hours.

^{ii} Particle median size. For 57, 91 and 128.5 μm, the particle size range is 39-75 μm, 76-106 μm and 107-150 μm respectively.

Table 5.4. Maximum and initial gradient of mass increase, and total and gradients of acid release of the ketoprofen-containing polymers in water over 18 weeks.

Code	Drug conc.	Max. mass increase	Initial mass increase		Total acid release	Acid release (μmoles/hr$^{0.5}$)		
	wt%	wt%	wt%/hr$^{0.5}$	R^2	μmoles	0-4 days	4days-18wk	Av. R^2
P34L8DMA	2.5	84	1.6	0.98	47	1.3	0.7	0.99
	10	disintegrated	1.3	1.00	69	1.4	1.3	0.99
P34L2DMA	2.5	20	1.2	0.94	34	1.7	0.4	0.98
	10	18	1.0	0.96	44	1.9	0.6	0.98
P17L4DMA	5	10	0.9	0.94	58	1.4	0.9	0.99
P7L8DMA	2.5	162	8.7	0.99	167	6.8	2.3	0.98
	10	130	8.2	0.96	165	5.7	2.5	0.98
P7L2DMA	2.5	4	0.7	0.89	103	3.5	1.5	0.99
	10	4	0.7	0.93	117	3.2	1.9	1.00

Table 5.5. Maximum and initial gradient of mass increase, and total and gradients of acid release of the prednisolone-containing polymers in water over 18 weeks.

Code	Drug conc.	Max. mass increase	Initial mass increase		Total acid release	Acid release (μmoles/hr$^{0.5}$)		
	wt%	wt%	wt%/hr$^{0.5}$	R^2	μmoles	0-4 days	4days-18wk	Av. R^2
P34L8DMA	2.5	98	1.5	0.98	34	1.6	0.4	0.93
	10	98	1.6	0.98	33	1.6	0.4	0.85
P34L2DMA	2.5	21	1.1	0.96	30	1.7	0.3	0.97
	10	39	1.2	0.99	32	2.0	0.3	0.96
P17L4DMA	5	11	0.8	0.88	39	0.9	0.6	0.99
P7L8DMA	2.5	188	5.6	0.98	137	6.2	1.6	0.96
	10	106	8.0	0.98	141	6.1	1.7	0.98
P7L2DMA	2.5	7	0.8	0.97	96	2.6	1.6	0.99
	10	7	0.8	0.95	91	3.5	1.3	0.96

5.3.3 Acid release

5.3.3.1 Chlorhexidine Diacetate

The pH of the storage solution was measured at each time point over 10 weeks. For all polymers the pH values dropped immediately within half an hour of specimen placement in water to between pH 4 and 5 and either fluctuated around these values or continued to decline for the remaining period. For the short PPG425 polymers the pH could drop to 3. The pH of the solutions was converted to cumulative moles of acid released per specimen to quantify relative rates of degradation in the polymers (see Equation 4.7 and 4.8, Chapter 4). Relative standard deviations of the mean acid release for the ten samples were on average 1 ± 2 %.

There was a burst release of acid with the short PPG polymers P7L2DMA and P7L8DMA in the first four hours (Figure 5.8). Acid release was then proportional to the square root of time for these polymers but the gradient for the 2.5 wt% drug level (1.53 and 1.32 μmoles/ $hr^{0.5}$ for P7L2DMA and P7L8DMA respectively) was higher than that of the 10 wt% drug level (1.36 and 0.84 μmoles/ $hr^{0.5}$ for P7L2DMA and P7L8DMA respectively). Acid release for P17L4DMA, P34L2DMA and P34L8DMA were also proportional to the square root of time albeit at slower rates (0.28 – 0.78 μmoles/ $hr^{0.5}$). The gradient for the 2.5 wt% drug level in P34L8DMA and P34L2DMA polymers (0.59 and 0.77 μmoles/ $hr^{0.5}$) was initially twice that of the 10 wt% drug level but was comparable after 4 days and 2 weeks respectively. Increasing drug particle size had on average no significant effect on acid release. At 10 weeks, cumulative acid release was higher with the 2.5 wt% than the 10 wt% drug level in most polymers despite drug levels having negligible effect on total polymer mass loss (see later in Section 5.3.4.1). This was due to the basic nature of the drug and the effect of CDA on solution acidity will be

(a)

(b)

Figure 5.8. Cumulative acid release per specimen as a function of the square root of time for the polymers containing the drug chlorhexidine diacetate. Filled and unfilled symbols represent 10 and 2.5 wt% drug levels in the polymer. Big and small symbols represent larger (median size 128.5 μm) and smaller (median size 57 μm) drug particles respectively. Results were averaged for the two duplicate formulations of the P17L4DMA samples.

discussed later in Section 5.4.2. On averaging the two drug levels cumulative acid release

at 10 weeks decreased in the order P7L2DMA $\approx$ P7L8DMA > P17L4DMA > P34L8DMA

$\approx$ P34L2DMA (see Table 5.3).

5.3.3.2 Ketoprofen

For all polymers the pH values dropped immediately within half an hour of

specimen placement in water to between pH 3 and 4 and fluctuated around these values

for the remaining time. For the short PPG425 polymers the pH could drop to 3. Relative

standard deviations of the mean acid release per sample for the ten samples were on

average 1 ± 1 % over 18 weeks.

Acid release was initially proportional to the square root of time in all polymers

but after 4 days the gradient of acid release versus square root of time declined (Figure

5.9). Increasing drug level from 2.5 to 10 wt% had limited effect (see Table 5.4).

Differences in acid release were however significant with changing compositions of the

polymers. Acid release from the short PPG425 polymers was approximately three to four

times faster than that from the longer PPG polymers. In the PPG425 polymers the

gradient of acid release for high lactide (i.e. P7L8DMA) could be twice that for low

lactide (i.e. P7L2DMA). Gradients of acid release versus square root of time were higher

than those with chlorhexidine-containing specimens after the initial burst release (see

Table 5.3 and Table 5.4). At 18 weeks, cumulative acid release decreased in the order

P7L8DMA > P7L2DMA > P17L4DMA $\approx$ P34L8DMA > P34L2DMA as with

chlorhexidine-containing specimens (see Table 5.4). The effect of ketoprofen release in

contributing to the acid release was found to be almost negligible as will be discussed

further in Section 5.4.2.
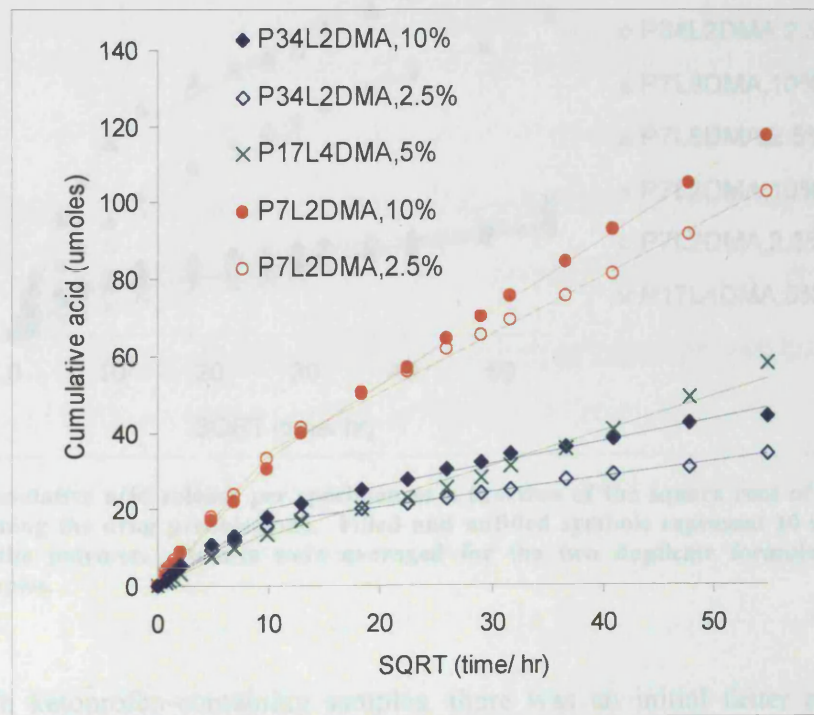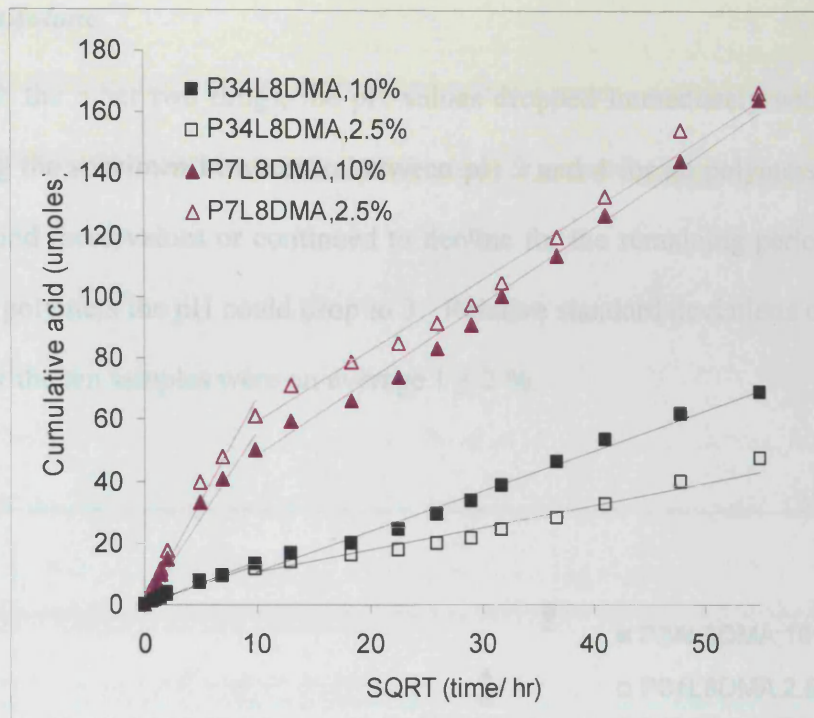
Figure 5.9. Cumulative acid release per specimen as a function of the square root of time for the polymers containing the drug ketoprofen. Filled and unfilled symbols represent 10 and 2.5 wt% drug levels in the polymer. Results were averaged for the two duplicate formulations of the P17L4DMA samples.

5.3.3.3 Prednisolone

As with the other two drugs, the pH values dropped immediately within half an hour of placing the specimen in water to between pH 3 and 4 for all polymers and either fluctuated around these values or continued to decline for the remaining period. For the short PPG425 polymers the pH could drop to 3. Relative standard deviations of the mean acid release for the ten samples were on average 1 ± 2 %.
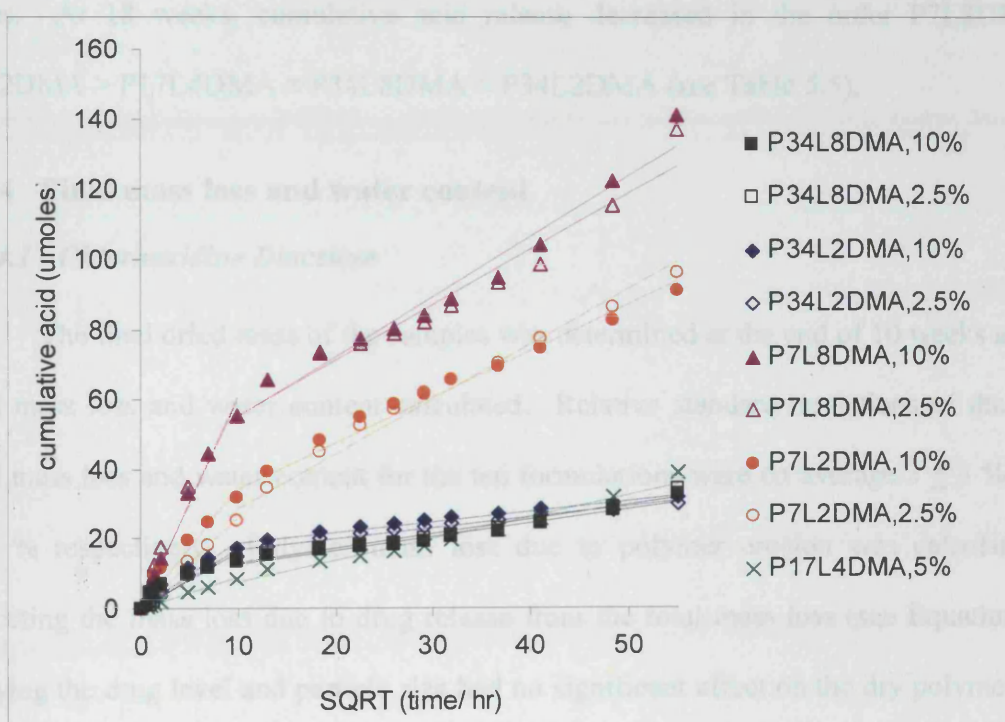
Figure 5.10. Cumulative acid release per specimen as a function of the square root of time for the polymers containing the drug prednisolone. Filled and unfilled symbols represent 10 and 2.5 wt% drug levels in the polymer. Results were averaged for the two duplicate formulations of the P17L4DMA samples.

As with ketoprofen-containing samples, there was an initial faster acid release phase up to 4 days with all polymers followed by a slower release phase over the remaining time period (Figure 5.10). In both phases acid release was linear with the

263

square root of time. Gradients of acid release was comparable to those obtained with

ketoprofen-containing specimens in the first 4 days but after this period became less than

those of ketoprofen (see Table 5.4 and Table 5.5). Varying drug level however had no

effect on the acid release. Acid release was the highest in the short PPG425 polymers and

when the lactide segment was long (P7L8DMA) the initial gradient could be twice that

containing short lactide (P7L2DMA). Acid release for P17L4DMA was two times slower

than that of P34L2DMA and P34L8DMA in the first 4 days but became faster at later

times. At 18 weeks, cumulative acid release decreased in the order P7L8DMA >

P7L2DMA > P17L4DMA ≈ P34L8DMA ≈ P34L2DMA (see Table 5.5).

5.3.4 Final mass loss and water content

5.3.4.1 *Chlorhexidine Diacetate*

The final dried mass of the samples was determined at the end of 10 weeks and the

total mass loss and water content calculated. Relative standard deviations of the mean

total mass loss and water content for the ten formulations were on average 3 ± 3 % and 6

± 2 % respectively. Polymer mass loss due to polymer erosion was calculated by

deducting the mass loss due to drug release from the total mass loss (see Equation 5.1).

Varying the drug level and particle size had no significant effect on the dry polymer mass

loss. Increasing drug level from 2.5 to 10 wt% increased slightly the water content for the

polymers P7L2DMA and P34L2DMA but decreased it when the lactide length was high

(see Table 5.6). The final water content at 10 weeks was between 11 and 53 wt%.

Polymer mass loss of the samples at 10 weeks ranged between 6 and 20 wt%. Polymer

mass loss per mole of acid release (Equation 4.9, Chapter 4) was on average equal to 0.7 ±

0.2 kg/mole of acid release. On changing the monomer structure, average mass loss

increased in the order P7L8DMA ≈ P7L2DMA > P17L4DMA ≈ P34L8DMA ≈

P34L2DMA similar to acid release; and water content followed in the order P7L8DMA >

P34L8DMA > P34L2DMA > P7L2DMA > P17L4DMA (see Table 5.6).

Table 5.6. Degraded material properties of the chlorhexidine diacetate-containing samples after 10 weeks in water.

Code	Drug conc.	Drug particle size	Total mass loss[i]	Polymer mass loss[ii]	Polymer mass / acid loss	Water content	Drug release
	Wt%	μm	wt%	wt%	kg/mol	wt%	%
P34L8DMA	2.5	39-75	7	6	0.4	43	50
	10	107-150	17	8	0.9	24	82
P34L2DMA	2.5	107-150	8	7	0.6	15	53
	10	39-75	13	7	1.0	19	69
P17L4DMA	5	76-106	10	8	0.5	11	38
P7L8DMA	2.5	107-150	22	20	0.6	53	55
	10	39-75	21	15	0.6	46	62
P7L2DMA	2.5	39-75	20	19	0.7	13	15
	10	107-150	23	19	0.7	16	36

[i] Total mass loss includes both polymer erosion and drug release
[ii] Polymer mass loss was calculated after correcting the total mass loss for drug release using Equation 5.1.

5.3.4.2 Ketoprofen

The total mass loss and water content were determined at 18 weeks for each

polymer sample. These could not be determined for the 34L8DMA specimens containing

10 wt% drug as they had disintegrated by this time. Relative standard deviations of the

mean mass loss and water content for the ten formulations were on average 3 ± 3 % and 6

± 4 % respectively. Varying the drug level had negligible effect on the polymer mass loss

or water content (see Table 5.7). Polymer mass loss of the samples at 18 weeks ranged

between 9 and 78 wt% and was on average equal to 0.6 ± 0.2 kg / mole of acid release.

The final water content at 18 weeks was between 18 and 55 wt%. On changing the

monomer structure, average mass loss increased in the order P7L8DMA > P7L2DMA >

P34L8DMA > P17L4DMA > P34L2DMA and water content increased in the order

P34L8DMA > P7L8DMA > P7L2DMA ≈ P34L2DMA ≈ P17L4DMA (see Table 5.7).

For polymers with long PPG lengths (i.e. PPG2000), 18-week water content was greater

than the total material loss. With polymers of PPG 425 g/mol the water content at 18

weeks was half of the total mass loss indicating some extent of material shrinkage.

Table 5.7. .Degraded material properties of the ketoprofen-containing samples after 18 weeks in water.

Code	Drug conc.	Total mass loss[i]	Polymer mass loss[ii]	Polymer mass / acid loss	Water content	Drug release
	Wt%	wt%	wt%	kg/mol	wt%	%
P34L8DMA	2.5	25	24	0.9	55	62
	10	*	*	*	*	49
P34L2DMA	2.5	11	9	0.4	19	62
	10	14	9	0.4	19	48
P17L4DMA	5	20	17	0.5	18	61
P7L8DMA	2.5	80	78	0.9	39	93
	10	86	78	0.8	33	99
P7L2DMA	2.5	34	33	0.6	18	51
	10	42	37	0.6	22	57

[i] Total mass loss includes both polymer erosion and drug release
[ii] Polymer mass loss was calculated after correcting the total mass loss for drug release using Equation 5.1.

5.3.4.3 Prednisolone

As with ketoprofen the total mass loss and final wet mass were determined at 18 weeks for each polymer sample. Relative standard deviations of the mean mass loss and water content for the ten formulations were on average 2 ± 2 % and 5 ± 3 % respectively.

Table 5.8. Degraded material properties of the prednisolone-containing samples after 18 weeks in water.

Code	Drug conc. wt%	Total mass loss[i] wt%	Polymer mass loss[ii] wt%	Polymer mass / acid loss kg/mol	Water content wt%	Drug release %
P34L8DMA	2.5	10	7	0.4	54	99
	10	16	7	0.4	57	96
P34L2DMA	2.5	11	8	0.5	18	104
	10	17	9	0.5	34	97
P17L4DMA	5	17	12	0.5	13	98
P7L8DMA	2.5	69	66	0.9	37	108
	10	69	61	0.9	43	94
P7L2DMA	2.5	31	29	0.6	19	96
	10	33	27	0.6	21	68

[i] Total mass loss includes both polymer erosion and drug release
[ii] Polymer mass loss was calculated after correcting the total mass loss for drug release using Equation 5.1.

Increasing the drug level from 2.5 to 10 wt% had negligible effect on the polymer mass loss but increased noticeably the water content (see Table 5.8). Polymer mass loss of the samples at 18 weeks ranged between 7 and 66 wt% and was on average equal to 0.6 $\pm$ 0.2 kg / mole of acid release. The water content at 18 weeks was between 13 and 57 wt%. On changing the monomer structure, average mass loss increased in the order P7L8DMA > P7L2DMA > P17L4DMA > P34L8DMA $\approx$ P34L2DMA and water content

increased in the order P34L8DMA > P7L8DMA > P34L2DMA ≈ P7L2DMA > P17L4DMA (see Table 5.8). Again with polymers of the shorter PPG lengths the 18-week water content was less than the material mass loss indicating some material shrinkage.

5.3.5 Drug release

Figure 5.11 to Figure 5.13 show example UV spectra of the storage solutions for the three different drugs before and after subtraction of the control spectra to determine absorbance due only to the drug. The three figures included spectra ranging from the fastest (i.e. P7L8DMA) to slower degrading samples (i.e. P7L2DMA and the slowest P34L2DMA) over different sampling time points when impurity was most prevalent (e.g. due to release of residual initiators and double bond-containing degradation products). The impurity-corrected spectrum of each drug after release from the polymer was consistent with that of the respective pure drug (Figure 5.4). This provides some evidence that the three drugs had not been affected by the curing process of the polymer or by the reduced pH of the solutions due to acidic degradation fragments of the polymers.
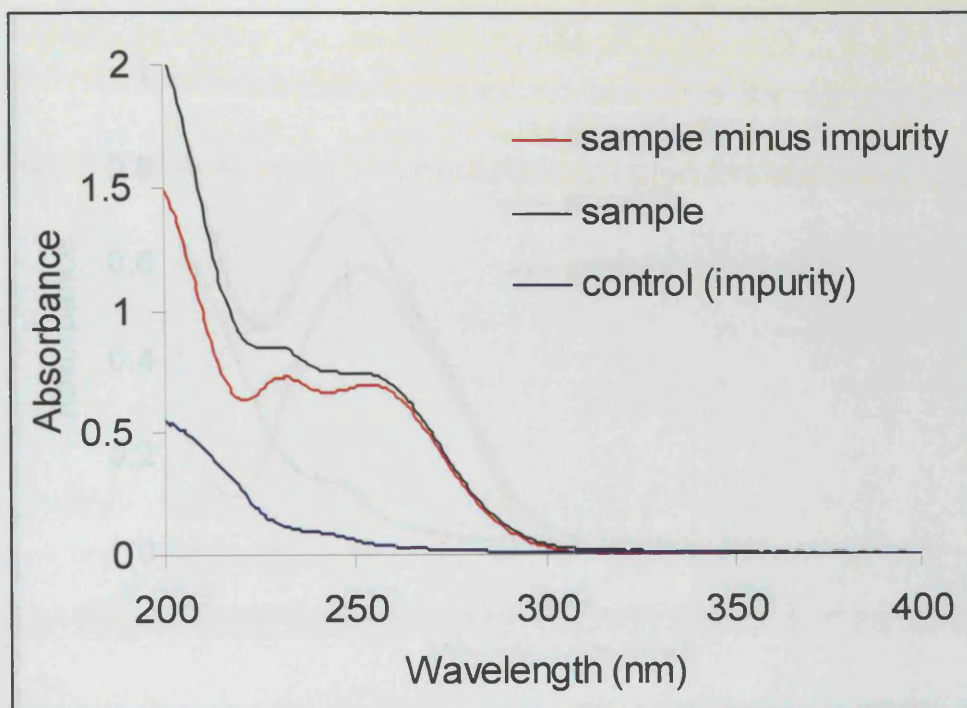
Figure 5.11. Example UV spectra of a chlorhexidine-containing sample (P7L2DMA) and a control (P7L2DMA) at 8 weeks of study. Subtracting the control spectrum from the sample spectrum reveals a spectrum due only to the drug component in the sample with peak maxima at λ_{231} and λ_{254}.
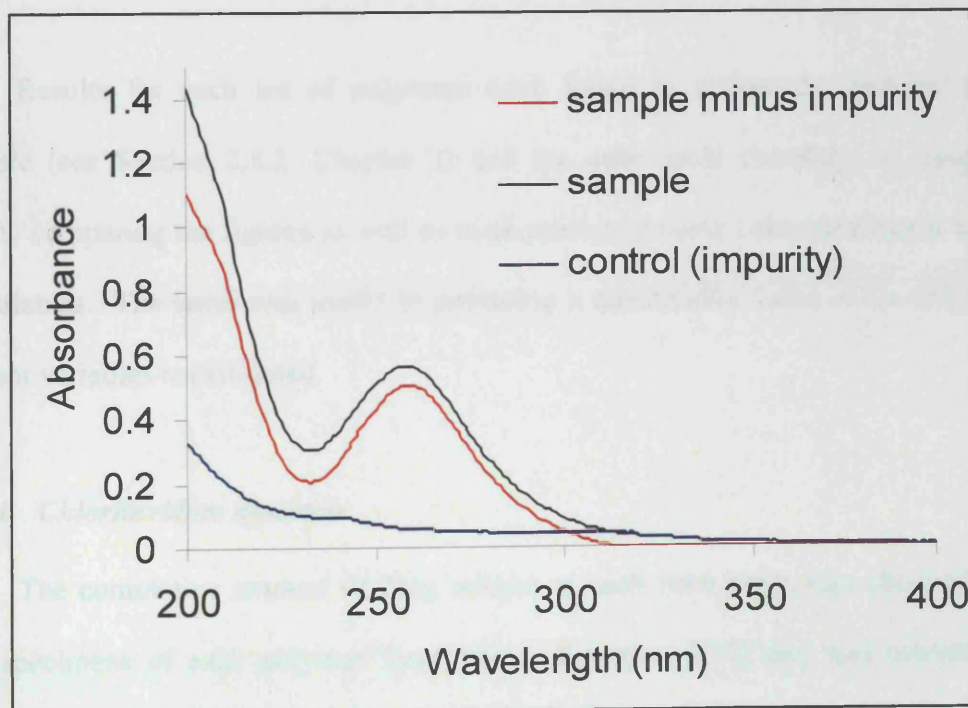
Figure 5.12. Example UV spectra of a ketoprofen-containing sample (P34L2DMA) and a control (P34L2DMA) at 2 weeks of study. Subtracting the control spectrum from the sample spectrum reveals a spectrum due only to the drug component in the sample with a peak maximum at λ_{261}.
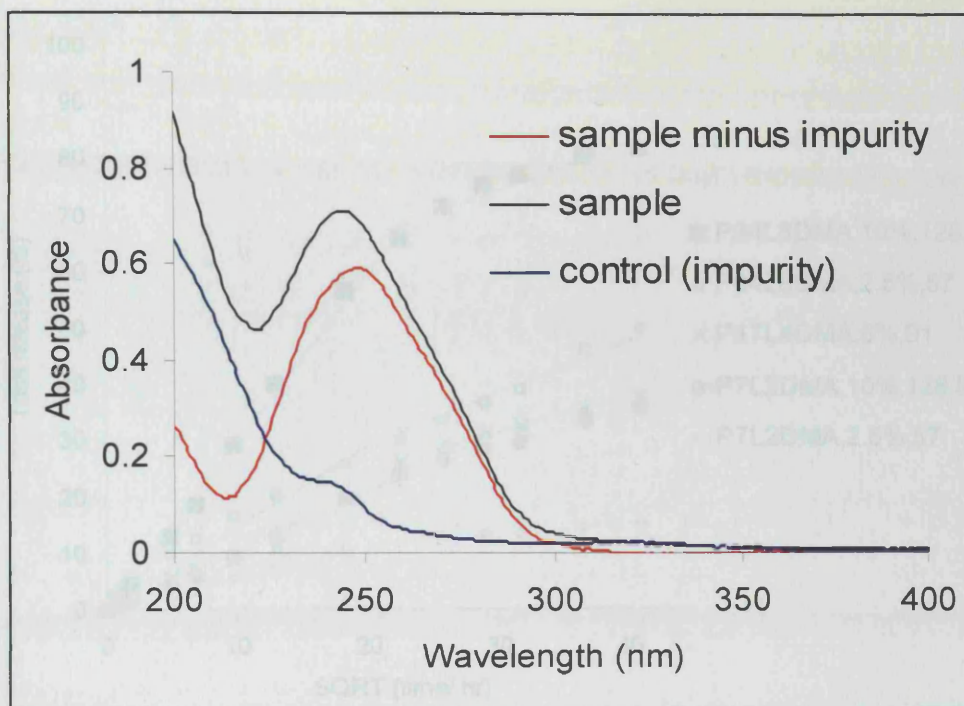
Figure 5.13. Example UV spectra of a prednisolone-containing sample (P7L8DMA) and a control (P7L8DMA) at 48 hours of study. Subtracting the control spectrum from the sample spectrum reveals a spectrum due only to the drug component in the sample with a peak maximum at λ_{247}.

Results for each set of polymers were found to follow the factorial analysis rationale (see Section 2.8.2, Chapter 2) and the data could therefore be analysed by visually comparing the figures as well as mathematically using calculated exp B values of the variables. The latter was useful in providing a quantitative value of the effect of the different variables investigated.

5.3.5.1 Chlorhexidine diacetate

The cumulative amount of drug release at each time point was obtained for the three specimens of each polymer formulation (Equation 5.11) and was converted into mean percentage release of the original drug mass over a 10-week period.
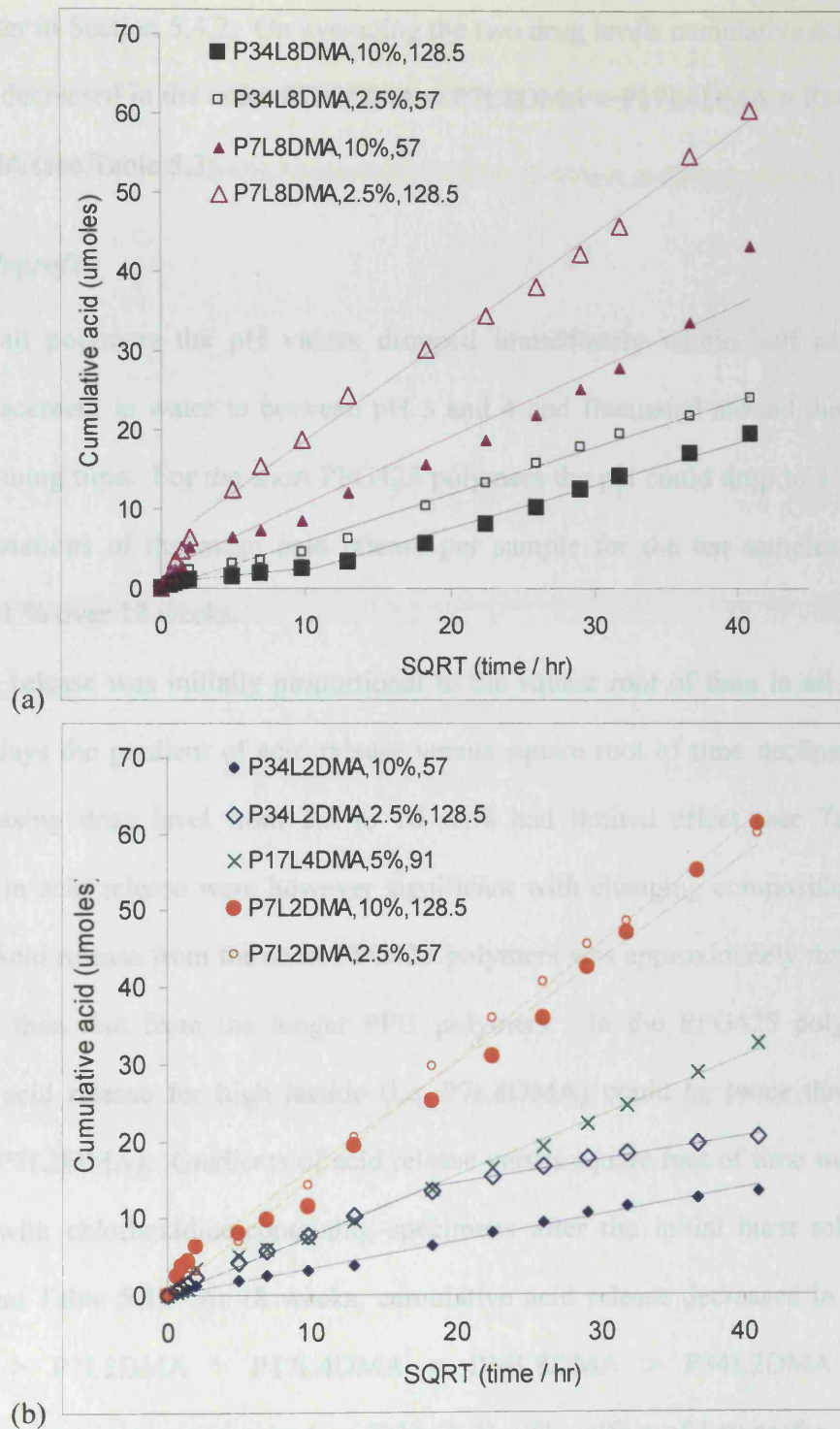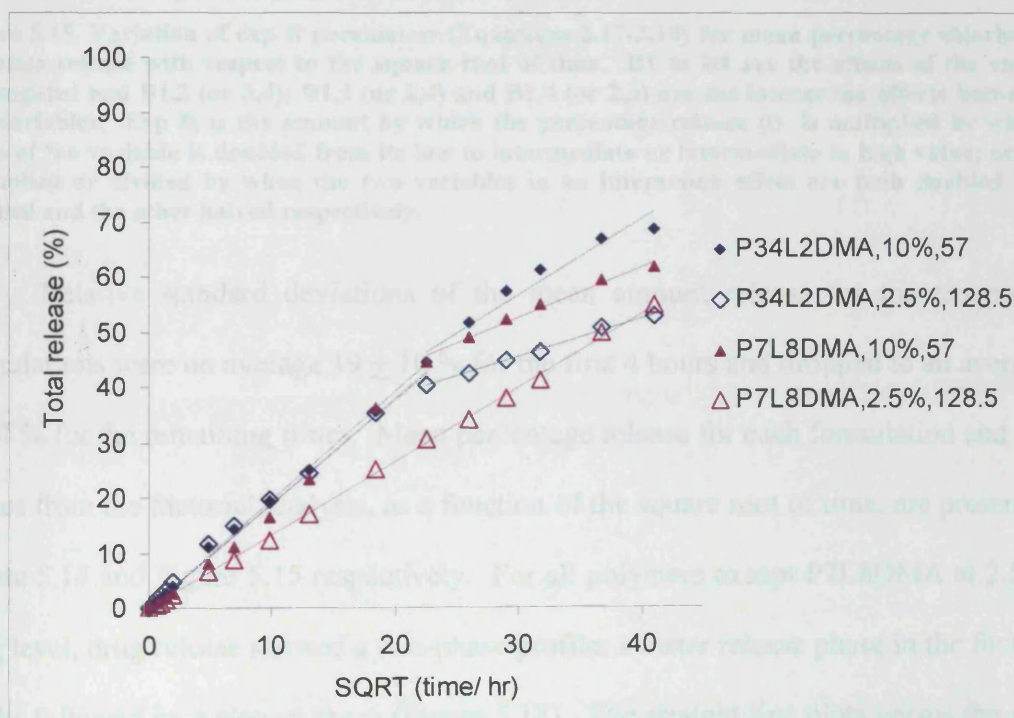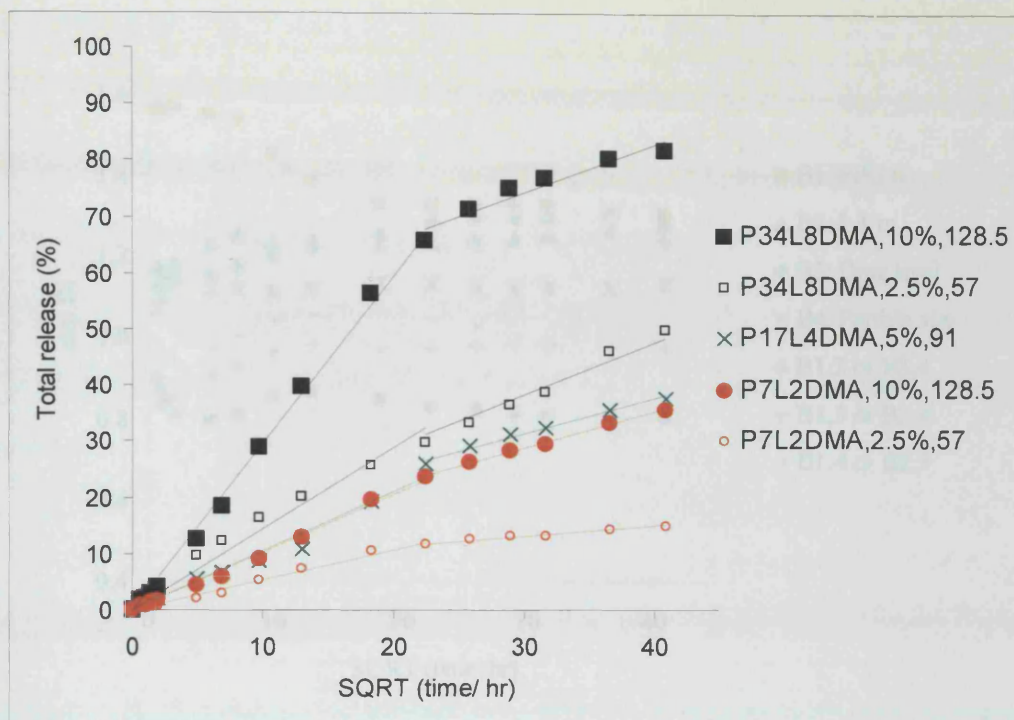
Figure 5.14. Percentage drug release per specimen as a function of the square root of time for the polymers containing the drug chlorhexidine diacetate. Filled and unfilled symbols represent 10 and 2.5 wt% drug levels in the polymer. Big and small symbols represent bigger (median size 128.5 μm) and small (median size 57 μm) size drug particles respectively. Results were averaged for the two duplicate formulations of the P17L4DMA samples.
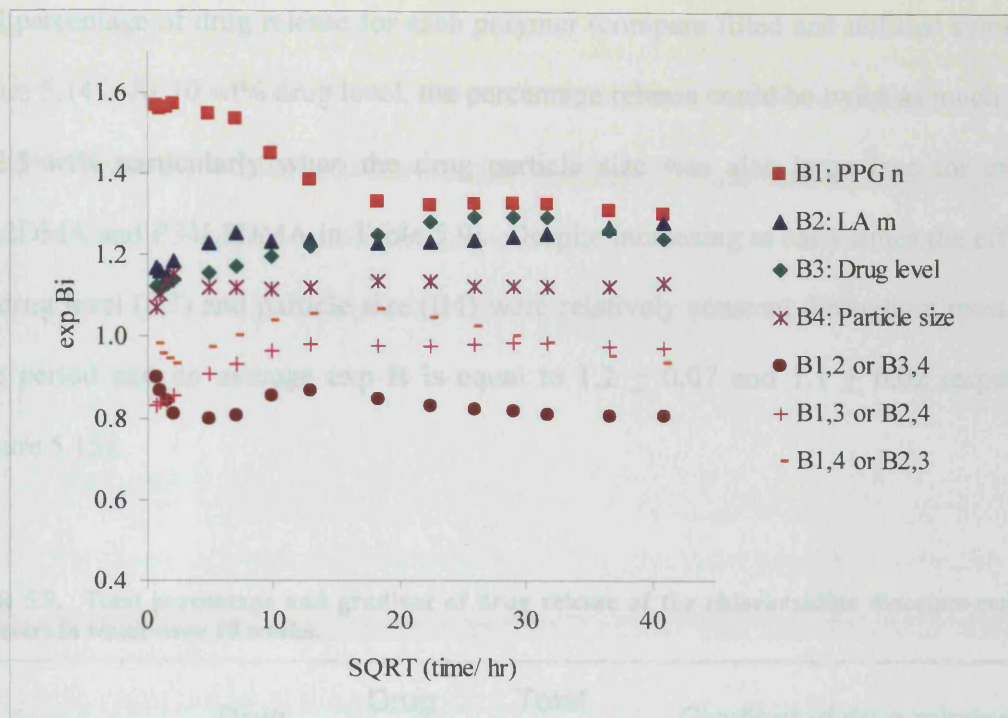
Figure 5.15. Variation of exp B parameters (Equations 2.17-2.18) for mean percentage chlorhexidine diacetate release with respect to the square root of time. B1 to B4 are the effects of the variables investigated and B1,2 (or 3,4); B1,3 (or 2,4) and B1,4 (or 2,3) are the interaction effects between the two variables. Exp B_i is the amount by which the percentage release (i) is multiplied by when the value of the variable is doubled from its low to intermediate or intermediate to high value; or (ii) is multiplied or divided by when the two variables in an interaction effect are both doubled or one doubled and the other halved respectively.

Relative standard deviations of the mean amount release for the ten polymer formulations were on average 19 ± 10 % for the first 4 hours and dropped to an average of 6 ± 4 % for the remaining times. Mean percentage release for each formulation and exp B values from the factorial analysis, as a function of the square root of time, are presented in Figure 5.14 and Figure 5.15 respectively. For all polymers except P7L8DMA at 2.5 wt% drug level, drug release showed a two-phase profile: a faster release phase in the first three weeks followed by a slower phase (Figure 5.14). The straight line plots versus the square root of time in both phases suggest that drug release was consistent with a diffusion mechanism. Raising the drug level from 2.5 to 10 wt% increased both the gradient and

total percentage of drug release for each polymer (compare filled and unfilled symbols in

Figure 5.14). At 10 wt% drug level, the percentage release could be twice as much as that

of 2.5 wt% particularly when the drug particle size was also large (see for example

P7L2DMA and P34L8DMA in Table 5.9). Despite increasing at early times the effects of

the drug level (B3) and particle size (B4) were relatively constant throughout most of the

time period and on average exp B is equal to 1.2 ± 0.07 and 1.1 ± 0.02 respectively

(Figure 5.15).

Table 5.9. Total percentage and gradient of drug release of the chlorhexidine diacetate-containing polymers in water over 10 weeks.

Code	Drug conc.	Drug particle size	Total drug release	Gradient of drug release $(\%/hr^{0.5})$		
	wt%	μm	%	0-3 wk	3-10wk	Av R^2
P34L8DMA	2.5	39-75	50	1.4	0.9	0.97
	10	107-150	82	3.0	0.8	0.96
P34L2DMA	2.5	107-150	53	1.9	0.7	0.99
	10	39-75	69	2.0	1.4	0.98
P17L4DMA	5	76-106	38	1.1	0.6	0.99
P7L8DMA	2.5	107-150	55	1.3	1.3	1.00
	10	39-75	62	1.9	0.9	0.99
P7L2DMA	2.5	39-75	15	0.5	0.2	0.99
	10	107-150	36	1.0	0.7	1.00

Varying monomer structures also affected drug release. Increasing PPG length

had the most significant effect on increasing the percentage drug release although this

effect became less with time (from exp $B_1 = 1.6$ to 1.3) (Figure 5.15). Lactide length (B2)

had similar effect as the drug level (B3). If the lactide length of the polymer was doubled,

the percentage drug release increased on average by a factor of 1.2 (as on average exp B_2 = 1.2, see Figure 5.15). At 10 weeks total percentage drug release ranged from 15 % for P7L2DMA (2.5 wt% drug-doped) to 82 % for P34L8DMA (10 wt% drug-doped). The average total percentage drug release for the different polymers decreased in the following order: P34L8DMA > P34L2DMA > P7L8DMA > P17L4DMA > P7L2DMA (see Table 5.9).

5.3.5.2   Ketoprofen

The mean percentage ketoprofen release in the specimens was obtained over a period of 18 weeks. Relative standard deviations of the mean amount release for the ten polymer formulations were on average 12 ± 6 %.
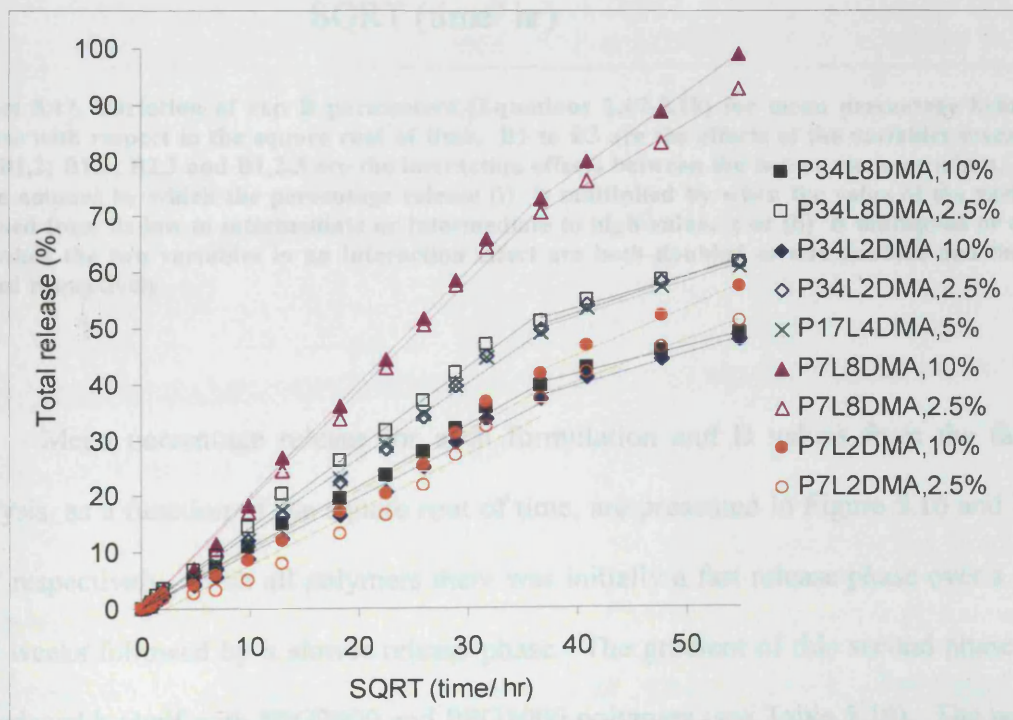
Figure 5.16. Percentage drug release per specimen as a function of the square root of time for the polymers containing the drug ketoprofen. Filled and unfilled symbols represent 10 and 2.5 wt% drug levels in the polymer. Results were averaged for the two duplicate formulations of the P17L4DMA samples.
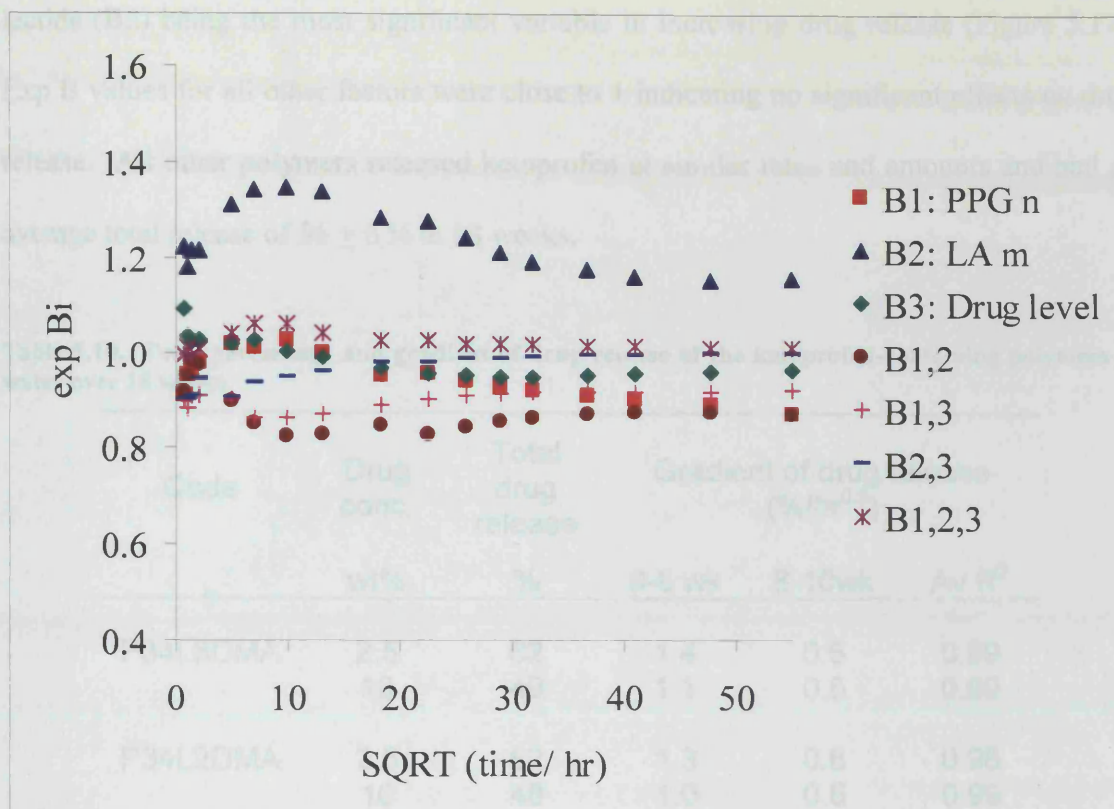
Figure 5.17. Variation of exp B parameters (Equations 2.17-2.18) for mean percentage ketoprofen release with respect to the square root of time. B1 to B3 are the effects of the variables investigated and B1,2; B1,3; B2,3 and B1,2,3 are the interaction effects between the two or more variables. Exp B_i is the amount by which the percentage release (i) is multiplied by when the value of the variable is doubled from its low to intermediate or intermediate to high value. ; or (ii) is multiplied or divided by when the two variables in an interaction effect are both doubled or one doubled and the other halved respectively.

Mean percentage release for each formulation and B values from the factorial analysis, as a function of the square root of time, are presented in Figure 5.16 and Figure 5.17 respectively. With all polymers there was initially a fast release phase over a period of 8 weeks followed by a slower release phase. The gradient of this second phase could be reduced by half with PPG2000 and PPG1000 polymers (see Table 5.10). The polymer P7L8DMA had the highest release of all with an average total release of 96 % that could be twice as high as the other polymers. The results for this polymer led to the effect of

lactide (B2) being the most significant variable in increasing drug release (Figure 5.17).

Exp B values for all other factors were close to 1 indicating no significant effects on drug

release. All other polymers released ketoprofen at similar rates and amounts and had an

average total release of 56 ± 6 % at 18 weeks.

Table 5.10. Total percentage and gradient of drug release of the ketoprofen-containing polymers in water over 18 weeks.

Code	Drug conc.	Total drug release	Gradient of drug release $(\%/hr^{0.5})$		
	wt%	%	0-8 wk	8-10wk	Av R^2
P34L8DMA	2.5	62	1.4	0.6	0.99
	10	49	1.1	0.5	0.99
P34L2DMA	2.5	62	1.3	0.6	0.98
	10	48	1.0	0.6	0.99
P17L4DMA	5	61	1.3	0.6	0.99
P7L8DMA	2.5	93	1.9	1.2	1.00
	10	99	2.0	1.4	1.00
P7L2DMA	2.5	51	1.0	0.7	0.98
	10	57	1.1	0.8	0.99

5.3.5.3 Prednisolone

Relative standard deviations of the mean prednisolone release for the ten polymer

formulations were on average 9 ± 5 % for the first 4 hours and dropped to an average of 5

± 3 % for the remaining times. Mean percentage release for each formulation and B

values from the factorial analysis, as a function of the square root of time, are presented in

Figure 5.18 and Figure 5.19 respectively.
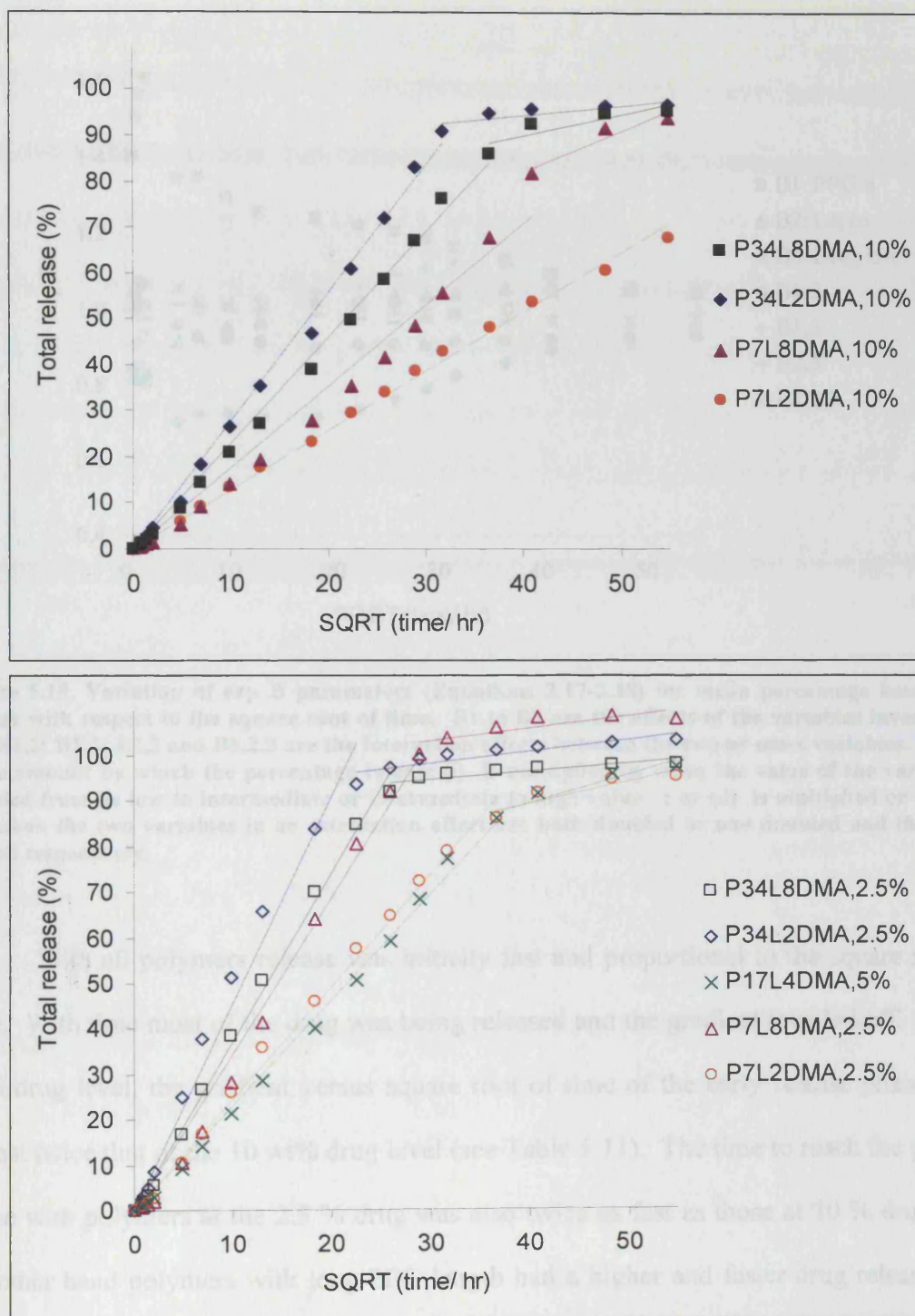
Figure 5.18. Percentage drug release per specimen as a function of the square root of time for the polymers containing the drug prednisolone. Filled and unfilled symbols represent 10 and 2.5 wt% drug levels in the polymer. Results were averaged for the two duplicate formulations of the P17L4DMA samples.
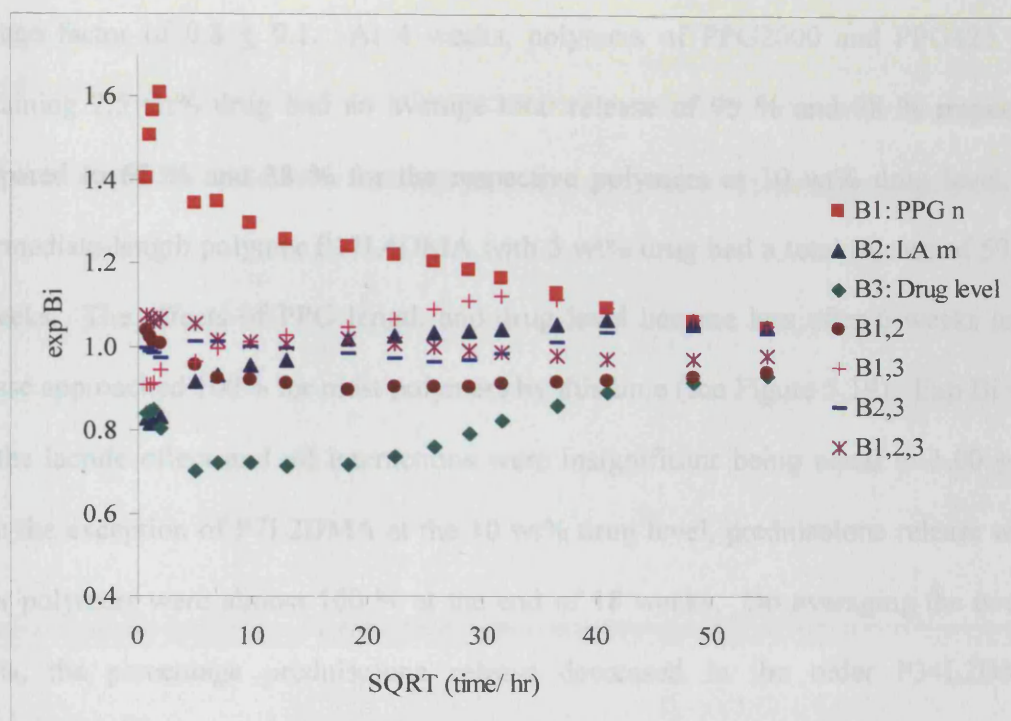
Figure 5.19. Variation of exp B parameters (Equations 2.17-2.18) for mean percentage ketoprofen release with respect to the square root of time. B1 to B3 are the effects of the variables investigated and B1,2; B1,3; B2,3 and B1,2,3 are the interaction effects between the two or more variables. Exp B_i is the amount by which the percentage release (i) is multiplied by when the value of the variable is doubled from its low to intermediate or intermediate to high value. ; or (ii) is multiplied or divided by when the two variables in an interaction effect are both doubled or one doubled and the other halved respectively.

With all polymers release was initially fast and proportional to the square root of time. With time most of the drug was being released and the gradient levelled off. At 2.5 wt% drug level, the gradient versus square root of time of the early release phase were almost twice that of the 10 wt% drug level (see Table 5.11). The time to reach the plateau phase with polymers at the 2.5 % drug was also twice as fast as those at 10 % drug. On the other hand polymers with long PPG length had a higher and faster drug release than those with short PPG (Figure 5.18). For the first 6 weeks doubling the length of PPG (B1) increased the percentage drug release by a factor of 1.3 $\pm$ 0.2 (Figure 5.19). Over the same period doubling the drug level (B3) would reduce the percentage drug release by an

average factor of 0.8 ± 0.1. At 4 weeks, polymers of PPG2000 and PPG425 g/mol

containing 2.5 wt% drug had an average total release of 95 % and 78 % respectively

compared to 65 % and 38 % for the respective polymers at 10 wt% drug level. The

intermediate-length polymer P17L4DMA with 5 wt% drug had a total release of 59 % by

4 weeks. The effects of PPG length and drug level became less after 6 weeks as drug

release approached 100% for most polymers by this time (see Figure 5.19). Exp Bi values

for the lactide effect and all interactions were insignificant being equal to 1.00 ± 0.07.

With the exception of P7L2DMA at the 10 wt% drug level, prednisolone release with all

other polymers were almost 100 % at the end of 18 weeks. On averaging the two drug

levels, the percentage prednisolone release decreased in the order P34L2DMA >

P34L8DMA > P7L8DMA > P17L4DMA ≈ P7L2DMA.

Table 5.11. Total percentage and gradient of drug release of the prednisolone-containing polymers in water over 18 weeks.

Code	Drug conc.	Total drug release	Gradient of drug release $(\%/hr^{0.5})$		
	wt%	%	Early[i]	Late	Av R^2
P34L8DMA	2.5	99	3.7	0.2	0.88
	10	96	2.3	0.5	0.88
P34L2DMA	2.5	104	4.6	0.3	0.90
	10	97	2.8	0.2	0.86
P17L4DMA	5	98	2.3	0.6	0.96
P7L8DMA	2.5	108	3.4	0.3	0.84
	10	94	1.8	0.9	0.95
P7L2DMA	2.5	96	2.5	0.5	0.92
	10	68	*	1.3	1.00

[i] Duration of this early phase for P34L8DMA: 4 wks (2.5 % drug) & 8 wks (10 % drug); for P34L2DMA: 3 wks (2.5 % drug) & 6 wks (10 % drug); for P17L4DMA: 8 wks; for P7L8DMA: 5 wks (2.5 % drug) & 10 wks (10 % drug); and for P7L2DMA: 8 wks (2.5 % drug) & 18 wks (10 % drug).

5.3.6   Comparison of the three drugs

5.3.6.1   *Polymer mass loss and water content*

Varying drug level and particle size had only slight effects on the polymer mass loss and water contents compared to monomer structures and results were therefore averaged for each polymer for ease of comparison. Figure 5.20 and Figure 5.21 show the polymer mass loss and water content respectively for samples containing the three different drugs over a period of 10 weeks (for CDA) or 18 weeks (for ketoprofen and prednisolone).
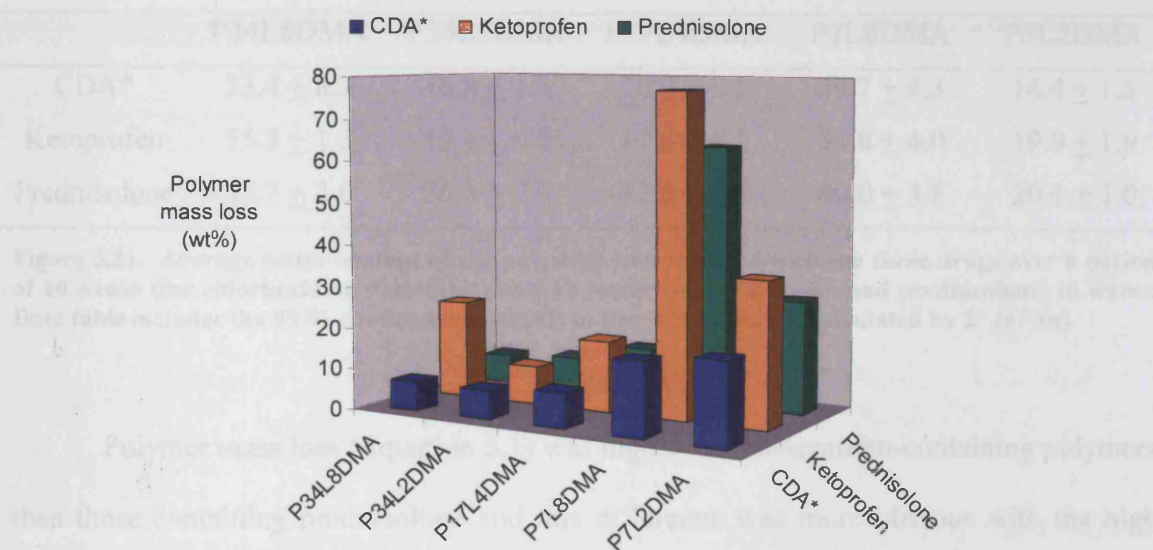
	P34L8DMA	P34L2DMA	P17L4DMA	P7L8DMA	P7L2DMA
CDA*	7.0 ± 1.3	7.0 ± 0.7	8.5 ± 0.1	17.9 ± 2.6	20.0 ± 0.2
Ketoprofen	23.6 ± 8.8	9.2 ± 0.4	17.3 ± 0.1	77.5 ± 2.1	35.0 ± 2.5
Prednisolone	7.0 ± 0.4	8.1 ± 0.2	12.2 ± 0.2	63.4 ± 3.8	27.4 ± 1.1

Figure 5.20. Average polymer mass loss of the polymers incorporated with the three drugs over a period of 10 weeks (for chlorhexidine diacetate*) and 18 weeks (for ketoprofen and prednisolone) in water. Data table includes the 95 % confidence intervals of the sample means calculated by 2* (s / √n).
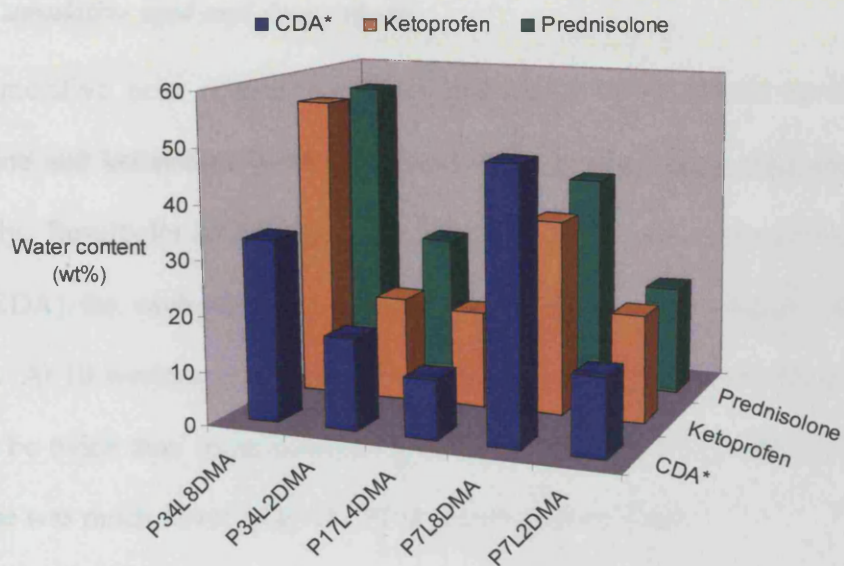
	P34L8DMA	P34L2DMA	P17L4DMA	P7L8DMA	P7L2DMA
CDA*	33.4 ± 8.7	16.8 ± 1.7	10.9 ± 0.3	49.7 ± 4.3	14.4 ± 1.5
Ketoprofen	55.3 ± 1.3	19.1 ± 0.8	17.8 ± 1.1	35.8 ± 4.0	19.9 ± 1.9
Prednisolone	55.7 ± 2.0	26.3 ± 7.3	12.6 ± 0.8	40.0 ± 3.8	20.1 ± 1.0

Figure 5.21. Average water content of the polymers incorporated with the three drugs over a period of 10 weeks (for chlorhexidine diacetate*) and 18 weeks (for ketoprofen and prednisolone) in water. Data table includes the 95 % confidence intervals of the sample means calculated by 2* (s / √n).

Polymer mass loss (Equation 5.1) was higher with ketoprofen-containing polymers than those containing prednisolone and this difference was more obvious with the high lactide length polymers (P34L8DMA and P7L8DMA). With all three drugs, polymers containing short PPG segments eroded the fastest particularly P7L8DMA whilst erosion extents with the intermediate and long length polymers (P34L8DMA, P34L2DMA and P17L4DMA) were much less and comparable with each other. In all three drugs the highest water sorption occurred with either P34L8DMA or P7L8DMA followed by P34L2DMA (see Figure 5.21). The polymers P17L4DMA and P7L2DMA had the least water sorption.

5.3.6.2   Cumulative acid and drug release

Cumulative acid release and total percentage drug release at 10 weeks for prednisolone and ketoprofen were compared with CDA in Figure 5.22 and Figure 5.23 respectively. Results for acid release were averaged over the two drug levels (and particle size for CDA) for each polymer as monomer structures gave bigger effects on this parameter. At 10 weeks acid release was the fastest with ketoprofen-containing polymers and could be twice than those containing CDA (see Figure 5.22). With all three drugs, acid release was much faster when the PPG segments were short.
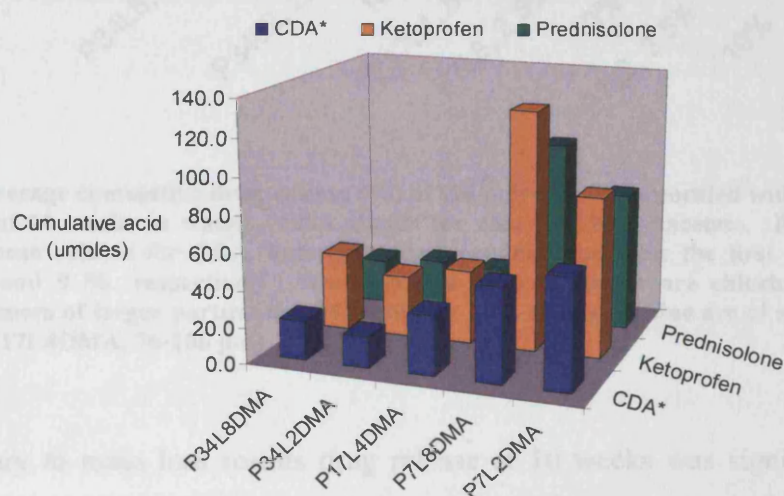
	P34L8DMA	P34L2DMA	P17L4DMA	P7L8DMA	P7L2DMA
CDA*	21.8	17.1	33.0	52.0	60.8
Ketoprofen	42.9	34.0	41.0	129.8	87.2
Prednisolone	24.6	27.6	26.0	101.2	75.9

Figure 5.22. Average cumulative acid release (µmoles) of the polymers incorporated with the three drugs over a period of 10 weeks in water. CDA stands for chlorhexidine diacetate. Relative standard deviations of mean acid release for each drug over 10 weeks were on average 1 %.
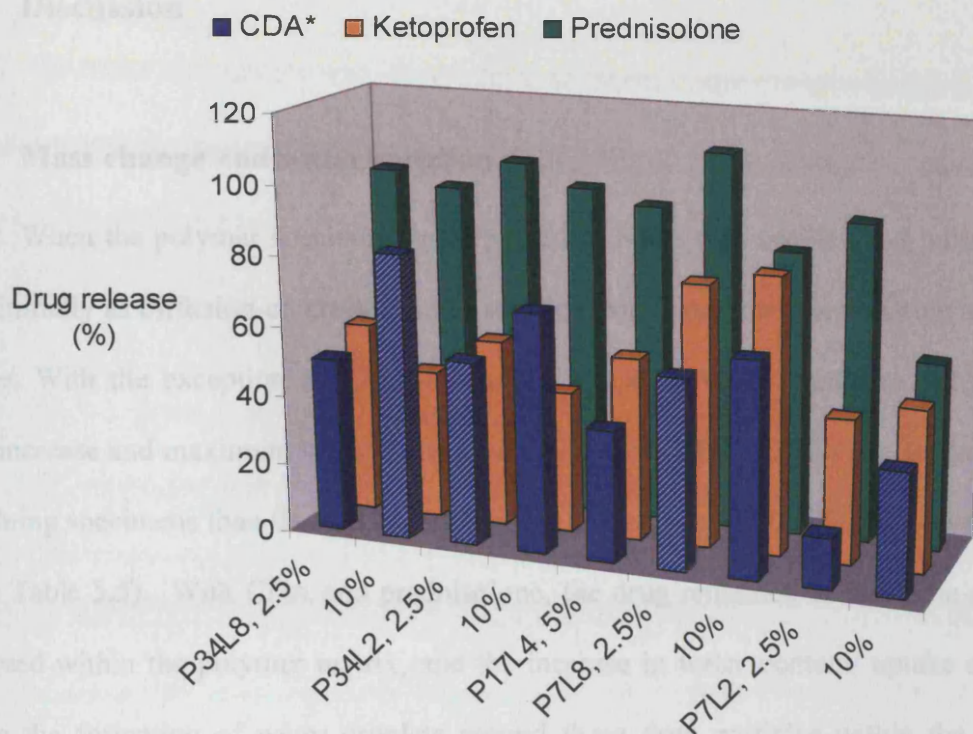
Figure 5.23. Average cumulative drug release (%) of the polymers incorporated with the three drugs over a period of 10 weeks in water. CDA stands for chlorhexidine diacetate. Relative standard deviations of mean release for CDA, ketoprofen and prednisolone after the first 4 hours were on average 6, 12 and 9 %. respectively *Data shaded in blue stripes are chlorhexidine diacetate containing polymers of larger particle size 107-150 μm; ones shaded in blue are of small particle size 39-75 μm (for P17L4DMA, 76-106 μm)

Contrary to mass loss results drug release at 10 weeks was significantly higher with all prednisolone-containing polymers when compared with those containing ketoprofen. For shorter and faster-degrading polymers (i.e. P7L2DMA and P7L8DMA) drug release was higher with those containing ketoprofen-than with CDA. With slow-eroding polymers of long PPG (i.e. P34L2DMA and P34L8DMA), however, there was a higher CDA than ketoprofen release at the 10 wt% drug level (see Figure 5.23). At 10 weeks, prednisolone release for all polymer samples averaged at 91 $\pm$ 16 %, compared to CDA and ketoprofen release of 51 $\pm$ 20 % and 55 $\pm$ 14 % respectively.

5.4   Discussion

5.4.1   Mass change and water sorption

When the polymer specimens were placed in water they swelled and increased in mass initially as diffusion-controlled water sorption dominated over degradation and drug release. With the exception of P34L8DMA and P7L8DMA, the gradient of this initial mass increase and maximum mass change were higher with both CDA- and prednisolone-containing specimens than those with ketoprofen, particularly at 10 wt% drug level (Table 5.3 to Table 5.5). With CDA and prednisolone, the drug remained as insoluble particles dispersed within the polymer matrix, and the increase in water content/ uptake could be due to the formation of water droplets around these drug particles within the sample. When water diffuses in and reaches a CDA or prednisolone inclusion, a droplet forms. This expands as water diffusing through the polymer flows along an osmotic gradient between the internal droplet and external solutions. This effect becomes more significant with increasing amount of drug particles in the polymers. The lower aqueous solubility of ketoprofen in the polymer reduces this osmolarity effect and hence water sorption was initially comparatively less.

As previously discussed in Chapter 4, the ability of the polymer to expand in response to water sorption, prior to degradation and drug release, is affected by the crosslinking density. This in turn is determined by both the monomer length (hence the distance between polymethacrylate blocks) and the extent of end group methacrylate termination. The polymers P34L8DMA and P7L8DMA used for this drug release study had a higher and lower percentage end group methacrylate termination, respectively, than

the similar polymers used previously for the degradation study (Table 5.12). The

methacrylate density (MA_{den}) i.e. crosslinking relative to the monomer length can be

estimated using Equation 5.12:

$$MA_{den} = \frac{2 \times MA\%}{M_{mw}}$$

                                                                                5.12

Where MA % and M_{mw} are the methacrylation percentage and the molecular weight of the

synthesised monomer respectively (see Table 3.7 and Equations 3.8 & 3.9, Chapter 3).

Despite the lower end group methacrylate percentage for P7L8DMA, the crosslinking

density of the polymers used in this drug release study increased in the same order as

found previously for those used for degradation study: P34L8DMA < P34L2DMA <

P7L8DMA <P17L4DMA < P7L2DMA (see Table 5.12).

Table 5.12. Methacrylate / crosslinking density for the polymers used in this drug release study compared to the polymers used previously for degradation study

	Drug release (this study)		Degradation (chapter 4)	
	% Methacrylation*	Methacrylate density x 10^{-4} (mol / g)	% Methacrylation*	Methacrylate density x 10^{-4} (mol / g)
P34L8DMA	61	4.3	40	2.5
P34L2DMA	74	6.3	81	6.7
P17L4DMA	85	10.1	81	9.7
P7L8DMA	48	7.2	65	9.0
P7L2DMA	60	15.5	88	20.8

*Data obtained from Table 3.7 in Chapter 3

With the longest polymer P34L8DMA the percentage of end group methacrylate termination is 61 % compared to 40 % previously and this allowed for better control of water sorption and disintegration of this polymer observed in this study. The P34L8DMA samples of the three drugs still swelled to a large extent, however, unlike those in the degradation study all but one sample remained intact over the study period. Conversely with the polymer P7L8DMA the percentage end group methacrylate termination is only 48 % compared to 65 % previously and this reduced level of methacrylation resulted in significantly high water sorption of this polymer observed in the above drug release study.

Decreasing the monomer length and increasing the percentage of methacrylate end termination (60– 85 % for P7L2DMA, P17L4DMA and P34L2DMA) raise the crosslink density such that with these polymers, water sorption was comparatively less and better controlled. With hydrolysis of the crosslinks and polymer erosion and drug release, water replaced material loss and further expansion of the matrix was allowed such that water contents could be twice or more than the total mass loss as in the case of all polymers containing long PPG (see Table 5.6 to Table 5.8). With all PPG425 polymers except CDA-containing P7L8DMA, final water contents were on average twice less than total mass loss indicating some extent of material shrinkage upon degradation and drug release. Water sorption balanced degradation product and drug release only in the intermediate polymer P17L4DMA.

5.4.2 Final mass loss and acid release

Total acid release and final mass loss (total or polymer) of the drug-containing formulations all followed the same trend as observed previously with undoped polymer samples (Chapter 4) with the following order: P7L8DMA > P7L2DMA > P17L4DMA ≥

P34L8DMA $\geq$ P34L2DMA (Table 5.6 to Table 5.8). As discussed previously the rate and level of degradation is affected by the concentration of ester / methacrylate and ether / ester bonds, the length of methacrylate blocks, the level of water sorption and the ease with which degradation products can diffuse out of the matrix. With polymers produced using PPG 425 g/mol, methacrylate blocks are short and the concentration of the more rapidly hydrolysed ether / ester and ester / methacrylate bonds is high resulting in faster degradation. With the polymer P7L8DMA containing a high lactide to PPG ratio, the degradation process was further accelerated by the high level of water sorption. In most samples a faster acid release phase was seen at early times (Figure 5.8 to Figure 5.10). This might be caused by degradation products being released from the specimen surface. The acid release gradient declined as the reaction occurred deeper within the polymer matrix.

Acid release and mass loss also varied between specimens of the same polymer but containing different drugs. Despite less water uptake, polymer erosion and acid release were faster in specimens containing ketoprofen than with CDA or prednisolone. At 10 weeks cumulative acid release with ketoprofen-containing specimens could be respectively 2 and 1.5 times than that with CDA and prednisolone–containing specimens (Figure 5.22). At 18 weeks, mass loss increased by 11–34 wt% with ketoprofen-containing specimens compared to those with prednisolone (Figure 5.20). This increase in acid release and mass loss in ketoprofen might be explained by the acidic nature of the drug (structure shown in Figure 5.2). With a pK$_a$ value of 4.45 (i.e. K$_a$= 3.55 x 10^{-5}), ketoprofen is acidic in nature whose equilibrium can be described by the following Bronsted-Lowery expression (232):

$C_{15}H_{13}OCOOH$ (aq) + H_2O (l) <---> H_3O^+(aq) + $C_{15}H_{13}OCOO^-$ (aq)
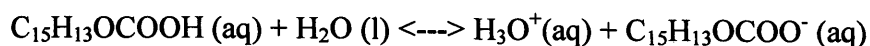
And the equation:

$$K_a = \frac{[H_3O^+][C_{15}H_{13}OCOO^-]}{[C_{15}H_{13}OCOOH]}$$

The molar concentrations of $[H_3O^+]$ and $[C_{15}H_{13}OCOO^-]$ are equal and so the numerator of the equation can be expressed as $[H_3O^+]^2$. At pH < 4.45 any ketoprofen released into the surrounding solution would be less than 50 % dissociated. The molar concentration of acid in the storage solution at 18 weeks contributed by the dissociation of the released ketoprofen can be calculated using the cumulative mass of drug release (C_D in 10 ml solution converted into molar concentration by dividing C_D by the drug molecular weight and multiplying by 100) and a rearranged equation of the above:

$$[H_3O^+] = \sqrt{(Ka \times [C_{15}H_{13}OCOOH])}$$

The molar concentration of H_3O^+ calculated can then be converted into acid release of ketoprofen in μmoles per specimen and compared to the total acid release obtained. Using this approach it was found that ketoprofen release contributed from ~2 % for the short, fast degrading polymers (PPG 425 g/mol) to ~6 % for the long, slow degrading polymers (PPG 2000 g/mol) to the total acid release obtained in this study. The limited effect of drug level on acid release (Table 5.4), and the constant values of the polymer mass loss per mole of acid release for a given sample (Table 5.7) also indicated that ketoprofen release was not a major contributor to the acid level measured with these specimens. Acid catalysis, however, caused by the dissociated carboxylic acid groups of

ketoprofen in the polymer matrix could possibly also increase the level of polymer degradation and acid release resulting in a higher mass loss compared to specimens containing the other two drugs.

With prednisolone, drug release rate with these specimens was much higher than their CDA-containing counterparts. High drug release resulted in formation of pores inside the specimens and facilitated easier movement of polymer degradation products out of the matrix; subsequently acid release and possibly mass loss of prednisolone were slightly higher than that of CDA. Drug release at the 10 wt% level was restricted in prednisolone-containing samples and consequently drug level had no effect on acid release and mass loss in this drug sample as will be explained below.

The relatively lower level of acid release from CDA-containing formulations might also be explained by the basic nature of the drug. Due to the amine groups in the structure (Figure 5.2) CDA has a pK_a of 10.8. Its acid / base equilibrium can be described by the following Bronsted-Lowery expression (232):

$$C_{22}H_{29}Cl_2N_9NH \text{ (aq)} + H_3O^+ \text{ (aq)} \longleftrightarrow H_2O \text{ (l)} + C_{22}H_{29}Cl_2N_9NH_2 \text{ (aq)}$$
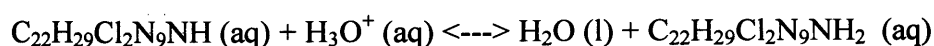
At the low pH of the storage solution due to acidic degradation products, the equilibrium would be driven to the right. When released into the surrounding solution, therefore, the CDA molecules could 'mop' up protons from the acidic degradation products and hence reduce the amount of acid in the water. Varying the CDA level caused negligible effect on polymer mass loss. With more CDA release at the 10 wt% drug level, however, more acidic products would be neutralised in the storage solution. Consequently a lower cumulative acid release was observed for the 10 wt% drug level than that for the

2.5 wt% drug level (Table 5.3). This could result in the calculated polymer mass loss per

mole of acid release (kg/ mol) being higher with 10 wt% drug (see for example results

with P34L8DMA and P34L2DMA polymers in Table 5.6). With these two polymers, acid

release was particularly low, and hence would be affected more significantly by a high

drug release level. Consequently, the polymer mass loss per mole of acid release for these

two polymers was observed to be twice as high for the 10 wt% drug level as that for the

2.5 wt%.

5.4.3 Drug release

The biphasic release profile observed with the square root of time with all three

drugs could be explained by the different stages of drug release (Figure 5.14, Figure 5.16

and Figure 5.18). Initially release was fast due to rapid dissolution of drug molecules on

or close to the specimen surface. With water ingress the polymer then expands and bonds

are hydrolysed resulting in the formation of channels that allow the encapsulated drug to

diffuse more rapidly out of the matrix. The significance of water sorption upon drug

release was shown by the higher drug release levels from polymers with high water uptake

including P34L2DMA, P34L8DMA and P7L8DMA. The release rates continuously

diminished with time due to the increasing distance that hindered drug must move through

as drug from the material surface is diminished. For the remaining deeply embedded drug

particles, release could only occur when degradation and erosion of polymer matrix

became sufficient.

The processes of drug release were complicated by factors including (i)

physicochemical properties, loading dose and particle size of the drug, and (ii) molecular

weight and methacrylate/ crosslinking density of the polymer. These resulted in the three

drugs exhibiting different drug release behaviour from the ten polymer formulations.

In specimens containing CDA, drug particles, with an aqueous solubility of 18

mg/ml at 15-25 °C, should dissolve easily in any absorbed water. With increasing

monomer length and reducing crosslinking (Table 5.12) the polymers become more

flexible and facilitate higher water uptake and droplet growth around the drug particles.

As a result, dissolution of the drug and its diffusion through the expanded polymer

structure were faster. With the shortest monomer containing a low lactide level,

P7L2DMA, the matrix was heavily crosslinked and droplet growth was restrained,

resulting in less dissolution and release of the drug. Raising drug level increased the

possibility of channel formation in the matrix causing enhanced drug release. With CDA

the shorter rapid-release phase (3 weeks vs. 8 weeks as with ketoprofen) suggests that

drug diffusion as opposed to polymer erosion is the rate-limiting step.

Commercially available Periochip$^{®}$ used for periodontal infections contains 2.5 mg

(~35 wt%) chlorhexidine gluconate and releases 80 % of the drug in four hours and a two-

week cumulative release of 7 mg/g (233). In another polymerisable methacrylate system

containing tetrahydrofurfuryl methacrylate (THFM)/ poly(ethyl methacrylate) (PEM)

doped with 5.6 wt% CDA (56), 2-week cumulative release in water was only 4 mg/g

sample, compared to 9 mg/g sample from the 5wt%-doped P17L4DMA polymer in this

study. With a more desirable longer term controlled release profile and cumulative release

comparative to commercial products, the polymers in this study may offer potentially

better sustained chlorhexidine release than other systems.

With specimens containing ketoprofen, the drug was soluble in the monomers.

With the exception of P7L8DMA, differences in monomer structure and drug level caused

insignificant effects on drug release rate. This phenomenon could be explained by the limited water solubility (0.1 mg/ml at 15-25 °C) and higher hydrophobicity (log P = 3.556) of the drug causing it to partition into the hydrophobic regions of the polymer domains. High water sorption in the long polymers (as in the case of polymers of PPG 2000 g/mol) would be expected to increase the diffusion medium in the polymer matrix and hence drug release, but in this case the ketoprofen molecules were likely to associate with the degraded hydrophobic PPG segments in the structure resulting in reduced drug release. These ketoprofen molecules would therefore not be released until degradation proceeds further with time and degraded PPG segments are released. With the short polymer P7L2DMA water sorption was less but polymer erosion was at least 4 times greater than that with the long polymers thereby increasing the likelihood of the hydrophobic ketoprofen release. With the polymer P7L8DMA initial mass increase due to water sorption was approximately 150 wt% and polymer erosion at 18 weeks was twice that of P7L2DMA. The combination of the highest water sorption and polymer erosion resulted in the most extensive ketoprofen release with this polymer. In addition, with the fast eroding polymers (P7L2DMA and P7L8DMA) 10-week drug release with ketoprofen-containing specimens was on average 1.6 times higher than that with CDA-containing specimens. The results suggest that, because of the hydrophobicity of ketoprofen, polymer erosion rather than diffusion was the governing factor for drug release. Average total drug release at 18 weeks was 96 % for P7L8DMA and 56 $\pm$ 6 % for all other polymers. By contrast Jeong et al incorporated ketoprofen into an injectable micelle forming PEG-PLGA-PEG hydrogel and obtained almost 100% release over 2 weeks (58). The polymer system in this study could therefore be applicable for an injectable more long term drug delivery device.

With specimens containing prednisolone, drug release at each drug level generally followed the same order as with CDA: P34L8DMA $\geq$ P34L2DMA $\geq$ P7L8DMA $>$ P17L4DMA $\geq$ P7L2DMA. As with CDA polymer formulations swelling and drug diffusion was the predominant factor controlling release rate. Again increasing water uptake and decreasing crosslinking density in polymers with long PPG and/ or high lactide facilitated drug diffusion, and drug release was enhanced. Increasing drug level from 2.5 to 10 wt%, however, caused a reduction in prednisolone release rather than an expected increase as seen with CDA. This might be due to the restricted solubility of prednisolone in water (0.1 – 1 mg/ml at 15-25 °C). In a 10 ml aqueous storage medium the maximum amount that the drug could dissolve would be 1 – 10 mg. It was observed that if the percentage drug release was converted into the mass of prednisolone release at each time period the biggest increment for a 10% drug-doped polymer was only 2.6 mg. Prednisolone had to be dissolved in water absorbed within the specimen before being diffused out of the material. It was postulated that as the amount of drug dissolved approached its saturation concentration in the diffusion medium, release rate would be restricted and further drug dissolution and release would not be possible until fresh unsaturated water diffused into the material. If this was the case, this restriction in drug release at 10 wt% drug level could be minimised by adding a surfactant into the release medium, such as Tween 20™, to increase the aqueous solubility of prednisolone (58).

Percentage release of prednisolone from the polymers could be almost twice that for the other two drugs over a ten-week period. This could be due to a combination of higher water sorption and faster drug dissolution. Water intake was generally higher with prednisolone-containing samples than those with CDA and ketoprofen. As a result this provided a higher diffusion medium and a greater expanded matrix that allowed

movement of the drug molecules through the structure. With prednisolone, the particles are much finer than those of CDA and with a similar texture to flour could be as small as 5 μm. In the fabrication process these smaller prednisolone particles were likely to agglomerate resulting in their effective particle size being higher than those of CDA. The less translucent appearance of prednisolone-containing specimens when compared to those with CDA (Figure 5.3) supported the cohesion of prednisolone powder in the polymer matrix. These fine particles nevertheless allowed prednisolone to have a faster drug dissolution rate than that of CDA. In the latter the crystalline nature of the particles might slow the effective drug dissolution in water despite its higher aqueous solubility.

The sustained drug release manner observed with the polymers in this study showed a profile that may be favourable over many PLGA devices. In the latter, drug release after the burst period can be negligible for a certain period of time then followed by a final dumping phase due to bulk erosion of the polymer (226). With the polymers in this study drug release can be controlled via a combination of monomer composition and drug loading level dependant upon the properties and nature of the drug to be incorporated. If diffusion is the rate limiting step for drug release the rapidly swellable long polymers may be preferred for use as the drug delivery vehicles (60). On the other hand when polymer erosion is the major factor in controlling drug release the faster eroding short polymers may be a better choice. The acidic microenvironment caused by the degradation products of the polymers would also pose problems if delicate biological agents such as peptides, proteins and DNA are to be incorporated. Further studies into addition of buffer particles to neutralise the internal pH (see Chapter 6), or encapsulation of such agents into protective spheres of another material might then be needed.

6 Polymer Composites

6.1   Background

In previous chapters the new poly(PG-co-lactide) dimethacrylate monomers have been structurally characterised, and their degradation, mechanical and drug release properties explored.   Potential disadvantages of these new formulations as bone cements include their release of acidic degradation products, slow rate of degradation and low modulus.   In this chapter, three composites were produced and investigated using one monomer with added phosphate-based glass particles or brushite forming particulate mixtures.

Composites of biodegradable polymers and various glasses / ceramics have been investigated in numerous studies in an attempt to combine advantages or alleviate problems associated with either class of biomaterials.   These include for example injectable poly(propylene fumarate)/ β-tricalcium phosphate composite (193), polycaprolactone/ phosphate glass composite (67) and polymer/ silica-based bioactive glass composites (234;235).   In these studies improved mechanical properties and better control of the overall degradation rates of the materials were observed.   In addition the levels of monomer and thereby polymerisation shrinkage, heat generation and toxicity would be reduced (73).

The monomer P17L4DMA was used for further investigations in this study as this monomer was the 'intermediate' formulation.   Results from the previous chapters also showed that the length of the lactide chains attached to the PPG, and the end group esterification and methacrylation efficiency were the most consistent and controllable between batches.   This monomer as a polymerised disc of 10 mm i.d. and 2 mm thickness degraded by a maximum of 10-11 wt% over 14 weeks and produced a surrounding pH of

between 3 and 4 in the dissolution medium. The aims of incorporating the filler particles were three-fold: (i) to modulate or increase the degradation rate of the polymer, (ii) to maintain a neutral pH balance of the surrounding solution upon degradation and (iii) to enhance the modulus of the polymer.

Two types of inorganic filler particles were used to create three composites. In the first two composites, phosphate glasses based on a ternary P_2O_5-CaO-Na_2O system were used with fixed P_2O_5 content of 45 mol% and either 30 or 40mol% CaO. The third composite formulation contained the monomer and an equimolar powder mixture of β-TCP and monocalcium phosphate monohydrate (MCPM). These two particular phosphates combine when mixed with water to form lower density dicalcium phosphate dihydrate (i.e. DCPD also known as brushite). Both types of inorganic filler particles are resorbable under physiological conditions and their biocompatibilities have been demonstrated in several *in vitro* and/ or *in vivo* studies (92-94;126).

This study was therefore to assess how polymerisation rates, degradation rate / mechanism and dynamic modulus are affected when high levels of degradable calcium phosphate particles are added to a degradable dimethacrylate monomer. Gravimetric studies were used to determine the mass, volume and density of both wet and dried samples as a function of time in water. Mathematical equations were derived to extract from this gravimetric data the individual rates of filler and polymer erosion. These were compared with rates of release of various ions into sample storage solutions quantified by pH and ion chromatography measurements. The effects of water sorption and degradation on the chemical homogeneity and modulus of the composites was assessed via Raman mapping and dynamic mechanical analysis respectively.

6.2   Materials and Methods

6.2.1   Sample preparation

6.2.1.1   Inorganic fillers

The bulk phosphate glass was prepared by Dr Ifty Ahmed (Eastman Dental Institute UCL). For $(P_2O_5)_{0.45}(CaO)_x(Na_2O)_{0.55-x}$ glass preparation, sodium dihydrogen orthophosphate (NaH_2PO_4), calcium carbonate ($CaCO_3$) and di-phosphorous pentoxide (P_2O_5) (BDH, U.K) were used as starting materials. The relative amounts of the precursors with respect to their expected molar ratios in the glass were calculated (236). The precursors were weighed (Table 6.1) and placed into a 200 ml platinum/10 % rhodium crucible. The crucible was placed in a furnace (Carbolite, RHF 1600, UK) initially at 300 °C for 30 min, then at 600 °C for 30 min and finally at 1050 °C for one hour. The resultant glass was poured onto a stainless steel plate, ground into powder form when cooled into solid, and sieved to obtain a particle size range between 20 and 45 μm.

Table 6.1. Amounts of precursors used for preparation of the two phosphate glass.

Glass system	NaH_2PO_4 (g)	$CaCO_3$ (g)	P_2O_5 (g)
$(P_2O_5)_{0.45}(CaO)_{0.30}(Na_2O)_{0.25}$	30.04	15	14.17
$(P_2O_5)_{0.45}(CaO)_{0.40}(Na_2O)_{0.15}$	18.03	20	21.28

The calcium phosphate mixture consists of equimolar sintered β-tricalcium phosphate (β-TCP) and monocalcium phosphate monohydrate (MCPM) (Rhodia, Birmingham, UK) with median final particle sizes of 11 and 62 μm respectively (as determined by laser diffraction particle sizing). These were supplied by Dr Mike Hoffman (Birmingham University) and Uwe Gbureck (University of Wurzburg, Germany). ß-TCP

had been prepared by sintering a 2:1 molar mixture of dicalcium phosphate anhydrous (DCPA, Mallinckrodt-Baker, Griesheim, Germany) and calcium carbonate (Merck, Darmstadt, Germany) at 1050°C for 24 hr followed by milling.

6.2.1.2 Poly(propylene glycol-co-lactide) dimethacrylate (PPGLADMA) monomer

The monomer P17L4DMA (lot number 111104) was synthesised using the method described in Section 3.2.2, Chapter 3 (overall reaction yield = 67 %). The product structure was confirmed using ATR-FTIR and Raman spectroscopy (Perkin Elmer series 2000 FTIR/ Raman spectrometer) and one dimensional ^{1}H-NMR (Varian *Unity plus* 500 MHz instrument using deuterated chloroform solvent). FT-IR and Raman spectra for the monomer were comparable with those previously reported for the monomers (Section 3.3.1.2 and 3.3.1.3, Chapter 3). From the NMR results and using Equations 3.5 to 3.8 (Chapter 3) the following were calculated: (i) calculated lactide *m* to PPG *n* ratio was 4.53, (ii) the efficiency of lactide attachment to the PPG was 97 % of that expected, and (iii) the lactoyl and methacrylate end capping efficiency were 68 % and 103 %, of that expected, respectively. The measured molecular weight of the monomer using Equation 3.9 was 1737 g/mole.

6.2.1.3 Formulations

Four formulations were prepared, the first F1 containing only an organic liquid phase, the second and third F2 and F3 additionally $(P_2O_5)_{0.45}(CaO)_x(Na_2O)_{0.55-x}$ filler powder with x equal to 0.3 and 0.4 respectively and the fourth F4 the above β-TCP and MCPM equimolar mixture (i.e. weight ratio of β-TCP to MCPM= 1.10: 0.90) (see Table 6.2). In all samples the liquid phase consisted of the P17L4DMA monomer, combined

with 1 wt% of each photoinitiator – CQ and DMPT, and 10 wt% HEMA (to aid dispersion of the initiators). The filler / liquid ratio for all the composites was 2:1 by weight which was sufficiently low to ensure all samples were viscous and workable over an adequate time period for clinical applications (i.e. > 5 min) before curing (237).

To prepare solid discs for degradation studies, formulations were placed into steel rings of approximately 8 mm diameter and 1 mm depth. With the top and bottom surfaces covered with acetate sheets these were then placed into a light box (Densply Trubyte Triad® 2000™ visible light cure system) and solidified using 10 mins (sufficient for >90 % cure for all samples, see Section 6.3.1) of blue light exposure (100 mW/ cm^2) before removal from the ring.

6.2.2 Photopolymerisation kinetic studies

To follow the rate of polymerisation at a depth of 1 mm at body temperature, 3 specimens of each unset formulation were placed in a 1 mm deep ring on a Golden Gate™ diamond ATR FTIR top-plate at 37 °C (maintained using a RS232 Specac 3000 Series™ temperature controller). They were then exposed to blue light (400 mW/ cm^3) for 80 s as FT-IR spectra were obtained every 23 s using Timebase software (Perkin Elmer) for 40 minutes. The final polymerisation percentages for formulations F1 to F3 were determined by comparing the height of the Raman methacrylate C=C 1640 cm^{-1} peak (in background subtracted and 2940 cm^{-1} peak normalised spectra) before and 24 hours after curing. With F4 this had to be estimated from a weaker FT-IR 1640 cm^{-1} peak because of its high fluorescence Raman background. The percentage reaction as a function of time was then obtained by combining final percentages with the FTIR absorbance change variation with time at 1716 and 1734 cm^{-1} using the method detailed in Section 3.3.3.2, Chapter 3. The

maximum reaction rate for each formulation was then determined from the gradient of the

calculated polymerisation percentages between 15 and 85 s since start of light exposure.

6.2.3 Degradation studies

For degradation studies, 25 specimens of each formulation of known initial mass,

W_0 (average of 72 mg for F1 and 120 mg for the composites) were placed upright in the

conical end of an individual sterilin tube, allowing contact with deionised water (10 ml

adjusted to pH 7 using ammonium hydroxide solution and incubated at 37 °C) on all sides.

For all specimens the water was exchanged at 0, 0.5, 1, 2 and 4 hours, 1, 2, 4, 7 and 10

days as well as 2, 3, 4, 7 and 10 weeks. In all analyses mean results from the three

specimens for each formulation were obtained and relative standard deviations calculated

by dividing the standard deviations by the means. These relative standard deviations

expressed the variability in the values measured relative to the magnitude of the calculated

mean as a fraction or percentage.

6.2.3.1 Mass, volumetric and density changes

At all the above time points, three specimens of each formulation were removed

from the tube, the external surface blotted dry with tissue paper and their mass, volume

and density assessed gravimetrically (using a Mettler Toledo density kit) before placing

back into fresh pH-adjusted deionised water. The mass and volume were converted to

total change as a percentage of initial values using Equations 4.2 and 4.6 respectively (see

Chapter 4)

The densities of the formulations at time 0 were first used to obtain the densities of

pure filler particles in the formulations. Equation 6.1 states that:

$$x_i = \frac{W_i}{\sum W_i}$$

In other words

$$\sum x_i = 1 \qquad\qquad\qquad 6.1$$

Where x_i and W_i are the mass fraction and mass of each pure component in the formulation. In this study i has value of 1, 2 or 3 each representing the polymer, filler and water respectively.

Assuming then the density of a mixture/ composite (ρ) is the sum of the total mass ($\sum W_i$) divided by the total volume of the individual components ($\sum V_i$) it will be given by Equation 6.2.

$$\rho = \sum \frac{W_i}{V_i}$$

which means

$$\frac{1}{\rho} = \sum \frac{V_i}{W_i}$$

And

$$\frac{1}{\rho} = \sum \frac{(W_i / \rho_i)}{W_i}$$

In expanded form

$$\frac{1}{\rho} = \frac{\left(W_1 / \rho_1\right) + \left(W_2 / \rho_2\right) + \left(W_3 / \rho_3\right)}{W_1 + W_2 + W_3}$$

Simplifying using Equation 6.1 gives

$$\frac{1}{\rho} = \sum \frac{x_i}{\rho_i} \qquad\qquad\qquad 6.2$$

Where ρ_i is the density of each pure component in the mixture.

At time 0 (before submersion in water), the mass and density of the specimen were determined by the polymer (i= 1) and filler (i= 2) components only. Using Equations 6.1 and 6.2 with the densities and the known mass fractions of the polymer and composites prior to their submersion in water an average density of the inorganic fillers (i.e. ρ_2) was obtained.

6.2.3.2 *Compositional changes and mass losses*

The dry mass (after vacuum drying to constant weight) of three specimens of each formulation were determined at 1 and 3 days and 1, 2, 7, 9 and 10 weeks and fractional mass loss, z and water content, x_3 calculated by comparison with the initial dry and final wet mass respectively. By expanding, combining and rearranging Equations 6.1 and 6.2, it can be shown that the fraction of polymer left in the wet composite at a given time, x_1, can be calculated using the densities of the composite, ρ, and pure components ρ_i, with Equation 6.3.

From Equation 6.2:

$$\frac{1}{\rho} = \frac{x_1}{\rho_1} + \frac{x_2}{\rho_2} + \frac{x_3}{\rho_3}$$

Rearranging Equation 6.1:

$$x_2 = \left(1 - x_1 - x_3\right)$$

Substituting the rearranged Equation 6.1 into Equation 6.2:

$$\frac{1}{\rho} = \frac{x_1}{\rho_1} + \frac{(1 - x_1 - x_3)}{\rho_2} + \frac{x_3}{\rho_3}$$

$$= \frac{x_1}{\rho_1} + \frac{1}{\rho_2} - \frac{x_1}{\rho_2} - \frac{x_3}{\rho_2} + \frac{x_3}{\rho_3}$$

Rearranging gives

$$\frac{1}{\rho} - \frac{1}{\rho_2} = x_1 \left[\frac{1}{\rho_1} - \frac{1}{\rho_2} \right] + x_3 \left[\frac{1}{\rho_3} - \frac{1}{\rho_2} \right]$$

and

$$x_1 \left[\frac{1}{\rho_1} - \frac{1}{\rho_2} \right] = \left[\frac{1}{\rho} - \frac{1}{\rho_2} \right] - x_3 \left[\frac{1}{\rho_3} - \frac{1}{\rho_2} \right]$$

which finally leads to

$$x_1 = \frac{\left[\frac{1}{\rho} - \frac{1}{\rho_2} \right] - x_3 \left[\frac{1}{\rho_3} - \frac{1}{\rho_2} \right]}{\left[\frac{1}{\rho_1} - \frac{1}{\rho_2} \right]} \qquad 6.3$$

Again the subscripts 1, 2 and 3 represent polymer, filler and water respectively. Once x_1 and x_3 are known, the fraction of filler in the composite, x_2 at a given time can be calculated from Equation 6.1. The fraction of dried composite that is polymer, y_1 and filler, y_2, is then given by Equation 6.4 and 6.5.

$$y_1 = \left[\frac{x_1}{x_1 + x_2} \right] \qquad 6.4$$

And

$$y_2 = 1 - y_1 \hspace{5cm} 6.5$$

As previously mentioned total mass loss fraction, z was calculated by comparison of the final dry mass with initial dry mass. From z and simple mass balance the mass fraction of polymer z_1 (or filler z_2) from the original composite (i.e. 33 wt% polymer, 67 wt% filler) that has dissolved at a given time is then obtained using Equation 6.6.

$$z_i = 1 - \frac{y_i}{y_{i,0}}(1 - z) \hspace{4cm} 6.6$$

With i equal to 1 or 2 and $y_{i,0}$ the initial fraction of polymer or filler in the composite at time 0. The mass fraction of polymer z_1 and filler z_2 from the original composite that has dissolved was then plotted against the square root of time.

6.2.3.3 pH measurement of storage solutions

The pH of the storage solutions at each time point was measured using a pH meter (Hanna Instruments, pH 211 Microprocessor pH meter). From this, the cumulative moles of acid released in the 10 ml storage solution per specimen, C_a was calculated using Equations 4.7 and 4.8 (see Chapter 4) and was converted into mM. This was plotted against the square root of time for the four formulations. Additionally the mass loss per mole of acid released was calculated for the polymer F1 using Equation 4.9 (see Chapter 4).

6.2.3.4 Ion release measurements

Ion release into the storage solutions up to 2 weeks was additionally monitored using two ion chromatography systems (Dionex, UK); one for cation release, and one for

anion release. In order to obtain results in the range of the calibration, all solutions for ion release were diluted by a factor of 20 with deionised water prior to analysis. Analysis of all solutions was completed within 30 minutes from the end of the sample storage period. Data analysis was performed using the Chromeleon® software package.

For the analysis of anion release (phosphates and polyphosphates), the system (Dionex ICS-2500) consisting of a 25-µl sample loop was equipped with an Ion Pac® AS16 separator column and an ASRS® self-regenerating suppressor, using deionised water as the mobile phase at a flow rate of 1.5 ml/ min. For the phosphate-glass composites four anionic species which might form as a result of the breakdown of the P_2O_5 network-forming backbone were quantified (Figure 6.1). These were namely, PO_4^{3-} (orthophosphate), which is the smallest phosphate species formed as a result of the hydrolysis of the P-O-P bonds; $P_2O_7^{4-}$ and $P_3O_{10}^{5-}$ (linear polyphosphates), formed as a result of hydration of the phosphate chains; and $P_3O_9^{3-}$ (cyclic trimetaphosphate) (122). Calibration was obtained with standard solutions containing 1, 10, 25 and 50 ppm of sodium phosphate tribasic (Na_3PO_4), trisodium trimetaphosphate ($Na_3P_3O_9$), pentasodium tripolyphosphate ($Na_5P_3O_{10}$) (all from Sigma) and tetrasodium pyrophosphate ($Na_4P_2O_7$) (BDH). Results were converted from ppm of the phosphate species to mM of phosphorus atom per specimen using Equation 6.7 and 6.8 to allow comparison with acid release and with the total phosphorus calculated from initial compositions to be originally in the samples. With composites of F4, PO_4^{3-} is the only anion expected.

$$I_{mM} = \frac{I_{ppm} \times \left(31 \times n \middle/ P_{mw}\right)}{31} \qquad\qquad 6.7$$

$$C_I = \sum_0^t [I_{mM}]_I \qquad\qquad 6.8$$

Where I_{mM} is ion release in units of mM of phosphorus atom, I_{ppm} is ion release in units of ppm (i.e. mg/l) of phosphate species, n is the number of phosphorus atoms in the phosphate species (e.g. 3 in $P_3O_9^{3-}$), 31 is the atomic weight per phosphorus atom, P_{mw} is the molecular weight of the phosphate species and C_I is the cumulative ion release.

Apart from phosphate anions, calcium and sodium cations were also released from their respective oxides which were used to act as network modifiers to the P_2O_5 network-forming oxide. For the analysis of sodium (Na^+) and calcium (Ca^{2+}) release, the system (Dionex ICS-1000) was used. Any organic residues (e.g. polymer degradation products), were removed by using a NG1 guard column (Dionex, UK), and the system was equipped with an Ion Pac® CS12A separator column and a CAES® electrolytic suppressor, using a mobile phase of 20 mM methylsulphonic acid solution in deionised water at a flow rate of 1 ml/min. An injection loop of 25 μl with an AS50 autosampler was used. Due to the binding of phosphates on to the CS12A column, all samples were pretreated with a Dionex Onguard® IIA cartridge to remove the phosphate species. Calibration was obtained with standard solutions containing 1, 10, 25 and 50 ppm of sodium chloride (Sigma) and calcium chloride (BDH) but final data again converted to cumulative mM specimen^{-1} to enable easier comparison with other ion release results.

(a)

PO_4^{3-}
[Orthophosphate]

(b)

$P_2O_7^{4-}$
[Pyrophosphate]

(c)

$P_3O_9^{3-}$
[Cyclic Trimetaphosphate]

(d)

$P_3O_{10}^{5-}$
[Tripolyphosphate].
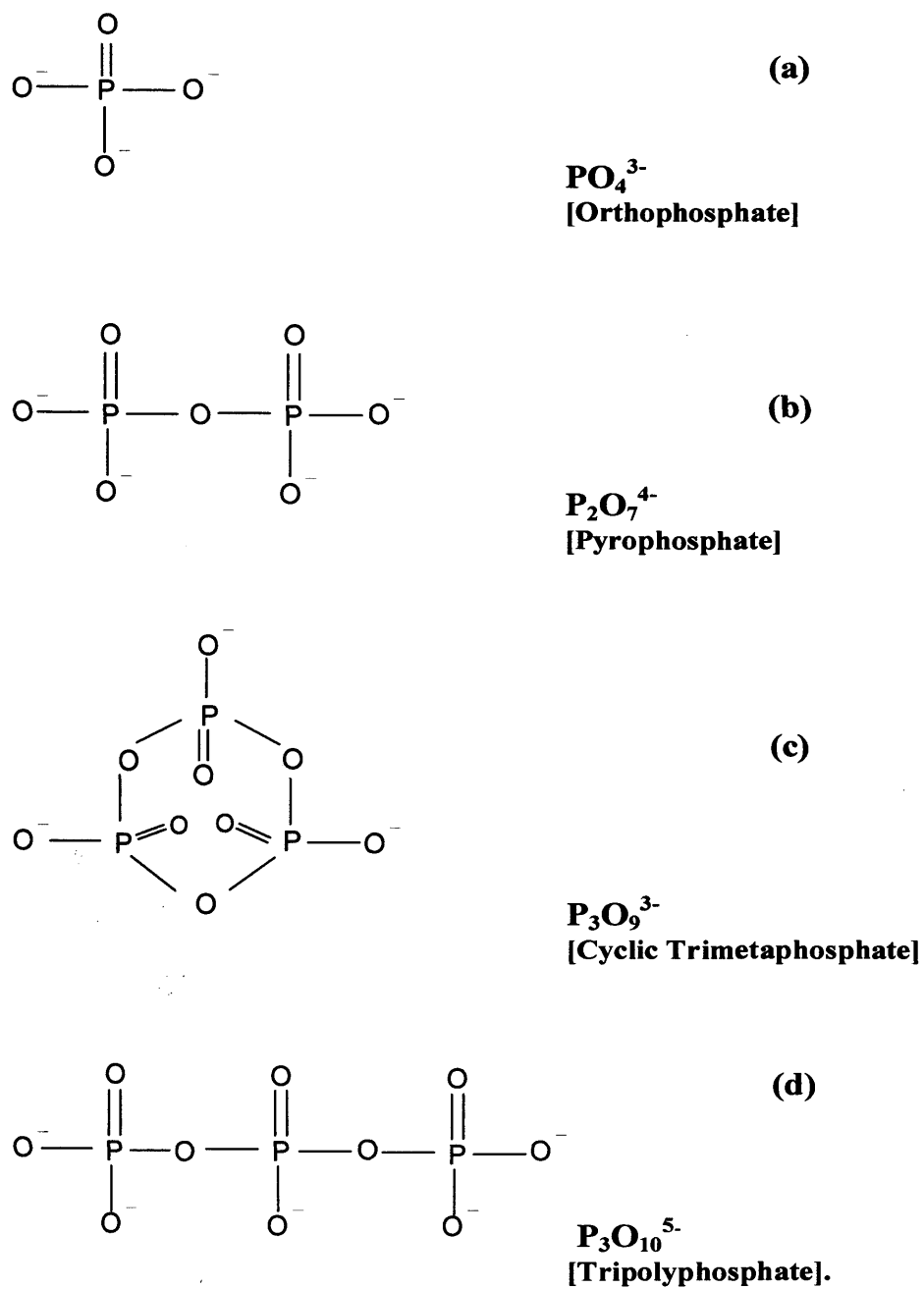
Figure 6.1. Structures of anions investigated in ion release measurements (122).

6.2.3.5   Mechanical analysis

At 0 and 4 hours, 1, 3, 6 and 9 days and 2, 3, 7 and 10 weeks, the specimens used in volumetric investigations above were additionally tested using a dynamic stress scan on a Perkin Elmer Dynamic Mechanical Analyser (DMA 7e, Perkin Elmer Instruments). A parallel plate setup was used, incorporating a 3 mm probe, with a static force of 5 mN and a superimposed dynamic compressive force of 4 mN at a frequency of 1 Hz. Testing was carried out at 25 °C for 60 s, and storage and loss modulus and tan delta recorded at 30 s of testing.

6.2.3.6   Raman mapping studies

The Raman mapping studies were carried out in collaboration with Horiba Yobin Yvon. With one specimen of each formulation, Raman chemical surface maps were obtained initially and after 4 days in water using a LabRAM 300 mapping spectrometer (Horiba Yobin Yvon) with a 633 nm laser and a long working distance objective (x 100) scanning over a wavenumber range of 500 and 1500 cm^{-1} with a step size of 4 µm over an area of at least 350 by 200 µm. Reference spectra of the individual components and of β–TCP reacted with MCPM in the presence of water were obtained over the same wavelength range to aid component identification in the maps.

6.3   Results

6.3.1 Photopolymerisation kinetics

Unlike specimens containing the three drugs (Chapter 5), photopolymerisation kinetics could be studied for the composites as the filler particles (phosphate glass and calcium phosphate) have absorption only in IR/ Raman region below 1500 cm^{-1}. The average relative standard deviation of mean polymerisation percentages for the four formulations was 0.02 ± 0.02. Polymerisation rates and conversion at 24 hours are given for all formulations in Table 6.2. Sample F4 containing β-TCP and MCPM reacted more slowly than F1, due to slight mismatch in refractive indices of the polymer and filler which caused light scattering reducing sample translucency and light penetration. The phosphate glass-containing composites F2 and F3, however, were more translucent specimens and had similar conversion rates to F1 achieving more than 80 % conversion at 1 mm depth by 80 s since light exposure. All four formulations were over 90 % polymerised by 24 hours (see Table 6.2).

Table 6.2. Polymer and composite formulations with their rate and extent of polymerisation with 80 seconds of blue light exposure.

Formu -lation no.	Inorganic filler	Average filler particle size (μm)	Maximum polymerisation rate (%/s)	Polymeri- sation at 80s (%)	Polymeri- sation at 24 hours (%)
F1	None	-	1.5	85	94
F2	$(P_2O_5)_{0.45}(CaO)_{0.30}(Na_2O)_{0.25}$	35	1.5	88	99
F3	$(P_2O_5)_{0.45}(CaO)_{0.40}(Na_2O)_{0.15}$	35	1.2	80	97
F4	β-TCP and MCPM	11 & 62	0.85	60	92

6.3.2 Degradation studies

6.3.2.1 Mass, volume and density change

The standard deviation divided by the mean value of mass or volume change or density was approximately constant for all 4 samples (excluding the first data point which has a significantly larger error in most of the measurements) and on average equal to 0.15 $\pm$ 0.13, 0.21 $\pm$ 0.27 or 0.02 $\pm$ 0.01 respectively over the study period (equivalent to 15, 21 or 2 % error). The large error on the mass and volume change is counteracted by its determination at many time points and fitting of trend lines through the data.

Percent mass changes for samples F1 to F4 versus the square root of time are given in Figure 6.2. For the first 4 hours mass increased almost proportional to the square root of time in all samples, as water sorption dominated over dissolution. Mass increase over this period was 2 wt% $hr^{-0.5}$ (R^2= 0.93) for the polymer F1, but was comparatively more rapid in all composites F2, F3 and F4 with an average slope of 3 $\pm$ 0.4 wt% $hr^{-0.5}$ (average R^2= 0.94). After 24 hours, mass change decreased dramatically for F2 and F3 before levelling off at 4 days, whereas F1 and F4 experienced only a slow decline with time. Maximum mass increases were approximately 5, 9, 15 and 11 wt% and 10 week final mass changes were -1, -26, -27 and 1 wt% for samples F1 to F4 respectively.
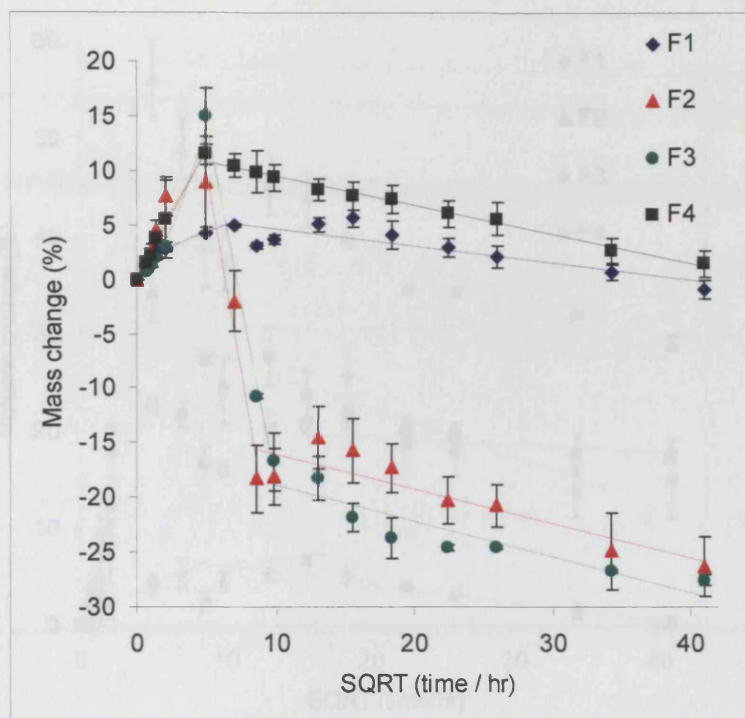
Figure 6.2. Mass change profiles of samples F1 to F4 as a function of the square root of time. (Later time data follow a straight line plot with additional intermediate ranges for fitting with sample F2 & F3 whereas the early time data are fitted assuming a power law i.e. y = mx^c)

Percent volume change for samples F1 to F4 versus the square root of time are given in Figure 6.3. For the polymer F1, over the first 4 hours, volume increased almost proportional to the square root of time with a slope of 1 vol% hr$^{-0.5}$ (R^2= 0.73). Volume increase over this period for all the composites F2, F3 and F4, however, was initially much more rapid and proportional to time with average proportionality constants of 5, 2 and 3 vol% hr^{-1} (R^2= 1.00, 0.96 and 0.98) respectively. After 24 hours, volume change decreased rapidly for F2 and F3 before levelling off but exhibited only a slight decline with time for F1 and F4 (see Figure 6.3). Maximum swelling was approximately 5, 56, 34 and 23 vol% and 10 week final volume expansions were 0, 29, 15 and 17 vol% for samples F1 to F4 respectively.
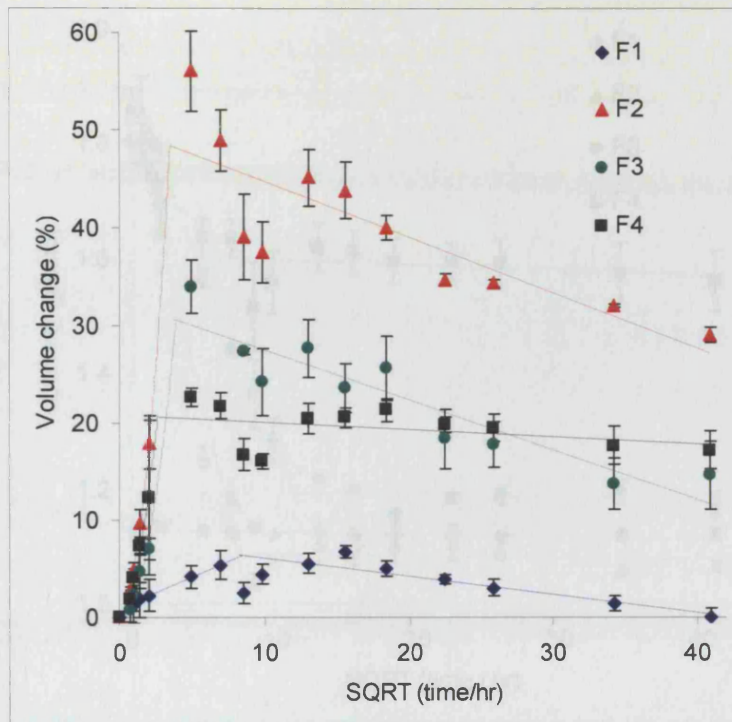
Figure 6.3. Volume change profiles of samples F1 to F4 as a function of the square root of time. (Later time data follow a straight line plot whereas the early time data are fitted assuming a power law i.e. y = mx^c)

The density (Figure 6.4) of the polymer F1 remained approximately constant at 1.13 g cm^{-3} throughout the study. The composites all had an initial density of 1.82 +/- 0.03 g cm^{-3} indicating from the pure polymer density and Equations 6.1 and 6.2 a filler density of 2.58 +/- 0.09 g cm^{-3}. The densities of F2, F3 and F4 decreased linearly with the square root of time in water with negative gradients of magnitude 0.10, 0.06 and 0.04 g cm^{-3} hr$^{-0.5}$ (R^2= 0.97, 0.99, 0.87) until 2, 7 and 1 days at which point they were close to their final densities of 1.06, 1.17 and 1.56 g cm^{-3} respectively (see Figure 6.4).
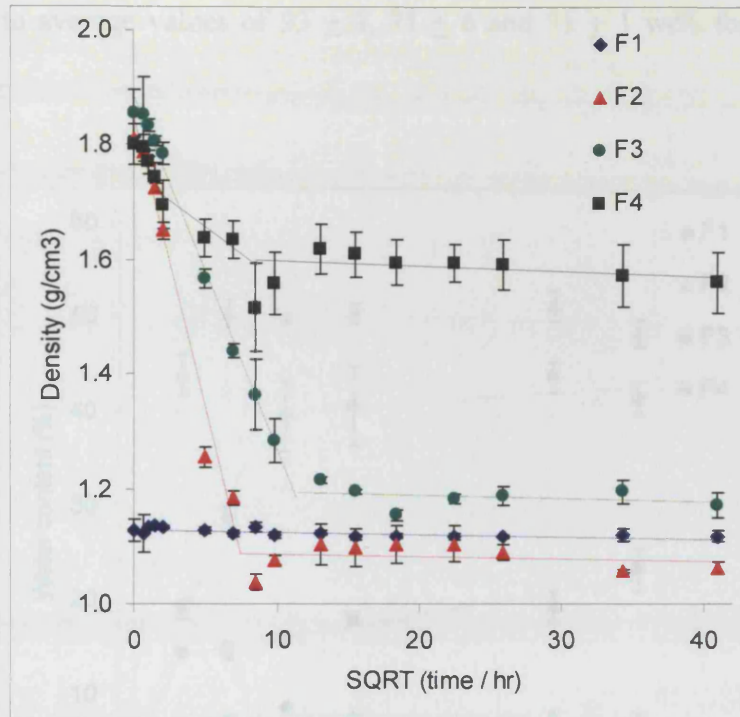
Figure 6.4. Density profiles of samples F1 to F4 as a function of the square root of time. (Straight lines are best fit through either early or later time data for samples F1 to F3 with an additional intermediate range for fitting with sample F4)

6.3.2.2 Compositional change and mass loss

The standard deviation of x_3 divided by its value (after the first time point) for all samples had an average value of 0.05 ± 0.04 (i.e. 5% error). The water content (x_3 in Figure 6.5) of polymer F1 was approximately constant between 24 hours and 10 weeks with an average value of 7.4 wt%. The glass-containing composites, F2 and F3, increased in water content rapidly to final plateaux values of 50 and ~40 wt% after 3 and 7 days respectively. x_3 of the β-TCP and MCPM containing formulation F4 increased linearly with the square root of time between 24 hours and 10 weeks from 14 to 23 wt% ($R^2 = 0.93$) (see Figure 6.5). After 3 days the fraction of dried composite that was polymer, y_1, (calculated using Equations 6.3 to 6.4 with water content and sample density) changed

314

from 33 wt% to average values of 93 ± 9, 71 ± 6 and 31 ± 1 wt% for F2, F3 and F4

respectively.
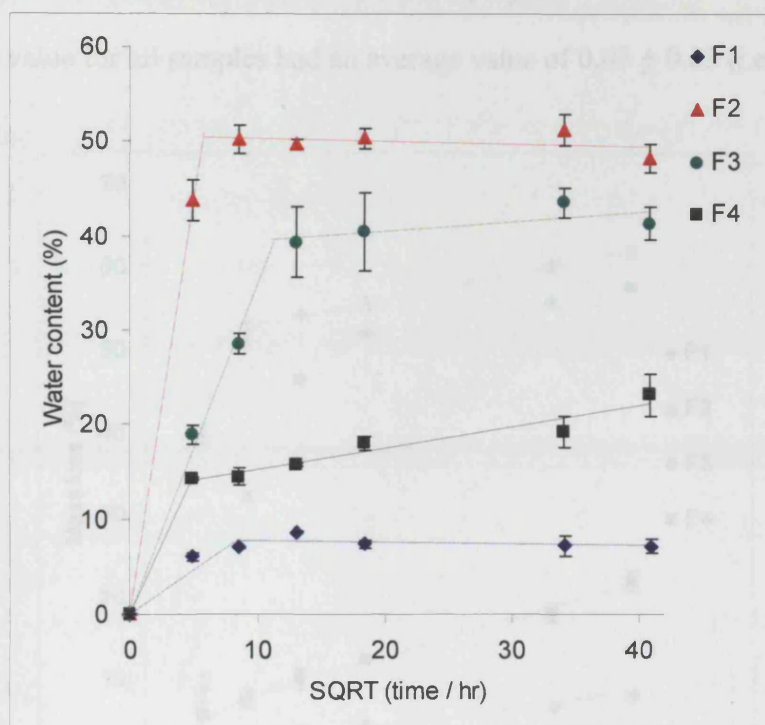
Figure 6.5. Water content profiles of samples F1 to F4 as a function of the square root of time. (Straight lines are best fit through either early (assuming a zero intercept) or later time data)

The total mass loss (z in Figure 6.6) of polymer F1 increased almost proportional

to the square root of time over the whole period of study with a gradient of 0.21 wt% $hr^{-0.5}$

($R^2 = 0.91$). Polymer final weight loss was 8 wt%. For the phosphate glass containing

composites F2 and F3 total mass loss was initially much steeper with gradients of 8.1 and

3.5 wt% $hr^{-0.5}$ up to 2 and 7 days respectively (average $R^2 = 0.97$) (see Figure 6.6). Lines

through data after the initial periods both had gradients of 0.3 wt% $hr^{-0.5}$ but intercepts of

50 and 45 wt% for F2 and F3 respectively and 10 week final mass loss was 62 and 57

wt%. Between 3 days and 10 weeks total mass loss of F4 increased linearly with the

square root of time with a best fit gradient of 0.42 wt% $hr^{-0.5}$ and intercept of 4.4 wt% ($R^2 =$

315

0.99) indicating an initial burst release of material followed by overall degradation at a rate double that for the pure polymer (see Figure 6.6). By 10 weeks the total mass loss for F4 was 22 wt% and 2.8 times that for the pure polymer. The standard deviation of z divided by its value for all samples had an average value of 0.03 ± 0.03 (i.e. 3 % error).
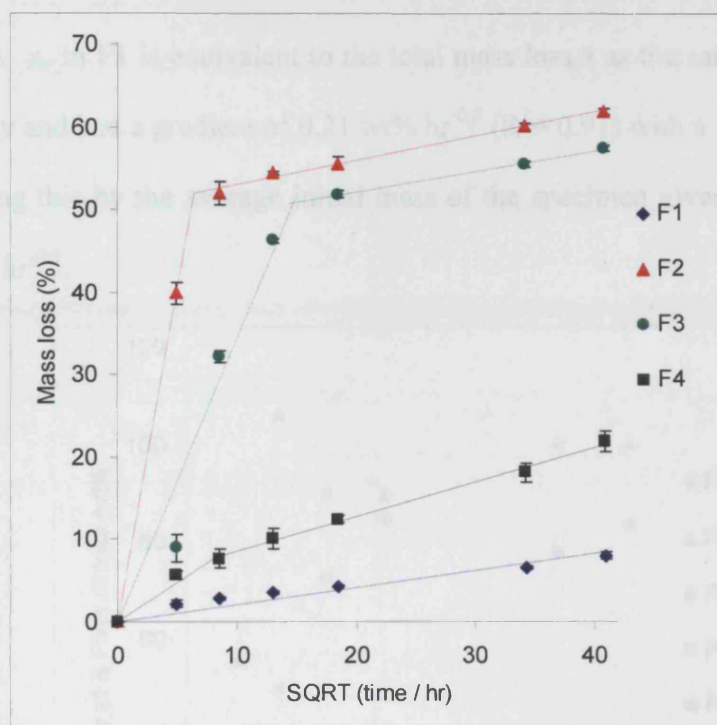
Figure 6.6. Mass loss profiles of samples F1 to F4 as a function of the square root of time. (Straight lines are best fit through either early (assuming an intercept of zero) or later time data)

Polymer and / or filler mass loss fractions (z_1 and z_2 respectively) calculated using Equation 6.6 for samples F1 to F4 versus the square root of time are given in Figure 6.7. Filler loss fractions z_2 increased rapidly at magnitudes of 12.2 and 5.4 wt% $hr^{-0.5}$ (average $R^2 = 0.97$) to maximum average values of 98 and 80 wt% after 1 week for F2 and F3 respectively. The fraction of filler lost by F4 showed a small initial burst of 3.4 wt% followed by a release gradient of 0.35 wt% $hr^{-0.5}$ ($R^2=0.95$) leading to 2 and 10 week total losses of 10 and 17 wt%. Polymer mass loss fractions, z_1, for F2 and F3 were negligible

316

in comparison with glass loss and therefore difficult to quantify accurately but were smaller than observed with the pure polymer. Polymer loss for F4, however, exhibited a burst release of 8 wt% in the first 24 hours followed by a linear increase with the square root of time of 0.50 wt% $hr^{-0.5}$ (R^2=0.87). By 10 weeks 32 wt% of the polymer from F4 was calculated to have dissolved which is 4 times that observed with the pure polymer F1 (see Figure 6.7). z_1 in F1 is equivalent to the total mass loss z as the sample consisted of the polymer only and had a gradient of 0.21 wt% $hr^{-0.5}$ (R^2= 0.91) with a 10-week loss of 8 wt%. Multiplying this by the average initial mass of the specimen gives a polymer mass loss of 0.15 mg $hr^{-0.5}$.
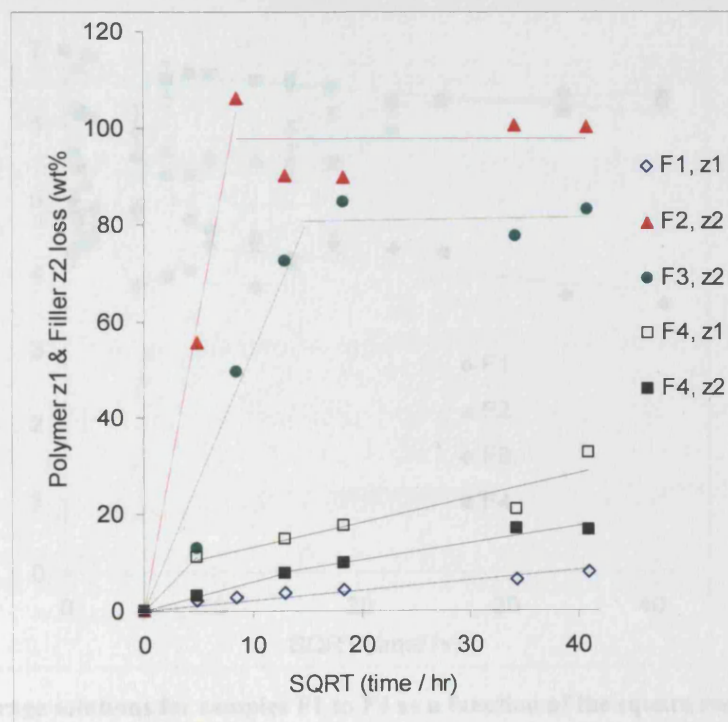
Figure 6.7. Polymer and filler mass loss profiles of samples F1 to F4 as a function of the square root of time. (Straight lines are best fit through either early (assuming an intercept of zero) or later time data)

6.3.2.3   Acid release

The storage solutions containing samples of F1 could decrease rapidly in pH to values around 4 in the first 24 hours and fluctuate around this pH for the remaining period (Figure 6.8). The pH of those containing samples F2 and F3 declined in the first week but never much below 5. By 4 weeks their pH increased to a constant pH of 6.4. The lowest average pH of sample F4 storage solutions was 4.5 in the first 24 hours but pH rose quickly to 6.5 at later times (see Figure 6.8). The relative standard deviations for all samples had an average value of 0.01 ± 0.01 (i.e. 1 % error).
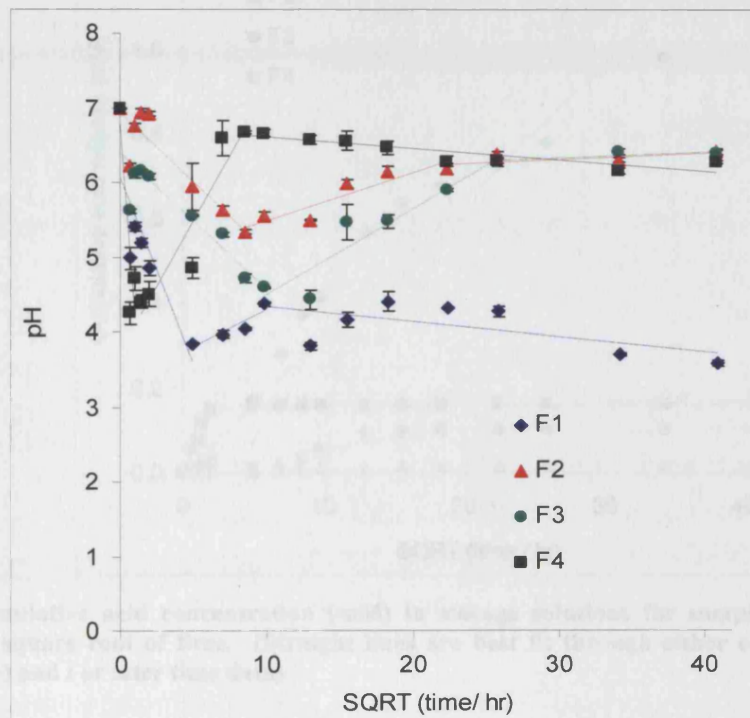
Figure 6.8. pH of storage solutions for samples F1 to F4 as a function of the square root of time. (The lines are for guidance only)

The cumulative acid release (C_a in units of mM) for all samples calculated using Equations 4.7 and 4.8 (Chapter 4) are given in Figure 6.9. C_a was proportional to the square root of time for the polymer F1 having a gradient of 0.032 mM hr$^{-0.5}$ specimen^{-1}

($R^2 = 0.95$). Ten-week cumulative acid released for F1was 1.24 mM (i.e. 1.24 x 10^{-5} mol in 10 ml storage solution). Using Equation 4.9 (Chapter 4) this gave the average degradation product mass per acid group (W_{Pmol}) of 0.47 kg/mol of acid. Calculated acid release from both F2 and F3 was small. That from F4 was initially greater than from the pure polymer but after 4 hours reached a maximum plateaux value of 0.16 mM specimen^{-1} (see Figure 6.9)
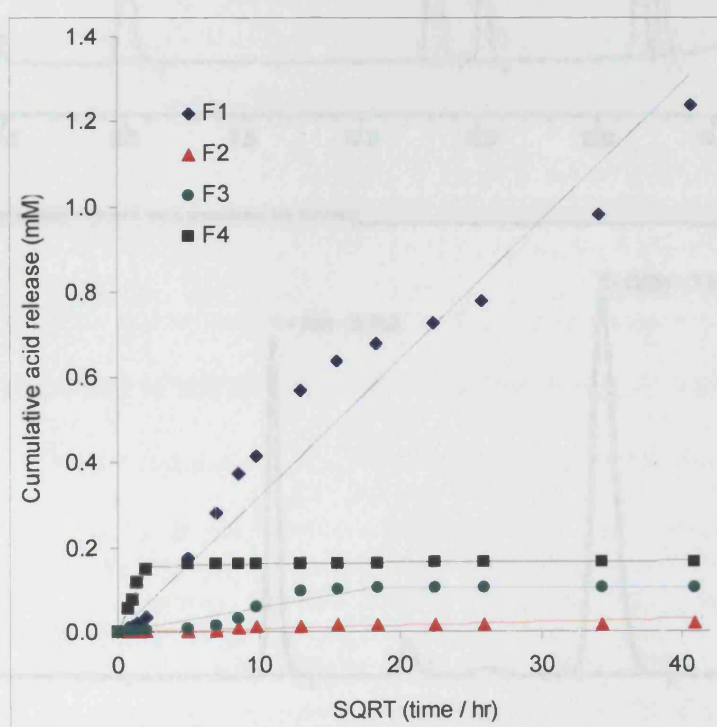
Figure 6.9. Cumulative acid concentration (mM) in storage solutions for samples F1 to F4 as a function of the square root of time. (Straight lines are best fit through either early (assuming an intercept of zero) and / or later time data)

6.3.2.4   Ion release

Typical IC chromatographs obtained for the anion and cation analyses, which show peaks of the ion species determined, are presented in Figure 6.10.

(a)

(b)
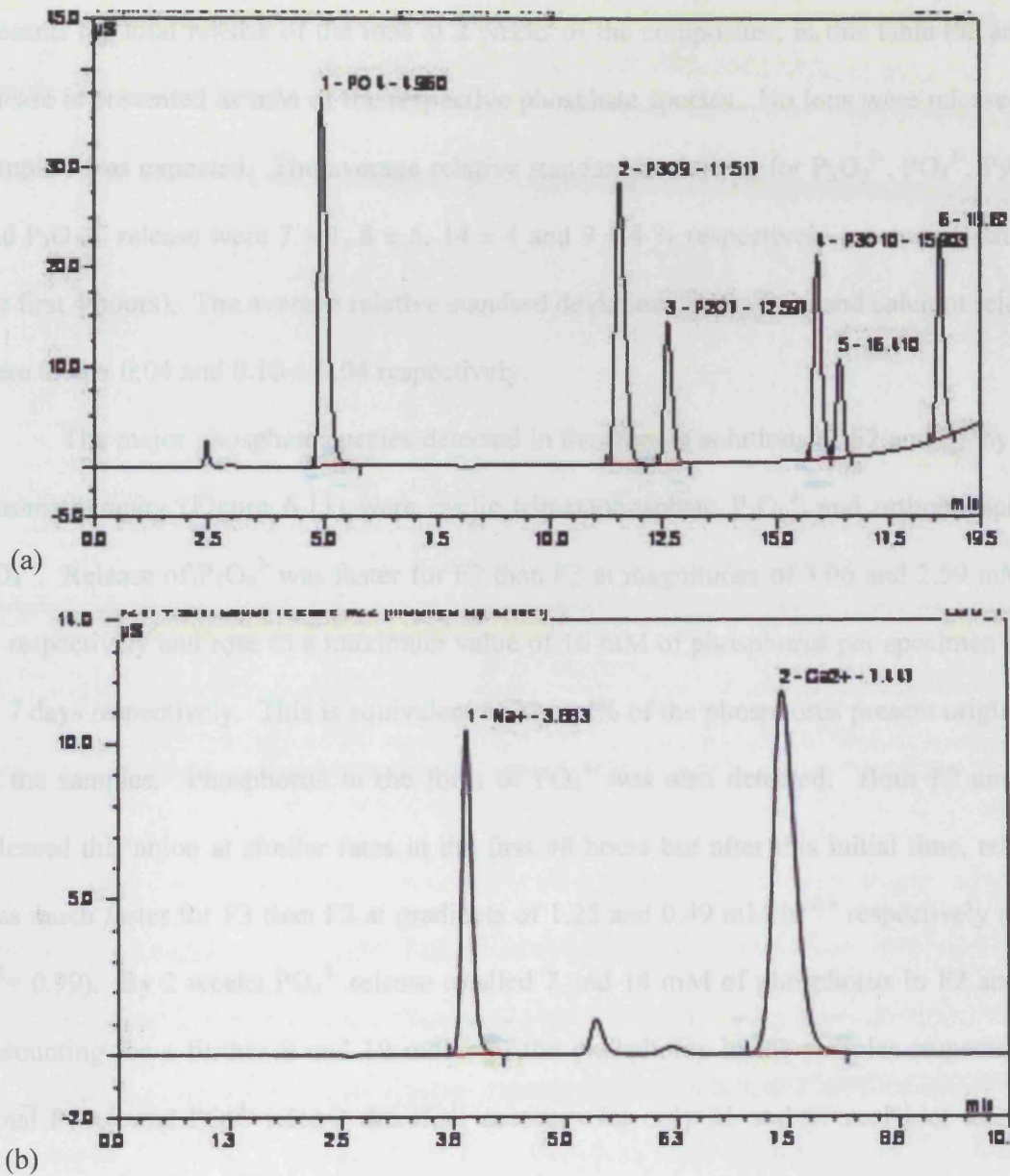
Figure 6.10. An example of an ion chromatograph for (a) anion analysis and (b) cation analysis of the composites F2 and F3. In the composite F4, only the PO_4^{3-} and Ca^{2+} peaks are present.

Figure 6.11 to Figure 6.14 show the anion and cation release profiles for the composites in water up to 2 weeks. All profiles are presented as cumulative mM release of an element (i.e. P, Na and Ca) with respect to the square root of time. Table 6.3

presents the total release of the ions at 2 weeks of the composites; in this table the anion

release is presented as mM of the respective phosphate species. No ions were released in

sample F1 as expected. The average relative standard deviations for $P_3O_9^{3-}$, PO_4^{3-}, $P_2O_7^{4-}$

and $P_3O_{10}^{5-}$ release were 7 ± 1, 8 ± 5, 14 ± 4 and 9 ± 4 % respectively (excluding data in

the first 4 hours). The average relative standard deviations for sodium and calcium release

were 0.08 ± 0.04 and 0.10 ± 0.04 respectively.

The major phosphate species detected in the storage solutions of F2 and F3 by ion

chromatography (Figure 6.11) were cyclic trimetaphosphate $P_3O_9^{3-}$ and orthophosphate

PO_4^{3-}. Release of $P_3O_9^{3-}$ was faster for F2 than F3 at magnitudes of 3.06 and 2.59 mMhr$^{-0.5}$ respectively and rose to a maximum value of 16 mM of phosphorus per specimen by 2

or 7 days respectively. This is equivalent to 22 mol% of the phosphorus present originally

in the samples. Phosphorus in the form of PO_4^{3-} was also detected. Both F2 and F3

released this anion at similar rates in the first 48 hours but after this initial time, release

was much faster for F3 than F2 at gradients of 1.25 and 0.49 mM hr$^{-0.5}$ respectively (both

R^2= 0.99). By 2 weeks PO_4^{3-} release totalled 7 and 14 mM of phosphorus in F2 and F3

accounting for a further 9 and 19 mol% of the phosphorus in the samples respectively.

Total $P_3O_9^{3-}$ and PO_4^{3-} release therefore accounts for only 31 and 41 mol% of the total

phosphorus in F2 and F3 specimens respectively.
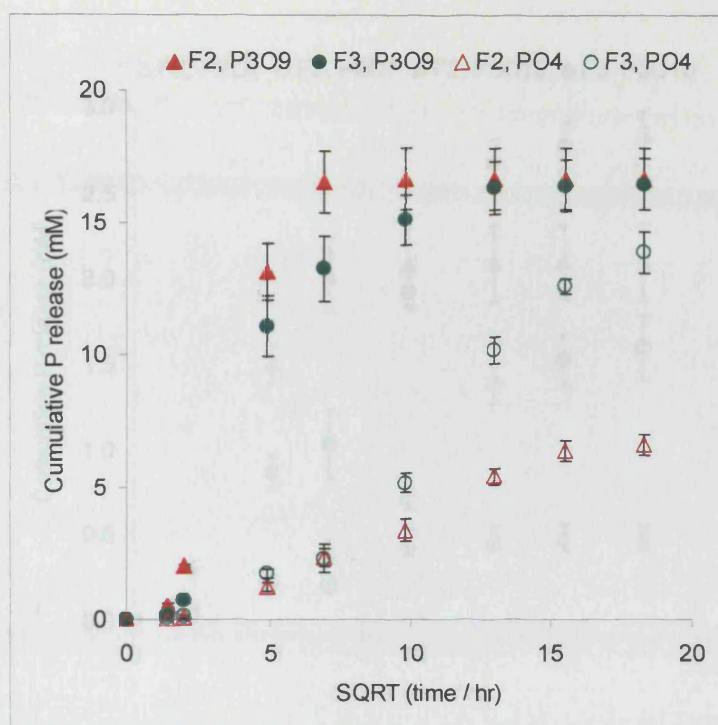
Figure 6.11. Cumulative phosphorous release as either trimetaphosphate ($P_3O_9^{3-}$) or phosphate (PO_4^{3-}) for samples F2 and F3 as a function of the square root of time.

Linear $P_2O_7^{4-}$ and $P_3O_{10}^{5-}$ anion chains were also detectable in the storage solutions and exhibited comparable release profiles as calcium (see later) release with ion release levelling off in F2, and increasing then levelling off in F3 from 48 hours onwards (Figure 6.12). By 2 weeks, $P_2O_7^{4-}$ and $P_3O_{10}^{5-}$ release totalled 0.5 and 2 mM of phosphorus respectively in F2, and 1.6 and 3 mM of phosphorus respectively in F3. These two phosphate species account for only 4 and 6 mol% of the total phosphorus in F2 and F3 specimens respectively. The $P_2O_7^{4-}$ release in F3 was approximately three times that in F2 (see Table 6.3). The absolute phosphorus molar levels released in the form of the four anions were 35 and 47 mol% in F2 and F3 respectively. The remainder of the phosphorus was released as larger unidentified anions (see unidentified peaks in Figure 6.10a).
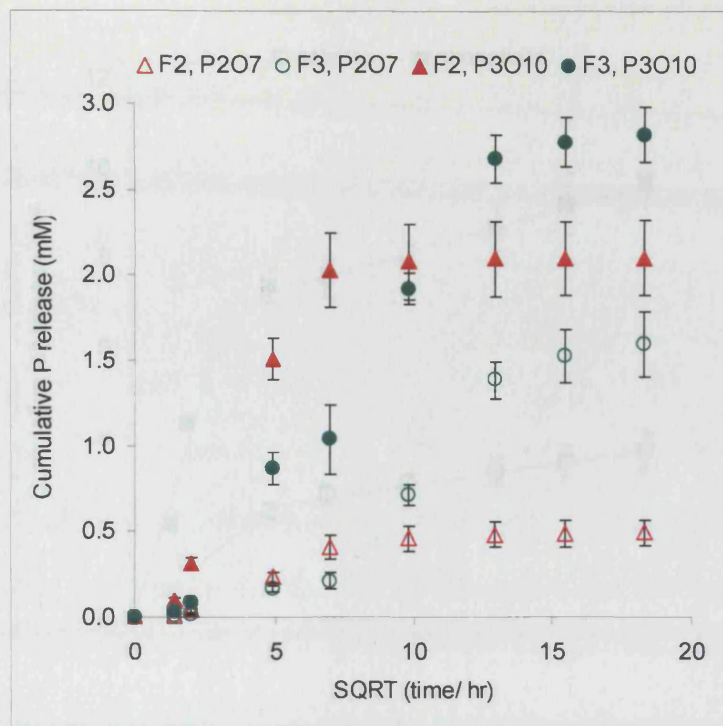
Figure 6.12. Cumulative phosphorous release as linear polyphosphates ($P_2O_7^{4-}$ and $P_3O_{10}^{5-}$) for samples F2 and F3 as a function of the square root of time.

Sample F4 released PO_4^{3-} as an initial burst of 6 mM of phosphorus in the first 24 hours followed by 0.18 mM $hr^{-0.5}$ ($R^2 = 0.98$) (Figure 6.13). This initial burst may be due to the dissolution of surface β-TCP which has a smaller particle size or MCPM which has a much higher solubility. By 2 weeks cumulative orthophosphate release was 10 mM of phosphorus which is calculated to be 16 mol% of that originally in the sample.
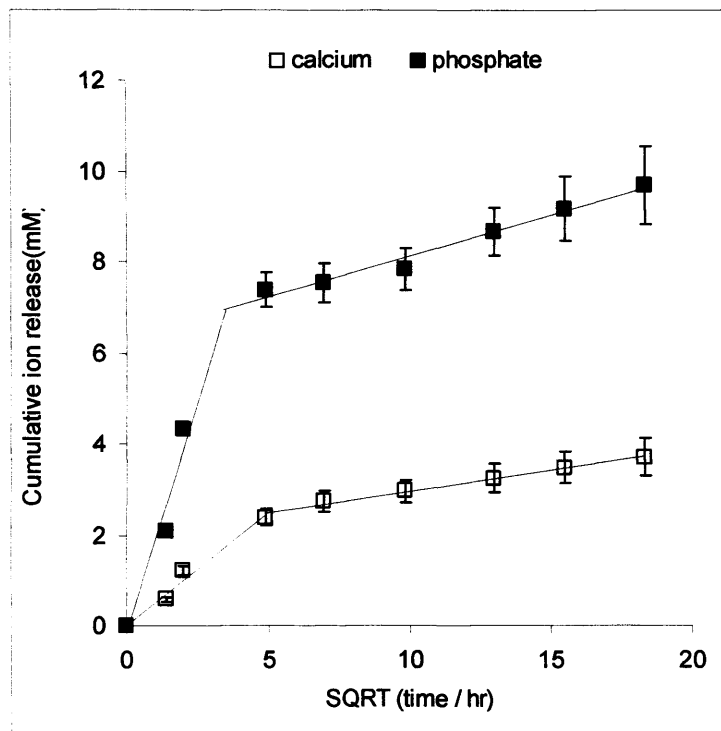
Figure 6.13. Cumulative phosphate (PO$_4^{3-}$) and calcium ion release from sample F4 as a function of the square root of time. (Straight lines are best fit through either early or later time data). N.B. release of PO$_4^{3-}$ is calculated as cumulative release of phosphorus.

Sodium ion release (Figure 6.14) was initially much faster in F2 than F3 at 7.8 versus 2.4 mM hr$^{-0.5}$ respectively (R^2= 0.99 and 0.98). Cumulative values obtained after 2 and 7 days were 36 and ~18 mM specimen^{-1} for F2 and F3 respectively which corresponds to 88 and 70 % of that calculated to be in the original samples. After this burst, sodium release in both samples was minimal and continued at a slow rate of 0.1 mM hr$^{-0.5}$ (average R^2= 0.86). By 2 weeks total sodium release was 37 and 18 mM corresponding to 91 and 71 % of sodium originally in F2 and F3 respectively. With F3 the amount of sodium release is three times that of P$_3$O$_9^{3-}$ (see Table 6.3).

Cumulative calcium ion release initially also exhibited a burst of 0.9 and 0.6 mM hr$^{-0.5}$ (R^2=0.99) up until 2 or 4 days for F2 and F3 respectively. By these times the cumulative levels of calcium in the storage solution were 4 and 6 mM which correspond

with, however, only 16 and 18 wt% of that in F2 and F3. After the burst release, calcium release continued at a slower gradient of 0.1 and 0.3 mM hr$^{-0.5}$ for F2 and F3 respectively (R^2= 0.96 and 0.97) (see Figure 6.14). By 2 weeks total calcium release was 5 and 8 mM for F2 and F3 respectively which account for 21 and 23 % of the calcium amounts originally in the samples.

With F4 (see Figure 6.13) no sodium release was detected as expected but cumulative calcium ion release exhibited an initial burst of ~2 mM in the first 24 hours and a total release of ~4 mM or 7 wt% of that in the sample at 2 weeks. After the initial burst, release rate of calcium was half that of PO$_4^{3-}$ and equal to 0.09 mM hr$^{-0.5}$ (R^2=0.99).
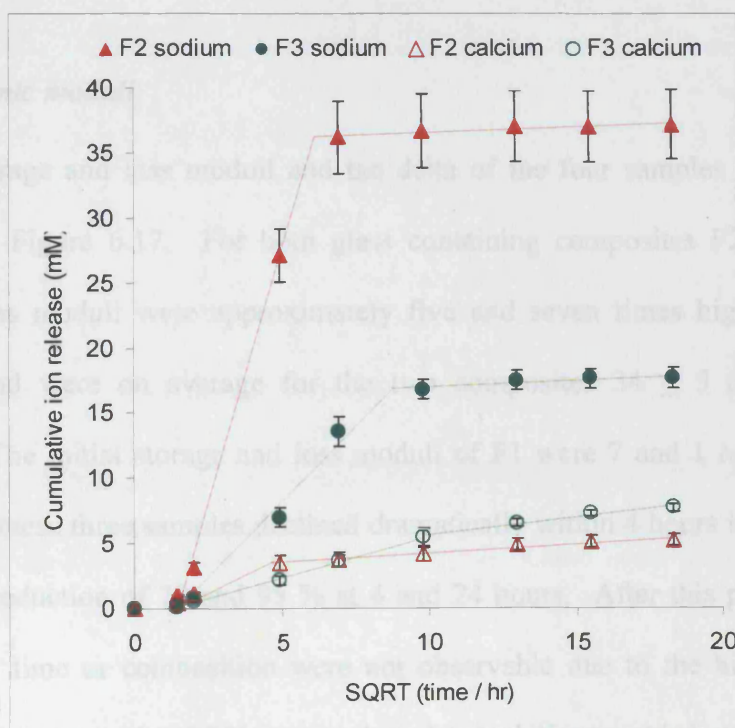
Figure 6.14. Cumulative sodium and calcium release from samples F2 and F3 as a function of the square root of time. (Straight lines are best fit through either early or later time data)

Table 6.3. Total release of identified ions from the three composites at 2 weeks. Note the release is presented as mM of the phosphate species not per phosphorus atom as presented in Figure 6.11 to Figure 6.13.

Ion release (mM)	F2	F3	F4
Na^+	37.18	17.68	*
Ca^{2+}	5.23	7.73	3.72
PO_4^{3-}	6.61	13.85	9.69
$P_3O_9^{3-}$	5.55	5.48	*
$P_2O_7^{4-}$	0.25	0.80	*
$P_3O_{10}^{5-}$	0.70	0.94	*

6.3.2.5 Dynamic moduli

The storage and loss moduli and tan delta of the four samples are presented in Figure 6.15 to Figure 6.17. For both glass containing composites F2 and F3, initial storage and loss moduli were approximately five and seven times higher than for the polymer F1 and were on average for the two composites 34 ± 5 and 7 ± 1 MPa respectively. The initial storage and loss moduli of F1 were 7 and 1 MPa respectively. The moduli of these three samples declined dramatically within 4 hours in water resulting in an average reduction of 79 and 95 % at 4 and 24 hours. After this period significant variations with time or composition were not observable due to the high variability in measurements (average 44 ± 26 % error) when the moduli were this low. Tan delta after 24 hours for F1, F2 and F3 fluctuated on average between 0.24 and 0.31 and again systemic variation could not be concluded due to the high variability of data (19 ± 15 % error) (see Figure 6.17). Although results for F4 were initially comparable with those of

F1, after 24 hours in water both storage and loss moduli rose from 3.5 and 1 MPa to 33 and 7 MPa respectively and relative standard deviations declined to an average of 4 ± 2 %. With F4, both storage and loss moduli then decreased almost linearly with the square root of time at magnitudes of 0.3 and 0.05 MPa hr$^{-0.5}$ ($R^2 = 0.88$ and 0.86) [5] to final values of 20 and 5 MPa respectively at 10 weeks (see Figure 6.15 & Figure 6.16). For F4, tanδ values after 24 hours were all equal to 0.23 ± 0.01 with a 2 ± 2 % error (Figure 6.17).
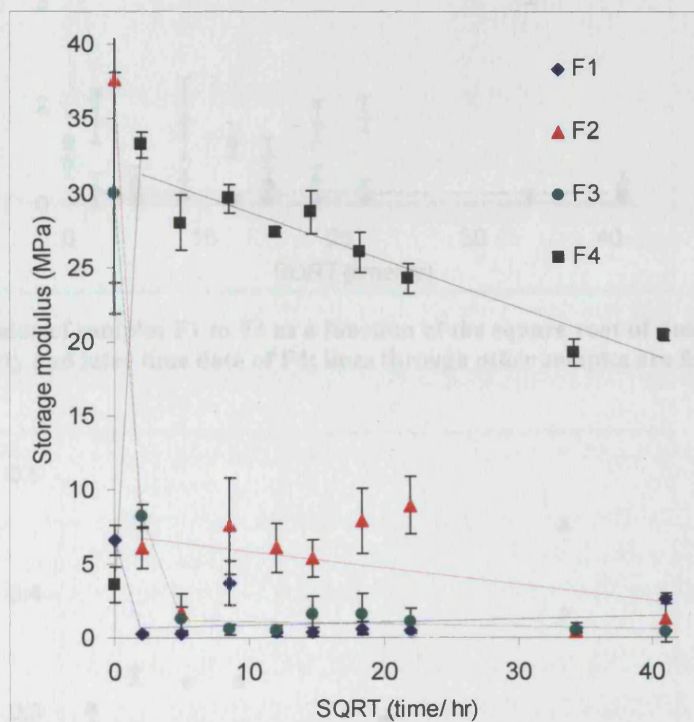
Figure 6.15. Storage modulus of samples F1 to F4 as a function of the square root of time. (Straight lines are best fit through early and later time data of F4; lines through other samples are for guidance only)
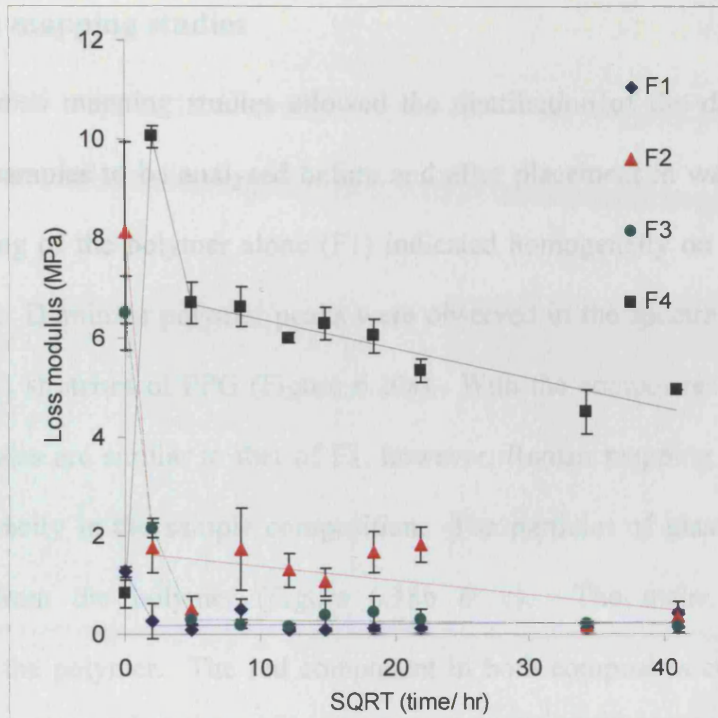
Figure 6.16. Loss modulus of samples F1 to F4 as a function of the square root of time. (Straight lines are best fit through early and later time data of F4; lines through other samples are for guidance only)
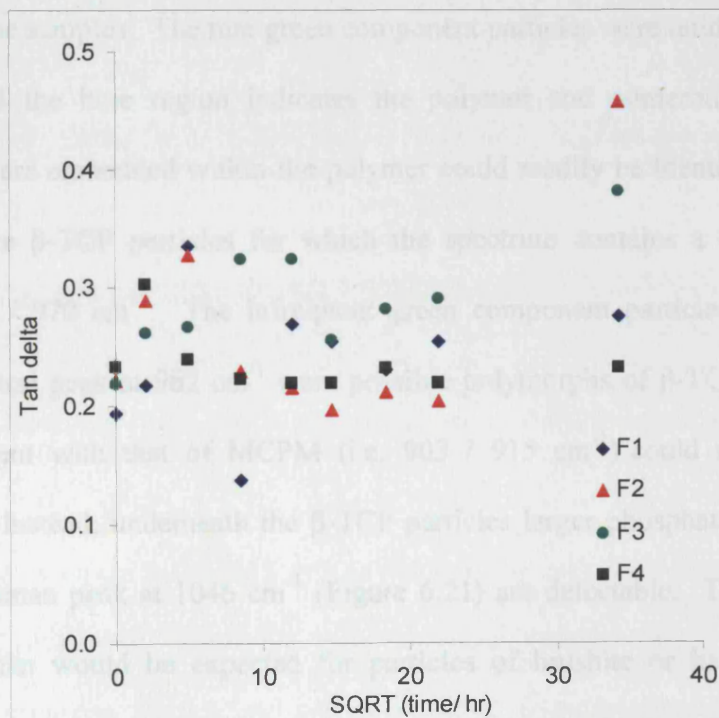
Figure 6.17. Tan delta of samples F1 to F4 as a function of the square root of time.

6.3.3 Raman mapping studies

The Raman mapping studies allowed the distribution of the different chemical species in the samples to be analysed before and after placement in water. The Raman mapping imaging of the polymer alone (F1) indicated homogeneity on the micron scale (Figure 6.18 a). Dominant polymer peaks were observed in the spectra at 870 and 1457 cm^{-1} due to C-H stretches of PPG (Figure 6.20a). With the composites F2 and F3, their visual appearances are similar to that of F1, however, Raman mapping images highlight strong heterogeneity in the sample composition. The particles of glass could easily be distinguished from the polymer (Figure 6.18b & c). The main blue component corresponds to the polymer. The red component in both composites corresponds to the $(P_2O_5)_{0.45}(CaO)_x(Na_2O)_{0.55-x}$ glass indicating two relatively broad but intense peaks at 693 and 1168 cm^{-1} (Figure 6.20b & c). These glass particles range in size from 3-50 μm over the surface of the samples. The rare green component particles were unidentified.

With F4 the blue region indicates the polymer and numerous small particles (purple) which are embedded within the polymer could readily be identified (Figure 6.18 d). These were β-TCP particles for which the spectrum contains a sharp PO stretch doublet at 945 / 970 cm^{-1}. The infrequent green component particles with a calcium phosphate spectral peak at 962 cm^{-1} were possible polymorphs of β-TCP. Regions with spectra consistent with that of MCPM (i.e. 903 / 915 cm^{-1}) could not, however, be distinguished. Instead, underneath the β-TCP particles larger phosphate particles with a major sharp Raman peak at 1046 cm^{-1} (Figure 6.21) are detectable. This is at a higher wavenumber than would be expected for particles of brushite or its anhydrous form monetite (~980 cm^{-1}) suggesting that the surface phosphate groups of MCPM may

possibly be interacting with the surrounding β–TCP and / or the polymer but not fully

converted to a new calcium hydrogen phosphate crystalline form. More work, such as

looking at MCPM particles alone in the polymer, would be required.

(a)   (b)

(c)   (d)
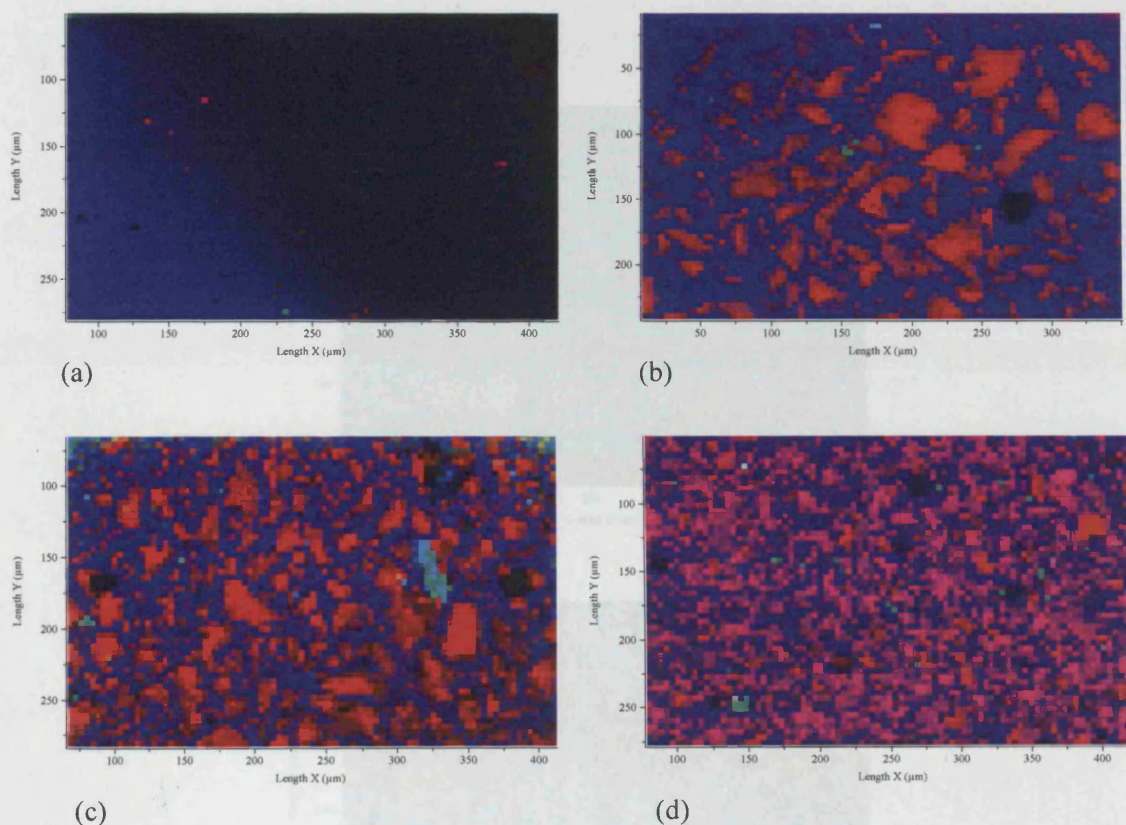
Figure 6.18. Raman mapping images of samples prior to immersion in water. Images are of areas of 250 by 400 micron with pixel dimensions of 4 micron square. (a) F1 consisting of polymer only (in blue); (b) F2 and (c) F3 showing phosphate particles (in red) dispersed within polymer (blue); (d) F4 with smaller βTCP particles (in purple) on top of larger areas with a dominant Raman peak at 1045 cm^{-1} (in red) both embedded within the polymer (in blue).

After placement in water for 4 days almost no calcium phosphate species could be

detected in the surfaces of either F2 or F3 but holes (regions with no distinguishing

Raman peaks) of comparable dimension to those of the particles were visible (see Figure

6.19a). Raman maps of sample F4 after 4 days in water were less clear still having

regions that could be assigned to all the individual components but also other areas with

poor Raman scattering. The later could be due to the formation of unidentified weak

Raman scattering components or pits in the surface. The number of β-TCP particles (in

purple), however, had dramatically decreased (Figure 6.19b).

(a)

(b)
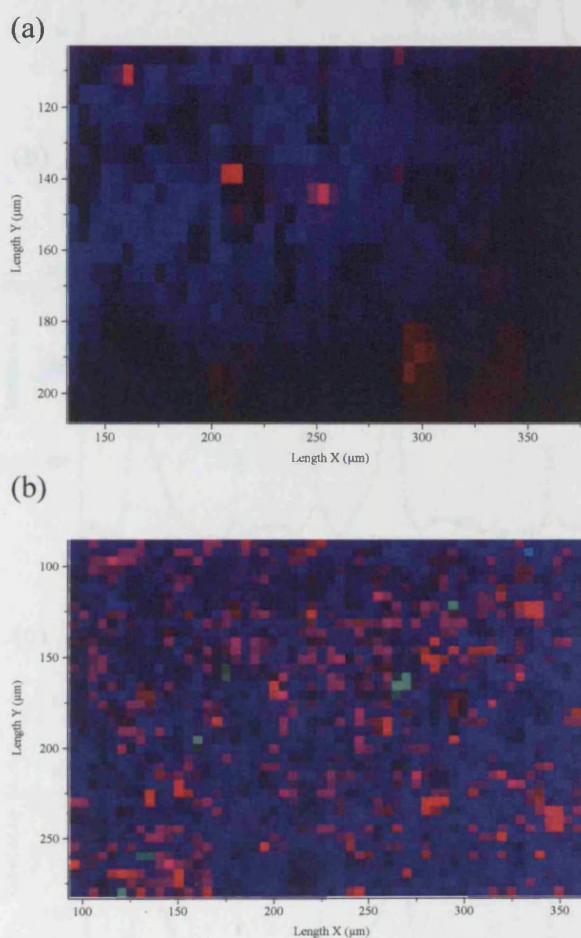
Figure 6.19. Raman mapping images of samples after immersion in water for 4 days. Images are of areas of 250 by 400 micron with pixel dimensions of 4 micron square. (a) F3 showing significantly reduced amounts of phosphate particles (in red) within polymer (blue) and holes (in black) with no Raman peaks; and (b) F4 with less β–TCP particles (in purple) and other particles (in red) both embedded within the polymer (in blue) and areas with poor Raman scattering.

Figure 6.20. Raman mapping spectra of different components in the samples corresponding to (a) the blue component in F1; (b) and (c) the red component in F2 and F3.
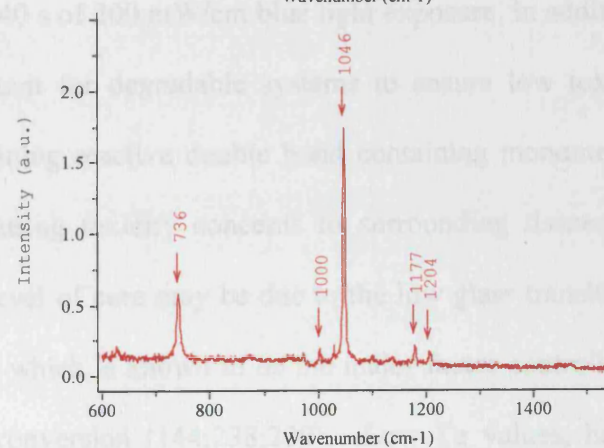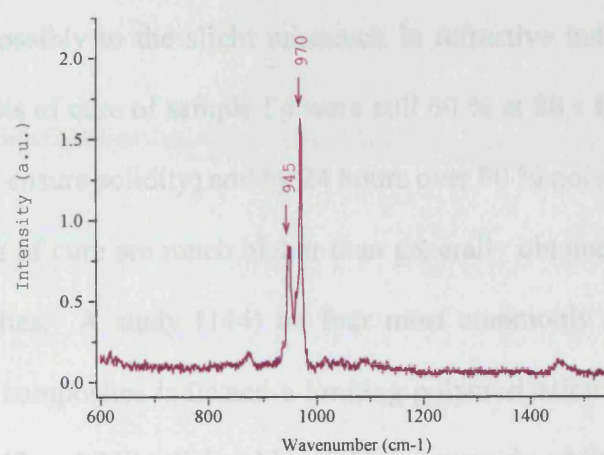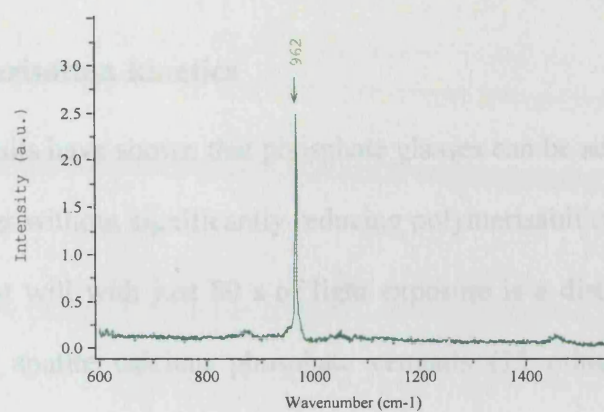
Figure 6.21. Raman mapping spectra of different components in the samples corresponding to the green, purple and red components in F4.

6.4   Discussion

6.4.1   Photopolymerisation kinetics

The above results have shown that phosphate glasses can be added to a degradable

methacrylate monomer without significantly reducing polymerisability. The ability to set

the polymer rapidly at will with just 80 s of light exposure is a distinct advantage over

much slower setting apatite calcium phosphate cements (15 minutes or more) (91).

Addition of β–TCP and MCPM phosphate particles did reduce the rate of monomer

polymerisation due possibly to the slight mismatch in refractive indices of the polymer

and filler, but the levels of cure of sample F4 were still 60 % at 80 s from the start of cure

(which is sufficient to ensure solidity) and by 24 hours over 90 % polymerised (Table 6.2).

These rates and levels of cure are much higher than generally obtained with methacrylate

based dental composites. A study (144) on four most commonly used dimethacrylate

monomers for dental composites indicated a limiting polymerisation level of between 39

and 76 % only with 240 s of 200 mW/cm blue light exposure. In addition, high conversion

is particularly important for degradable systems to ensure low toxicity of degradation

products. Any remaining reactive double bond containing monomer would be released

upon degradation causing toxicity concerns to surrounding tissues. As mentioned in

Chapter 3, the high level of cure may be due to the low glass transition temperature (Tg)

of the final polymers which is known to be the major factor controlling final equilibrium

levels of monomer conversion (144;238;239). Low Tg values, however, will lead to

materials of low modulus that for improved suitability for bone repair would benefit from

the addition of higher modulus fillers.

The polymerisation shrinkage (vol %) of the polymer F1 and the composites can be calculated using Equation 6.11:

$$Vol = \Delta V_{MA} \times \rho \times \left(\frac{f \times m}{M_{MA}} \right) \qquad\qquad 6.11$$

Where ΔV_{MA} is the volume change per mole of any methacrylate (i.e. 22.5 cm^3/ mole (240)), ρ is the density of polymer/ composite (g/ cm^3), f is the polymerisation fraction, m is the polymer mass content (wt%) and M_{MA} is the molecular weight per mole of methacrylate (g/ mole).

With a polymer density of 1.13 g/cm^3, a polymerisation fraction close to 1 and a measured monomer molecular weight per methacrylate group of 869 g/mol, the polymerisation shrinkage of the pure polymer F1 is calculated to be 2.9 vol%, which is comparable with that observed in dental composites (241). Since the molecular weight of methyl methacrylate is 100 g/mol and the density of PMMA is 1.19 g/cm^3, this shrinkage is 9 times smaller than that expected for full polymerisation of PMMA (i.e. 26.8 vol%). Using the composite densities obtained (i.e. 1.82 g/cm^3 for all composite samples, section 6.3.2.1) and the polymer mass content of 33 wt%, polymerisation shrinkage in the composites is calculated to be 1.6 vol% which is almost half of that for the polymer F1.

The amount of heat generated by polymerisation (Heat, kcal/ cm^3) of the pure polymer and new composites can be calculated via a similar equation (Equation 6.12).

$$Heat = H \times \rho \times \left(\frac{f \times m}{M_{MA}} \right) \qquad\qquad 6.12$$

Where H is the heat per mole of methacrylate monomer reacted (i.e. 14 kcal/mole (242)). Again with a polymerisation fraction of close to 1, the amounts of heat generated by F1

and the composite polymerisation are calculated to be 1.82 and 0.97 kcal/ cm^3. This is 9 and 17 times, respectively lower than that calculated for PMMA cements (i.e. 16.7 kcal/ cm^3).

6.4.2 Degradation studies

6.4.2.1 Polymer F1

Within the first 24 hours in solution the polymer F1 increases in volume by 5 vol% due to water sorption and a maximum water content of 7.4 wt% is reached (Figure 6.3 and Figure 6.5). This level of swelling may be beneficial because it is of the correct order of magnitude to compensate for polymerisation shrinkage as calculated above. After 24 hours the volume slowly declines due to polymer degradation but the water content remains stable. This level of water sorption is not sufficient to significantly alter the sample density. The results show that polymer mass loss (z) and acidic degradation product (C_a) release are all proportional to the square root of time ($t^{0.5}$) and therefore that degradation rate (i.e. dz/ dt or dC_a/ dt) declines with time (Figure 6.7 and Figure 6.9). The mass of the degradation products per acid group obtained in this study (i.e. 0.47 kg/mol) is comparable with that previously observed for a similar polymer of twice the specimen depth (~0.8 kg/mol) (Section 4.3.4, Chapter 4).

During degradation, water is expected to attack the C-O bonds of the crosslinking ester groups of the polymer. Previous FT-IR studies have shown upon degradation of these polymers, small poly (methacrylic-co-lactic) acid molecules and PPG are formed (Section 4.3.6, Chapter 4). Whereas the former are released into solution, the hydrophobic PPG tends to remain within the specimen. Due to the restricted water sorption the degradation occurs largely at the specimen surface but the growing percentage of PPG and

decline in reactive groups in this surface region is likely to cause the observed decline in

degradation rate with time (as discussed in Section 4.4, Chapter 4). With degradable bone

cements it is generally preferable to have a linear rate of degradation but it has been

shown in Chapter 4, that through modification of the molecular weight of the monomer,

this may be achieved. Of further concern, however, is the reduction of pH to below 4

during degradation of the polymer. The acidic products could irritate any tissue

surrounding the implanted material thus providing another rationale for the use of fillers

that may, in addition to raising modulus, neutralise these acids.

The results have shown that addition of inorganic fillers to the polymer matrix had

significant effects on the degradation and stiffness behaviours of the composites when

compared to the polymer formulation alone.

6.4.2.2   Phosphate glass – containing composites F2 and F3

The initial swelling of the polymer due to water sorption was found to increase in

magnitude and level by several fold on addition of phosphate glass filler particles (Figure

6.3). Maximum swelling was ~56 and 34 vol% for F2 and F3 respectively. This might be

because (i) reduction in the amount of crosslinking (with less monomer in a given volume)

allows greater expansion of the composite and (ii) dissolution of soluble inorganic

particles in water within the composites increases the internal osmotic pressure. Previous

studies on ternary phosphate glasses in bulk form indicated that at this level of phosphorus,

degradation products are pH neutral and their dissolution rate is inversely proportional to

the CaO content within the glass (121;122;124;126). The faster dissolution of the filler in

F2, with 30 mol% CaO, might then explain its more rapid water sorption when compared

with F3 with 40 mol% CaO. As explained before some expansion can be beneficial in that

it counteracts polymerization shrinkage of the monomer (typically ~ 5-10%) but the large

dimensional expansion of the composites F2 and F3 may need to be better understood and

controlled.

The maximum level of water in the composites increased to 50 and 40 wt% by 3

and 7 days in F2 and F3 respectively (Figure 6.5). During these periods over 80 wt% of

the inorganic filler had also been released (Figure 6.7). Water content (%) remained

constant after these times but there was a reduction in the sample volume with time. The

inorganic components in the bulk of the material should dissolve first in the absorbed

water prior to their release. This release of the filler might then reduce the composite

internal osmotic pressure thereby allowing the remaining polymer to contract again. The

levels of sample expansion and contraction and ion release are all likely to be affected by

the relative rates of composite water sorption, and inorganic component solubility and

dissolution kinetics. Further work, in for example phosphate buffered solutions and with

other phosphate glasses of differing solubility would be required, however, to assess better

the likely expansion and contraction *in vivo* and determine exactly how to control this

potential problem with soluble - glass – containing composites.

The initial polymer to filler weight ratio of each composite sample was 33 to 67

wt%. Using the glass particle and polymer densities obtained and with density defined as

mass over volume, the fillers are calculated to occupy initially ~46 vol% of the sample.

This level of filler / liquid ratio was sufficient to produce clinically workable pastes for at

least 5 minutes. Inorganic component release from the F2 and F3 composites leaves, as

the Raman mapping studies proved, water–containing holes in the specimens of

comparable dimensions and volume to the glass particles. This can be beneficial as it

provides a means to develop materials of controllable porosity (as the range of glass

particle size is known), which can affect the effectiveness of bone ingrowth (9;62;63). Although F2 and F3 were initially stiffer than the pure polymer F1, the fast dissolution of the glass resulted in 95 % loss in modulus over a period of 24 hours (Figure 6.15). Further studies with other phosphate glasses of slower dissolution may allow balance between the desired pore formation and stiffness reduction to be better controlled. Despite the large polymer surface area in contact with water with such structures, both acid release studies and gravimetric investigations indicated a decline rather than increase in the rate of polymer erosion when compared to the pure polymer F1. This suggests that water sorption is not the rate limiting factor in the polymer erosion mechanism but as previous studies with the pure polymers have suggested may largely be determined by the rate at which the degraded polymer can be released from the specimen surface (Chapter 4). It is also possible that the Ca^{2+} ions could be crosslinking some of the degradation products reducing their solubility in water.

By 2 days with F2, and 7 days with F3, ion chromatography showed that over 88 and 70 wt% of the sodium in the specimens were released respectively into the surrounding water. Rates and levels of loss of this ion (Figure 6.14) showed similar trends to that of total filler loss estimated from gravimetric measurements (Figure 6.7). The cyclic $P_3O_9^{3-}$ metaphosphate anion had the highest release of all four anions suggesting that a significant proportion of this anion was present in the original glass structure as has been found for similar ternary based phosphate-glass system (122). This was also supported by a previous study (121), which identified, via X-ray powder diffraction (XRPD) studies, $Na_4Ca(PO_3)_6$ (a calcium bridged trimetaphosphate) as the main crystalline phase in the $P_{45}Ca_{30}Na_{25}$ glass (as in F2). On the other hand two crystalline phases in the $P_{45}Ca_{40}Na_{15}$ glass (as in F3) were detected: the main $NaCa(PO_3)_3$ (a sodium

calcium metaphosphate) phase, and $Ca_2P_2O_7$ (a calcium pyrophosphate) of which small quantities were detected. Additionally this cyclic $P_3O_9^{3-}$ metaphosphate anion could also be formed upon for example hydrolysis of the phosphate chains, when the negative charge on a phosphate chain end (O^-) 'bends' around three P groups down the chain and forms a bond with the P atom on the hydrolysed P-O bond. With F3 the amount of Na^+ release is at least three times that of $P_3O_9^{3-}$ at all times suggesting that these species may be released together. Correlation in the release profiles between these two ions has been observed previously which suggested that the remaining negative charge on the mostly unbranched $P_3O_9^{3-}$ anion was ionically linked with the Na^+ ion (122). For F2, however, a comparable level of $P_3O_9^{3-}$ was released but twice as much Na^+ as with F3 (Table 6.3). The higher sodium release with F2 was expected because its level was 1.7 times that in F3 and its replacement of calcium increased glass dissolution rate. Some of this 'additional' sodium in F2 must therefore, be associated with the PO_4^{3-} and longer linear polyphosphates that were released. Ion release studies of the four phosphate anions accounted only for 35 and 47 % of the phosphorus amount in F2 and F3 respectively and many of the longer polyphosphates could not be quantified by ion chromatography due to the large number that can be formed and lack of available commercial standards (P > 4).

Gravimetric studies suggest that by the end of the experiment most of the phosphorus is likely to have been released from both F2 and F3. The cumulative levels of calcium detected in the storage solutions for F2 and F3 after two weeks were, however, much lower than calculated to be in the original specimens (only accounted for 21 and 23 % of calcium) suggesting that this ion might in part be retained within the polymer and/ or crosslinked with the polymer when the other components of the glass were released. An alternative explanation could be, however, that these cations were strongly chelated with

the longer polyphosphate species and were removed by the Dionex Onguard® IIA cartridge before detection. It has been stated that Ca^{2+} ions form chelates that can strongly complex with linear polyphosphates (243). At higher CaO content, these linear phosphate anions were more likely to be crosslinked with the Ca^{2+} ions acting as chelates, with a consequent decrease in their release rates (122). This might explain why release rates for $P_2O_7^{4-}$ and $P_3O_{10}^{5-}$ were initially lower in F3 than F2 (Figure 6.12). At later times hydration of these crosslinked phosphate chains resulted in their faster release in F3 as well as Ca^{2+} ions. At these times the higher release of Ca^{2+} ions was expected for F3 as its level is 1.3 times that in F2. With F3 the amount of $P_2O_7^{4-}$ release was three times than that of F2 at these later times suggesting that this species is more prevalent in the former. As mentioned earlier XRPD study (121) showed $Ca_2P_2O_7$ as one minor crystalline phase present in the $P_{45}Ca_{40}Na_{15}$ glass (as in F3)

The pH of solution dropped initially in the first week in both F2 and F3 composites (Figure 6.8). This could be due to release of some of the polymer from the surface of the specimens where the concentration of the phosphate glass might be low. With time the pH slowly rose to almost neutral as degradation products mainly consisted of the glass, which was found to be neutral as previously studied (121).

6.4.2.3 β–TCP and MCPM - containing composite F4

The initial rapid water sorption of the β-TCP and MCPM containing F4 composite formulation might also be explained by reduced methacrylate crosslinking and partial dissolution of the filler raising the internal composite osmotic pressure. The maximum level of swelling of F4, however, was only 23 % (compare with 56 and 34 % in F2 and F3, Figure 6.3). This might be a consequence of lower solubility of β–TCP and MCPM ($K_{sp} =$

2.07 x 10^{-33} and 7.18 x 10^{-2} at 25 °C respectively) or their reacted brushite product (K_{sp} =

2.59 x 10^{-7} at 25 °C) (244). Water sorption was expected in F4 to encourage reaction

between the different phosphate species and promote transfer of hydrogen ions from the

MCPM to the β-TCP. This transfer gives rise to crystals of brushite in accordance with

the following stoichiometric equation (245).

β-$Ca_3(PO_4)_2$ + $Ca(H_2PO_4)_2.H_2O$ + 7 H_2O → 4 $CaHPO_4. 2H_2O$
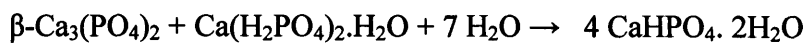
In conventional calcium phosphate cements containing MCPM and β-TCP the

particles dissolve in water and then reprecipitate solidifying the cement and forming

brushite or its anhydrous form monetite (dicalcium phosphate anhydrous (DCPA))

crystallites. It has been found that blade-like brushite crystals of ~20-30 μm in length and

~2 μm in width were obtained (246). One of the additional aims of this study was to

assess if the restricted water sorption could encourage this process within the fully

polymerised composite and cause the phosphate particles to dissolve and reform brushite

species thereby affecting mechanical properties and degradation mechanism.

Although the Raman spectra at 4 days provided no conclusive proof for the

formation of the brushite species, the reduction in MCPM and β-TCP regions in the

Raman maps combined with the large increase in modulus after placement in water did

suggest water sorption-induced chemical processes were occurring. It was possible that

hydrogen ion transfer as in MCPM / β-TCP cements did occur but that the highly

crosslinked structure of the polymer prevented precipitation of well defined large brushite

crystals that could then be identified in a Raman map. The formation of fine crystals that

might interpenetrate on the nanometre scale with the polymer network might then provide

explanation as to why the modulus of F4 increased by an order of magnitude upon water

sorption from 4 hours onwards (from 3.5 to 33 MPa) and significantly higher than with the

pure polymer or with incorporating any of the phosphate fillers studied above (Figure 6.15). Although the modulus of this sample is still not as high as most bone, the formulation has yet to be fully optimised. For example, as discussed in Chapter 4, by altering the length of the monomers the initial modulus of the polymer itself can be raised by a factor of almost 10 providing a higher initial starting point which the addition of the filler would raise further.

Unlike the other 3 samples, F4 increased in water content throughout the whole 10 week study period providing further evidence that water might be being consumed in a reaction process between the β–TCP and MCPM (Figure 6.5). After the first 24 hours, however, water sorption-induced swelling was balanced by composite degradation leading to stability in overall dimensions with minimal volume change (Figure 6.3). Gravimetric studies indicated a four fold increase in the percentage polymer degradation (z_1) at 10 weeks with the addition of the F4 filler particles (32 wt% compared to 8 wt% in F1, see Figure 6.7) but this was not accompanied by an increase in the level of acid detected in the storage solutions (Figure 6.9). The latter suggests that after the initial period most of the acidic degradation products from the polymer were being neutralised either within the composite specimen prior to their release or within the storage solution by association with PO_4^{3-}.

The acid dissociation constant (K_a) of an acid is given by this expression (232):

$$K_a = \frac{[H^+][A^-]}{[HA]}$$

$$-\log K_a = pK_a$$

In dilute solution the three dissociation constants of phosphoric acid (H_3PO_4) and its first two conjugate bases ($H_2PO_4^-$ and HPO_4^{2-}) (pK_a's = 2.1, 7.2 and 12.7 respectively at 25°C)(232) and total PO_4^{3-} and H^+ concentrations will determine the levels of association between orthophosphate and hydrogen ions and thereby the solution pH and concentrations of the different associated species (Figure 6.22). In the stoichiometric reaction between β-TCP and MCPM, MCPM is the acid donating a hydrogen ion to the basic β-TCP with formation of the brushite salt. With polymer degradation, acid is produced adding hydrogen ions into the solution. In non-buffered solution as in F1 this acid formation resulted in lowering of the pH. The brushite-forming system in F4, however, acts as a buffer for the solution maintaining its pH close to the pK_a of its conjugated acid MCPM according to the Henderson-Hasselbalch equation (see below) and the ratio of the concentrations of weak acid to conjugate base or of weak base to conjugate acid (232). If for example acid is produced, the brushite (4 $CaHPO_4$. $2H_2O$) will 'mop up' the acid proton and drive the equilibrium to form MCPM ($Ca(H_2PO_4)_2.H_2O$). Consequently the solution should be buffered and have a pH close to the pK_a of MCPM i.e. 7.2. This was observed for the F4 storage solutions after the first 24 hours. This control of pH may be beneficial in reducing irritation to any tissue surrounding the implanted material. It could also reduce the possibility of sudden catastrophic core degradation of the material caused by acid build-up.

$$pH = pK_a - \log\left(\frac{[acid]}{[base]}\right)$$ **The Henderson-Hasselbalch Equation**
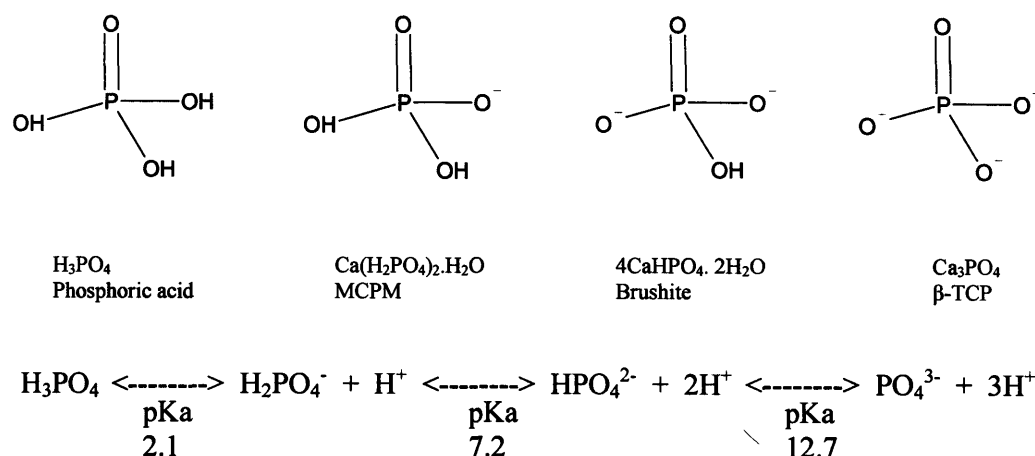
Figure 6.22. Structures of the different phosphate species from the calcium phosphate particles in composite F4 and their acid dissociation constants.

With the F4 composite, PO_4^{3-}, H^+ and Ca^{2+} are present in equimolar ratios in the filler (see stoichiometric equation above). Determining the level of phosphorus released from sample F4 is much easier than with F2 or F3 because after passing through the ion exchange columns only one anionic species PO_4^{3-} will be present for detection. The orthophosphate release of 16 wt% (9.7 mM phosphorus) in 2 weeks detected by ion chromatography from F4 is higher than the total filler loss of 10 wt% estimated from gravimetric studies but the calculated calcium ion release is lower at 7 wt% (3.7 mM Ca^{2+}) (Figure 6.13 & Figure 6.7). This is consistent with the brushite reacting with acid produced by polymer degradation. Polymer mass loss for F4 is observed to be 4 times that for F1 (Figure 6.7). At 2 weeks acid release was ~0.7 mM for F1 (Figure 6.13), and assuming no neutralisation of acid occurred acid release from F4 would be expected to be ~2.8 mM. On the other hand dissolution of the brushite particles (4 $CaHPO_4$. $2H_2O$) would theoretically release P and Ca ions at 1:1 ratio. As described above the neutralisation of acid from polymer degradation products, however, results in conversion

of the brushite particles into MCPM ($Ca(H_2PO_4)_2.H_2O$), which when dissolved, gives a 2 :

1 release of P and Ca ions. With a 9.7 mM of phosphorus release, therefore, the amount

of Ca^{2+} release would be expected to be 4.9 mM. Of this amount, however, ~1.4 mM of

the Ca^{2+} ions would be associated with the neutralised polymer degradation fragments (i.e.

2 R-COOH + Ca^{2+} → $Ca(R\text{-}COO^-)_2$ + $2H^+$) and hence not be detected as they are

removed by the Dionex NG1 guard column prior to analysis. The amounts of P and Ca^{2+}

ions (9.7 and 3.7 mM respectively) obtained from the IC analysis were therefore

consistent with the buffering reaction of the brushite particles and the neutralisation of

polymer degradation products. The neutralisation of the polymer hydrolysis products

might drive the polymer esterification / hydrolysis equilibrium within the specimens

further towards the hydrolysis products hence an increase in rate of polymer erosion.

As with the polymer release, the rate of filler loss decreased with the square root of

time (Figure 6.7) suggesting that the formation of a PPG rich surface polymer layer

inhibited both the filler and polymer erosion. Nevertheless the gradual composite mass

loss profile in F4 compared to F2 and F3 (Figure 6.6) would be more suitable if the

material is used in load bearing application. Further work is now required to assess if the

total composite degradation can be made linear with time by using new monomer

formulations that by themselves have a linear degradation profile.

Since the completion of this project, further research within the department on the

sample F4 has provided supporting evidence for the formation of brushite in the sample

after submersion in water. This is enclosed in Appendix 1.

7 Summary, Conclusion & Future work

7.1   Synthesis and Polymerisation Kinetics of Monomers- summary

Five ABA triblock poly(lactide-co-PG-co-lactide)s with 7, 17 or 34 propylene glycol and 2, 4 or 8 lactic acid units in each B and A block respectively end capped with methacrylate groups were prepared. Qualitative and quantitative structural analyses using FTIR, Raman and NMR confirmed success of the monomer syntheses and indicated that the lactide to PPG ratios were controllable and in reasonable agreement with those expected from reactant molar ratios. Their polymerisation reaction kinetics at 37 °C upon blue light exposure for 60, 120 or 240 s using 0.5, 1 or 2 wt% initiators was determined by a combination of time-based ATR-FTIR and Raman methods.

The monomers started to polymerise immediately on light exposure. At early times, PPG n level had the most significant effect on reaction rate with samples of high n polymerising more slowly than those of low n. At later times the effect of light exposure time, as a single factor or in interaction with the PPG n factor, became prominent. Extending light exposure time to 240 s increased the rate of polymerisation of monomers with $n=34$. The shortest monomer, P7L2DMA, with 0.5 wt% initiator achieved 96 % polymerisation by 120 s after the start of 60 s illumination indicating its suitability as a fast setting cement. Raising initiator concentration reduced polymerisation rate on the lower surface of the samples. The lactide chain length showed insignificant effects on the monomer polymerisation. With all the monomers, 60 s light exposure gave final levels of methacrylate conversion of greater than 90 %. Synthesis of triblock poly(glycolide-co-PG-co-glycolide) dimethacrylates in this study was less successful due to their poor reaction yields and uncontrollable glycolide to PPG ratios on changing reactant molar ratios.

7.2   Polymer Degradation- summary

The physical, degradation and mechanical properties of the five ABA poly(PG-co-lactide) dimethacrylate polymers in pH-neutralised water over 14 weeks at 37 °C were assessed using a combination of gravimetrical, FT-IR, pH and mechanical analyses.

The early rate of polymer degradation was faster than expected for pure PLA suggesting that the ester / methacrylate and ether / ester bonds may degrade more rapidly than the ester / ester bonds.   Incompletely degraded poly(methacrylic-co-lactic acid) fragments were initially released upon immersion in water with the hydrophobic PPG largely remaining in the discs.

The polymethacrylate block length determines the number of degradable poly(PG-co-lactide) chains that crosslink them to other polymethacrylate blocks.   It was proposed that the higher initial static modulus observed on decreasing initiator concentration from 2 to 0.5 wt% was due to increased polymethacrylate block lengths.   The longer polymethacrylate blocks would also mean a higher number of ether / ester or ester / methacrylate bonds that require scission before erosion could occur.   This was used to explain a slower degradation but fuller hydrolysis of the ester/ ester bonds prior to any fragment release with lower initiator concentration.

Decreasing monomer length and increasing methacrylate end group termination (i.e. polymers of PPG 425 g/mol) increased the number of methacrylate groups per unit volume and hence crosslinking density and consequent stiffness of the polymerised material.   This resulted in limited expansion and better controlled water sorption of the material.   As material degraded, water replaced the material loss in the matrix and volume

was maintained or increased except in the case of one polymer P7L2DMA. With P7L2DMA degradation product release was almost linear with time.

In addition, decreasing monomer length raised the concentration of ester / methacrylate and ether / ester bonds and caused faster polymerisation which was associated with shorter polymethacrylate block lengths. Both these factors were proposed to contribute to faster degradation of the crosslink chains, production of shorter fragmentation products and faster erosion. Polymer erosion could also be enhanced by high water sorption which could allow faster diffusion of fragmentation products out of the polymer and possibly also greater reaction within the bulk of the samples. At 14 wks polymer mass loss was, on average for the two initiator levels, 60 wt% for P7L8DMA and 19 wt% for P7L2DMA. With reduced crosslinking through degradation and water sorption, however, these polymers lost on average 80 % of their stiffness within 2 weeks in water. The results suggested that erosion rate in polymers with long PPG length was further limited by the increased molecular weight of the hydrophobic PPG left in the sample surfaces after initial surface degradation. With these samples 14-week polymer loss was only 11 wt% for P17L4DMA and 7 wt% for P34L2DMA. Their decline in stiffness in water was however slower losing on average 50 % of their elastic modulus by 2 weeks.

7.3   Drug release- summary

Drug release from the five ABA poly(PG-co-lactide) dimethacrylate polymers in pH-neutralised water at 37 °C was investigated over 10 weeks for specimens containing CDA, and over 18 weeks for specimens containing ketoprofen or prednisolone. Drug

release and degradation characteristics were assessed using UV/vis spectroscopy and gravimetrical and pH analyses respectively.

Initial water sorption was faster with specimens containing the more water soluble drugs CDA and prednisolone due to an increased internal osmotic pressure within the material. With ketoprofen, particles were miscible with the monomers producing translucent specimens with relatively less water sorption. As with undoped samples in the above degradation study, decreasing monomer length and increasing methacrylate endcapping percentage raised polymer crosslink density and gave restricted expansion but better controlled water sorption. With the short PPG polymers degradation was faster which in the case of P7L8DMA was further enhanced by its high water sorption.

Despite less water uptake, polymer erosion and acid release were faster possibly as a result of acid catalysis with specimens containing acidic ketoprofen than with those containing prednisolone or basic CDA. Higher drug release could allow increased formation of pores inside the matrix and thereby greater movement of degradation products such that acid release with prednisolone-containing specimens was comparatively higher than with CDA. With CDA, acid release due to polymer degradation products could be neutralised.

Drug release with all three drugs was biphasic. Release profiles can be affected by the physicochemical properties and loading dose of the drug as well as polymer molecular weight and methacrylate / crosslinking density. With specimens containing CDA, drug dissolution and diffusion were enhanced by high water sorption which occurred on increasing monomer length and reducing crosslinking. With this drug, release was further facilitated with increased channel formation upon the material releasing a higher drug

level. Diffusion through the polymer rather than erosion appeared to be the primary rate limiting factor for drug release with CDA.

Release of ketoprofen was by contrast affected more by polymer-erosion as the hydrophobic drug was likely to remain with the degraded hydrophobic PPG segments within the matrix. With this drug, release could only be fast with rapid-eroding, high water-absorbing polymers (e.g.P7L8DMA).

Release of prednisolone showed a profile similar to that of CDA being strongly affected by polymer swelling and diffusion through the polymer rather than erosion rate-controlled. With prednisolone, however, percentage drug release was lower at 10 wt% than at 2.5 wt% drug level. This might be due to the restricted aqueous solubility of the prednisolone resulting in saturation of any water within the polymer and thereby limiting release. On average, however, percentage prednisolone release was higher than that with the other two drugs which could be due to a combination of relatively higher water uptake and faster drug dissolution. Ten-week release was, on average for all polymer samples, 91 %, 51 % and 55 % for prednisolone, CDA and ketoprofen respectively.

7.4   Polymer composites- summary

Poly(PG-co-lactide) dimethacrylate composites were produced using the monomer P17L4DMA with 67 wt% of three phosphate fillers. Methacrylate photo-curing kinetics were assessed using FTIR and Raman spectroscopy. Dimensional stability, degradation kinetics, chemical homogeneity and modulus of the fully polymerised materials in water were quantified over 10 weeks, via gravimetric, pH, ion chromatography, Raman mapping and dynamic mechanical analysis. Formulation F1 contained no filler but F2 and F3,

phosphate glass particles, $(P_2O_5)_{0.45}(CaO)_x(Na_2O)_{0.55-x}$ with x equal to 0.3 or 0.4 respectively. The filler for composite F4 was a reactive mixture of equimolar β-tricalcium phosphate (β-TCP) and monocalcium phosphate monohydrate (MCPM).

Methacrylate groups in F4 were 60 % polymerised but in F1, F2 and F3 over 80 % reacted by 80 s of blue light exposure at 37 °C. Addition of fillers increased water sorption-induced swelling but the effect was less with F4 than F2 and F3. Water sorption enabled release of over 80 wt% of the phosphate glasses in F2 and F3 within 3 and 7 days respectively leaving polymeric structures with water filled holes of comparable dimensions to the original fillers. Conversely with F4, water sorption caused an order of magnitude increase in the material modulus in comparison with either the dry sample, or the other three formulations. This suggested, with the degradation and Raman map studies, that a hydrogen ion exchange reaction between the two fillers rather than release is encouraged by water sorption. In 10 weeks 8 wt% of F1 had eroded giving acidic products. Filler addition reduced the rate of polymer erosion in F2 and F3 but increased it by four fold with F4. Despite the more rapid polymer degradation, simultaneous filler release from the surface of F4 was able to buffer the storage solution pH.

7.5 Overall conclusion

In this project fluid poly(PG-co-lactide) dimethacrylate monomers have been produced that can photocrosslink rapidly and completely on blue light exposure if the PG and lactide segments are kept short. Initiator concentrations of 0.5 wt% are preferable to 2 wt% to prevent possible incomplete cure of thicker specimens. Through reducing the monomer length the polymers can change from highly flexible to semi rigid rubbers.

Degradation behaviour can be modified via changing the monomer structure producing polymers that could degrade linearly with time and exhibit good dimensional stability as in P7L2DMA. Drug release can be controlled by varying monomer composition and drug loading level. The rapidly swellable long polymers may be preferred for use as the drug delivery vehicles when diffusion is the rate limiting step for drug release, whereas the fast eroding short polymers may be a better choice when polymer erosion is the factor controlling drug release.

Improved polymer properties have been obtained by adding calcium phosphate fillers at high levels. This was achieved without losing the rapid set advantage of the methacrylate. The addition of highly soluble phosphate glasses provide a means to develop porosity of controllable level and structure whilst additionally providing the elements that are required for bone formation. Replacement of phosphate glass with β-TCP and MCPM filler can increase the modulus of the polymer by an order of magnitude upon water sorption because of reaction between the fillers. These β-TCP and MCPM fillers additionally act as a buffer neutralising the acidic degradation products of the polymer and raise its erosion rate significantly.

This project has demonstrated the potential of these poly(PG-co-lactide) dimethacrylate monomers as injectable and biodegradable adhesives or implants for tissue engineering and controlled drug release applications. Use of phosphate glass of different compositions, in combination with calcium phosphates would no doubt enable further manipulations of the polymer / composite properties and allow tailor-made materials to be fabricated to suit different applications.

7.6   Future work

7.6.1   Chemical Curing system

The monomers in this study have been polymerised with the use of the photoinitiator, CQ, upon blue light exposure within a couple of minutes. Light curing, however, is impractical for use in deep crevices in some bones. A chemical means of polymerising these monomers could include using chemical initiators and activators such as benzoyl peroxide and DMPT. Use of a combination of light and chemical cure can also be studied.

7.6.2   Composite formulations

Addition of fillers to different monomers should also be studied in order to assess if improved modulus or composite erosion linear with time can be made using monomer formulations that by themselves are more rigid and have a linear degradation profile. In addition, phosphate glass fillers of varying compositions having different dissolution properties or β-TCP and MCPM fillers of varying ratios should be incorporated into the monomers in order to produce composites of controllable porosity, swelling ratio and moderate decline in stiffness with time.

7.6.3   Cell attachment studies

Biocompatibility of the monomers can be assessed by evaluating whether cells e.g. osteoblast-like cells can attach and proliferate successfully on the polymer surfaces. Incorporation of osteoinductive proteins and peptides, such as recombinant growth factors

and bone morphogenetic proteins into the polymers could be studied in order to further enhance tissue cellular growth.

7.6.4 Monomer composition and Stereolithography

Figure 7.1 shows an image of a 3-D object produced with P17L4DMA (batch no 091104) using stereolithography. Using images obtained from X-ray, NMR or ultrasonic tornography and advanced computer software, images of missing structures in a patient can be produced. The monomers in this study can then be converted via rapid prototyping stereolithography into 3-D implants of the images (247). In this way complex implant dimensions and structure can be made for individual patients and medical problems.

Furthermore, multicrosslinking monomers can also be produced through replacement of PPG with tetra functional pentaerythritol [C(CHOH)$_4$] and various polyvinylalcohols in order to gain greater control over mechanical, water sorption and degradation properties of the final polymer without compromising fluidity required for both injectable cements and stereolithography methods. Combinations of formulations in different ratios can also be experimented with to give materials suitable for different clinical applications in both implant and injectable adhesive form.

Figure 7.1. **Implant (ca. 4x 6 mm) produced with P17L4DMA and the photoinitiator Irgacure 651™ (2,2-dimethoxy-2-phenylacetophenone) after exposure to UV light at 325 nm using stereolithography. (Courtesy of Dr. Alexander Evseev and Dr. Michail Markov at Institute of Laser and Information Technologies, Russian Academy of Sciences, Moscow).**

7.6.5 DNA delivery

DNA has previously been incorporated within similar polymers to those in this study to produce controlled delivery systems for gene therapy (196;248-250), or alternatively entrapped within calcium phosphate as nanoparticles (<100 nm) (GeneCaP) (251;252). The polymers in this study could therefore be further studied as a DNA delivery device for controlled release of gene-containing calcium phosphate nanoparticles. Using the reactive calcium phosphate fillers, for example, the DNA can become entrapped within the calcium phosphates as they dissolve and re-precipitate as brushite (as occurs upon precipitation of DNA-calcium phosphate mixtures via water-in-oil microemulsions (250)). The gene-containing nanoparticles can be dispersed directly within the fluid monomers. Placement of genes within the calcium phosphate nanoparticles would provide a means to protect the DNA from free radicals or acid produced during polymer curing or degradation. Through modification of the monomer used, release rate of the

entrapped nanoparticles could be controlled. If the DNA is then released with the calcium

phosphate its uptake by cells could also be improved and it would also be better protected

from degradative enzymes and acid as it traverses across the cell to the nucleus.

8 Appendices

8.1   Appendix 1: Polymer composites-supporting evidence for F4

8.1.1   Background

In Chapter 6 the composite formulation F4 contained the monomer P17L4DMA and an equimolar powder mixture of β-tricalcium phosphate (β-TCP) and monocalcium phosphate monohydrate (MCPM). These two particular phosphates, when placed in water, dissolve and re-precipitate forming lower density dicalcium phosphate dihydrate (i.e. DCPD also known as brushite). Evidence suggesting that water sorption-induced chemical processes had occurred after the composite F4 was placed in water included (i) Raman spectra at 4 days showed reduction in MCPM and β-TCP regions in the Raman maps; (ii) large increase in modulus after placement in water; and (iii) water content increased throughout the whole 10 week study period indicating consumption of water. Conclusive proof for the formation of the brushite species between MCPM and β-TCP in the sample F4, however, had not been obtained.

Since the completion of this project, continuing research conducted within the department on the sample F4 by Dr Anne Young has provided supporting evidence for the formation of brushite within the polymer matrix after submersion in water. The results will be discussed briefly in the following.

8.1.2   Analytical methods

Surface hardness

Indentation depth for the polymer F1 and composite F4 were determined in water using a Wallace hardness indentation test at the following time points: 0, 10 and 30 mins,

1, 2, 2.5 and 18 hours, 1, 2, 3, 6, 10 and 13 days. A specimen of each formulation was placed in 10 ml deionised water incubated at 37 °C. At each time point, the specimen was removed from the water and blotted dry with tissue paper. A 300 g load using a Wallace indentation hardness tester was applied onto the surface of the specimen and the indentation depth measured. Eight readings, four on each side of the specimen, were taken.

Scanning electron microscopy and EDAX

Scanning electron microscopy (SEM) images and energy dispersive X-ray (EDAX) analysis (with the aid of Nicky Mordan at the Eastman Dental Institute) were obtained for the composite F4 when dry and after submersion in water for 2 weeks. SEM images allow the topographies of the specimen to be inspected at high magnifications while EDAX analysis enables the elemental composition of an area of the specimen to be identified. The specimen was split into slices longitudinally. The cut specimen was fixed in 3% (v/v) gluteraldehyde at 4 °C overnight, then dehydrated with alcohol, followed by coating with gold and palladium (Polaron E5000 sputter coater) prior to examination of the cut surface with SEM (Cambridge 90B, Leica) equipped with EDAX analysis (Inca 300, Oxford Instruments Analytical). Five SEM images of different areas on the specimen cut surface were taken, within each image 32 EDAX spectra were obtained producing in total of 160 points of EDAX analysis. At each point the ratio of the elements calcium to phosphorus (Ca/P) was calculated, and mean, standard deviation and 95 % confidence interval (i.e. 2* s/ √n) obtained.

X-ray diffraction

X-ray diffraction (XRD) patterns, which allow the type of crystal structure and the spacing between atoms to be determined, were obtained for the composite F4 when dry and after 24 hours in water by Professor Jonathan. Knowles. An X-ray diffraction pattern is obtained when a crystal diffracts an X-ray beam passing through it to produce beams at specific angles depending on the X-ray wavelength, the crystal orientation, and the structure of the crystal. The specimen was placed in an X-ray diffractometer (Philips PW1780), and the data was collected using Cu K_α radiation. Data was collected from $10°$ to $40° 2\theta$ with a step size of $0.02°$ and a count time of 12 seconds. The crystallised phases were identified using the Crystallographica Search-Match software (Oxford Cryosystems, Oxford, UK) and the International Centre for Diffraction Data (ICDD) database (volumes 1 – 45).

8.1.3 Results and discussion

Surface hardness

Figure 8.1 presents the indentation depth as a square root of time for the polymer F1 and the composite F4. The level of penetration of the weight into the specimen was much greater with the polymer than the composite. The initial increase in depth for both the polymer and composite is linear with the square root of time, and occurs because of a decrease in surface hardness, arising with water sorption. After the first 24 hours, however, the surface hardness became stable despite further water sorption and degradation of the composite.
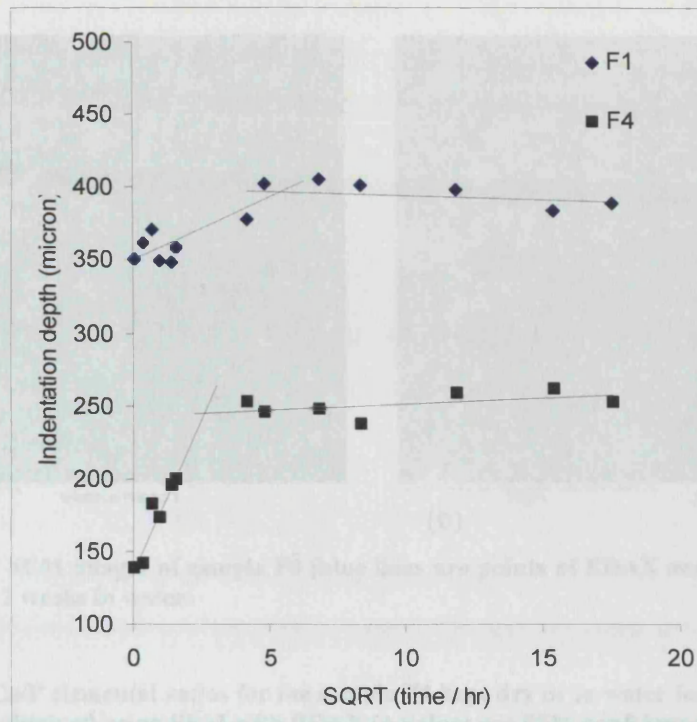
Figure 8.1. Wallace hardness indentation depth as a function of the square root of time for polymer F1 and composite F4.

Scanning electron microscopy and EDAX

From SEM images it can be seen that after placement in water the particles in the composite F4 are finer (Figure 8.2). From EDAX analysis results (Table 8.1) the dry sample particles were found to have larger scatter of Ca/P ratios with values tending to 1.5 or 0.5 as expected for either β– TCP [β-Ca$_3$(PO$_4$)$_2$]or MCPM [Ca(H$_2$PO$_4$)$_2$.H$_2$O] respectively. After 2 weeks in water the Ca/P ratio, although not significantly different on average throughout the composite, was observed to have a much narrower standard deviation as expected with reaction of β-TCP and MCPM to form brushite. The Ca/P ratio is close to 1 (4 CaHPO$_4$. 2H$_2$O) as expected for brushite.
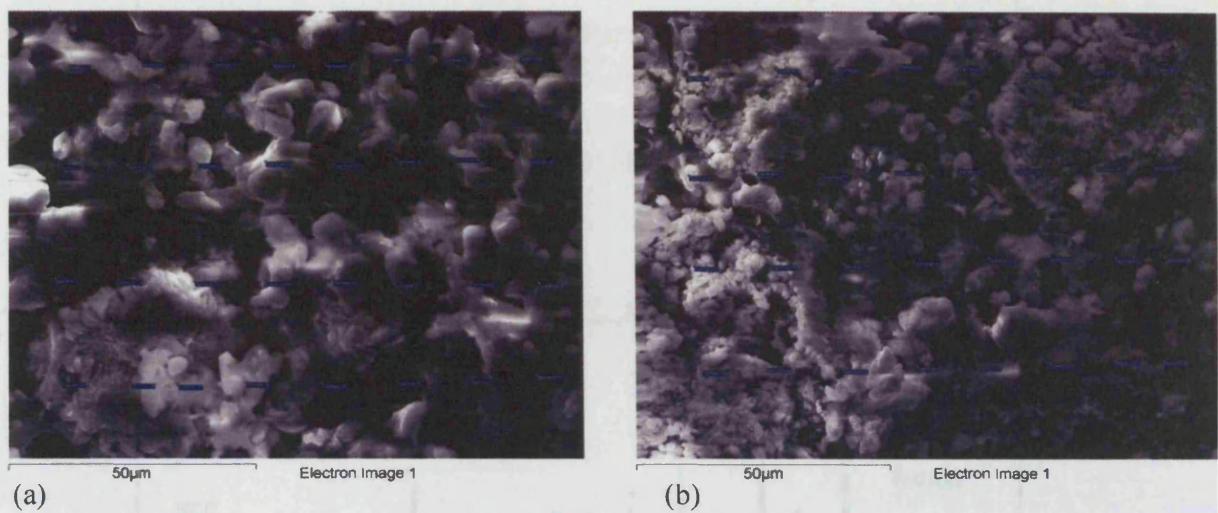
Figure 8.2. Example SEM images of sample F4 (blue lines are points of EDAX analysis for Table 8.1 (a) dry and (b) after 2 weeks in water

Table 8.1. Average Ca/P elemental ratios for the sample F4 kept dry or in water for 2 weeks and their standard deviations obtained using SEM with EDAX (± values are 95% confidence intervals obtained using 5 images (see for example Figure 8.2) for each specimen with a total of 160 measurements)

	Mean Ca/ P	Standard deviation
Dry	1.24 ± 0.12	0.63
After 2 weeks in water	1.16 ± 0.05	0.31

X-ray diffraction

Figure 8.3 shows the XRD patterns obtained for the composite F4 when dry and after 24 hours in water. The presence of MCPM, β-TCP and brushite in the specimen were identified by comparing the XRD patterns with patterns in the ICDD Database (vols 1 – 45). From X-ray diffraction data it is clear that when the specimen was dry only β-TCP and MCPM particles were present. After 24 hours in water, however, a large proportion of the fillers in the composite were converted into brushite, although some β-TCP was still present. The presence of monetite (dicalcium phosphate anhydrate, DCPA) has been attributed to the dehydration of the brushite crystals (245).
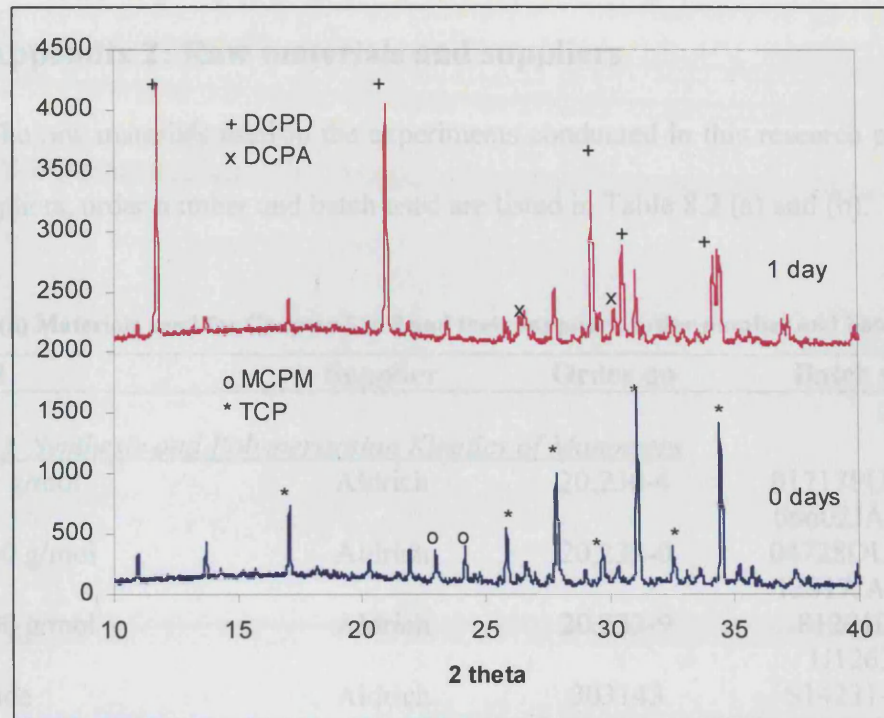
Figure 8.3. XRD spectra of composite specimen F4 initially and after 24 hours in water. Peaks that match those of monocalcium phosphate monohydrate (MCPM), β-tricalcium phosphate (TCP), dicalcium phosphate dihydrate (DCPD, brushite), and dicalcium phosphate anhydrate (DCPA, monetite) are marked with symbols correspondingly.

8.1.4 Conclusion

Data obtained form surface hardness, EDAX with SEM, and XRD patterns have provided further evidence that the filler particles β-TCP and MCPM react within the fully polymerised composite. This occurs when water is absorbed and results in brushite formation that affects the polymer mechanical and degradation properties described in Chapter 6.

8.2   Appendix 2: Raw materials and suppliers

The raw materials used in the experiments conducted in this research project, and

their suppliers, order number and batch used are listed in Table 8.2 (a) and (b).

Table 8.2 (a) Materials used for Chapter 3 to 5 and their suppliers, order number and batch number.

Material	Supplier	Order no	Batch no.
Chapter 3 Synthesis and Polymerisation Kinetics of Monomers			
PPG 425 g/mol	Aldrich	20,230-4	01717PU-413
			06602JA-273
PPG 1000 g/mol	Aldrich	20,232-0	04728DU-462
			13817JA-413
PPG 2000 g/mol	Aldrich	20,233-9	81201012
			U12634
D,L-lactide	Aldrich	303143	S14231-263
Glycolide	Purasorb	Special order	0305000324
TEA (99 %)	Aldrich		00210008
MAC (≥ 97 %)	Fluka	64120	5338/1
CQ (97 %)	Aldrich	124893	1935799
DMPT	Aldrich	D18900-6	C109103TU
HEMA (99 %)	Aldrich	477028	09020TA
Dichloromethane (99.6 %)	Aldrich	43318-7	U05780
			U00507
Hexane	Aldrich	270504	-
Deuterated chloroform (99.9 atom%)	Aldrich	151823	
Acetone	BDH	152966P	-
Propan-2-ol	BDH		-
Stannous Octoate	Sigma	S-3252	18H0666
Chapter 4 Polymer Degradation			
CQ (97 %)	Aldrich	12489-3	1935799
DMPT	Aldrich	D18900-6	C109103TU
HEMA (99%)	Aldrich	477028	09020TA
Chapter 5 Drug release			
Chlorhexidine diacetate	Sigma	C6143	19H0417
Ketoprofen	Sigma	K1751	043K0684
Prednisolone	Sigma	P-6004	102K1460
CQ	Aldrich	12489-3	0029282
DMPT	Aldrich	D18900-6	C109103TU
HEMA	Aldrich	477028	09020TA

Table 8.3 (b) Materials used for Chapter 6 and their suppliers, order number and batch number.

Material	Supplier	Order no	Batch no.
Chapter 6 Polymer Composites			
$(P_2O_5)_{0.45}(CaO)_{0.30}(Na_2O)_{0.25}$	See (i)		
$(P_2O_5)_{0.45}(CaO)_{0.40}(Na_2O)_{0.15}$	See (i)		
β-TCP	See (ii)		
MCPM	See (ii)		
CQ	Aldrich	12489-3	0029282
DMPT	Aldrich	D18900-6	C109103TU
HEMA	Aldrich	477028	09020TA

(i)   Made by Dr Ifty Ahmed, the Eastman Dental Institute, UCL

(ii)   Supplied by Dr Mike Hoffman, Birmingham University and Dr Uwe Gbureck, University of Wurzburg, Germany

Abbreviations:

PPG	Poly(propylene glycol)
TEA	Triethylamine
MAC	Methacryloyl chloride
CQ	Camphorquinone
DMPT	N,N-dimethyl-p-toluidine
HEMA	Hydroxyethyl methacrylate
$(P_2O_5)_{0.45}(CaO)_{0.30}(Na_2O)_{0.25}$	Ternary phosphate glass containing 45 mol% P_2O_5, 30 mol% CaO and 25 mol% Na_2O
$(P_2O_5)_{0.45}(CaO)_{0.40}(Na_2O)_{0.15}$	Ternary phosphate glass containing 45 mol% P_2O_5, 40 mol% CaO and 15 mol% Na_2O
β-TCP	β- tricalcium phosphate
MCPM	Monocalcium phosphate monohydrate

8.3   Appendix 3: List of presentations and publications

1. <u>S.M. Ho</u>, J.C. Knowles, A.M. Young. *Characterisation of injectable biodegradable methacrylate/calcium phosphate composites*
Poster, 1ˢᵗ Annual Biomaterials Workshop, Cranfield University. Shrivenham.   Mar. 2003

2. <u>S.M. Ho.</u> *Injectable biodegradable methacrylate polymers for bone tissue engineering and drug delivery applications*
Oral presentations at
UK Society of Biomaterials Conference, Brighton.   July 2004
EPSRC Summer School on Cell Interaction in Tissue Engineering, Nottingham.   Sept. 2004

3. A.M. Young, D. Leung, <u>S.M. Ho</u>, Y.T. Sheung, J. Pratten, D. Spratt. *New injectable antibacterial polymers for bone and tooth repair.*
Book chapter, Medical Polymers 2004. Shawbury: Rapra Technology Ltd.   Nov. 2004

4. <u>S.M. Ho</u>, A.M. Young. *Reaction kinetics and degradation behaviour of injectable biodegradable ABA triblock poly(lactide- co-propylene glycol-co-lactide) methacrylate polymers for bone tissue engineering.*
Poster, 2ⁿᵈ World Congress on Regenerative Medicine, Leipzig, Germany.   May 2005

5. <u>S.M. Ho</u>, A.M. Young. *Synthesis, polymerisation and degradation of poly(lactide-co-propylene glycol) dimethacrylate adhesives*
Journal, European Polymer Journal; 42: 1775-1785   May 2006

6. <u>S.M. Ho</u>, A.M. Young. *Reactive calcium phosphate fillers for biodegradable polymers.*
European Patent application submitted.   June 2006

7. <u>S.M. Ho</u>, I. Ahmed, S.N. Nazhat, A.M. Young. *Degradation behaviour and ion release characteristics of injectable oligo (lactic acid-co-propylene glycol) methacrylate composites.*
Journal, in preparation.   2006

9 References

Reference List

(1)   Gunatillake PA, Adhikari R. Biodegradable synthetic polymers for tissue engineering. European Cells and Materials 2003; 5:1-16.

(2)   http://www.who.int/world-health-day/2004/en/traffic_facts_en.pdf. 2004. World Health Organisation.
Ref Type: Internet Communication

(3)   https://www.nos.org.uk/osteo.asp. 2004.   The National Osteoporosis Society.
Ref Type: Internet Communication

(4)   Langer R, Vacanti JP. Tissue Engineering. Science 1993; 249:1527-1532.

(5)   James K, Kohn J. New biomaterials for tissue engineering. MRS Bulletin 1996; 21:22-26.

(6)   Sipe JD. Tissue engineering and reparative medicine. Annual New York Academy of Sciences 2002; 961:1-9.

(7)   Einhorn TA. Clinically applied models of bone regeneration in tissue engineering research. Clinical Orthopaedics and Related Research 1999; 1(367S):S59-S67.

(8)   Stevens MP. Basic principles. Polymer Chemistry: An Introduction. New York: Oxford University Press Inc., 1999: 3-34.

(9)   Hollinger JO, Battistone GC. Biodegradable Bone Repair Materials. Clinical Orthopaedics and Related Research 1986; 207:290-305.

(10) Rubinstein M, Colby RH. Introduction. Polymer Physics. Oxford: Oxford University Press, 2003: 1-45.

(11) Middleton JC, Tipton AJ. Synthetic biodegradable polymers as orthopedic devices. Biomaterials 2000; 21(23):2335-2346.

(12) Stevens MP. Chemical structure and polymer morphology. Polymer Chemistry: An Introduction. New York: Oxford University Press Inc., 1999: 61-95.

(13) Temenoff JS, Mikos AG. Injectable biodegradable materials for orthopedic tissue engineering. Biomaterials 2000; 21(23):2405-2412.

(14) Hendriks JGE, Van Horn JR, Van Der Mei HC, Busscher HJ. Backgrounds of antibiotic-loaded bone cement and prosthesis-related infection. Biomaterials 2004; 25:545-556.

(15) An YH, Woolf SK, Friedman RJ. Pre-clinical in vivo evaluation of orthropaedic bioabsorbable devices. Biomaterials 2000; 21:2635-2652.

(16) Jain RA. The manufacturing techniques of various drug loaded biodegradable poly(lactide-co-glycolide) (PLGA) devices. Biomaterials 2000; 21:2475-2490.

(17) Chung I, Xie D, Puckett AD, Mays JW. Synthesis and evaluation of biodegradable multifunctional polymer networks. European Polymer Journal 2003; 39:1817-1822.

(18) Domb AJ, Elmalak O, Shastri VR, Ta-Shma Z, Masters DM, Ringel I et al. Polyanhydrides. In: Domb AJ, Kost J, Wiseman DM, editors. Handbook of Biodegradable Polymer. Amsterdam: Overseas Publishers Association, 1997: 135-159.

(19) Rosen HB, Chang J, Wnek GE, Linhardt RJ, Langer R. Bioerodible polyanhydrides for controlled drug delivery. Biomaterials 1983; 4(2):131-133.

(20) Peter SJ, Miller MJ, Yaszemski MJ, Mikos AG. Poly(propylene fumarate). In: Domb AJ, Kost J, Wiseman DM, editors. Handbook of Biodegradable polymers. Amsterdam: Overseas Publishers Association, 1997: 87-97.

(21) Domb AJ, Manor N, Elmalak O. Biodegradable bone cement compositions based on acrylate and epoxide terminated poly(propylene fumarate) oligomers and calcium salt compositions. Biomaterials 1996; 17:411-417.

(22) Vehof JWM, Fisher JP, Dean D, Van Der Waerden JCM, Spauwen PHM. Bone formation in transforming growth factor b-1-coated porous poly(propylene fumarate) scaffolds. Journal of Biomedical Materials Research 2002; 60:241-251.

(23) Frazier DD, Lathi VK, Gerhart TN, Hayes WC. Ex vivo degradation of a poly(propylene glycol-fumarate) biodegradable particulate composite bone cement. Journal of Biomedical Materials Research 1997; 35:383-389.

(24) Hedberg EL, Shih CK, Lemoine JJ, Timmer MD, Liebschner MAK, Jansen JA et al. In vitro degradation of porous poly(propylene fumarate)/ poly(DL-lactic-co-glycolic acid) composite scaffolds. Biomaterials 2005; 26:3215-3225.

(25) Passuti N, Gouin F. Antibiotic-loaded bone cement in orthopedic surgery. Joint Bone Spine 2003; 70:169-174.

(26) Kuhn K-D. Bone Cements. New York: Springer-Verlag, 2000.

(27) Leenslang JW, Pennings AJ, Ruud RM, Rozema FR, Boering G. Resorbable materials of poly(L-lactide). VI. Plates and screws for internal fracture fixation. Biomaterials 1987; 8:70-73.

(28) Kellomaki M, Niiranen H, Puumanen K, Ashammakhi N, Waris T, Tormala P. Bioabsorbable scaffolds for guided bone regeneration and generation. Biomaterials 2000; 21:2495-2505.

(29) Hutmacher DW. Scaffolds in tissue engineering bone and cartilage. Biomaterials 2000; 21:2529-2543.

(30) Gross KA, Rodriguez-Lorenzo LM. Biodegradable composite scaffolds with an interconnected spherical network for bone tissue engineering. Biomaterials 2004; 25:4955-4962.

(31) Chang CH, Lin FH, Lin CC, Chou CH, Liu HC. Cartilage tissue engineering on the surface of a novel gelatin-calcium-phosphate biphasic scaffold in a double-chamber bioreactor. Journal of Biomedical Materials Research Part B: Applied Biomaterials 2004; 71B(2):313-321.

(32) Saito N, Murakami N, Takahashi J, Horiuchi H, Ota H, Kato H et al. Synthetic biodegradable polymers as drug delivery systems for bone morphogenetic proteins. Advanced Drug Delivery Reviews 2005; 57:1037-1048.

(33) Madsen S, Mooney DJ. Delivering DNA with polymer matrices: applications in tissue engineering and gene therapy. Pharmaceutical Science & Technology Today 2000; 3(11):381-384.

(34) Fernandez M, Parra J, Vazquez B, Lopez-Bravo A, San Roman J. Self-curing controlled release systems for steroids. Application of prednisolone-based polymeric systems to ear diseases. Biomaterials 2005; 26:3311-3318.

(35) Takaoka K, Miyamoto S, Saito N, Okada T. New synthetic degradable polymers as carrier materials for BMP. In: Wise DL, Tarantolo DJ, Lewandrowski K, Gresser JD, Cattanio MV, Yaszemski MJ, editors. Biomaterials Engineering and Devices: Human Applications, Volume 1. New Jersey: Humana Press Inc., 2000: 239-249.

(36) Athanasou NA. Colour Atlas of Bone, Joint, and Soft Tissue Pathology. Oxford University Press, 1999.

(37) Jackson DW, Simon TM. Tissue engineering principles in orthopaedic surgery. Clinical Orthopaedics and Related Research 1999; 1(367S):S31-S45.

(38) Caplan AI, Elyaderani M, Mochizuki Y, Wakitani S, Goldverg VM. Overview: principles of cartilage repair and regeneration. Clinical Orthopaedics and Related Research 1997; 1(342):254-269.

(39) Anseth KS, Metters AT, Bryant SJ, Martens PJ, Elisseeff JH, Bowman CN. In situ forming degradable networks and their application in tissue engineering and drug delivery. Journal of Controlled Release 2002; 78:199-209.

(40) Bergsma JE, de Bruijn WC, Rozema FR, Bos RRM, Boering G. Late degradation tissue response to poly(-lactide) bone plates and screws. Biomaterials 1995; 16(1):25-31.

(41) Muggli DS, Burkoth AK, Anseth KS. Crosslinked polyanhydrides for use in orthopedic applications: Degradation behavior and mechanics. Journal of Biomedical Materials Research 1999; 46(2):271-278.

(42) Burg KJL, Porter S, Kellam JF. Biomaterial developments for bone tissue engineering. Biomaterials 2000; 21(23):2347-2359.

(43) Capes JS, Ando HY, Cameron RE. Fabrication of polymeric scaffolds with a controlled distribution of pores. Journal of Materials Science:Materials in Medicine 2005; 16:1069-1075.

(44) Itoh H., Aso Y., Furuse M., Noishiki Y., Miyata T. A Honeycomb Collagen Carrier for Cell Culture as a Tissue Engineering Scaffold. Artificial Organs 2001; 25(3):213-217.

(45) Gresser JD, Nagaoka HX, Trantolo DJ, Gangadharam PRJ, Hsu YY, Wise DL. Incorporation of active agent into biodegradable cement. In: Wise DL, Tarantolo DJ, Lewandrowski K, Gresser JD, Cattanio MV, Yaszemski MJ, editors. Biomaterials Engineering and Devices: Human Applications, volume 1. New Jersey: Humana Press Inc., 2000: 225-237.

(46) Saito N, Okada T, Toba S, Miyamoto S, Takaoka K. New synthetic absorbable polymers as BMP carriers: plastic properties of poly-D,L-lactic acid-polyethylene glycol block copolymers. Journal of Biomedical Materials Research 1999; 47:104-110.

(47) Witt C, Mader K, Kissel T. The degradation, swelling and erosion properties of biodegradable implants prepared by extrusion or compression moulding of poly(lactide-co-glycolide) and ABA triblock copolymers. Biomaterials 2000; 21:931-938.

(48) Kim YJ, Choi S, Koh JJ, Lee M, Ko KS, Kim SW. Controlled release of insulin from injectable biodegradable triblock copolymer. Pharmaceutical Research 2001; 18:548-550.

(49) Cleek RL, Ting KC, Eskin G, Mikos AG. Microparticles of poly(-lactic-co-glycolic acid)/poly(ethylene glycol) blends for controlled drug delivery. Journal of Controlled Release 1997; 48(2-3):259-268.

(50) Wang EA, Rosen V, D'Alessandro JS, Bauduy M, Cordes P, Harada T et al. Recombinant Human Bone Morphogenetic Protein Induces Bone Formation. Proceedings of the National Academy of Sciences of the United States of America 1990; 87(6):2220-2224.

(51) Gopferich A, Tessmar J. Polyanhydride degradation and erosion. Advanced Drug Delivery Reviews 2002; 54:911-931.

(52) Huang X, Brazel CS. On the importance and mechanisms of burst release in matrix-controlled drug delivery systems. Journal of Controlled Release 2001; 73:121-136.

(53) Griffith LG. Polymeric biomaterials. Acta Materialia 2000; 48:263-277.

(54) Kaneko TS, Bell JS, Pejcic MR, Tehranzadeh J, Keyak JH. Mechanical properties, density and quantitative CT scan data of trabecular bone with and without metastases. Journal of Biomechanics 2004; 37(4):523-530.

(55) Okada M. Chemical syntheses of biodegradable polymers. Progress in Polymer Science 2002; 27:87-133.

(56) Riggs PD, Braden M, Patel M. Chlorhexidine release from room temperature polymerising methacrylate systems. Biomaterials 2000; 21:345-351.

(57) Wu N, Wang LS, Tan DCW, Moochhala SM, Yang YY. Mathematical modeling and in vitro study of controlled drug release via a highly swellable and dissoluble polymer matrix: polyethylene oxide with high molecular weights. Journal of Controlled Release 2005; 102:569-581.

(58) Jeong B, Bae YH, Kim SW. Drug release from biodegradable injectable thermosensitive hydrogel of PEG-PLGA-PEG triblock copolymers. Journal of Controlled Release 2000; 63:155-163.

(59) Hedberg EL, Tang A, Crowther RS, Carney DH, Mikos AG. Controlled release of an osteogenic peptide from injectable biodegradable polymeric composites. Journal of Controlled Release 2002; 84(3):137-150.

(60) Lou X, Munro S, Wang S. Drug release characteristics of phase separation pHEMA sponge materials. Biomaterials 2004; 25:5071-5080.

(61) Hentze HP, Antonietti M. Porous polymers and resins for biotechnological and biomedical applications. Reviews in Molecular Biotechnology 2002; 90:27-53.

(62) Chen F, Chen S, Tao K, Feng X, Liu Y, Lei D et al. Marrow-derived osteoblasts seeded into porous natural coral to prefabricate a vascularised bone graft in the shape of a human mandibular ramus: experimental study in rabbits. British Journal of Oral Maxillofacial Surgery 2004; 42(6):532-537.

(63) Kose GT, Ber S, Korkusuz F, Hasirci V. Poly(3-hydroxybutyric acid-co-3-hydroxyvaleric acid) based tissue engineering matrices. Journal of Materials Science:Materials in Medicine 2003; 14(2):121-126.

(64) Perren SM, Gogolewski S. Clinical requirements fro bioresorbable implants in internal fixation. In: Leung KS, Hung LK, Leung PC, editors. Biodegradable Implants in Fracture Fixation. Hong Kong: Department of Orthopaedics and Traumatology, The Chinese University of Hong Kong, 1994: 35-44.

(65) Peter SJ, Miller ST, Zhu G, Yasko AW, Mikos AG. In vivo degradation of a poly(propylene fumarate)/b-tricalcium phosphate injectable composite scaffold. Journal of Biomedical Materials Research 1998; 41(1):1-7.

(66) Peter SJ, Kim P, Yasko AW, Yaszemski MJ, Mikos AG. Crosslinking characteristics of an injectable poly(propylene fumarate)/ b-tricalcium phosphate paste and mechanical properties of the crosslinked composite for use as a biodegradable bone cement. Journal of Biomedical Materials Research 1999; 44:314-321.

(67) Prabhakar RL, Brocchini S, Knowles JC. Effect of glass composition on the degradation properties and ion release characteristics of phosphate glass-polycaprolactone composites. Biomaterials 2005; 26:2209-2218.

(68) He S, Yaszemski MJ, Yasko AW, Engel PS, Mikos AG. Injectable biodegradable polymer composites based on poly(propylene fuamrate) crosslinked with poly(ethylene glycol)-dimethacrylate. Biomaterials 2000; 21:2389-2394.

(69) Behravesh E, Yasko AW, Engel PS, Mikos AG. Synthetic biodegradable polymers for orthopaedic applications. Clinical Orthopaedics and Related Research 1999; 1(367S):S118-S129.

(70) Corden TJ, Jones IA, Rudd CD, Christian P, Downes S. Initial development into a novel technique for manufacturing a long fibre thermoplastic bioabsrobable composite: in situ polymerisation of poly-e-caprolactone. Composites Part A: Applied Science and Manufacturing 1999; 30:737-746.

(71) Corden TJ, Jones IA, Rudd CD, Christian P, Downes S, McDougall KE. Physical and biocompatibility properties of poly-e-caprolactone produced using in situ polymerisation: a novel manufacturing technique for long-fibre composite materials. Biomaterials 2000; 21:713-724.

(72) Pascual B, Vazquez B, Gurruchaga M, Goni I, Ginebra MP, Gil FJ et al. New aspects of the effect of size and size distribution on the setting parameters and mechanical properties of acrylic bone cements. Biomaterials 1996; 17:509-516.

(73) Kharas GB, Kamenetsky M, Simantirakis J, Beinlich KC, Rizzo A-MT, Caywood GA et al. Synthesis and characterization of fumarate-based polyesters for use in bioresorbable bone cement composites. Journal of Applied Polymer Science 1997; 66(6):1123-1137.

(74) Migliaresi C, Fambri L, Kolarik J. Polymerization kinetics, glass transition temperature and creep of acrylic bone cements. Biomaterials 1994; 15:875-881.

(75) Gerhart TN, Roux RD, Horowitz G, Miller RL, Hanff P, Hayes WC. Antibiotic release from an experimental biodegradable bone cement. Journal of Orthopaedic Research 1998; 6:585-592.

(76) Perrin DE, English JP. Polyglycolide and polylactide. In: Domb AJ, Kost J, Wiseman DM, editors. Handbook of biodegradable polymers. Amsterdam: Overseas Publishers Association, 1997: 3-27.

(77) Uhrich KE, Ibim SEM, Larrier DR, Langer R, Laurencin CT. Chemical changes
      during in vivo degradation of poly(anhydride-imide)matrices. Biomaterials 1998;
      19:2045-2050.

(78) Masatsugu I, Shin-ichiro O, Teruo A, Yasuharu Y, Kazuhiko I, Nobuo N. Bone
      morphogenetic protein encapsulated with a biodegradable and biocompatible
      polymer . Journal of Biomedical Materials Research 1996; 32(3):433-438.

(79) Jeong B, Bae YH, Lee DS, Kim SW. Biodegradable block copolymers as
      injectable drug-delivery system. Nature 1997; 388:860-862.

(80) Tojo K, Aoyagi H, Kurita T. Surface dissolution-bulk erosion model of drug
      release from biodegradable polymer rods. Journal of Chemical Engineering of
      Japan 1998; 31(4):648-651.

(81) Purasorb: Monomers and Biodegradable Polymers. 2002. The Netherlands,
      PURAC Biochem.
Ref Type: Catalog

(82) Korhonen H, Helminen A, Seppala JV. Synthesis of polylactides in the presence of
      co-initiators with different numbers of hydroxyl groups. Polymer 2001;
      42(18):7541-7549.

(83) Coullerez G, Lowe C, Pechy P, Kausch HH, Hilborn J. Synthesis of acrylate
      functional telechelic poly(lactic acid) oligomer by transesterification. Journal of
      Materials Science:Materials in Medicine 2000; 11:505-510.

(84) Xu XJ, Sy JC, Shastri VP. Towards developing surface eroding poly(a-hydroxy
      acids). Biomaterials 2006; 27:3021-3030.

(85) Frank A, Rath SK, Boey F, Venkatraman S. Study of the initial stages of drug
      release from a degradable matrix of poly(d,l-lactide-co-glycolide). Biomaterials
      2004; 25:813-821.

(86) Perrin DE. Polycaprolactone. In: Domb AJ, Kost J, Wiseman DM, editors.
      Handbook of Biodegradable Polymer. Amsterdam: Overseas Publishers
      Association, 1997: 63-77.

(87) Pitt CG. Poly-e-caprolactone and its copolymers. In: Chasin M, Langer R, editors.
      Biodegradable polymers as drug delivery systems. New York: Marcel Dekker,
      1990: 71.

(88) Goraltchouk A, Freier T, Shoichet MS. Synthesis of degradable poly(l-lactide-co-
      ethylene glycol) porous tubes by liquid-liquid centrifugal casting for use as nerve
      guidance channels. Biomaterials 2005; 26:7555-7563.

(89) Geiger M, Li RH, Friess W. Collagen sponges for bone regeneration with rhBMP-
      2. Advanced Drug Delivery Reviews 2003; 55(12):1613-1629.

(90) Wallace DG, Rosenblatt J. Collagen gel systems for sustained delivery and tissue engineering. Advanced Drug Delivery Reviews 2003; 55(12):1631-1649.

(91) Bohner M. Calcium orthophosphates in medicine: from ceramics to calcium phosphate cements. Injury: International Journal of the Care of the Injured 2000; 31(S-D37):S-D47.

(92) Kuemmerle JM, Oberle A, Oechslin C, Bohner M, Frei C, Boecken I et al. Assessment of the suitability of a new brushite calcium phospate cement for cranioplasty- an experimental study in sheep. Journal of Cranio-Maxillofacial Surgery 2005; 33:37-44.

(93) Fraysinnet P, Gineste L, Conte P, Fages J, Rouquet N. Short-term implantation effects of a DCPD based calcium phosphate cement. Biomaterials 1998; 19:971-977.

(94) Grover LM, Knowles JC, Fleming GJP, Barralet JE. In vitro ageing of brushite cement. Biomaterials 2003; 24:4133-4141.

(95) Joosten U, Joist A, Frebel T, Brandt B, Diederichs S, Von Eiff C. Evaluation of an in situ setting injectable calcium phosphate as a new carrier material for gentamicin in the treatment of chronic osteomyelitis: Studies in vitro and in vivo. Biomaterials 2004; 25(18):4287-4295.

(96) Legeros RZ. Calcium phosphate materials in restorative dentistry: A review. Advances in Dentistry Research 1988; 2:164-168.

(97) Dee KC, Puleo DA, Bizics R. Biomaterials. An Introduction to Tissue-Biomaterial Interactions. New Jersey: JohnWiley & Sons Inc., 2002: 1-12.

(98) Qiao M, Chen D, Ma X, Liu Y. Injectable biodegradable temperature-responsive PLGA-PEG-PLGA copolymers: Sythesis and effect of copolymer composition on the drug release from the copolymer-based hydrogels. International Journal of Pharmaceutics 2005; 294:103-112.

(99) Sawhney AS, Pathak CP, Hubbell JA. Bioerodible hydrogels based on photopolymerised poly(ethylene glycol)-co-poly(á-hydroxy acid) diacrylate macromers. Macromolecules 1993; 26:581-587.

(100) Kim BS, Hrkach JS, Langer R. Biodegradable photo-crosslinked poly(ether-ester) networks for lubricious coatings. Biomaterials 2000; 21(3):259-265.

(101) Muggli DS, Burkoth AK, Keyser SA, Lee HR, Anseth KS. Reaction behavior of biodegradable, photo-cross-linkable polyanhydrides. Macromolecules 1998; 31(13):4120-4125.

(102) Burkoth AK, Anseth KS. A review of photocrosslinked polyanhydrides: in situ forming degradable networks. Biomaterials 2000; 21(23):2395-2404.

(103) Anseth KS, Shastri VR, Langer R. Photopolymerizable degradable polyanhydrides with osteocompatibility. Nature Biotechnology 1999; 17:156-159.

(104) Gresser J, Hsu S, Nagaoka H, Lyons CM, Nieratko DP, Wise DL et al. Analysis of a vinyl pyrrolidone/poly(propylene fumarate) resorbable bone cement. Journal of Biomedical Materials Research 1995; 29:1241-1247.

(105) Yaszemski M, Payne R, Hayes W, Langer R, Mikos A. In vitro degradation of a poly(propylene fumarate)-based composite materials. Biomaterials 1996; 17:2127.

(106) Burkoth AK, Burdick J, Anseth KS. Surface and bulk modifications to photocrosslinked polyanhydrides to control degradation behavior. Journal of Biomedical Materials Research 2000; 51(3):352-359.

(107) Cai Q, Bei J, Wang S. Synthesis and properties of ABA-type triblock copolymers of poly(glycolide-co-caprolactone) (A) and poly(ethylene glycol) (B). Polymer 2002; 43:3585-3591.

(108) Wei H, He J, Sun LG, Zhu K, Feng ZG. Gel formation and photopolymerization during supramolecular self-assemblies of [alpha]-CDs with LA-PEG-LA copolymer end-capped with methacryloyl groups. European Polymer Journal 2005; 41:948-957.

(109) Han DK, Hubbell JA. Synthesis of polymer network scaffolds from L-lactide and poly(ethylene glycol) and their interaction with cells. Macromolecules 1997; 30:6077-6083.

(110) Hubbell JA. Synthetic biodegradable polymers for tissue engineering and drug delivery. Current Opinion in Solid State & Materials Science 1998; 3:246-251.

(111) Nguyen KT, West JL. Photopolymerizable hydrogels for tissue engineering applications. Biomaterials 2002; 23:4307-4314.

(112) Jain JP, Modi S, Domb AJ, Kumar D. Role of polyanhydrides as localized drug carriers. Journal of Controlled Release 2005; 103:541-563.

(113) Chiu LL, Deng J, Stephens D. Polyanhydride implant for antibiotic delivery--from the bench to the clinic. Advanced Drug Delivery Reviews 2002; 54:963-986.

(114) He S, Timmer MD, Yaszemski MJ, Yasko AW, Engel PS, Mikos AG. Synthesis of biodegradable poly(propylene fumarate) networks with poly(propylene fumarate)-diacrylate macromers as crosslinking agents and characterisation of their degradation products. Polymer 2001; 42(3):1251-1260.

(115) Lewandrowski K, Gresser JD, Wise DL, White RL, Trantolo DJ. Osteoconductivity of an injectable and bioresorbable poly(propylene glycol-co-fumaric acid) bone cement. Biomaterials 2000; 21:293-298.

(116) Peter SJ, Miller MJ, Yasko AW, Yaszemski MJ, Mikos AG. Polymer concepts in tissue engineering. Journal of Biomedical Materials Research 1998; 43:422-427.

(117) Chemicals products for the pharmaceutical industry: extensive lines of excipients, vitamins and active substances for all dosage forms-technical information. 2001. Germany, BASF Aktiengesellschaft Fine Chemicals Division.
Ref Type: Catalog

(118) Peter SJ, Nolley JA, Widmer MS, Merwin JE, Yaszemski MJ, Yasko AW et al. *In vitro* degradation of a poly(propylene fumarate)/b-tricalcium phosphate composite orthopaedic scaffold. Tissue Engineering 1997; 3:207-215.

(119) Heller J, Barr J, Ng SY, Shen HR, Schwach-Abdellaoui K, Gurny R et al. Development and applications of injectable poly(ortho esters) for pain control and periodontal treatment. Biomaterials 2002; 23:4397-4404.

(120) Heller J. Poly(ortho esters). In: Domb AJ, Kost J, Wiseman DM, editors. Handbook of Biodegradable Polymer. Amsterdam: Overseas Publishers Association, 1997: 99-118.

(121) Ahmed I, Lewis M, Olsen I, Knowles JC. Phosphate glasses for tissue engineering: Part 1. Processing and characterisation of a ternary-based P_2O_5-CaO-Na_2O glass system. Biomaterials 2004; 25:491-499.

(122) Ahmed I, Lewis MP, Nazhat SN, Knowles JC. Quantification of anion and cation release from a range of ternary phosphate-based glasses with fixed 45 mol% P_2O_5. Journal of Biomaterial Application 2005; 20(1):65-80.

(123) Franks K, Abrahams I, Knowles JC. Development of soluble glasses for biomedical use. Part I: In vitro solubility measurement. Journal of Materials Science:Materials in Medicine 2000; 11:609-614.

(124) Knowles JC. Phosphate based glasses for biomedical applications. Journal of Material Chemistry 2003; 13:2395-2401.

(125) Ahmed I, Lewis M, Olsen I, Knowles JC. Phosphate glasses for tissue engineering: Part 2. Processing and characterisation of a ternary-based P_2O_5-CaO-Na_2O glass fibre system. Biomaterials 2004; 25:501-507.

(126) Salih V, Franks K, James M, Hastings GW, Knowles JC. Development of soluble glasses for biomedical use. Part 2: The biological response of human osteoblast cell lines to phosphate-based soluble glasses. Journal of Materials Science:Materials in Medicine 2000; 11:615-620.

(127) Gough JE, Christian P, Scotchford CA, Jones IA. Long-term craniofacial osteoblast culture on a sodium phosphate glass. Journal of Biomedical Materials Research 2003; 66A:233-240.

(128)   Ahmed I, Collins CA, Lewis MP, Olsen I, Knowles JC. Processing, characterisation and biocompatibility of iron-phosphate glass fibres for tissue engineering. Biomaterials 2004; 25:3223-3232.

(129)   Ahmed I, Ready D, Wilson M, Knowles JC. The antimicrobial effect of silver doped phosphate glasses. Journal of Biomedical Materials Research Part A. In press.

(130)   Brocchini S, James K, Tangpasuthadol V, Kohn J. Structure-property correlations in a combinatorial library of degradable materials. Journal of Biomedical Materials Research 1998; 42:66-75.

(131)   Brocchini S. Combinatorial chemistry and biomedical polymer development. Advanced Drug Delivery 2001; 53:123-130.

(132)   Leong K, Brott B, Langer R. Bioerodible polyanhydrides as drug-carrier matrices. I: Characterisation, degradation, and release characteristics. Journal of Biomedical Materials Research 1985; 19:941-955.

(133)   Kohn DH, Ducheyne P. In: Cahn R, Haasen P, Kramer E, editors. Materials Science and Technology. New York: VCH, 1992: 29-110.

(134)   Watts DC. In: Cahn R, Haasen P, Kramer E, editors. Materials Science and Technology. New York: VCH, 1992: 209-258.

(135)   Anseth KS, Kline LM, Walker TA, Anderson KJ, Bowman CN. Reaction kinetics and volume relaxation during polymerisations of multiethylene glycol dimethacrylates. Macromolecules 1995; 28:2491-2499.

(136)   Priola A, Gozzelino G, Ferrero F, Malucelli G. Properties of polymeric films obtained from u.v. cured poly(ethylene glycol) diacrylates. Polymer 1993; 34(17):3653-3657.

(137)   Kalachandra S, Kusy RP. Comparison of water sorption by methacylate and dimethacrylate monomers and their corresponding polymers. Polymer 1991; 32(13):2428-2434.

(138)   Fujisawa S, Atsumi T, Kadoma Y. Cytotoxicity of methyl methacrylate (MMA) and related compounds and their interaction with dipalmitoylphosphatidylcholine (DPPC) liposomes as a model for biomembranes. Oral Diseases 2000; 6(4):215-221.

(139)   Van Miller JP, Garman RH, Hermansky SJ, Mirsalis JC, Frederick CB. Skin irritaion, basal epithelial cell proliferation, and carcinogenicity evaluations of a representative specialty acrylate and methacrylate. Regulatory Toxicology and Pharmacology 2003; 37:54-65.

(140) Yoshii E. Cytotoxic effects of acrylates and methacrylates: relationships of monomer structures and cytotoxicity. Journal of Biomedical Materials Research 1997; 37:517-524.

(141) Carraher JCE. Step-reaction polymerization or polycondensation reactions. Seymour/ Carraher's Polymer Chemistry. New York: Marcel Dekker Inc., 2000: 230-285.

(142) Carraher JrCE. Free radical chain polymerization (addition polymerization). Seymour/ Carraher's Polymer Chemistry. New York: Marvel Dekker Inc., 2000: 322-357.

(143) Kohn J, Abramson S, Langer R. Bioresorbable and bioerodible materials. In: Ratner BD, Hoffman AS, Schoen FJ, Lemons JE, editors. Biomaterials Science: An Introduction to Materials in Medicine. London: Academic Press Inc., 2004: 115-127.

(144) Sideridou I, Tserki V, Papanastasiou G. Effect of chemical structure on degree of conversion in light-cured dimethacrylate-based dental resins. Biomaterials 2002; 23(8):1819-1829.

(145) Kowalski A, Duda A, Penczek S. Mechanism of cyclic ester polymerization initiated with tin(II) octoate. 2.† Macromolecules fitted with tin(II) alkoxide species observed directly in MALDI-TOF spectra . Macromolecules 2000; 33(3):689-695.

(146) Schwach G, Coudane J, Engel R, Vert M. More about the polymerization of lactides in the presence of stannous octoate. Journal of Polymer Science Part A: Polymer Chemistry 1997; 35:3431-3440.

(147) Kricheldorf HR, Kreiser-Saunders I, Stricker A. Polylactones 48. SnOct2-initiated polymerizations of lactide: a mechanistic study. Macromolecules 2000; 3(3):702-709.

(148) Moller M, Kange R, Hedrick JL. Sn(OTf)2 and Sc(OTf)3: efficient and versatile catalysts for the controlled polymerization of lactones. Journal of Polymer Science Part A: Polymer Chemistry 2000; 38:2067-2074.

(149) Witzke DR, Narayan R, Kolstad JJ. Reversible kinetics and thermodynamics of the homopolymerization of L-lactide with 2-ethylhexanoic acid tin(II) salt. Macromolecules 1997; 30(23):7075-7085.

(150) Dobrzynski P, Kasperczyk J, Janeczek H, Bero M. Synthesis of biodegradable glycolide/ L-lactide copolymers using iron compounds as initiators. Polymer 2002; 43:2595-2601.

(151) Myers M, Connor EF, Glauser T, Mock A, Nyce G, Hedrick JL. Phosphines: nucleophilic organic catalysts for the controlled ring-opening polymerization of

lactides. Journal of Polymer Science: Part A: Polymer Chemistry 2002; 40:844-851.

(152)   Hiltunen K, Seppala JV, Harkonen M. Effect of catalyst and polymerization conditions on the preparation of low molecular weight lactic acid polymers. Macromolecules 1997; 30(373):379.

(153)   Winter K, Pagoria D, Geurtsen W. The effect of antioxidants on oxidative DNA damage induced by visible-light-irradiated camphorquinone/N,N-dimethyl-p-toluidine . Biomaterials 2005; 26:5321-5329.

(154)   Rydholm AE, Bowman CN, Anseth KS. Degradable thiol-acrylate photopolymers: polymerization and degradation behavior of an in situ forming biomaterial. Biomaterials 2005; 26:4495-4506.

(155)   Hile DD, Pishko MV. Emulsion copolymerization of D,L-lactide and glycolide in supercritical carbon dioxide. Journal of Polymer Science: Part A: Polymer Chemistry 2001; 39(4):562-570.

(156)   Stassin F, Halleux O, Jerome R. Ring-opening polymerization of e-caprolactone in supercritical carbon dioxide. Macromolecules 2001; 34:775-781.

(157)   Timmer MD, Ambrose CG, Mikos AG. Evaluation of thermal- and photo-crosslinked biodegradable poly(propylene fumarate)-based networks. Journal of Biomedical Materials Research Part A 2003; 66A(4):811-818.

(158)   Weniger K, Helfmann J, Muller G. Penetration depth of light for argon laser curing of dental composites. Medical Laser Application 2005; 20:71-76.

(159)   Williams DF. The Williams Dictionary of Biomaterials. Liverpool: Liverpool University Press, 1999.

(160)   Gopferich A. Mechanisms of polymer degradation and elimination. In: Domb AJ, Kost J, Wiseman DM, editors. Handbook of Biodegradable Polymer. Amsterdam: Overseas Publishers Association, 1997: 451-471.

(161)   Schliecker G, Schmidt C, Fuchs S, Kissel T. Characterization of a homologous series of D,L-lactic acid oligomers; a mechanistic study on the degradation kinetics in vitro. Biomaterials 2003; 24:3835-3844.

(162)   Von Burkersroda F, Schedl L, Gopferich A. Why degradable polymers undergo surface erosion or bulk erosion. Biomaterials 2002; 23:4221-4231.

(163)   Timmer MD, Ambrose CG, Mikos AG. In vitro degradation of polymeric networks of poly(propylene fumarate) and the crosslinking macromer poly(propylene fumarate)-diacrylate. Biomaterials 2006; 24:571-577.

(164)   Gopferich A. Mechanisms of polymer degradation and erosion. Biomaterials 1996; 17:103-114.

(165) Domb AJ, Nudelman R. In vivo and in vitro elimination of aliphatic polyanhydrides. Biomaterials 1995; 16:319-323.

(166) Gopferich A, Langer R. Modeling of polymer erosion. Macromolecules 1993; 26:4105-4112.

(167) Mathiowitz E, Jacob J, Pekarek K, Chickering III D. Morphological characterization of bioerodible polymers. 3. Characterization of the erosion and intact zones in polyanhydrides using scanning electron microscopy. Macromolecules 1993; 26(25):6756-6765.

(168) Clement J, Bernqvist J, Ginebra MP, Planell JA. Effect of the polymer degradation on the *in vitro* behaviour of a polylactic acid / calcium phosphate glass composite material for biomedical applications. Polymers in Medicine and Surgery PIMS 2000. IOM Communications Chameleon Press Ltd (2000), 2000: 71-78.

(169) Klopffer W. Introduction to Polymer Spectroscopy. New York: Springer-Verlag, 1984.

(170) Koenig JL. Spectroscopy of Polymers. Washington, D.C.: American Chemical Society, 1992.

(171) Drake AF. Optical Spectroscopy. In: Jones C, Mulloy B, Thomas AH, editors. Methods in Molecular Biology, Vol. 22: Microscopy, Optical Spectroscopy, and Macroscopic Techniques. Totowa N.J.: Humana Press Inc., 1994: 151-171.

(172) Spectrum GX FT-IT User's Guide. Perkin Elmer, 1998.

(173) Urban MW. Attenuated Total Reflectance Spectroscopy of Polymers. Washington, D.C.: American Chemical Society, 1996.

(174) FT-IR Spectroscopy Attenuated Total Reflectance (ATR) Technical Notes. Perkin Elmer, 1998.

(175) FT-IR Spectroscopy Spectrum 2000R NIR FT-Raman User's Reference. Perkin Elmer, 1998.

(176) Williams DH, Fleming I. Spectroscopic Methods in Organic Chemistry. 5th ed. Berkshire: McGraw-Hill Publishing Co., 1995.

(177) Stevens MP. Evaluation, characterisation, and analysis of polymers. Polymer Chemistry: An Introduction. New York: Oxford University Press Inc., 1999: 129-163.

(178) LabRam Software and Hardware-User Guide. Horiba Jobin Yvon, 2006.

(179) Li Y, Kissel T. Synthesis, characteristics and in vitro degradation of star-block copolymers consisting of L-lactide, glycolide and branched multi-arm poly(ethylene oxide). Polymer 1998; 39(18):4421-4427.

(180) Espartero JL, Rashkov I, Li SM, Manolova N, Vert M. NMR analysis of low moleculare weight poly(lactic acid)s. Macromolecules 1996; 29:3535-3539.

(181) McCann DL, Heatley F, D'Emanuele A. Characterization of chemical structure and morphology of eroding polyanhydride copolymers by liquid-state and solid-sate H-1 NMR. Polymer 1999; 40(8):2151-2162.

(182) Introduction to the Spectroscopy of Biological Polymers. London: Academic Press Inc., 1976.

(183) McMurray J. Organic Chemistry. 3rd ed. California: Brooks/ Cole Publishing Company, 1992.

(184) Skoog DA, West DM, Holler FJ, Crouch SR. Analytical Chemistry- An Introduction. 7th ed. New York: Harcourt College Publishers, 2000.

(185) Tyron M, Horowitz E. Analytical Chemistry of Polymers. New York: Wiley-Interscience, 1962.

(186) Carraher JCE. Testing and spectrometric characterization of polymers. Seymour/ Carraher's Polymer Chemistry. New York: Marcel Dekker Inc., 2000: 96-132.

(187) Cromoglu T, Gonul N, Baykara T. Preparation and in vitro evaluation of modified release ketoprofen microsponges. II Farmaco 2003; 58:101-106.

(188) Mason SF. Molecular electronic absorption spectra. Quarterly Reviews of Chemical Society 1961; 15:287-371.

(189) Jones DS. Dynamic mechanical analysis of polymeric systems of pharmaceutical and biomedical significance. International Journal of Pharmaceutics 1999; 179:167-178.

(190) Bashaiwoldu AB, Podczeck F, Newton JM. Application of dynamic mechanical analysis (DMA) to determine the mechanical properties of pellets. International Journal of Pharmaceutics 2004; 269:329-342.

(191) Menard KP. Dynamic Mechanical Analysis Basics: Part 1 - How it works. Perkin Elmer Thermal Analysis Technical notes 2002.

(192) ICS-1000 Ion Chromatography System Operator's Manual. Dionex 2003; Document number. 031879 Revision 01.

(193) Peter SJ, Kim P, Yasko AW. Crosslinking characteristics of an injectable poly(propylene fumarate)/-tricalcium phosphate paste and mechanical properties of the crosslinked composite for use as a biodegradable bone cement. Journal of Biomedical Materials Research 1999; 44:314-321.

(194) Peter SJ, Miller ST, Zhu G, Yasko AW, Mikos AG. *In vivo* degradation of a poly(propylene fumarate)/-tricalcium phosphate injectable composite scaffold. Journal of Biomedical Materials Research 1998; 41(1):1-7.

(195) Quick DJ, Macdonald KK, Anseth KS. Delivering DNA from photocrosslinked, surface eroding polyanhydrides. Journal of Controlled Release 2004; 97:333-343.

(196) Quick DJ, Anseth KS. DNA delivery from photocrosslinked PEG hydrogels: encapsulation efficiency, release profiles, and DNA quality. Journal of Controlled Release 2004; 96:341-351.

(197) Usumez S, Buyukyilmaz T, Karaman AI. Effects of fast halogen and plasma arc curing lights on the surface hardness of orthodontic adhesives for lingual retainers. American Journal of Orthodontics and Dentofacial Orthopedics 2003; 123:641-648.

(198) Packhaeuser CB, Oster CG, Kissel T. In situ forming parenteral drug delivery systems: an overview. European Journal of Pharmaceutics and Biopharmaceutics 2004; 58:445-455.

(199) Cook WD. Photopolymerisation kinetics of dimethacrylates using the camphoroquinone/ amine initiator system. Polymer 1992; 33:600-609.

(200) Schmatloch S, Meier MAR, Schubert US. Instrumentation for combinatorial and high-throughput polymer research: a short overview. Macromolecular Rapid Communications 2003; 24:33-46.

(201) Xie HQ, Guan JG, Guo JS. Synthesis and properties of ionic conducting crosslinked polymer and copolymer based on dimethacryloyl poly(ethylene glycol). European Polymer Journal 2001; 37(10):1997-2003.

(202) coullerez g, lowe c, pechy p, kausch hh, hilborn j. Synthesis of acrylate functional telechelic poly(lactic acid) oligomer by transesterification. Journal of Materials Science:Materials in Medicine 2000; 11:505-510.

(203) Young AM, Rafeeka SA, Howlett JA. FTIR investigation of monomer polymerisation and polyacid neutralisation kinetics and mechanisms in various aesthetic dental restorative materials. Biomaterials 2004; 25(5):823-833.

(204) Stevens MP. Polyesters. Polymer Chemistry: An Introduction. New York: Oxford University Press Inc., 1999: 338-363.

(205) Leung D, Spratt DA, Pratten J, Gulabivala K, Mordan NJ, Young AM. Chlorhexidine-releasing methacrylate dental composite materials. Biomaterials 2005; 26:7145-7153.

(206) Gauthier MA, Stangel I, Ellis TH, Zhu XX. A new method for quantifying the intensity of the C=C band of dimethacrylate dental monomers in their FTIR and Raman spectra. Biomaterials 2005; 26:6440-6448.

(207) Stevens MP. Free radical polymerization. Polymer Chemistry: An Introduction. New York: Oxford University Press Inc., 1999: 167-202.

(208) Young RJ, Lovell PA. Synthesis. Introduction to Polymers. London: Chapman & Hall, 1991: 15-137.

(209) Lovestead TM, Burdick JA, Anseth KS, Bowman CN. Understanding multivinyl monomer photopolymerization kinetics through modeling and GPC investigation of degradable networks. Polymer 2005; 46(16):6226-6234.

(210) Burdick JA, Peterson AJ, Anseth KS. Conversion and temperature profiles during the photoinitiated polymerization of thick orthopaedic biomaterials. Biomaterials 2001; 22(13):1779-1786.

(211) Pagoria D, Lee A, Geurtsen W. The effect of camphorquinone (CQ) and CQ-related photosensitizers on the generation of reactive oxygen species and the production of oxidative DNA damage. Biomaterials 2004.

(212) Elisseeff J, Anseth K, Sims D, McIntosh W, Randolph M, Langer R. Transdermal photopolymerization for minimally invasive implantation. PNAS 1999; 96(6):3104-3107.

(213) Claes LE. Mechanical characterisation of biodegradable implants. Clinical Materials 1992; 10:41-46.

(214) Burkersroda FV, Schedl L, Gopferich A. Why degradable polymers undergo surface erosion or bulk erosion. Biomaterials 2002; 23:4221-4231.

(215) Proikakis CS, Mamouzelos NJ, Tarantili PA, Andreopoulos AG. Swelling and hydrolytic degradation of poly(d,l-lactic acid) in aqueous solutions. Polymer Degradation and Stability 2006; In Press, Corrected Proof.

(216) Taddei P, Simoni R, Fini G. Spectroscopic study on the in vitro degradation of a biodegradable composite periodontal membrane. Journal of Molecular Structure 2001; 565-566:317-322.

(217) Li SM, Vert M. Morphological changes resulting from the hydrolytic degradation of stereocopolymers derived from L- and DL-lactides. Macromolecules 1994; 27(1307):1310.

(218) Haglund BO, Joshi R, Himmelstein KJ. An in situ gelling system for parenteral delivery. Journal of Controlled Release 1996; 41:229-235.

(219) Heller J, Barr J, Ng SY, Abdellauoi KS, Gurny R. Poly(ortho esters): synthesis, characterization, properties and uses. Advanced Drug Delivery Reviews 2002; 54:1015-1039.

(220) Marks KE, Nelson CL, Lautenschlager EP. Antibiotic-impregnated acrylic bone cement. Journal of Bone Joint Surgery 1976; 5:358-364.

(221) Corry D, Moran J. Assessment of acrylic bone cement as a local delivery vehicle for the application of non-steroidal anti-inflammatory drugs. Biomaterials 1998; 19:1295-1301.

(222) Markou CP, Lutostansky EM, Ku D, Hanson SR. A novel method for efficient drug delivery. Annual Review of Biomedical Engineering 1998; 26:502-511.

(223) Lewis DH. Controlled release of bioactive agents from lactide / glycolide polymers. In: Chasin M, Langer R, editors. Biodegradable polymers as drug carrier systems. New York: Marcel Dekker, 1990: 1-42.

(224) Patel MP, Cruchley AT, Coleman DC, Swai H, Braden M, Williams DM. A polymeric system for the intra-oral delivery of an anti-fungal agent. Biomaterials 2001; 22:2319-2324.

(225) Roskos KV, Fritzinger BK, Rao SS, Armitage GC, Heller J. Development of a drug delivery system for the treatment of periodontal disease based on bioerodible poly(orthoester). Biomaterials 1995; 16:313-317.

(226) Sanders LM, Kent JS, McRae GI, Vickery BH, Tice TR, Lews DH. Controlled release of a luteinizing hormone-releasing hormone analogue from poly(d,l-lactide-co-glycolide) microspheres. Journal of Pharmaceutical Science 1984; 73:1294-1297.

(227) Singh M, Shirley B, Bajwa K, Samara E, Hora M, O'Hagan D. Controlled recombinant insulin-like growth factor from a novel formulation of polylactide-co-glycolide microparticles. Journal of Controlled Release 2001; 70:21-28.

(228) Jones CG. Chlorhexidine: is it still the gold standard? Periodontology 2000; 15:55-62.

(229) British National Formulary. 50th ed. British Medical Association, 2005.

(230) Martindale-The Extra Pharmacopoeia. 28th ed. London: The Pharmaceutical Press, 1982.

(231) British Pharmacopoeia. British Pharmacopoeia Commission, 2000.

(232) Atkins PW. Part 1: Equilibrium. In: Atkins PW, editor. Physical Chemistry. Oxford: Oxford University Press, 1994: 19-311.

(233) Young AM, Leung D, Ho SM, Sheung YT, Pratten J, Spratt D. New injectable antibacterial polymers fro bone and tooth repair. Medical Polymers 2004. Shawbury: Rapra Technology Ltd., 2004.

(234) Greish YE, Brown PW. Characterisation of bioactive glass reinforced HAP-polymer composites. Journal of Biomedical Materials Research 2000; 52(4):687-694.

(235) Lu H, El-Amin S, Scott K, Laurencin C. Three-dimentsional, bioactive, biodegradable, polymer-bioactive glass composite scaffolds with improved mechanical properties support collagen synthesis and mineralisation of human osteoblasts-like cells in vitro. Journal of Biomedical Materials Research 2003; 64A:465-474.

(236) Ahmed I. Phosphate Based Glasses and Glass-Fibres for Tissue Engineering. Eastman Dental Institute, University College London, 2005.

(237) Khairoun I, Boltong MG, Driessens FCM, Planell JA. Limited compliance of some apatitic calcium phosphate cements with clinical requirements. Journal of Materials Science:Materials in Medicine 1998; 9:667-671.

(238) Kloosterboer JG, Lijten GFCM. Photopolymers exhibiting a large difference between glass transition and curing temperatures. Polymer 1990; 31(1):95-101.

(239) Cook WD. Thermal aspects of the kinetics of dimethacrylate polymerisation. Polymer 1992; 33(10):2152-2161.

(240) Rueggeberg F, Tamareselvy K. Resin cure determination by polymerization shrinkage. Dental Materials 1995; 11:265-268.

(241) Dewaele M, Truffier-Boutry D, Devaux J, Leloup G. Volume contraction in photocured dental resins: The shrinkage-conversion relationship revisited. Dental Materials 2006; 22:359-365.

(242) O'Brien WJ. Dental Materials and Their Selection. 2nd ed. IL: Quintessence Publishing Co. Inc., 1997.

(243) Wazer JRV, Campanella DA. Structure and properties of the condensed phosphates IV. Complex ion formation in polyphosphate solutions. Journal of the American Ceramics Society 1950; 72(2):639-643.

(244) Elliott JC. General chemistry of the calcium orthophosphate. Structure and Chemistry of the Apatites and Other Calcium Orthophosphates (Studies in Inorganic Chemistry). Elsevier, 1994: 1-61.

(245) Grover LM, Gbureck U, Young AM, Wright AJ, Barralet JE, Source JE. Temperature dependent setting kinetics and mechanical properties of beta-TCP-pyrophosphoric acid bone cement. Journal of Material Chemistry 2005; 15(46):4955-4962.

(246) Barralet JE, Grover LM, Gbureck U. Ionic modification of calcium phosphate cement viscosity. Part II: hypodermic injection and strength improvement of brushite cement. Biomaterials 2004; 25:2197-2203.

(247) Popov VK, Evseev AV, Ivanov AL, Roginski W, Volozhin AI, Howdle SM. Laser stereolithography and supercritical fluid processing or custom-designed implant fabrication. Journal of Materials Science:Materials in Medicine 2004; 15:123-128.

(248) Chun KW, Lee JB, Kim SH, Park TG. Controlled release of plasmid DNA from photo-cross-linked pluronic hydrogels. Biomaterials 2005; 26(16):3319-3326.

(249) Jang JH, Shea LD. Controllable delivery of non-viral DNA from porous scaffolds. Journal of Controlled Release 2003; 86(1):157-168.

(250) Li Y, Ogris M, Pelisek J, Roedl W. Stability and release characteristics of poly(-lactide-co-glycolide) encapsulated CaPi-DNA coprecipitation. International Journal of Pharmaceutics 2004; 269(1):61-70.

(251) Roy I, Mitra S, Maitra A, Mozumdar S. Calcium phosphate nanoparticles as novel non-viral vectors for targeted gene delivery. International Journal of Pharmaceutics 2003; 250(1):25-33.

(252) Bisht S, Bhakta G, Mitra S, Maitra A. pDNA loaded calcium phosphate nanoparticles: highly efficient non-viral vector for gene delivery. International Journal of Pharmaceutics 2005; 288(1):157-168.